NASA CONTRACTOR REPORT

NASA CR-1718

NASA CR-1718

TURBULENCE AND LATERAL-DIRECTIONAL FLYING QUALITIES

by James A. Franklin

NATIONAL AERONAUTICS AND SPACE ADMINISTRATION • WASHINGTON, D. C. • APRIL 1971

1. Report No. NASA CR-1718	2. Government Accession No.	3. Recipient's Catalog No.
4. Title and Subtitle TURBULENCE AND LATERAL-DIRECTIONAL FLYING QUALITIES		5. Report Date April 1971
		6. Performing Organization Code
7. Author(s) James A. Franklin		8. Performing Organization Report No. Report No. 890
9. Performing Organization Name and Address Princeton University Princeton, New Jersey 08540		10. Work Unit No.
		11. Contract or Grant No. NSR-31-001-104
		13. Type of Report and Period Covered
12. Sponsoring Agency Name and Address National Aeronautics & Space Administration Washington, D. C. 20546		Contractor Report
		14. Sponsoring Agency Code

15. Supplementary Notes

16. Abstract Flight evaluations using a variable stability airplane were made to determine independence and interacting effects of turbulence induced aerodynamic disturbances and lateral-directional dynamics on flying qualities associated with a precision heading control task. Trends in pilot rating obtained in the test program for variations in turbulence disturbances and airplane dynamics are explained in terms of measures of precision of task performance, pilot control workload, and pilot compensatory behavior derived from time histories of the flight evaluations. Pilot-vehicle systems analyses substantiate the performance-workload data and provide a more fundamental understanding of the heading control task in turbulence.

The significant influence of turbulence on the evaluation task was found to be the rms disturbance magnitude, with yaw disturbances having a more profound effect than roll disturbances. Spectral bandwidth had less bearing on flying qualities than disturbance magnitude, although bandwidth did have an apparent influence for frequencies below $V_0/L \doteq 1.0$ radian/ second. Reductions in either roll damping or directional stability adversely affected flying qualities. Additional roll damping and directional stability were desired when the level of turbulence was increased. Data obtained in this investigation for variations in aileron yaw indicate that favorable yaw is detrimental to the heading tracking task, particularly for low directional stability and when roll disturbances due to turbulence are large.

17. Key Words (Selected by Author(s)) Flying qualities Lateral directional Atmospheric turbulence In-flight simulation Variable stability Pilot workload Pilot describing function Closed loop system analysis Directional stability Roll damping Dutch roll damping Aileron yaw		18. Distribution Statement Unclassified - Unlimited	
19. Security Classif. (of this report) Unclassified	20. Security Classif. (of this page) Unclassified	21. No. of Pages 347	22. Price $3.00

FOREWORD

This research program was sponsored by Headquarters, National Aeronautics and Space Administration. It was conducted by the Flight Research Laboratory of Princeton University under Contract No. NSR 31-001-104. Mr. R. J. Wasicko was the Project Monitor for NASA. Professor Edward Seckel was the Principal Investigator and Mr. James A. Franklin was the Project Engineer for Princeton University.

A unique tribute should be paid to the project evaluation pilots and safety pilot for their endurance of numerous hours of unpleasant flying conditions. The evaluation pilots were Mr. W. B. Nixon of Princeton University, Mr. J. W. Olcott of Aeronautical Research Associates of Princeton, Mr. G. W. Hall of the Cornell Aeronautical Laboratory, and Mr. L. Person of NASA Langley Research Center. Mr. D. R. Ellis, Manager of Variable Stability Flight Research at Princeton, was the safety pilot.

ABSTRACT

This report presents the results of an experimental investigation into the influences of atmospheric turbulence on lateral-directional flying qualities. In-flight evaluations of various combinations of turbulence-induced aero-dynamic disturbances and open loop airplane dynamics were made for a precision heading control task. Test configurations were chosen to permit a thorough study of the effects of turbulence to be made for a set of satisfactory dynamics and further to assess the interacting influences of turbulence and airplane dynamics. The turbulence characteristics were specified in terms of rms magnitudes of roll and yaw disturbances, turbulence spectral bandwidth, and correlation between the roll and yaw disturbances. Selective variations of these characteristics were made for several combinations of airplane dynamics which included variations in roll damping (or roll subsidence time constant), directional stability (or Dutch roll natural frequency), Dutch roll damping ratio, and aileron yaw characteristics. Data in the form of pilot ratings and commentary were obtained. Time histories of the pertinent airplane response and control variables were digitally processed to produce rms measures of task performance and control workload. Selective measures of pilot describing functions were also made to determine the extent of pilot compensation.

The dominant influences on flying qualities associated with the heading control task are the precision of task performance, the pilot's control workload, and the pilot's compensation in the pertinent control loops. Turbulence disturbances and airplane dynamics are found to be important insofar as they bear on these three factors. Closed loop pilot-airplane systems analysis substantially verify the pilot rating and flight test performance-workload data in this report.

This investigation showed that the significant influence of turbulence is the rms disturbance magnitude. Yaw disturbances have a more profound effect than roll disturbances on the evaluation task. Spectral bandwidth has less bearing on flying qualities than disturbance magnitude, although bandwidth does have an apparent influence for frequencies on the order of one radian/second or less. Roll-yaw correlation is of little consequence to the task.

Both roll damping and directional stability were found to profoundly affect flying qualities by determining in part the magnitude of the airplane's response to turbulence and the closed loop control characteristics. Reductions in either roll damping or directional stability adversely affect flying qualities in this regard. An increase in the level of turbulence seems to have a more degrading effect on flying qualities when either roll damping or directional stability are low. Turbulence bandwidth influences seem to be essentially independent of roll subsidence time constant and Dutch roll natural frequency. Increasing the Dutch roll damping ratio offers an improvement in flying qualities for the low directional stability configuration, particularly in the presence of large yaw disturbances. Taken as a whole the data obtained in this investigation for variations in aileron yaw indicate that favorable yaw is detrimental to the heading tracking task, particularly for low directional stability and when roll disturbances due to turbulence are large. Control of heading excursions with the rudder is required to achieve acceptable precision in heading tracking. Scatter in the pilot rating data for variations in aileron yaw is felt to be due to the willingness and skill of the pilots in using the rudder. A larger sample of pilots would be necessary to more conclusively define the influence of aileron yaw on flying qualities in turbulence.

TABLE OF CONTENTS

LIST OF FIGURES

LIST OF FIGURES (continued)

LIST OF FIGURES (continued)

LIST OF FIGURES (continued)

LIST OF FIGURES (continued)

xv

LIST OF TABLES

NOTATION AND SYMBOLS

A   Turbulence scale factor

AR   Aspect ratio

A_r Gain factor of the $r/\delta r$ transfer function

A_β Gain factor of the $\beta/\delta a$ transfer function

$A_{\varphi \delta a}$ Gain factor of the $\varphi/\delta a$ transfer function numerator

$A_{\varphi \delta r}$ Gain factor of the $\varphi/\delta r$ transfer function numerator

C. L.   Closed loop

C_{ℓ_β} Nondimensional dihedral effect derivative $\dfrac{1}{qSb} \dfrac{\partial L}{\partial \beta}$

C_{n_β} Nondimensional directional stability derivative $\dfrac{1}{qSb} \dfrac{\partial N}{\partial \beta}$

C_{ℓ_p} Nondimensional roll damping derivative $\dfrac{1}{qSb} \dfrac{\partial L}{\partial \left(\dfrac{pb}{2V}\right)_o}$

$F_x(\omega)$ Fourier transform of x

$H_i(\omega)$ Fourier transform of $h_i(t)$; transfer function defining variable i in the frequency domain due to a gust input

I_x, I_y, I_z Moments of inertia about the x, y, and z axes (slug-ft^2)

I_{xz} Cross product of inertia between the x and z axes (slug-ft^2)

K_d/K_{ss} Dutch roll excitation parameter for roll response

K_0, K_1 Modified Bessel functions of the second kind

$K_0(x-\xi, y-\eta)$ Kernel function for defining downwash at point (x, y) due to local pressure at point (ξ, η)

K_φ Pilot gain in the bank angle control loop (inch/deg)

K_ψ Pilot gain in the $\psi \rightarrow \delta r$ control loop (inch/deg) or in the $\psi \rightarrow \delta a$ loop (deg/deg)

L   Rolling moment (ft-lb); turbulence scale length (ft)

$$L' = \dfrac{L + \dfrac{I_{xz}}{I_x} N}{1 - \dfrac{I_{xz}^2}{I_x I_z}}$$ Primed rolling moment derivative

L_β, L_{β_g} Dihedral effect $\dfrac{1}{I_x} \dfrac{\partial L}{\partial \beta}$; roll due to β gust $\dfrac{1}{I_x} \dfrac{\partial L}{\partial \beta_g}$ (rad/sec^2 per rad)

L_p, L_{p_g} Roll damping $\dfrac{1}{I_x} \dfrac{\partial L}{\partial p}$; roll due to w gust field $\dfrac{1}{I_x} \dfrac{\partial L}{\partial p_g}$ (rad/sec^2 per rad/sec)

L_r Roll due to yaw rate $\dfrac{1}{I_x} \dfrac{\partial L}{\partial r}$ (rad/sec^2 per rad/sec)

$L_{\delta a}$ Aileron effectiveness $\dfrac{1}{I_x} \dfrac{\partial L}{\partial \delta_a}$ (rad/sec^2 per inch)

$L_{\delta r}$ Rudder roll $\dfrac{1}{I_x} \dfrac{\partial L}{\partial \delta_r}$ (rad/sec^2 per inch)

L_{w_g}, L_{v_g} Rolling moment due to vertical and lateral gusts (ft-lb); roll acceleration due to vertical and lateral gusts (rad/sec^2)

N_j^i Open loop transfer function numerator relating the response i to an input j

N'^i_j Transfer function numerator relating the response i to an input j with an inner loop (typically $\varphi \rightarrow \delta_a$) closed

N   Yawing moment (ft-lb); limit of integer index n

$$N' = \dfrac{N + \dfrac{I_{xz}}{I_z} L}{1 - \dfrac{I_{xz}^2}{I_x I_z}}$$ Primed yawing moment derivative

N_β, N_{β_g} Directional stability $\dfrac{1}{I_z} \dfrac{\partial N}{\partial \beta}$; yaw due to β gust $\dfrac{1}{I_z} \dfrac{\partial N}{\partial \beta_g}$ (rad/sec^2 per rad)

N_p Yaw due to roll $\dfrac{1}{I_z}\dfrac{\partial N}{\partial p}$ (rad/ sec^2 per rad/ sec)

N_r Yaw damping $\dfrac{1}{I_z}\dfrac{\partial N}{\partial r}$ (rad/ sec^2 per rad/ sec)

$N_{\delta a}$ Aileron yaw $\dfrac{1}{I_z}\dfrac{\partial N}{\partial \delta_a}$ (rad/ sec^2 per inch).

$N_{\delta r}$ Rudder effectiveness $\dfrac{1}{I_z}\dfrac{\partial N}{\partial \delta_r}$ (rad/ sec^2 per inch)

N_{w_g}, N_{v_g} Yawing moment due to vertical and lateral gusts (ft -lb); yaw acceleration due to vertical and lateral gusts (rad/ sec^2)

O. L.   Open loop

POR   Pilot opinion rating

R   Spatial dimension scalar; terrain roughness factor

R_e Real part of a complex number

R_{ij} Autocorrelation function for the variable i (if i = j); cross correlation function for the variables i and j (if i $\neq$ j)

Rms   Root mean square

S   Wing area (ft^2)

T   Time length of record (sec)

T_i Time constant of the ith factor of the nth order polynomial approximation to rolling or yawing moment spectra

T_{L_φ} Pilot lead time constant in the bank angle control loop (sec)

T_{L_ψ} Pilot lead time constant in the heading control loop (sec)

T_N Time constant associated with human neuromuscular lag (sec)

T_R Roll mode time constant (sec)

T_R' Time constant of the numerator root of the $\psi/\delta r$ transfer function ($\varphi \rightarrow \delta a$ loop closed) associated with the roll mode (sec)

T_S	Spiral mode time constant (sec)
T_{v_1}	Time constant associated with the power spectral densities of rolling and yawing moments due to lateral gusts (sec)
T_{w_1}, T_{w_2}	Time constants associated with the power spectral density of rolling moment due to vertical gusts (sec)
T_{ψ_1}	Low frequency numerator time constant of the $\psi/\delta r$ transfer function ($\varphi \to \delta a$ loop closed) (sec)
T_{φ_1}	Time constant of the numerator root of the $\varphi/\delta r$ transfer function (sec)
T_{β_1}, T_{β_2}	Time constants of the factors of the numerator of the $\beta/\delta a$ transfer function (sec)
$T_{r_1}, T_{r_2}, T_{r_3}$	Time constants of the numerator factors of the $r/\delta r$ transfer function (assuming 3 first order factors) (sec)
VT	Vertical tail
V_o	True airspeed (miles/hour, ft/sec)
$\bar{V}$	Mean wind velocity (ft/sec)
Y_A	Generalized transfer function of airplane response to control inputs
Y_G	Generalized transfer function of airplane response to turbulence disturbances
Y_p	Generalized pilot transfer function
$Y_{p_{\delta a}}$	Pilot transfer function for aileron control
$Y_{p_{\delta r}}$	Pilot transfer function for rudder control
Y	Side force (lbs)
Y_v	Side force due to lateral velocity $\dfrac{1}{m}\dfrac{\partial Y}{\partial v}$ (per sec)

Y_{v_g} Side force due to lateral gusts (lbs); side force due to lateral gusts $\frac{1}{m} \frac{\partial Y}{\partial v_g}$ (per sec)

$Y_{\delta r}^*$ Side force due to rudder deflection $\frac{1}{mV_o} \frac{\partial Y}{\partial \delta r}$ (per in. sec)

$a \quad = \quad \frac{b}{L} \sqrt{1 + (\frac{L}{V_o} \omega)^2}$

a_i i^{th} coefficient of an nth order polynomal

a_t Gain of the transient analog representation of the turbulence disturbance

b   Wing span (ft)

c   Generalized command input

$\bar{c}$ Mean aerodynamic chord; mean chord S/b (ft)

c(y)   Wing chord at spanwise location y (ft)

$c_\ell(y)$ Section lift coefficient at spanwise location y

db   Decibels, $20 \log_{10} | \ |$

e   Exponential function

eas   Equivalent airspeed $v_{eas} = v_{true} (\frac{\rho}{\rho_o})^{\frac{1}{2}}$

f   Generalized turbulence disturbance

f(r)   Longitudinal correlation function for isotropic turbulence

g(r)   Transverse correlation function for isotropic turbulence

g   Acceleration due to gravity (ft/sec^2)

$h_i(t)$ Indicial (step) response influence function in the time domain of the variable i

i   Generalized variable; index

j   Generalized variable; index; imaginary number $\sqrt{-1}$

$k_1(t)$ Transient lift response function to a step gust input

$\ell(y)$ Section lift (lbs/ft)

ℓ_v, ℓ_t Tail length for vertical and horizontal tail nominally measured from c.g. to the 1/4 chord of the tail m.a.c. (ft)

n General integer number

$p_o(x, y)$ Local pressure at point (x, y)

q Dynamic pressure $\frac{1}{2} \rho V^2$ (lb/ft^2)

$r, \underline{r}$ Generalized response; spatial separation scalar; spatial separation vector

s Laplace operator $\sigma \pm j\omega$

t, t_o, t_1 Time; initial time; dummy time variable (sec)

u, v, w Longitudinal, lateral, vertical perturbation velocities (ft/sec)

u_g, v_g, w_g Longitudinal, lateral, vertical gust velocities (ft/sec)

u_{d_e} Equivalent derived gust velocity (ft/sec eas)

u_L, u_T Gust velocities associated with the longitudinal (L) and transverse (T) direction (ft/sec)

$w_o(x, y)$ Local downwash at point (x, y)

x, x_o Distance along the longitudinal axis (typically associated with the airplane's flight path); initial longitudinal position (ft)

y Distance along the lateral (spanwise) axis (ft)

Δy Incremental spanwise separation (ft)

$z_i(x, y)$ Mode shape associated with point (x, y)

α Angle of attack (deg., rad.)

β Sideslip angle (deg)

$\gamma_{L_{w_g}}(y)$ Dimensionless lift distribution in roll

$\Gamma(\Delta y)$ Autoconvolution of $\gamma(y)$

Δ Open loop lateral-directional characteristic equation or matrix

Δ', Δ'' Closed loop lateral-directional characteristic equation or matrix, typically with $\varphi \to \delta a$ loop closed; $\varphi \to \delta a$ and $\psi \to \delta r$ loops closed

δ_a, δ_{as} Aileron control deflection (rad, deg); lateral stick deflection (inches, lbs)

δ_r, δ_{rp} Rudder control deflection (rad, deg); rudder pedal deflection (inches, lbs)

δ_{ij} Dirac delta function $\delta_{ij} = \begin{matrix} 1 & i = j \\ 0 & i \neq j \end{matrix}$

∇ Del operator, $\underline{i} \dfrac{\partial}{\partial x} + \underline{j} \dfrac{\partial}{\partial y} + \underline{k} \dfrac{\partial}{\partial z}$

ϵ Generalized error (c-r)

ζ_d Dutch roll damping ratio

ζ'_d, ω'_d Dutch roll damping ratio and frequency as modified by the $\varphi \to \delta a$ loop closure

ζ''_d, ω''_d Dutch roll damping ratio and frequency as modified by consecutive $\varphi \to \delta a$, $\psi \to \delta r$ loop closures

ζ_N, ω_N Damping ratio and natural frequency of the human neuro-muscular system

ζ_{SR}, ω_{SR} Damping ratio and natural frequency of the coalesced roll-spiral mode resulting from the $\varphi \to \delta a$ loop closure

$\zeta_\varphi, \omega_\varphi$ Damping ratio and natural frequency of the $\varphi/\delta a$ transfer function numerator

ζ_ψ, ω_ψ Damping ratio and natural frequency of the second order factor of the $\psi/\delta r$ transfer function numerator ($\varphi \to \delta a$ loop closed) associated with the roll-spiral mode

ζ_r, ω_r — Damping ratio and natural frequency of the second order numerator factor of the $r/\delta r$ transfer function (assuming one first order and one second order factor)

λ — Inverse time constant of the transient analog representation of the turbulence disturbance

ρ — Air density (slugs/ft^3)

ρ_{LN} — Normalized cross correlation between roll and yaw distur-bances $\rho_{LN} = \dfrac{R_{LN}(0)}{\sigma_L \sigma_N}$

σ_i — Root mean square of the variable i

τ — Time lag (sec)

τ_e — Equivalent pilot time lag (sec)

τ_e' — Time constant associated with the closed loop root originating at $\sigma = -\dfrac{2}{\tau_e}$ in the $\varphi \to \delta a$ control loop

Φ_{ij} — Power spectral density of the variable i ($i = j$); cross spectral density of the variables i and j ($i \neq j$)

$\Phi_{w_e}(\omega)$ — Power spectral density of vertical gusts weighted to give effective spanwise gust gradient

φ — Bank angle (deg)

$\dot{\varphi}, p$ — Roll rate (rad/sec, deg/sec)

$\varphi_k(\omega)$ — Sears function for unsteady lift during gust penetration

φ_m — Phase margin (deg)

φ_ϵ — Error in the roll attitude loop $\varphi_\epsilon = \varphi_c - \varphi$ (deg)

ψ — Heading (deg)

$\dot{\psi}$, r   Yaw rate (rad/sec, deg/sec)

ψ_ϵ Error in the heading loop $\psi_\epsilon = \psi_c - \psi$ (deg)

$\underline{\Omega}$ Three dimensional spatial frequency (wave number) vector

$$|\Omega| = \sqrt{\Omega_x^2 + \Omega_y^2 + \Omega_z^2} \quad \text{(rad/ft)}$$

Ω_i Spatial frequency (wave number) in the ith direction, where $i = x, y, z$ (rad/ft)

ω Angular frequency (rad/sec)

ω_c, ω_{co} Crossover frequency (rad/sec) ω for $|Y_A Y_p| = 1.0$

ω_f Frequency bandwidth of the generalized disturbance input f

ω_d Dutch roll frequency (rad/sec)

ω_n Natural frequency (rad/sec)

ω_{v_1} Break frequency associated with the power spectral densities of rolling and yawing moments due to lateral gusts (rad/sec)

$\omega_{w_1}, \omega_{w_2}$ Break frequencies of the power spectral density of rolling moment due to vertical gusts (rad/sec)

[ ]* Complex conjugate of the quantity [ ]

$|(\ )|$ Absolute value of ( )

$\sphericalangle$ ( )   Angle of ( )

$\doteq$ Approximately equal to

SECTION 1

INTRODUCTION

Turbulence, whether encountered in VFR cruise flight or under a pre-
cisely controlled IFR terminal area maneuver, whether encountered as a pilot
or as a passenger, can be a highly disconcerting, discomforting, and a poten-
tially dangerous experience. And yet, in the history of study of airplane flying
qualities, a conspicuously small amount of attention has been paid, either theo-
retically or experimentally, to the effects of atmospheric turbulence on the
pilot's capability to control the airplane. Certainly there has been some de-
gree of awareness that the airplane's turbulence response characteristics play
a part in determining its overall handling characteristics. NACA Report No. 1
(Reference 1), titled "Report on Behavior of Aeroplanes in Gusts" is an indica-
tion of the early interest in the general subject. Ample evidence is available
from pilot commentary collected during operational use, airplane flight test
programs, variable stability airplane programs, and the like, of the dele-
terious effects of turbulence on the pilot's ability to control the airplane satis-
factorily. However, to this date, no systematic study has been made to define
in general the relationship of turbulence to flying qualities.

Research conducted at Princeton University in recent years, using a
variable stability airplane to evaluate flying qualities in the landing approach,
incorporated one of the more realistic simulations of the turbulent environ-
ment attempted up to that time (References 2 through 5). More specifically,
the turbulence simulation was designed to represent spectral characteristics
of the gust environment and to scale the aerodynamic moments induced by
these disturbances consistently with the aerodynamic configuration being
simulated. One of the latest flying qualities studies for fighter aircraft
conducted by Cornell Aeronautical Laboratory (Reference 6) has also

1

accounted for the gust environment in the aforementioned manner. It has been quite apparent from these programs that turbulence has had a decided influence on flying qualities. In each case the turbulence simulation has represented an attempt to accurately reproduce the flight environment associated with specific airplanes and specific segments of the flight regime.

Prior to the Princeton and Cornell studies, the simulation of gust inputs, either for in-flight or ground based simulators or for analytical studies, was approached in a less precise manner. Some work at Cornell and NASA, for example, noted in References 7, 8, and 9, illustrate the technique of using unfiltered noise or sums of sinusoids to generate a random disturbance, introduced either through the controls or through a tracking display. In these instances, neither the spectral characteristics of turbulence or the magnitude of the disturbance induced forces and moments were simulated in a manner which reflected the character of turbulence or the aerodynamic configuration of the vehicle under study. Analytical flying qualities investigations, such as that of Reference 10, also have adopted this approach. Notwithstanding the simplified representation of turbulence used in these cases, it has been characteristic that introduction of the random disturbance has made the pilot's task more difficult.

From the results of these various studies, it has been amply demonstrated that turbulence must be considered as one of the more significant influences on airplane flying qualities. As a start toward achieving an understanding of this influence, a thorough analytical and experimental investigation which defines the important parameters of airplane response to turbulence, including influences of the turbulence induced force and moment disturbances, dynamics of the pilot-airplane system, and their interrelationships relevant to flying qualities is a necessity. From this type of generalized approach, implications for airframe and automatic control system design, aimed at improving the piloting task in turbulence, can be drawn more logically.

The research effort discussed in this report represents a beginning in this regard. It is a generalized study of the problems of lateral-directional flying qualities in turbulence. It is directed toward the general aviation class of airplane when such a distinction is appropriate. As in the case of analysis of airplane dynamics, the problem of turbulence response may be simplified by decoupling the six-degree of freedom system into two separate three-degree of freedom problems. The lateral-directional case is considered in this report.

The problem may be illustrated conceptually with reference to Figure 1. The response r of the pilot-airplane system to the error signals ε and to the turbulence induced disturbances f may be generally expressed, using transform notation

$$r(s) = Y_P Y_A \; \varepsilon(s) + Y_G \; f(s) \tag{1}$$

and in terms of the command inputs c of the closed loop pilot-airplane system

$$r(s) = \frac{Y_P Y_A}{1 + Y_P Y_A} \; c(s) + \frac{Y_G}{1 + Y_P Y_A} \; f(s) \tag{2}$$

In a compensatory tracking task which requires that the error between the airplane's response and command input vanish or be minimized, the expression for the tracking error is of interest.

$$\varepsilon(s) = \frac{1}{1 + Y_P Y_A} \; c(s) - \frac{Y_G}{1 + Y_P Y_A} f(s) \tag{3}$$

3
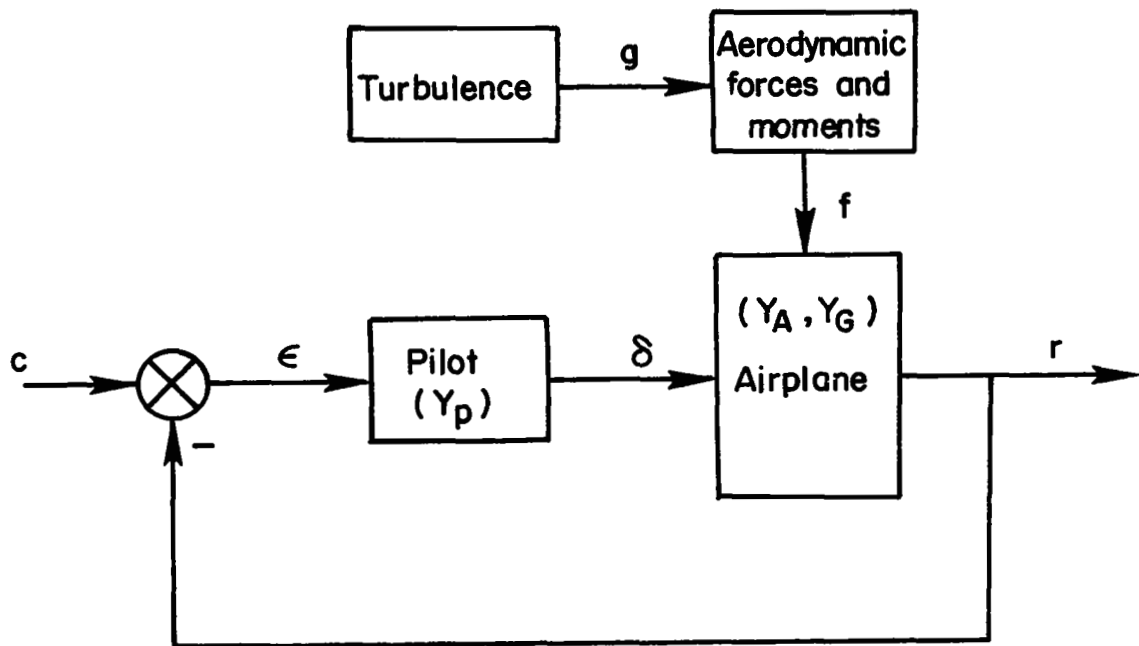
Figure 1.   Block Diagram of Pilot-Airplane System

A suitable statistical description of the airplane's response and one which is commonly employed in random process analysis is the power spectral density. The power spectral density of the airplane's response to the various inputs, where there is no correlation between the command inputs and turbulence, is generally know to be (see Reference 11 for example)

$$\Phi_{\epsilon\epsilon} = \left|\frac{1}{1 + Y_P Y_A}\right|^2 \Phi_{cc} + \left|\frac{Y_G}{1 + Y_P Y_A}\right|^2 \Phi_{ff} \tag{4}$$

The problem at hand deals with the second of the two terms in equation (4). The form of the term describing the contribution of turbulence suggests a subdivision of the problem into two sections. The first area of study involves the turbulence disturbances, Φ_{ff}, which in turn requires separate consideration of the atmospheric gust velocities and of the aerodynamic forces and moments induced by these gusts. The second area of study concerns the closed loop transfer function, $\frac{Y_G}{1 + Y_P Y_A}$, relating airplane response to the gust disturbances. The role of the open loop airplane transfer function, Y_A, the pilot's compensatory characteristics in the loop, Y_P, and the open loop turbulence response transfer function, Y_G, will be included here.

Section 2 of this report is devoted to an analytical description of atmospheric turbulence. A considerable amount of work has been done in this area in the past. The purpose of this section is to outline the mathematical description most suitable to the problem at hand, based on a review of the existing literature. No extensive reinterpretation of the existing information or collection of additional data is attempted.

In Section 3, the relationships between the gust components and the force and moment disturbances are presented. The basis for this analysis is in the literature, and although much of the previous work was directed

toward prediction of structural loads, it is applicable in general to the problem at hand. Approximations to the disturbance spectra are developed in this section to facilitate the simulation of the turbulence disturbances in the flight test program.

An experimental flight program to explore the influence of the turbulence disturbances on the airplane's closed loop response characteristics and hence on its flying qualities is discussed in Section 4. The parameters studied in the test program are outlined and the data pertinent to the evaluation of flying qualities are summarized.

Finally, in Section 5 the flight test results are presented and discussed in detail, including pilot opinion data and measures of task performance and pilot workload. A detailed pilot-vehicle systems analysis is undertaken to provide a fundamental understanding of the flight data.

SECTION 2

DESCRIPTION OF TURBULENCE

Properties of Turbulence

The nondeterministic nature of atmospheric turbulence makes it necessary to utilize statistical measures for the definition of the time or spatial variation of the turbulence field. In this regard, the tools of random process theory, particularly the correlation function and power spectral density, lend themselves to a description of turbulence suitable for airplane dynamic response analysis.

Before considering the statistical description of turbulence, four important properties typically associated with the gust field and which greatly simplify the mathematical model should be considered. These properties are stationarity, homogeneity, compliance with Taylor's hypothesis, and isotropy. A brief description of each of these properties follows.

Stationarity of the field of turbulence exists if such statistical properties as the mean wind intensity, rms gust intensity, time correlation function, and power spectral density are invariant within the time period of interest. This implies no significant variation in meteorological conditions over the specified time period.

Turbulence is considered to be homogeneous if the aforementioned statistical properties are independent of spatial position. This characteristic implies no variation in meteorological conditions or in the character of the terrain within the spatial confines of interest.

Taylor's hypothesis infers an invariance of the turbulence field on a short time basis. The significance of this characteristic is the implication of equivalence of the time and spatial correlation functions. This assumption has been shown to be valid for a patch of turbulence transported past a stationary point or for an airplane penetrating a gust field at a speed much

7

greater than the rms gust intensity. Therefore, to an airplane traversing the gust field, the field appears to be "frozen." In this case, conversion between time and spatial measures may be made by the relationship

$$(x - x_o) = V_o(t - t_o) \tag{5}$$

Isotropy suggests a turbulence field whose statistical characteristics are invariant with rotation and reflection of the coordinate system in which the turbulence is measured. In general, the turbulence field is assumed to be isotropic in three dimensions, although circumstances occasionally dictate a two-dimensional isotropy or axisymmetry. Isotropy further implies specific relationships between statistical properties of the three gust components. The gust field must be homogeneous to satisfy the definition of isotropy. No correlation can exist between gust velocity components at a point in space. Correlation between the same gust component at two different points in space exists and will be defined in the following discussion.

Mathematical Models of Isotropic Turbulence

A useful tool for defining the characteristics of turbulence on the average, and one which readily lends itself to dynamic response analysis is the correlation function. Based on the aforementioned properties, isotropic turbulence may be defined by two spatial correlation functions corresponding to the longitudinal and transverse velocity vectors associated with two points in space (Figure 2). These two correlation functions are defined in general as

$$f(r) = \frac{\overline{u_{L_A} u_{L_B}}}{\sigma_{u_L}^2} = \lim_{T \to \infty} \frac{1}{2T} \int_{-T}^{T} \frac{u_{L_A} u_{L_B}}{\sigma_{u_L}^2} \, dt \tag{6}$$

for the longitudinal velocity components and
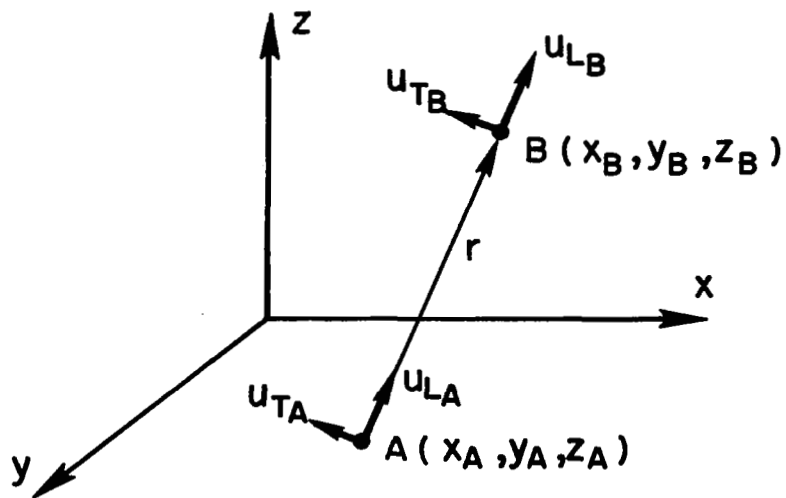
Figure 2. Longitudinal and Transverse Turbulence Velocity Vectors
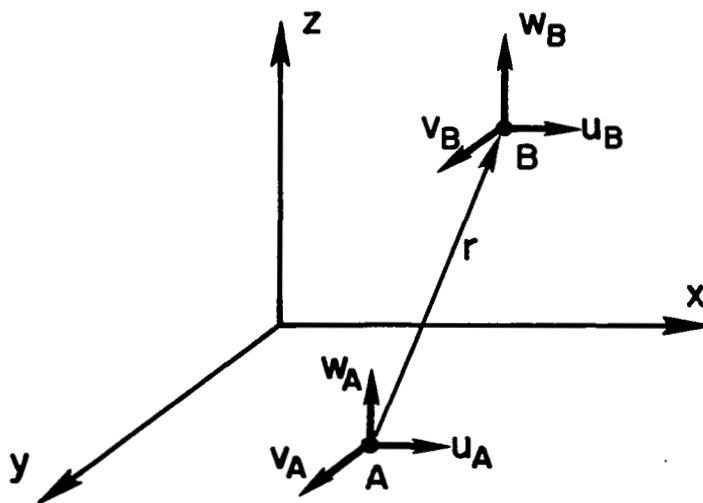
Figure 3. Cartesian Velocity Components

9

$$g(r) = \frac{\overline{u_{T_A} u_{T_B}}}{\sigma_{u_T}^2} = \lim_{T \to \infty} \frac{1}{2T} \int_{-T}^{T} \frac{u_{T_A} u_{T_B}}{\sigma_{u_T}^2} \, dt \tag{7}$$

for transverse velocity components. These two correlation functions are sufficient to describe the gust field due to the independence of the axis system orientation in which the turbulence velocities are measured. Knowledge of these correlation functions also allows a correlation tensor to be defined

$$R_{ij}(\underline{r}) = \lim_{T \to \infty} \frac{1}{2T} \int_{-T}^{T} u_i u_j \, dt \tag{8}$$

where the indices i and j refer to any one of the three components in a cartesian coordinate system. Figure 3 illustrates the velocities of interest. Correlation functions of the three velocity components u, v, and w may be related to the longitudinal and transverse velocity correlations associated with points A and B by the expressions

$$R_{uu}(\underline{r}) = \frac{f(r) - g(r)}{r^2} (x_B - x_A)^2 + g(r) \tag{9}$$

$$R_{vv}(\underline{r}) = \frac{f(r) - g(r)}{r^2} (y_B - y_A)^2 + g(r) \tag{10}$$

$$R_{ww}(\underline{r}) = \frac{f(r) - g(r)}{r^2} (z_B - z_A)^2 + g(r) \tag{11}$$

$$R_{uv}(\underline{r}) = \frac{f(r) - g(r)}{r^2} (x_B - x_A)(y_B - y_A) \tag{12}$$

$$R_{uw}(\underline{r}) = \frac{f(r) - g(r)}{r^2} (x_B - x_A)(z_B - z_A) \tag{13}$$

$$R_{vw}(\underline{r}) = \frac{f(r) - g(r)}{r^2} (y_B - y_A)(z_B - z_A) \tag{14}$$

10

As noted in Reference 12, these expressions result from a coordinate transformation from the generalized coordinates used in the definition of the longitudinal and transverse correlation functions to the cartesian set noted in Figure 3. One further simplification of this group of equations may be made by relating the longitudinal and transverse correlation functions through application of the principle of conservation of mass. For the case of incompressible flow, this is satisfied by the continuity equation $\nabla \cdot V = 0$, or as applied to the velocity correlation tensor $\nabla \cdot R_{ij} = 0$. The relationship between $f(r)$ and $g(r)$ which results is

$$g(r) = f(r) + \frac{r}{2} \frac{df(r)}{dr} \tag{15}$$

Thus from the knowledge of either the longitudinal or transverse velocity correlation along any path in the turbulent field, the correlation functions describing any component of turbulence may be defined.

Since the power spectral density of the turbulence induced disturbances are ultimately desired (equation 4), the spectral densities of the various turbulence components are of interest. Given the three-dimensional velocity correlation function, a three-dimensional power spectral density may be obtained using the Fourier transform in three-dimensional form

$$\Phi_{ij}(\underline{\Omega}) = \frac{1}{\pi^3} \int_{-\infty}^{\infty} R_{ij}(\underline{r}) e^{-i\underline{r} \cdot \underline{\Omega}} d\underline{r} \tag{16}$$

The spectral function derived here is in terms of spatial frequency, $\underline{\Omega}$. The component of this spatial frequency along the flight path, Ω_x, can readily be converted to angular frequency, ω, in radians per second using the relationship implicit in Taylor's hypothesis

$$\Omega_x = \frac{\omega}{V_o} \tag{17}$$

11

The spectral function is an isotropic tensor of second order and may be defined in terms of a three-dimensional spectral density function $\Phi(\underline{\Omega})$ as

$$\Phi_{ij}(\underline{\Omega}) = -\frac{\Phi(\Omega)}{4\pi\Omega^2}\left(\frac{\Omega_i\Omega_j}{\Omega^2} - \delta_{ij}\right) \tag{18}$$

Hinze, among others, has shown (Reference 12) that in the lower frequency range the three-dimensional spectra vary as a function of Ω^4. The Ω^4 proportionality follows from a power series expansion of the spectral density with the imposition of the additional requirement that the function be analytic and finite at $\Omega = 0$.

At frequencies in the inertial subrange identified by Kolmogoroff (wavelengths on the order of a few thousand feet to .01 feet) the spectra have been shown by similarity theory to be functions of $\Omega^{-5/3}$. No energy creation or dissipation is assumed to take place at these wavelengths. Instead, energy is presumed to be transferred from the longer wavelength to the shorter wavelength eddies through action of turbulent shear stresses resulting from the interaction of these eddies. These stresses act to break the larger eddies into smaller ones while causing no net loss in energy. This being the case, the process can be assumed to be independent of viscosity effects and the original source of energy. Based on this reasoning, Kolmogoroff derived the relationship of spectral power to the -5/3 power of wave number or frequency.

Finally in the very high frequency region (wavelengths less than .01 feet) viscous dissipation of the turbulent energy dominates. As Reference 12 notes, Heisenberg is credited with demonstrating spectral dependence on Ω to the -7 power in this region.

A useful approximation to the three-dimensional spectra, which asymptotically satisfies the Ω^4 character at low frequency and $\Omega^{-5/3}$ relationship in the inertial subrange, was developed by von Karman (Reference 13). This form of the spectra is

$$\Phi(\underline{\Omega}) = \frac{55}{9} \frac{L}{\pi} \sigma_u^2 \frac{(1.339 \, L \, \underline{\Omega})^4}{[1 + (1.339 \, L \, \underline{\Omega})^2]^{17/6}} \tag{19}$$

This form, which serves as an interpolation formula between the Ω^4 and $\Omega^{-5/3}$ ranges, was derived assuming large Reynolds numbers. As a result, the dissipation range (where viscous effects dominate) is not included. The dissipation process takes place at such short wavelengths and at such low energy levels that the corresponding range of the gust spectrum is of no interest to airplane flying quality analysis. Definition of a turbulence model will be confined to the energy input and inertial subranges of the spectrum.

While the three-dimensional spectra provide the most rigorous definition of isotropic turbulence, a two-dimensional representation in the horizontal (flight) plane is sufficient for the purposes of this study. The implication of this simplification is that there is essentially no variation in the turbulence field for displacements normal to the plane of flight. It is justified by the relatively small dimensions of the airplane along its vertical axis. The two-dimensional spectra are defined in terms of the three-dimensional spectra by the relationship

$$\Phi_{ij}(\Omega_x, \Omega_y) = \int_{-\infty}^{\infty} \Phi_{ij}(\underline{\Omega}) \, d\Omega_z \tag{20}$$

In some particular instances where the spanwise dimension of the airplane is very small compared to the characteristic turbulence wavelength, a one-dimensional spectrum will provide a suitable representation of the turbulence field. Based on the three-dimensional spectra, this is

$$\Phi_{ij}(\Omega_x) = \iint_{-\infty}^{\infty} \Phi_{ij}(\underline{\Omega})\, d\Omega_z\, d\Omega_y \qquad . \tag{21}$$

Another form of the spectral density function in addition to the von Karman spectra has seen wide use in the description of isotropic turbulence. This is the Dryden spectrum and is based on experimental wind tunnel measurements of the one-dimensional correlation function. The longitudinal velocity correlation function was empirically found to be well approximated by

$$R_{uu}(r) = \sigma_u^2\, e^{-r/L} \tag{22}$$

The three-dimensional spectral density function associated with this velocity correlation function is

$$\Phi(\underline{\Omega}) = \frac{8L}{\pi}\, \sigma_u^2\, \frac{(L\underline{\Omega})^4}{[1 + (L\underline{\Omega})^2]^3} \tag{23}$$

A noteworthy point for the range of spectral frequencies over which isotropy is expected to prevail is that the von Karman and Dryden spectral models are nearly equivalent. This may be seen in Figure 4 which compares the one-dimensional form of these two models for longitudinal and transverse velocity components. Significant divergence in the two models occurs only for reduced frequencies of $L\frac{\omega}{V_o} > 30$ ($\omega > 30\frac{V_o}{L}$). While the von Karman spectrum has a sounder theoretical basis because the high frequency attenuation is proportional to $\Omega^{-5/3}$ in accordance with Kolmogoroff's reasoning, the Dryden spectrum, by virtue of being a function of integer powers of frequency Ω, is somewhat easier to manipulate mathematically and is considerably easier to implement in the flight test simulation performed as part of this research. Experimental measurements of turbulence spectra made in recent years (Reference 14, for example) appear to favor the von Karman model in that the data seem to follow a -5/3 power of frequency. Nevertheless, in the frequency

$$\frac{\Phi(\Omega)}{\sigma_w^2 \frac{L}{\pi}} \text{, db}$$

Reduced Frequency, $L \frac{\omega}{V_o}$

Dryden Spectrum ———
von Karman Spectrum — — —
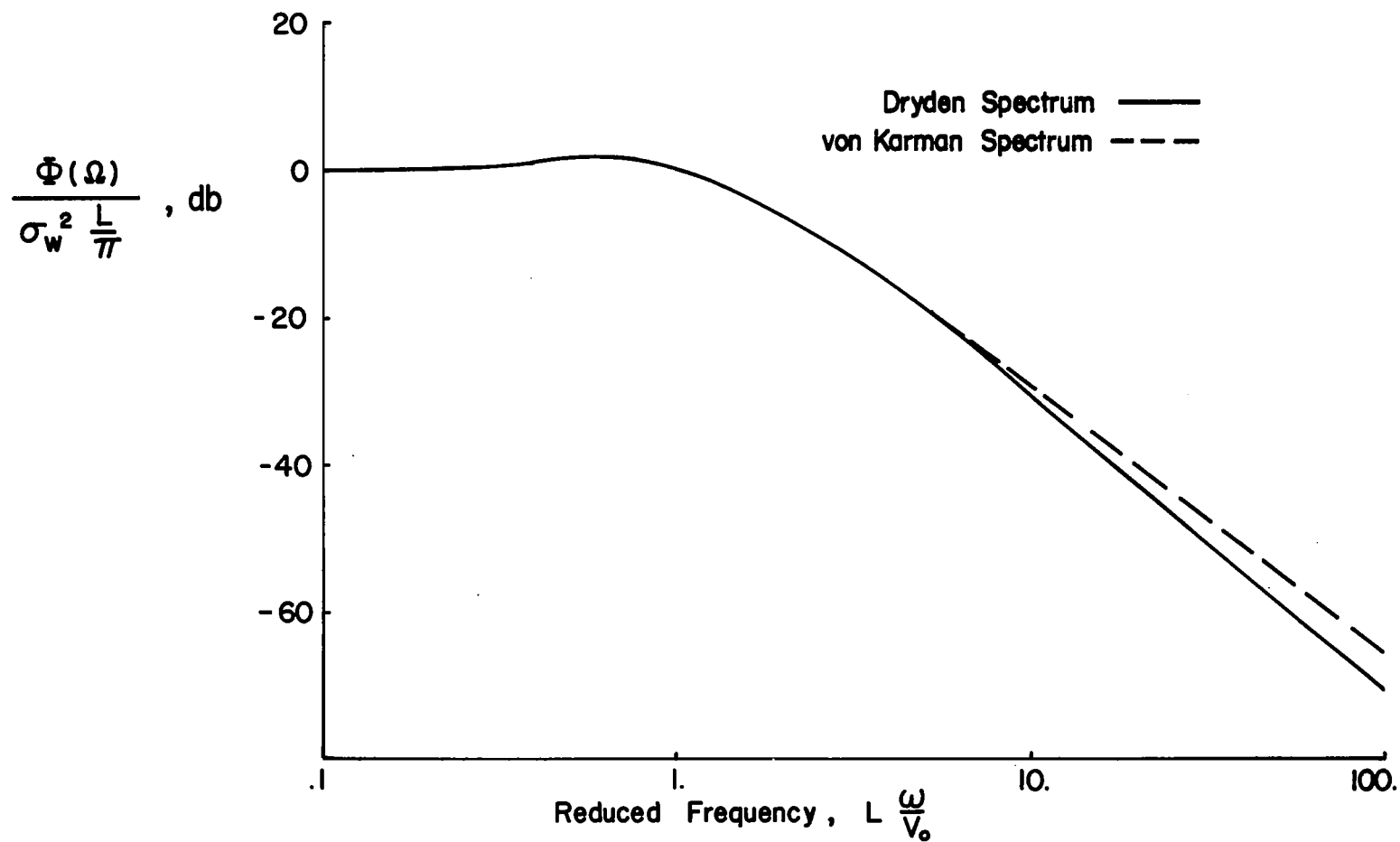
Figure 4.   Comparison of the Dryden and von Karman Spectral Models

range of interest, there is little to choose between the two models on either a theoretical or experimental basis. Because of its relative ease of manipulation in analysis, the Dryden spectrum will be used in the subsequent analyses.

Mathematical expressions of the Dryden spectra in their one-dimensional form for the velocity components u, v, and w are

$$\Phi_{uu} = \frac{2L}{\pi} \sigma_u^2 \frac{1}{1 + L^2 \Omega_x^2} \tag{24}$$

$$\Phi_{vv} = \frac{L}{\pi} \sigma_v^2 \frac{1 + 3L^2 \Omega_x^2}{(1 + L^2 \Omega_x^2)^2} \tag{25}$$

$$\Phi_{ww} = \frac{L}{\pi} \sigma_w^2 \frac{1 + 3L^2 \Omega_x^2}{(1 + L^2 \Omega_x^2)^2} \tag{26}$$

Another form into which the spectral model may be manipulated, and one which will be subsequently shown to be of interest is a so-called cross-spectral form. A physical feeling for this function is readily obtained by considering two parallel paths through space, separated laterally by a distance y and along which the turbulence field is to be sampled. The situation is illustrated in Figure 5. If the correlation function $R_{ij}(\underline{r})$ is transformed into the Ω_x dimension, the result will be a function of the variables Ω_x and r and may be interpreted as a cross-spectral density of the gust velocities w_{y_1} and w_{y_2}, $\Phi_{ij}(\Omega_x, r)$. If interest is restricted to the x-y plane, the function becomes $\Phi_{ij}(\Omega_x, \Delta y)$. This transform relationship is

$$\Phi_{ij}(\Omega_x, \Delta y) = \frac{1}{\pi} \int_{-\infty}^{\infty} R_{ij}(\underline{r}) e^{-i\Omega_x x} \, dx \tag{27}$$

where $r = \sqrt{\Delta x^2 + \Delta y^2}$.
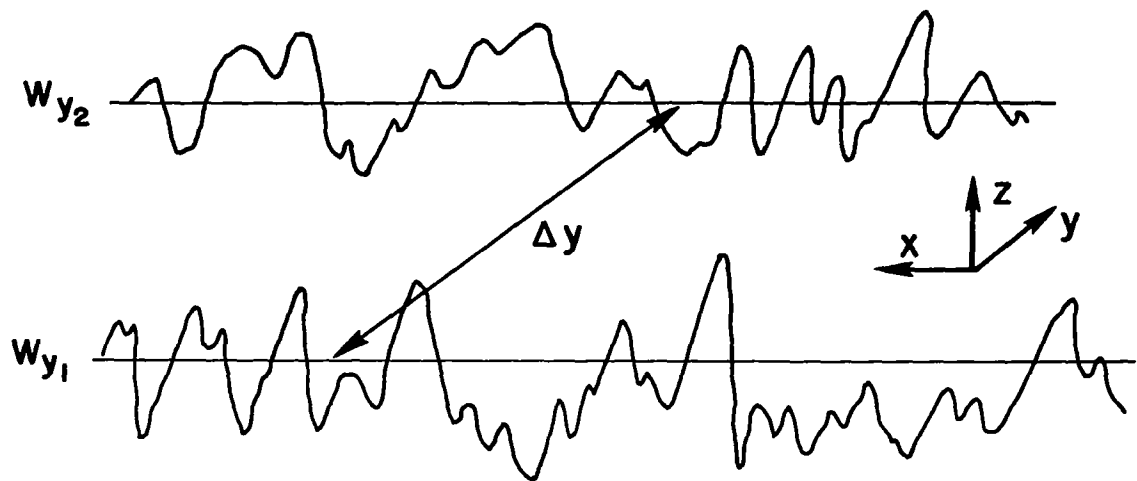
Figure 5. Vertical Gust Field for Two Parallel Paths

This cross-spectral form is of particular interest for the definition of the span-wise variation of vertical gusts which give rise to rolling moments due to vertical gusts. In the case of the Dryden model, the cross-spectral density function for the vertical gust component is

$$\Phi_{ww}(\Omega_x, \Delta y) = \frac{L}{\pi} \sigma_w^2 \left\{ \frac{-\frac{\Delta y}{L}}{(1 + L^2 \Omega_x^2)} K_0 \left(\frac{\Delta y}{L} \sqrt{1 + L^2 \Omega_x^2} \right) \right.$$

$$\left. + \frac{\Delta y}{L} \frac{(1 + 3 L^2 \Omega_x^2)}{(1 + L^2 \Omega_x^2)^{3/2}} K_1 \left(\frac{\Delta y}{L} \sqrt{1 + L^2 \Omega_x^2} \right) \right\}$$

(28)

Validity of the Isotropic Model

It is appropriate at this stage to comment on the validity of the assumption of isotropy as related to specific ranges of gust wavelength (or eddy size) in the spectra. Local isotropy has been assumed to exist in the inertial sub-range. Energy is transferred to eddies in this wavelength range from the larger eddies of the energy input region which were created through wind shear or thermal activity. While turbulence in the input region is aniso-tropic, the process of energy transfer from longer to shorter wavelengths through the turbulence shear stresses and the action of pressure stresses serves to distribute turbulent energy equally among the gust components. Consequently, the turbulence is rendered isotropic for the smaller size ed-dies which result from these processes. Experimental verification of the isotropic character of turbulence in the inertial subrange has been accom-plished to a considerable degree in a number of studies. Reference 14 shows strong evidence of isotropy in this subrange for low altitude turbulence (250 and 750 feet). Relationships between the longitudinal and transverse correla-tion functions comply with the characteristics of an isotropic gust field for spatial wave numbers above .001 cycles per foot. Lack of correlation be-tween gust components in this region adds further support to the isotropic

assumption. In Reference 15 two different measurements to evaluate the degree of isotropy in the horizontal plane were made, one being a comparison of spectra for upwind and crosswind components, the other a comparison of longitudinal, lateral, and vertical components along a flight path. Over a range of wavelengths up to several hundred feet, the spectra of the upwind and crosswind components virtually coincide, implying an independence of orientation of the reference axis, i.e., isotropy. Comparison of the lateral and vertical component spectra show good agreement over a similar range of wavelengths, as would be expected for transverse components from isotropic theory. The longitudinal and vertical spectra which extend further into the long wavelength range do not agree as well with isotropic theory, at least at the longest wavelengths observed. However, over a band of wavelengths comparable to the other two sets of data, the theory is supported quite well. The general conclusion to be drawn is that turbulence is isotropic with qualifications, namely that the longer wavelength components tend less and less to exhibit this property.

Spectral measurements of turbulence also exist which give an indication, perhaps somewhat limited, of the validity of the properties of homogeneity and stationarity attributed to the gust field. Some examples are noted in References 18 and 28. Measurements of vertical gust velocity taken at different times and spatial positions are in good agreement for high spatial frequencies while they differ somewhat at lower frequencies. This implies a homogeneous and stationary character of the shorter wavelength gust components and a divergence from these properties for the longer wavelength components.

The frequency range of the turbulence spectra which is of the greatest interest in this study of flying qualities corresponds to frequencies on the order of 0.5 to 10 radians per second. Relationships between eddy wavelengths in the turbulence field and angular frequencies in the spectral density function are illustrated in Figure 6. It is apparent that the frequency range of interest coincides with the range of wavelength associated with isotropic turbulence, namely for gust wavelengths less than a few thousand feet.
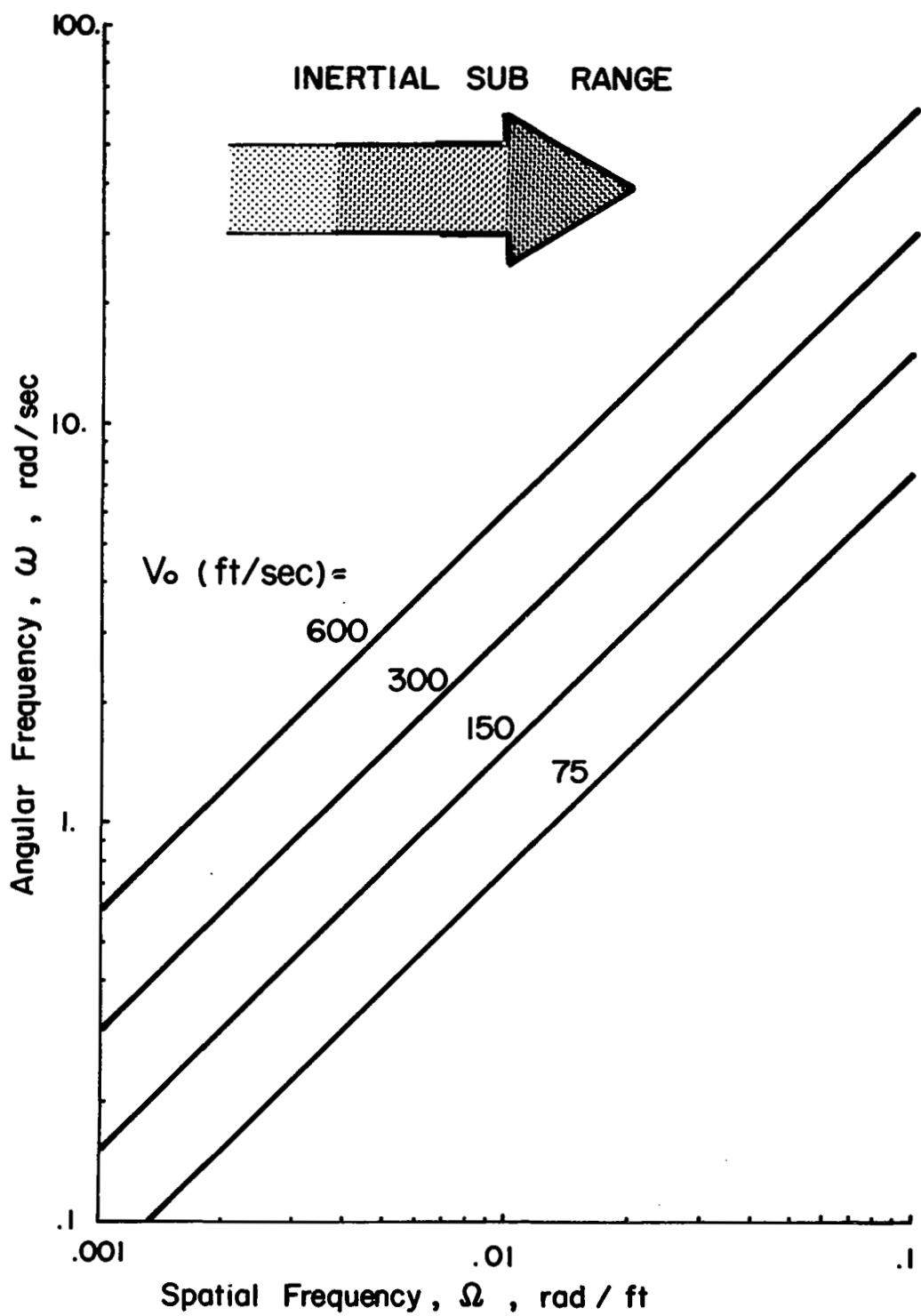
Figure 6. Identification of Inertial Sub-Range in Terms of Spatial and Angular Frequencies

20

Parameters of the Turbulence Model

The descriptive parameters of the turbulence model are the mean square gust velocity, σ_u^2, and the integral scale, L. The mean square gust velocity is defined by either of two relationships (using the longitudinal component as an example)

$$\sigma_u^2 = \int_0^\infty \Phi_{uu} (\Omega_x) \, d\Omega_x \qquad (29)$$

$$= R_{uu} (o) \qquad (30)$$

The integral scale is defined to be

$$L = \int_0^\infty f(r) \, dr \qquad (31)$$

in terms of the longitudinal correlation function, or

$$L = 2 \int_0^\infty g(r) \, dr \qquad (32)$$

in terms of the transverse correlation function. According to Reference 24, a reasonable physical interpretation would associate this scale length with the distance between two points in a gust field on the order of the spatial separation for which the correlation of velocity components vanishes. In this regard, because of transform relationships between the spatial and frequency domains, the scale length also is an indication of the frequency bandwidth of the spectral density.

Experimental measurements of atmospheric turbulence have indicated a relationship between these two parameters and the sources of turbulent energy. Turbulence is created as a result of wind shear, convective or

thermal activity and air motion over irregular terrain. Wind shear is generally related to the mean wind speed, and to its velocity gradient with height. Turbulence is generated by the shearing stresses coincident with a velocity gradient. Thermal activity is associated with atmospheric instability as defined by the vertical gradient of temperature (lapse rate). Instability gives rise to vertical motion of large masses of air which in turn creates eddies through the shear with the surrounding air. Irregularities in the Earth's surface also serve to create turbulent motion in an air mass moving over the terrain.

Each of these turbulence generating processes is distinctly anisotropic in nature while the concern here is with an isotropic turbulence model. However, turbulent energy appears initially in the form of large eddies which generally are well out of range of the region of the turbulence spectra of interest in this problem. By the time the energy containing eddies are reduced to a size compatible with the frequency range noted on page 14, the turbulent shear stresses and pressure stresses will have acted to redistribute energy among the gust components. As a consequence, the turbulence is rendered locally isotropic for the pertinent spectral region, and the isotropic model adopted previously should be valid. Exceptions to this case may be noted for flight at low altitude where the turbulence becomes anisotropic in that the characteristics of the vertical gust component are no longer equivalent to those of the longitudinal or lateral components. The constraint imposed by the terrain confines the energy input of the vertical component to a higher frequency region of the spectrum, which may well be in the frequency range of interest to the flying qualities problems under consideration. Fortunately, evidence exists to indicate that the turbulence is axisymmetric, in other words isotropic in the horizontal plane, for these conditions. This behavior would permit the spectral model to be used for low level flight at essentially constant altitude. It is not clear, however, whether the last one to two hundred feet of a landing approach are compatible with the axisymmetric turbulence model.

A number of investigations have been made to experimentally define the influence of the three sources of turbulent energy on the spectral density of the gust field. Reference 16 represents a recent attempt to collect results of various studies in order to more completely define the relation between gust intensity and scale length and the factors which characterize the energy source, namely wind speed, lapse rate, and surface roughness. While universal agreement does not exist between all sources of data and the results presented in Reference 16, the trends shown in this report provide an indication of the relationships involved.

Mean square gust intensity turns out to be quite strongly influenced by wind shear and stability, particularly for the vertical velocity component (Figure 7). Altitude above terrain and surface roughness are also factors of note for the vertical component. Variations in the parameter $\frac{\sigma}{R\overline{V}}$ by a factor of five or more seem possible. A rather limited and inconclusive set of data were used in Reference 16 to establish relationships between the vertical gust velocity and the lateral and longitudinal components of turbulence. Ratios $\frac{\sigma_v}{\sigma_w}$ and $\frac{\sigma_u}{\sigma_w}$ are shown in Reference 16 as functions of lapse rate and altitude, with little or no evidence of the effects of wind speed.

Scale length appears as a function of altitude and lapse rate (Figure 8). For an altitude of 200 feet, scale length is shown to change by a factor of five or more for varying degrees of atmospheric stability. Scale lengths of the lateral and longitudinal components are related as a function of altitude to vertical scale.

Numerous documents exist which represent the character and scope of experimental data on atmospheric turbulence. A sample is given in References 17 through 21 in addition to those references previously quoted. Two helpful texts which present the physical theory of turbulence and which evaluate at least some test data on atmospheric turbulence are those of References 12 and 22.
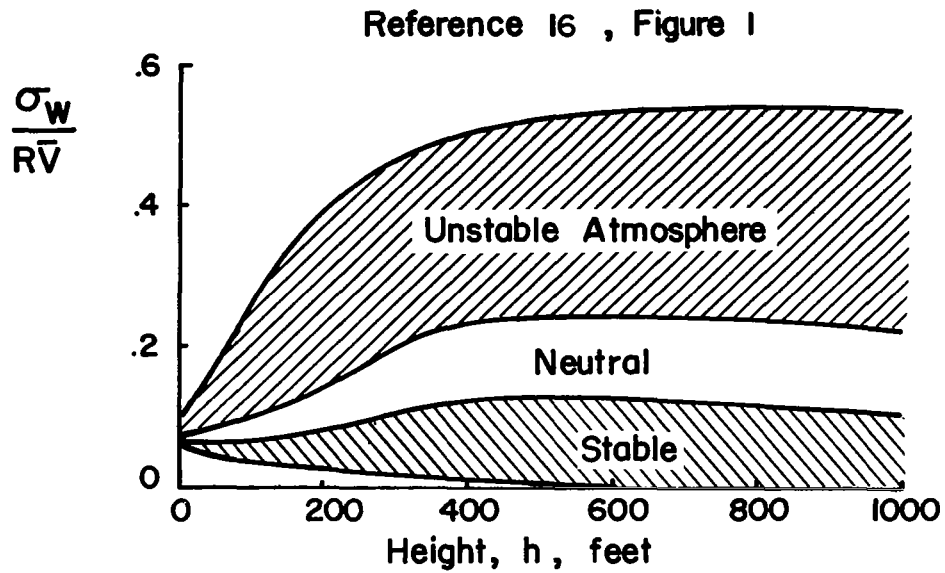
Figure 7. Influences on Turbulence Spectrum Intensity
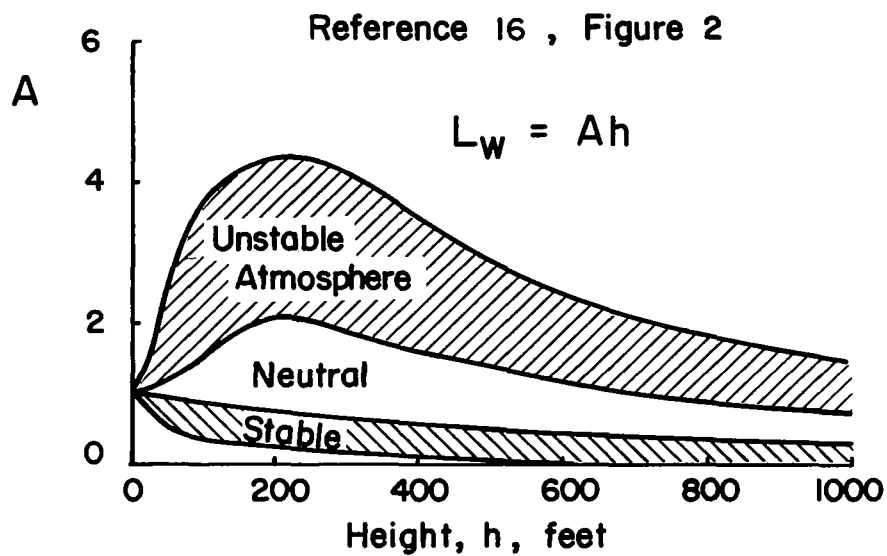
Figure 8. Influences on Turbulence Spectrum Scale

Summary of the Turbulence Model

Having reviewed the available theory and experimental data on atmospheric turbulence, the following conclusions have been reached regarding the analytical description of turbulence most suitable to this test program:

- A homogeneous, isotropic model of the turbulence spectra is appropriate to the frequency range of interest in this program.

- Taylor's hypothesis is valid for the flight speeds involved, hence spatial frequencies and angular frequencies may be interrelated.

- The power spectral density of the gust field may be adequately represented by the Dryden model. Although the von Karman model is considered to be a more precise representation on a theoretical basis, the difference in aerodynamic forces and moments between the Dryden and von Karman models is insignificant in the frequency range of interest in this program. Furthermore, the Dryden spectrum is easier to manipulate mathematically and is more readily simulated than the von Karman model. This is a factor worth considering since it creates no compromise in the analysis and simulation involved in this program.

- The parameters of the turbulence spectra which should be considered are the mean square intensity and scale length. This description should suffice to bracket turbulence characteristics associated with cruise flight and with altitudes corresponding to landing approach to within a few hundred feet of the ground.

25

SECTION 3

TURBULENCE INDUCED AERODYNAMIC DISTURBANCES

General Approach

Perturbations in the relative motion of the airplane with respect to the atmosphere create incremental variations in the aerodynamic forces and moments from the steady flight case. In this regard it is immaterial whether these perturbations arise from airplane motion or turbulence associated gust velocities. It is of interest to this lateral-directional analysis to define the variation in side force, rolling moment, and yawing moment which are associated with the longitudinal, lateral, and vertical gust velocities u_g, v_g, and w_g.

Before getting into the development of these aerodynamic relationships, it is worthwhile to consider which of these turbulence induced disturbances have an important bearing on the problem and which may be eliminated for sake of a clearer and simpler representation of the problem. One reasonable simplification may be made by disregarding the side force disturbance. This simplification is warranted after consideration of the contribution of side force to the airplane's response to a lateral gust. It is apparent from Figures 3 through 11b of Reference 23 that side force disturbances contribute very little to the open loop roll, yaw, and sideslip response for the scope of airplanes considered in that study. A typical comparison of the relative contribution of side force to the airplane's response in roll, yaw, and sideslip, is reproduced in Figure 9. Even the airplane's lateral acceleration response to side gusts is not unduly compromised by the lack of fidelity of the side force simulation. This behavior is indicated in Figure 10. The proper response characteristic for lateral acceleration due to a side gust is indicated by the solid line. The response of the variable stability airplane is indicated in comparison by the dashed line. It should be understood that some side force results in the
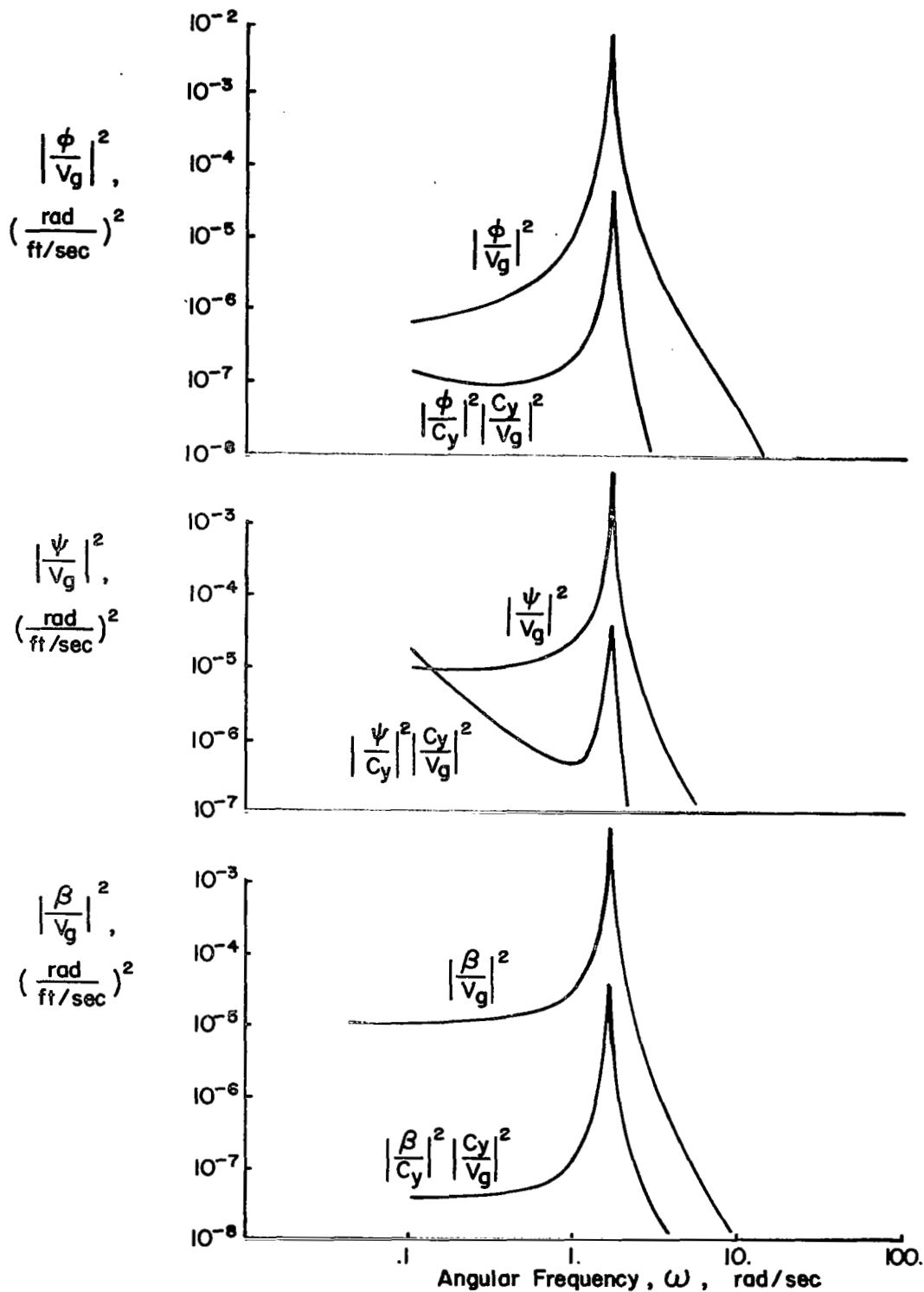
Figure 9. Contribution of Side Force to Airplane Response

27

$\left| \dfrac{a_y}{V_g} \right|$, db

Angular Frequency , ω , rad/sec

Actual a_y ($Y_{vg} = Y_v$)

Simulated a_y

$\left(Y_{vg} = \dfrac{Y_{\delta r}}{V_o} \dfrac{N_{\beta g}}{N_{\delta r}} , N_{\beta g} = 5 \right)$
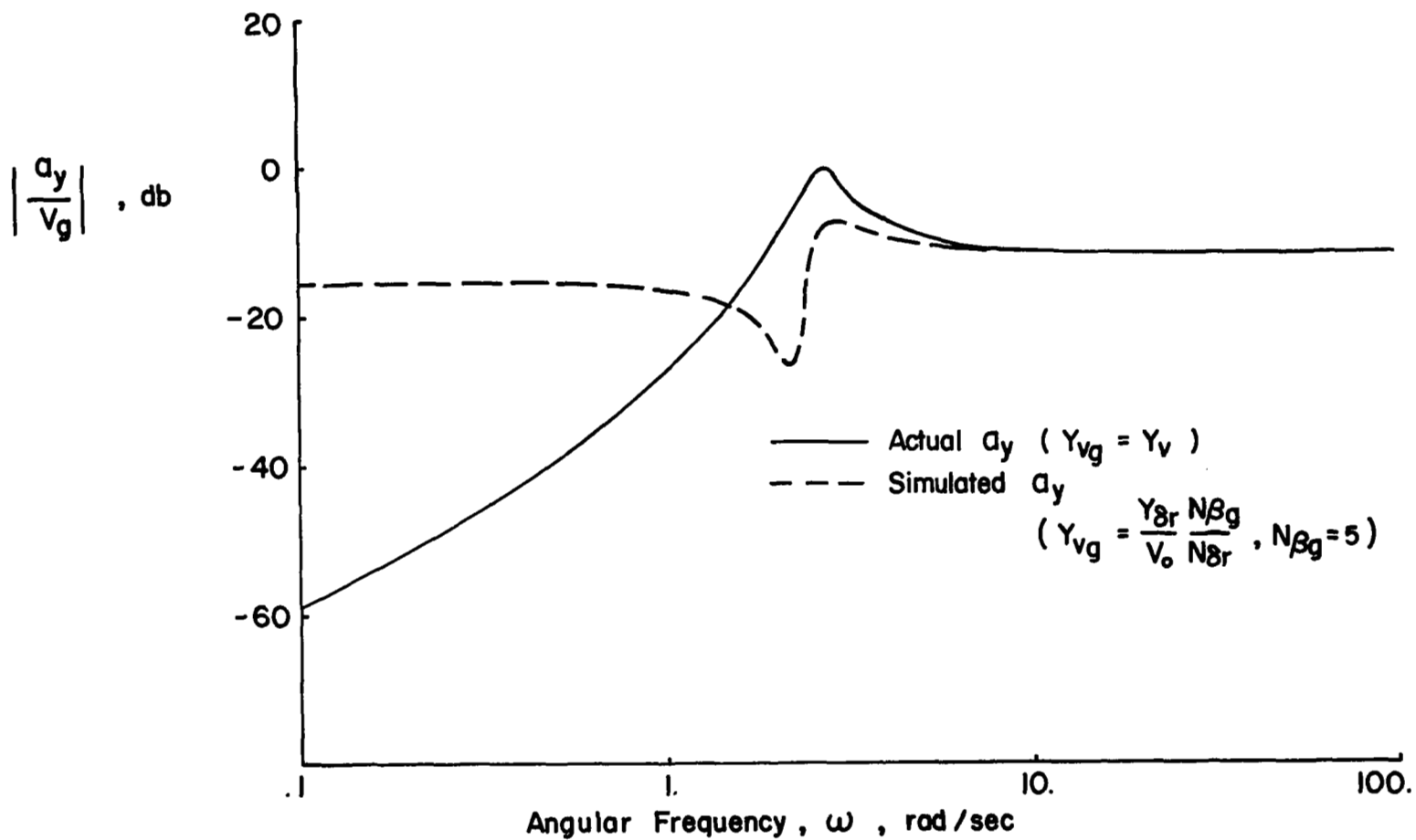
Figure 10. Effect of Side Force Contribution Due to Lateral Gusts on Lateral Acceleration Response

28

variable stability simulation from the rudder which is actuated to produce
yawing moment upsets due to the simulated lateral gust disturbances. In
this case the effective side force derivative is

$$Y_{v_g} = \frac{Y_{\delta r}}{V_o} \frac{N_{\beta g}}{N_{\delta r}}$$

If $Y_{v_{g \text{simulation}}} = Y_{v_{\text{Navion}}}$, the lateral acceleration resulting in the simu-
lation would be precisely correct. For the example shown, where the $N_{\beta g}$
derivative corresponds to the base level of $N_{\beta g}$ tested in the evaluation
program, the significant difference between the two cases occurs at low fre-
quency ($\omega < 1.$ radian/second). This shortcoming in the simulation should
be of little consequence to a closed loop tracking task. However, the pre-
sence of large low frequency accelerations has been found to be disconcert-
ing to pilots in previous studies, and steps have been taken to rectify this
problem. Further discussion is presented on page 90 and in Reference 2.

With side force excluded, rolling moment and yawing moment distur-
bances remain to be considered. Contributions to these moment disturbances
arise due to forces and moments generated by the wing, fuselage, horizontal
and vertical stabilizers, including their mutual interference effects. Specific
contributions of these components of the airplane to the rolling and yawing
moment disturbances are listed in Table 1. From this table it becomes ap-
parent that the lifting surfaces such as the wing and the vertical stabilizer
produce the significant disturbances experienced by the airplane. The fuse-
lage's effects are of secondary importance by comparison, even though in
the case of yawing moments they may be of similar magnitude to those of
the vertical stabilizer. However, in this instance, the total disturbance
magnitude is unlikely to be of a sufficient level to impair the pilot's task
performance, and it will be ignored for the purpose of identifying the first
order of magnitude influences of turbulence on flying qualities.

TABLE 1

CONTRIBUTIONS TO ROLLING AND YAWING MOMENT DISTURBANCES

Distur- bance	Airframe Component	Gust Component		
		u	v	w
Rolling Moment	Wing	Small compared to v and w dis- turbances	Significant. Mag- nitude depends on the amount of di- hedral	Significant. Depends on level of roll damping
	Fuselage	No contribution	Interference effect to be considered with wing compo- nent	No contribu- tion
	Vertical Stabilizer	No contribution	Generally small compared to wing	No contribu- tion
	Horizontal Stabilizer	Negligible	Small compared to wing	Small com- pared to wing
Yawing Moment	Wing	Small compared to v contributions of tail	Small, except for configurations with large dihedral or sweep	Small, except for configura- tions with large yaw due to roll
	Fuselage	No contribution	Generally moder- ate to small	No contribu- tion
	Vertical Stabilizer	No contribution	Dominant	No contribu- tion

30

From the results of Reference 23 it is also apparent that the contribution of the longitudinal (u) velocity component to the airplane's turbulence response is of little consequence, compared to the lateral (v) and vertical (w) components. Figures 3 through 11a of Reference 23 demonstrate this quantitatively. Typical data of lateral response to the three gust components is reproduced in Figure 11.

Having made the simplifications in the problem as indicated in the foregoing discussion, the remaining elements of the turbulence disturbance field are listed in Table 2.

TABLE 2

DOMINANT CONTRIBUTIONS TO ROLLING AND
YAWING MOMENT DISTURBANCES

Disturbance	Airplane Component	Gust Component
Rolling Moment	Wing	v, w
Yawing Moment	Vertical Stabilizer	v

In general, it may be said that the most rigorous description of turbulence induced disturbances is obtained using lifting surface theory. Reference 24, as an example, shows that the lift force generated by a wing penetrating turbulence can be represented by the integral over the airfoil surface of all the pressure forces acting on each infinitesimal increment of surface area.

$$L = \iint P_o(x, y) \, dx \, dy \qquad (33)$$

The pressure at each surface location is defined in turn by the integral equation relating the local downwash to the pressure

$$\Phi^* = \frac{\Phi}{\sigma_g^2 \frac{L}{\pi}} \quad \left(\frac{rad/(ft/sec)^2 ft}{rad/sec} \right)$$
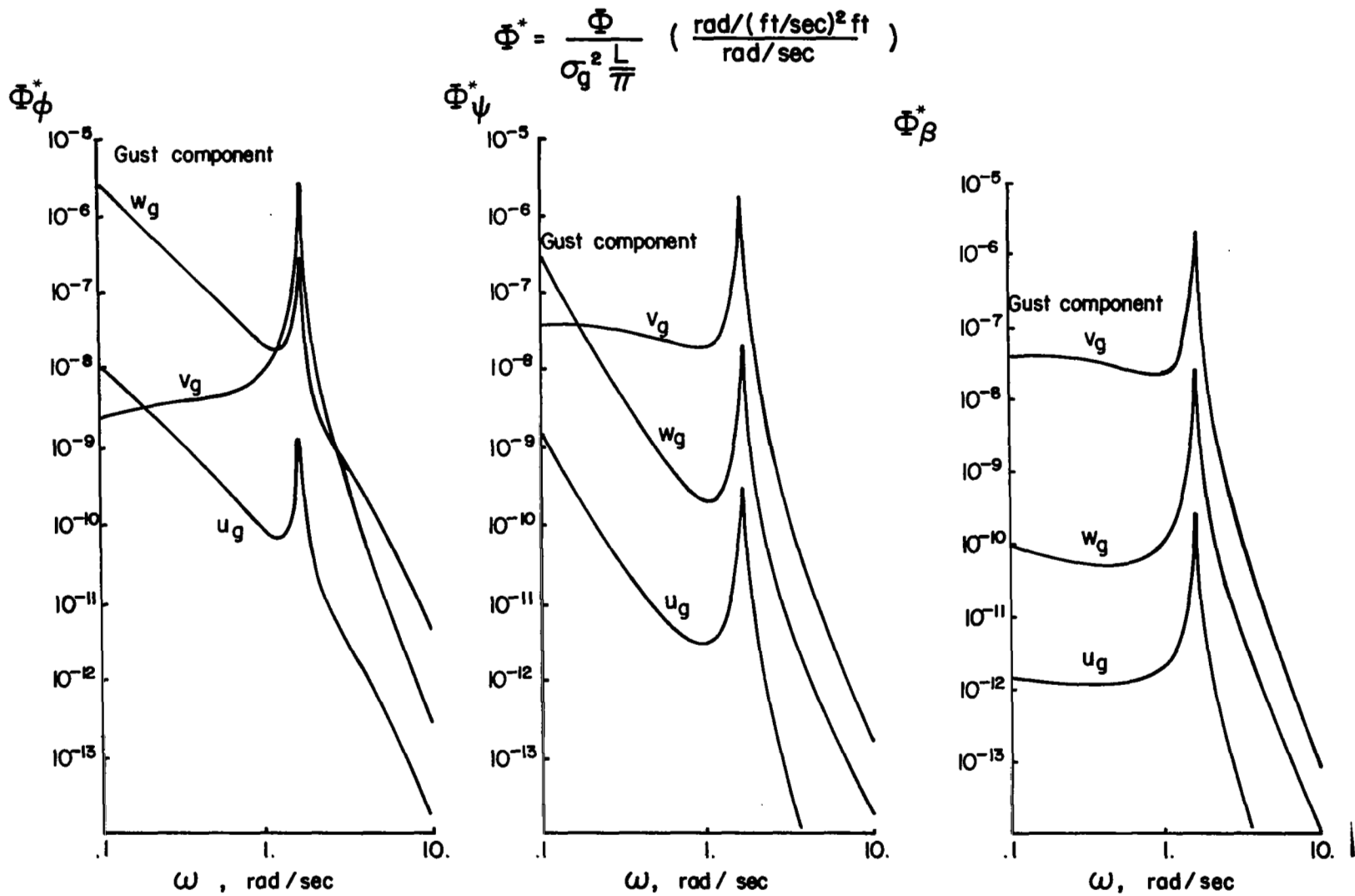
Figure 11. Comparative Contributions of Gust Components to Airplane Response

$$w_o(x, y) = \frac{V}{8\pi q} \iint p_o(x, y)\, K_o(x - \xi,\, y - \eta)\, d\xi\, d\eta \tag{34}$$

The complication of this approach, associated with the solution of the integral equation which defines $p_o(x, y)$ as a function of $w_o(x, y)$, is unwarranted for the class of airplanes considered in this program. General aviation aircraft typically have airfoil planforms of relatively high aspect ratio and little or no sweep. For such configurations, spanwise and streamwise aerodynamic behavior tend to be uncoupled, in the sense that pressure perturbations taking place across the span and along the chord of the airfoil are essentially independent of each other. The analysis of the airfoil's force and moment characteristics may be accordingly simplified while retaining the significant effects of wing geometry and turbulence environment on rolling moment and yawing moment disturbances.

The work of Diederich and others at NASA (References 25, 26, and 27) provides a suitable method for defining the aerodynamic disturbances of interest. This approach represents the application of modified strip theory to the prediction of the spanwise load distribution on an airfoil for an arbitrary spanwise variation in angle of attack. The theory of this method hinges on the assumption that the spanwise load distribution is independent of the transient variations in lift as the airfoil penetrates the gust field. As previously noted this behavior can be expected to prevail for reasonably high aspect ratio airfoils. Wind tunnel measurements of air loads on an oscillating wing have shown the spanwise load distribution to be independent of the period of oscillation, thereby confirming the validity of the aforementioned approach. It is therefore permissible to adopt a spanwise load distribution representative of the steady flight case and account separately for transient aerodynamic effects by a streamwise penetration factor. This approach has been used with a great deal of success in predicting structural mode frequencies and amplitude ratios for flexible aircraft with wings of moderate

sweep ($30°$-$40°$). Such agreement between experimental results and analytical predictions provides further assurance that modified strip theory can be applied to the gust disturbance problem for a rigid airframe.

Another approach to the definition of the turbulence disturbances which relies on a representation of the gust field by its spectral components is discussed in detail in Reference 28. This is equivalent to a superposition of sinusoidal waves of varying wavelength and magnitude. This representation may be expressed in turn by a Taylor series approximation in the vicinity of the point of interest (the airplane's c.g.). If the series is limited to first order terms, the gust field is defined by the local gust velocity at the point of interest and by linear spatial gradients along the flight path and in the spanwise direction. For example, the lateral gust velocity at any point along the length of the airplane would be expressed as

$$v_g \doteq v_{g_{cg}} + \left(\frac{\partial v_g}{\partial x}\right)_{cg} \Delta x \qquad (35)$$

It is apparent that this representation by local gust velocities and linear gradients may also be interpreted in terms of equivalent rigid body motion of the airplane. As a result, the turbulence disturbances may be approximated by products of the airplane's stability derivatives and these equivalent rigid body motions. Using the yawing moment due to lateral gusts as an illustration

$$N_{v_g} \doteq N_\beta \frac{v_{g_{cg}}}{V_o} + N_r \left(\frac{\partial v_g}{\partial x}\right)_{cg} \qquad (36)$$

An obvious limitation of this first order series approximation is posed by the airplane's size as well as by the planform shape and flexibility characteristics noted previously. This limitation compromises the accuracy of the simulation in the higher frequency regions. While this first order approximation will not be pursued further in this section, a comparison of the results of this technique with those of the modified strip theory approach is presented in

34

Appendix A. Based on the results of the flight test program, some observations are made on the significance of the differences between the strip theory and spectral component representations to the flying qualities problems of interest.

Rolling Moment Spectra

The strip theory approach developed in Reference 27 may be demonstrated using the rolling moment due to vertical gusts as an example. Rolling moment generated by a wing penetrating a two dimensional vertical gust field may be expressed as

$$L_{w_g}(t) = \frac{1}{b^2} \int_{-\infty}^{\infty} \int_{-b/2}^{b/2} h_{L_{w_g}}(t_1) \, \gamma_{L_{w_g}}(y) \, w[V_o(t-t_1), y] \, dy \, dt_1 \qquad (37)$$

The influence function $h_{L_{w_g}}$ accounts for streamwise penetration of the gust field and is expressed as

$$h_{L_{w_g}}(t_1) = \lceil C_{\ell_p} \frac{qSb}{V_o} \rceil k(t_1) \qquad (38)$$

The spanwise rolling moment distribution may be written

$$\gamma_{L_{w_g}}(y) = [-\frac{c_\ell(y) \, c(y)}{C_{\ell_p} \bar{c}}]_{\alpha=y} \qquad (39)$$

A better understanding of this distribution function and its significance in the rolling moment expression may be gained by defining the rolling moment for a steady, spanwise varying angle of attack distribution. The rolling moment may be written

$$L_{w_g} = \int_{-b/2}^{b/2} \ell(y)]_{\alpha(y)=1} \frac{w(y)}{V_o} y \, dy \qquad (40)$$

where

$$\ell(y) = c_\ell(y)]_{\alpha(y)=1} \, c(y) \, q \tag{41}$$

Reciprocity theorems of linearized airfoil theory given in Reference 29 state that the rolling moment of a wing due to an arbitrary spanwise angle of attack is equivalent to the spanwise integral of the product of the spanwise lift distribution due to a linearly varying angle of attack and the angle of attack distribution across the span. Analytically expressed, this is

$$L_{w_g} = \int_{-b/2}^{b/2} \ell(y)]_{\alpha=y} \, \frac{w(y)}{V_o} \, dy \tag{42}$$

Equation (42) follows from (40) since the $\ell(y)]_{\alpha=y}$ terms result from the multiplication of $\ell(y)]_{\alpha=1}$ by $\alpha = y$. If (42) is nondimensionalized by qSb, and further if $\ell(y)$ is normalized by C_{ℓ_p}, the resulting expression for the nondimensional rolling moment coefficient is

$$C_{\ell_{w_g}} = -\frac{C_{\ell_p}}{b^2} \int_{-b/2}^{b/2} \left[\frac{c_\ell(y)c(y)}{-C_{\ell_p}\,\bar{c}} \right]_{\alpha=y} \frac{w(y)}{V_o} \, dy \tag{43}$$

With inclusion of the term for transient aerodynamic effects, $h_{L_{w_g}}(t_1)$, and after multiplying by qSb to restore (43) to dimensional form, the similarity of this equation with (37) is apparent. The term $\left[\dfrac{c_\ell(y)c(y)}{-C_{\ell_p}\,\bar{c}} \right]_{\alpha=y}$ is the normalized form of the spanwise lift distribution due to a linear spanwise variation of angle of attack which is referred to in equation (39) as the rolling moment distribution. Examples of this rolling moment distribution for several spanwise load distributions (for constant spanwise angle of attack) are shown in Figure 12.
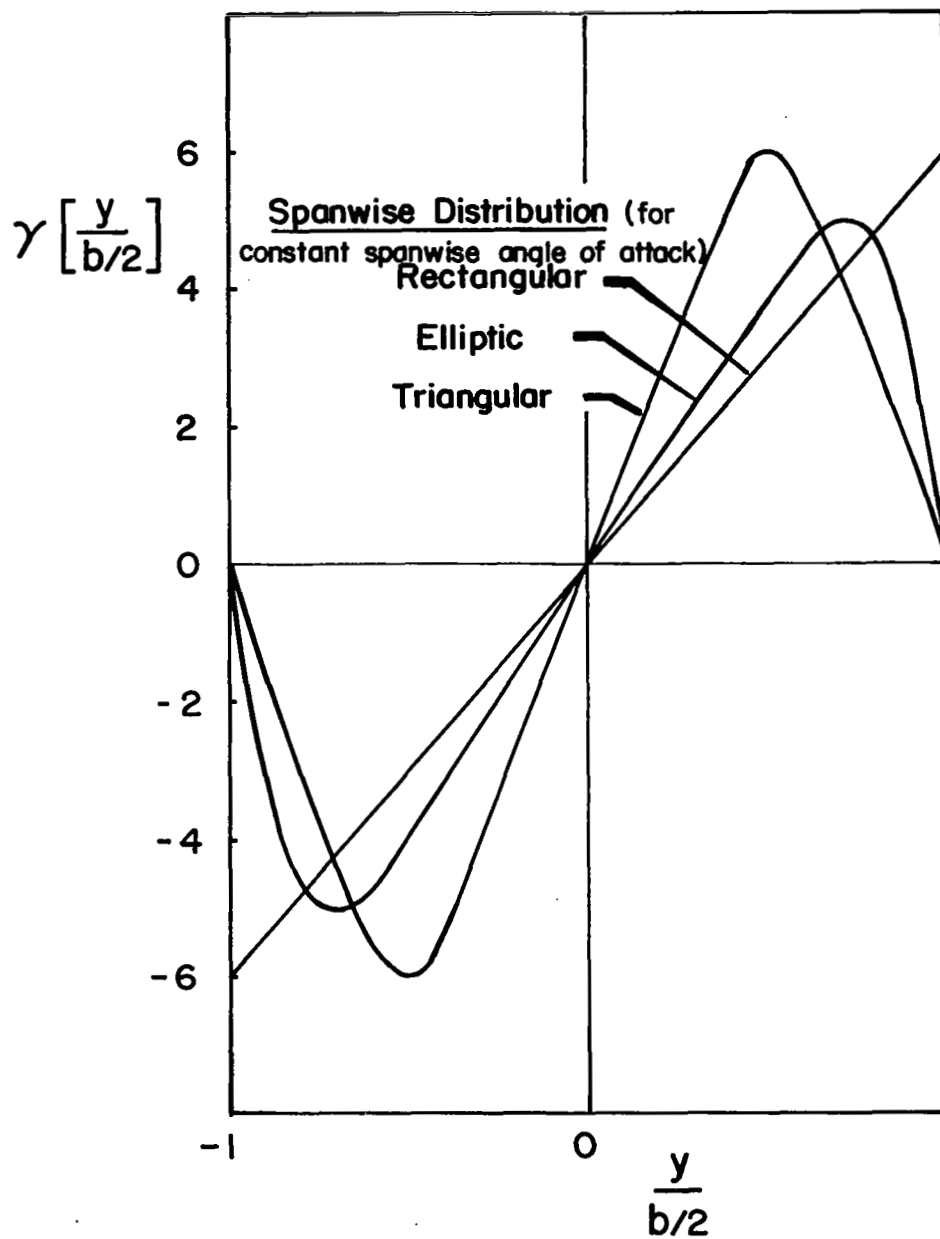
Figure 12. Variation of Rolling Moment Distribution with Span

The gust velocity term $w[V_o(t-t_1), y]$ represents a two-dimensional gust field where according to Taylor's hypothesis the streamwise spatial dimension and the time variable are related by $x-x_o = V_o(t-t_o)$.

The expression for rolling moment may be transformed to spectral form and would then appear as

$$\Phi_{L_{w_g}}(\omega) = |H_{L_{w_g}}(\omega)|^2 \Phi_{w_e}(\omega) \qquad (44)$$

where the function $H_{L_{w_g}}(\omega)$ is the Fourier transform of $h_{L_{w_g}}(t)$, that is

$$H_{L_{w_g}}(\omega) = [C_{\ell_p} \frac{qSb}{V_o}] \varphi_k(\omega) \qquad (45)$$

$\varphi_k(\omega)$ is the transform of $k_1(t)$ and is the Sears function for transient lift which is discussed in Reference 30. For the airfoil planforms of interest and for the range of frequency significant in this study, the function $\varphi_k(\omega)$ for infinite aspect ratio is adequate. This form of the Sears function as given in Reference 30 is

$$|\varphi_k(\omega)|^2 = \frac{1}{1 + \pi \frac{c}{V_o} \omega}$$

Except for very low aspect ratios (on the order of $AR < 3$) results of Reference 30 indicate that the departure of this function for finite aspect ratios from the two-dimensional case is apparent only at frequencies above the range of interest.

The function $\Phi_{w_e}(\omega)$ is related to the spanwise rolling moment distribution $\gamma_{w_g}(y)$ and the cross-spectral density function for vertical gusts, $\Phi_{ww}(\omega, \Delta y)$, which was previously given on page 18. The expression for $\Phi_{w_e}(\omega)$ is

$$\Phi_{w_e}(\omega) = \frac{1}{b^2} \int_o^b [\frac{2}{b^2} \int_{-b/2}^{b/2-\Delta y} \gamma_{L_{w_g}}(y) \gamma_{L_{w_g}}(y+\Delta y) \Phi_{ww}(\omega, \Delta y) dy] d(\Delta y) \qquad (46)$$

A physical interpretation of equation (46) can be found by considering the rolling moment of the wing to be composed of a sum of the rolling moment contributions of discrete spanwise segments of the wing. Each segment is associated with a one-dimensional strip of the gust field in the streamwise direction as shown in Figure 13. An expression for the total rolling moment may be written

$$L_{w_g}(t) = \sum_i L_{w_{g_i}}(t) = \sum_i \frac{1}{b^2} \int_{-\infty}^{\infty} h_{L_{w_g}}(t_1) \gamma_{L_{w_g}}(y_i) w_i [V_o(t-t_o)] dt_1 \qquad (47)$$

If the power spectral density of $L_{w_g}(t)$ is formed, the individual terms will appear as follows:

$$\Phi_{L_{w_g}}(\omega) = \frac{1}{b^2} |H_{L_{w_g}}(\omega)|^2 \{ [\gamma^2_{L_{w_g}}(y_1) \Phi_{w_1}(\omega) + \gamma^2_{L_{w_g}}(y_2) \Phi_{w_2}(\omega) + ---]$$

$$+ [2\gamma_{L_{w_g}}(y_1) \gamma_{L_{w_g}}(y_2) \Phi_{w_1 w_2}(\omega) + 2\gamma_{L_{w_g}}(y_2) \gamma_{L_{w_g}}(y_3) \Phi_{w_2 w_3}(\omega) + ---]$$

$$+ [2\gamma_{L_{w_g}}(y_1) \gamma_{L_{w_g}}(y_3) \Phi_{w_1 w_3}(\omega) + 2\gamma_{L_{w_g}}(y_2) \gamma_{L_{w_g}}(y_4) \Phi_{w_2 w_4}(\omega) + ---]$$

$$+ [2\gamma_{L_{w_g}}(y_1) \gamma_{L_{w_g}}(y_4) \Phi_{w_1 w_4} + 2\gamma_{L_{w_g}}(y_2) \gamma_{L_{w_g}}(y_5) \Phi_{w_2 w_5}(\omega) + ---]$$

$$+ ----\}$$

$$(48)$$

This equation may be rearranged to obtain a form consistent with equation (44), that is
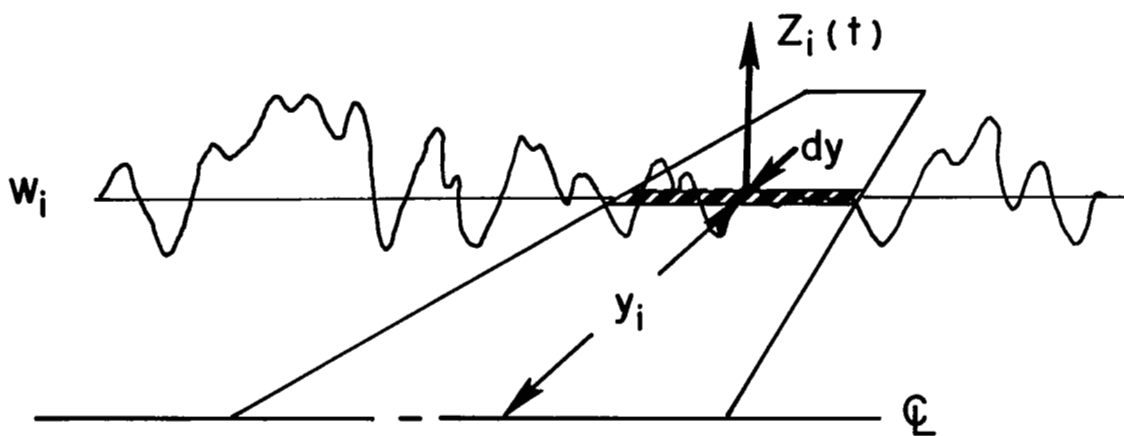
Figure 13. Contribution of a Wing Segment to Rolling Moments Due to
Vertical Gusts

$$\Phi_{L_{w_g}}(\omega) = \frac{1}{b^2} |H_{L_{w_g}}(\omega)|^2 \{ [\gamma^2(y_1) + \gamma^2(y_2) + \gamma^2(y_3) + ---] \Phi_{w_1}(\omega)$$

$$+ 2[\gamma(y_1)\gamma(y_2) + \gamma(y_2)\gamma(y_3) + \gamma(y_3)\gamma(y_4) + ---]\Phi_{w_1 w_2}(\omega)$$

$$+ 2[\gamma(y_1)\gamma(y_3) + \gamma(y_2)\gamma(y_4) + \gamma(y_3)\gamma(y_5) + ---]\Phi_{w_1 w_3}(\omega)$$

$$+ ---$$

$$+ 2[\gamma(y_1)\gamma(y_n) + \gamma(y_2)\gamma(y_{n+1}) + ---]\Phi_{w_1 w_n}(\omega)$$

$$+ ---\} \tag{49}$$

Equation (49) follows from (48) based on the assumptions that the power spectra for all of the one-dimensional gusts are equal, i.e., $\Phi_{w_1} = \Phi_{w_2} = \Phi_{w_n}$ and that the cross-spectra for gust components with equal spanwise separation are equal, i.e., $\Phi_{w_1 w_2} = \Phi_{w_2 w_3} = \Phi_{w_3 w_4}$, $\Phi_{w_1 w_3} = \Phi_{w_2 w_4} = \Phi_{w_3 w_5}$, etc.

Comparing equations (46) and (49) it should be apparent that $\Phi_{w_e}(\omega)$ and the term within the braces { } are equivalent. The integrals over y and Δy may be related to similar summations in (49). The products $\gamma_{L_{w_g}}(y) \gamma_{L_{w_g}}(y+\Delta y)$ have their counterparts in (49) and the spectral function $\Phi_{ww}(\omega, \Delta y)$ appears either as the power spectral density $\Phi_{w_i w_i}(\omega)$ for $\Delta y = 0$ or as a cross-spectral density $\Phi_{w_i w_j}(\omega)$ for $\Delta y = y_i - y_j$. Variation of this cross-spectral density function with frequency for several values of the dimensionless spanwise separation parameter Δy is shown in Figure 14. The attenuating effects of ω and Δy are apparent.
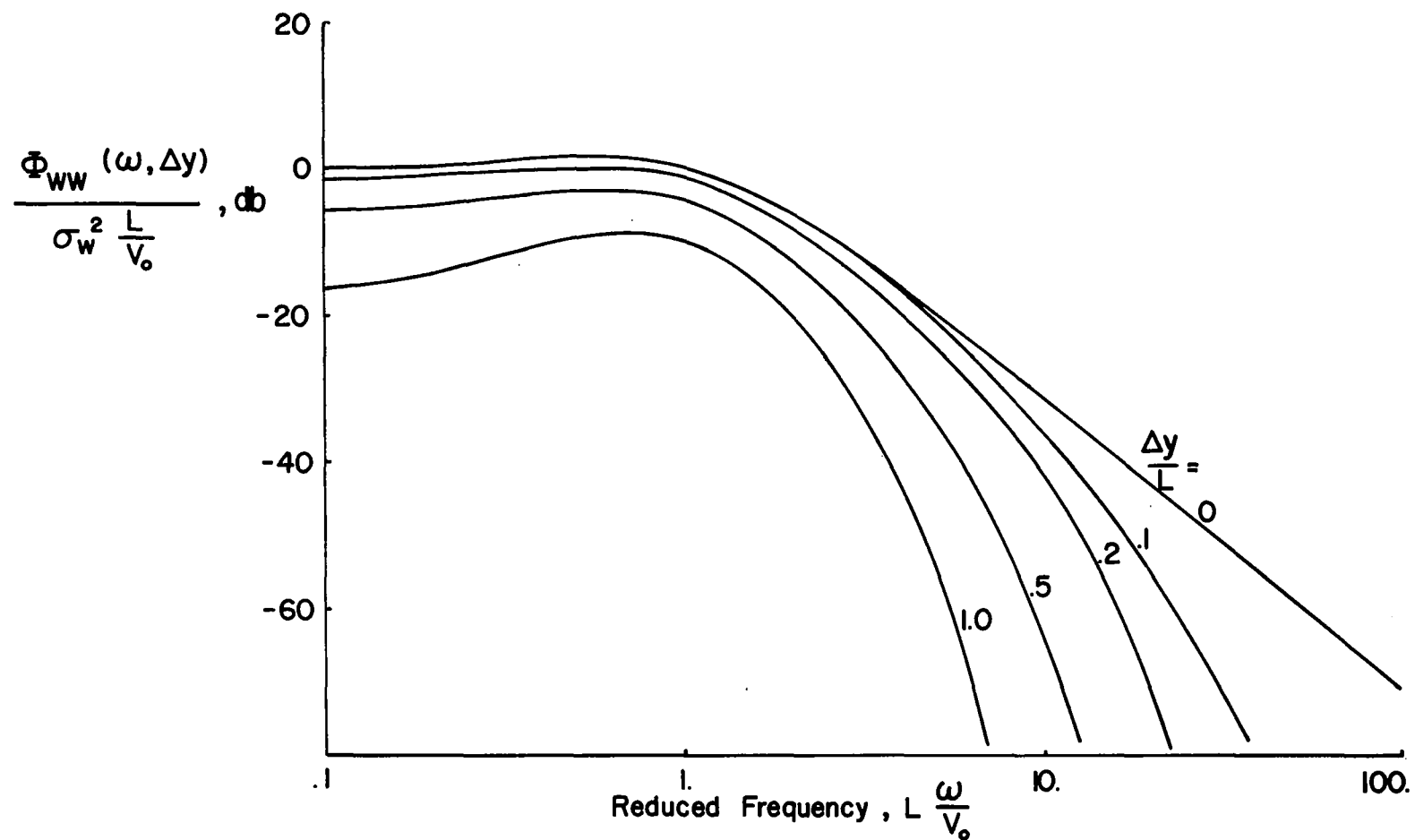
Figure 14. Effect of Frequency and Spanwise Separation on Vertical Gust Cross Spectra

An additional simplification normally made to the form of Φ_{w_e} as it appears in (46) is

$$\Phi_{w_e}(\omega) = \frac{1}{b} \int_0^b \Gamma_{L_{w_g}}(\Delta y)\, \Phi_{ww}(\omega, \Delta y)\, d(\Delta y) \tag{50}$$

where $\Gamma_{L_{w_g}}(\Delta y)$ is the auto-convolution of $\gamma_{L_{w_g}}(y)$

$$\Gamma_{L_{w_g}}(\Delta y) = \frac{2}{b^3} \int_{-b/2}^{b/2 - \Delta y} \gamma_{L_{w_g}}(y)\, \gamma_{L_{w_g}}(y + \Delta y)\, dy \tag{51}$$

The spectral function $\Phi_{w_e}(\omega)$ which results after performing the integration of equation (46) is

$$\Phi_{w_e}(\omega) = \frac{18}{\pi}\, \sigma_w^{\,2}\, \frac{L}{V_o} \left[\frac{1}{a^4(1 + L^2\Omega_x^{\,2})^2} \right] \left\{ a^3 (L\Omega_x)^2 \int_0^a K_o(x)\, dx \right.$$

$$+ \left[a^4 + 16a^2(1 - L^2\Omega_x^{\,2})\right] K_o(a) + \left[2a^3(3 - L^2\Omega_x^{\,2}) + 32a(1 - L^2\Omega_x^{\,2})\right] K_1(a)$$

$$\left. + 2a^2(1 - 3L^2\Omega_x^{\,2}) - 32(1 - L^2\Omega_x^{\,2}) \right\} \tag{52}$$

for the case of a uniform spanwise load distribution where $\gamma_{L_{w_g}} = 6\,\frac{y}{b/2}$. This so-called average or weighted vertical gust spectrum is a function of the frequency parameter $L\frac{\omega}{V_o}$ and the ratio of wing span to turbulence scale, b/L. An interesting feature of this spectrum is that variations in spanwise load distribution seem to have little or no effect on its magnitude. Plots of Φ_{w_e} for uniform, elliptic, and triangular load distributions are shown in Figure 15 for $\frac{b}{L} = .125$. Differences exhibited in this figure for the three specified cases would be of no consequence to this investigation. Hereafter, the form of the spectra used in these analyses will be for the uniform load distribution.

$$\frac{\Phi_{W_e}(\omega)}{\sigma_W^2 \frac{L}{\pi V_o}} \text{, db}$$

Spanwise Load Distribution (for constant spanwise angle of attack)

Uniform ————
Elliptic —— ——
Triangular ————

Reduced Frequency, $\frac{\omega L}{V_o}$
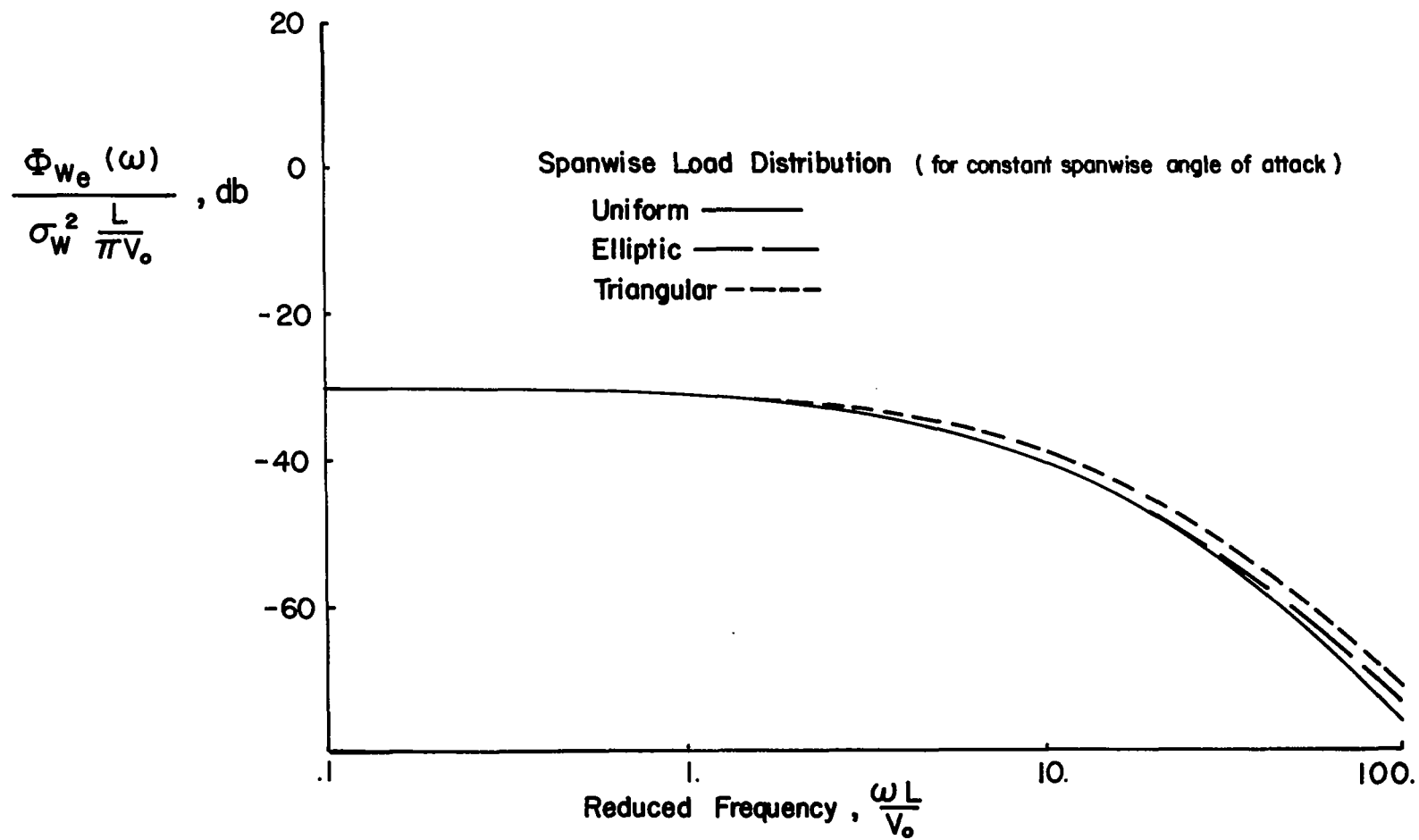
Figure 15. Effect of Spanwise Load Distribution on Integrated Spectra

44

The complete form of the rolling moment spectra, given in equation (40), may now be considered. It is shown in Figure 16 as a function of angular frequency, ω. Both the rms level of the vertical gust field and the magnitude of the roll damping derivative determine the overall level of the disturbances. Wing geometry has an influence on the spectra due to the averaging effect of the wing which spans eddies in the lateral dimension (V_o/b being the definitive parameter) and due to the attenuating effect of transient lift buildup following streamwise penetration of turbulence (where V_o/c is the definitive parameter). Planform influences such as aspect ratio and taper are inherent in the roll damping derivative which in part determines the spectral magnitude.

Rolling moment disturbances due to lateral gusts may be defined in a manner similar to that presented for the vertical gust case. In the case of lateral gusts the spanwise variation in gust velocity plays a secondary part in the determination of roll disturbances. This is in contrast to the case of roll disturbances induced by vertical gusts where the spanwise variation in the gust field was of singular importance. Reference 28 (Figure 10) reveals that the effect of spanwise variation in the lateral gust field only serves to attenuate the turbulence spectrum in the high frequency region where the level of turbulence is already low and where the airplane's transfer function will already have significantly attenuated the airplane's roll response. Thus a one dimensional (streamwise) representation will be used in this analysis.

The rolling moment expression for a one-dimensional lateral gust field is

$$L_{v_g}(t) = \int_{-\infty}^{\infty} h_{L_{v_g}}(t_1) \, v_g [V_o(t - t_1)] \, dt_1 \tag{53}$$

For the lateral gust case, the influence function is

$$h_{L_{v_g}}(t_1) = C_{\ell_\beta} \frac{qSb}{V_o} k(t_1) \tag{54}$$

45
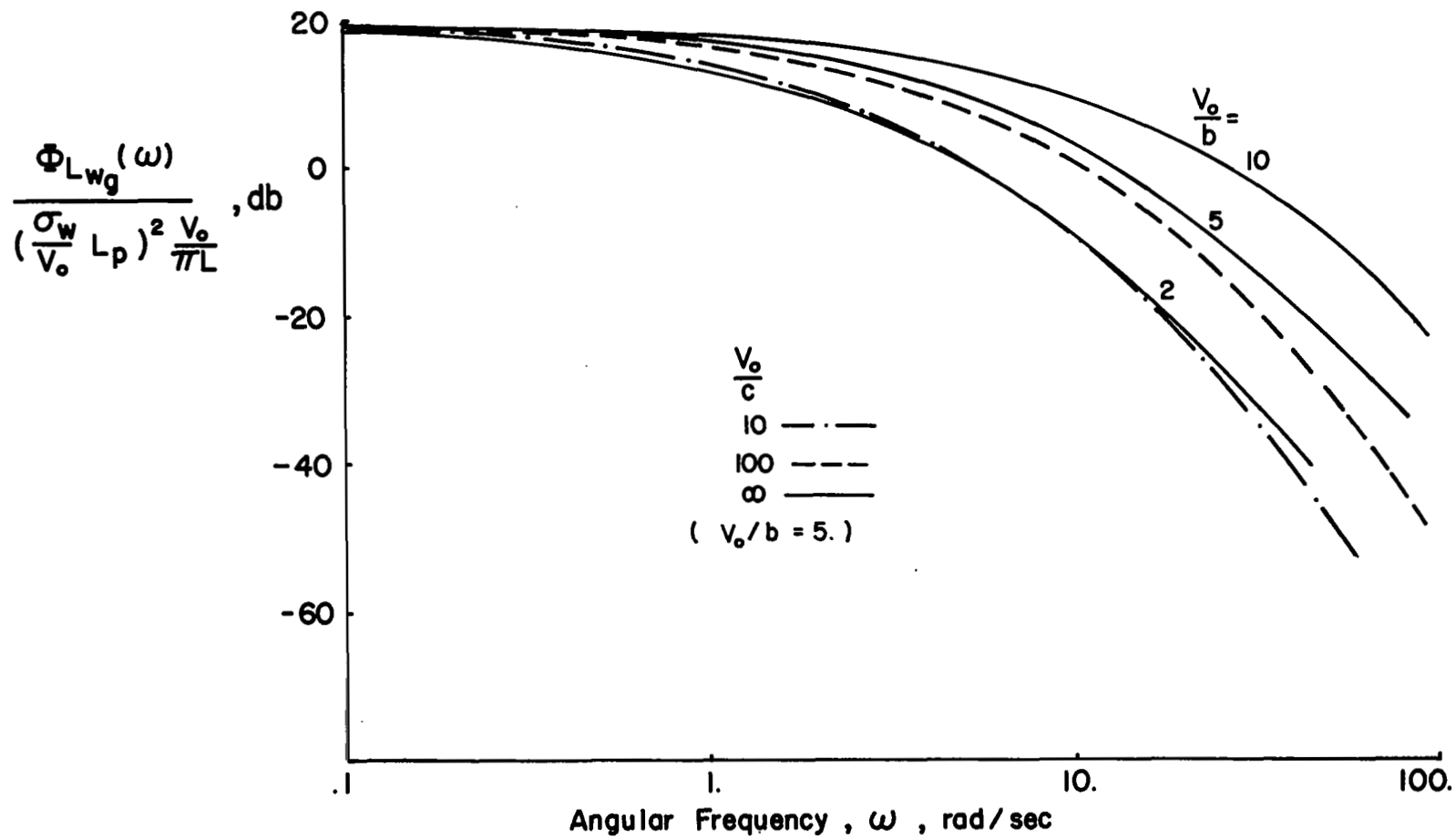
Figure 16. Rolling Moment Spectra Due to Vertical Gusts

46

The spanwise load distribution is not taken into account since the lateral gust field is uniform across the span. Transformation of this rolling moment equation into the frequency domain produces the appropriate rolling moment spectrum,

$$\Phi_{L_{v_g}}(\omega) = |H_{L_{v_g}}(\omega)|^2 \, \Phi_{vv}(\omega) \tag{55}$$

and

$$H_{L_{v_g}}(\omega) = C_{\ell_\beta} \frac{qSb}{V_o} \varphi_k(\omega) \tag{56}$$

where φ_k is the Sears function. The lateral gust spectrum corresponds to the one-dimensional form of equation (25), with an additional contribution provided by the Sears function to account for transient aerodynamic effects.

The rolling moment spectrum plotted as a function of frequency appears in Figure 17. Spectral amplitude is a function of the rms gust intensity and the dihedral effect derivative. Wing geometry influences the high frequency attenuation as a function of V_o/c just as in the vertical gust case. The other planform influence is in the dihedral effect derivative. The turbulence parameter V_o/L determines the spectral bandwidth.

Yawing Moment Spectra

The dominant yawing moment disturbances are produced by the vertical stabilizer as it encounters lateral gusts. Previous definition of the turbulence field has limited the gust velocity representation to the plane of flight. Thus, no spatial variations of gust velocities along the vertical axis are recognized; all gust velocities above or below the flight plane are identical to their in-plane counterparts. This restriction presents no appreciable penalty to the analysis. The vertical tail span is considerably smaller than the dominant gust wavelengths. For these purposes, turbulence appears one-dimensional to the airplane along its vertical axis.
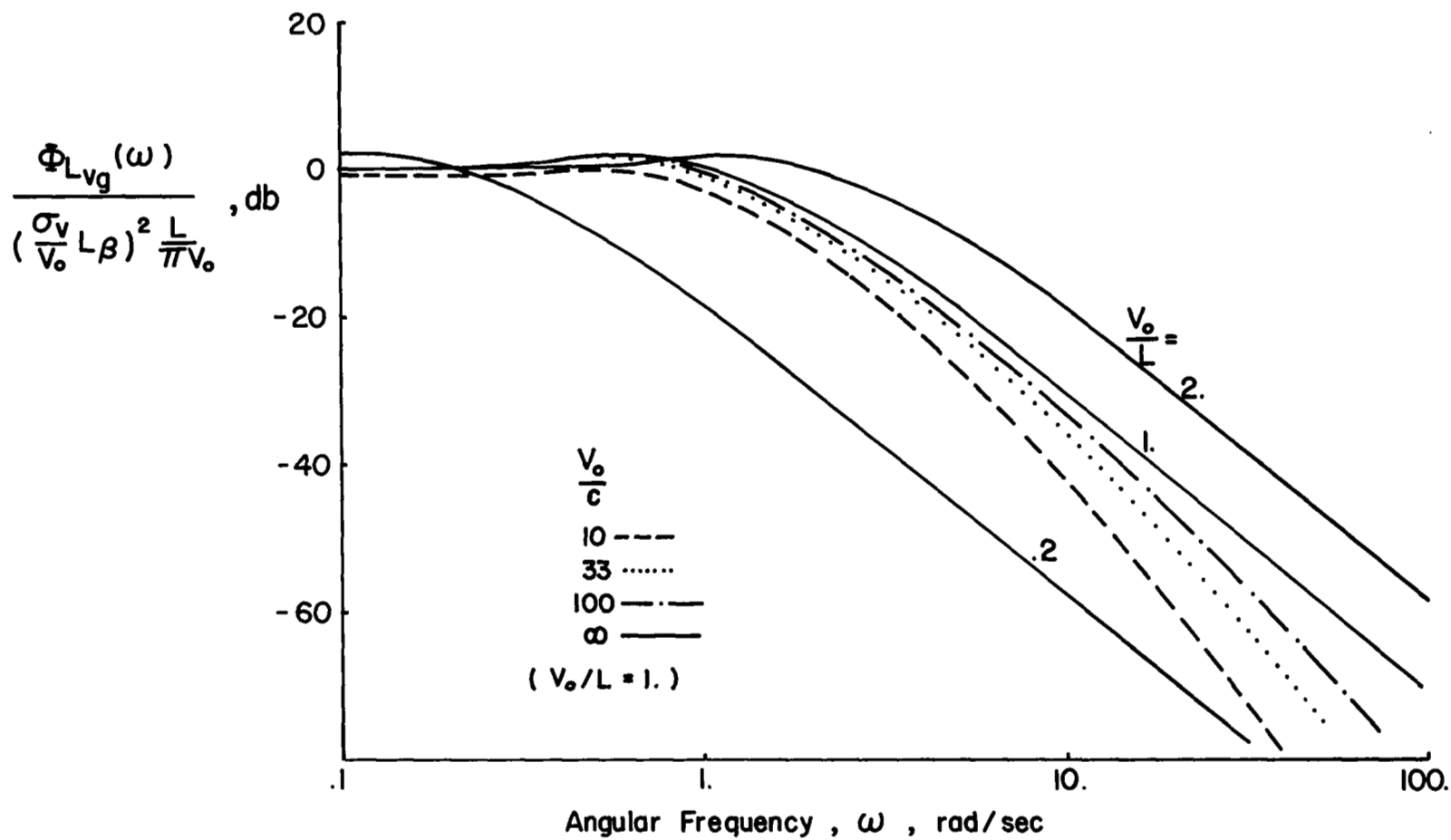
Figure 17. Rolling Moment Spectra Due to Lateral Gusts

48

As a result of these qualifications, yawing moment disturbances may be defined by

$$N_{v_g}(t) = \int_{-\infty}^{\infty} h_{N_{v_g}}(t_1) \, v_g \left[V_o(t - t_1 - \frac{\ell_v}{V_o}) \right] dt_1 \tag{57}$$

The influence function is

$$h_{N_{v_g}}(t_1) = C_{n\beta_{VT}} \frac{qSb}{V_o} k(t_1) \tag{58}$$

As in the case of rolling moments for lateral gusts, the spanwise load distribution has no significance here.

The spectral density of yawing moment is

$$\Phi_{N_{v_g}}(\omega) = |H_{N_{v_g}}(\omega)|^2 \, \Phi_{vv}(\omega) \tag{59}$$

and

$$H_{N_{v_g}}(\omega) = C_{n\beta_{VT}} \frac{qSb}{V_o} \varphi_k(\omega) \, e^{-\frac{\ell_v}{V_o}s} \tag{60}$$

Strictly speaking, the transient penetration effect associated with V_o/c will attenuate this spectrum at high frequency. For the class of airplanes involved in this study, the vertical tail chord is small enough compared to the flight speed V_o that the influence of streamwise penetration may be ignored. The resulting yawing moment spectrum is shown in Figure 18. Directional stability and the rms gust velocity combine to establish the spectral amplitude while V_o/L determines the frequency bandwidth. The effect of tail length, which causes the yaw disturbance to lag the roll disturbance due to lateral gusts, is noted in the exponential term.

$$\frac{\Phi_{N_{v_g}}(\omega)}{(\frac{\sigma_v}{V_o} N\beta_{VT})^2 \frac{L}{\pi V_o}} \text{ , db}$$

20

0

-20

-40

-60

$\frac{V_o}{L} =$

2.

1.

.2

.1   1.   10.   100.

Angular Frequency , ω , rad / sec
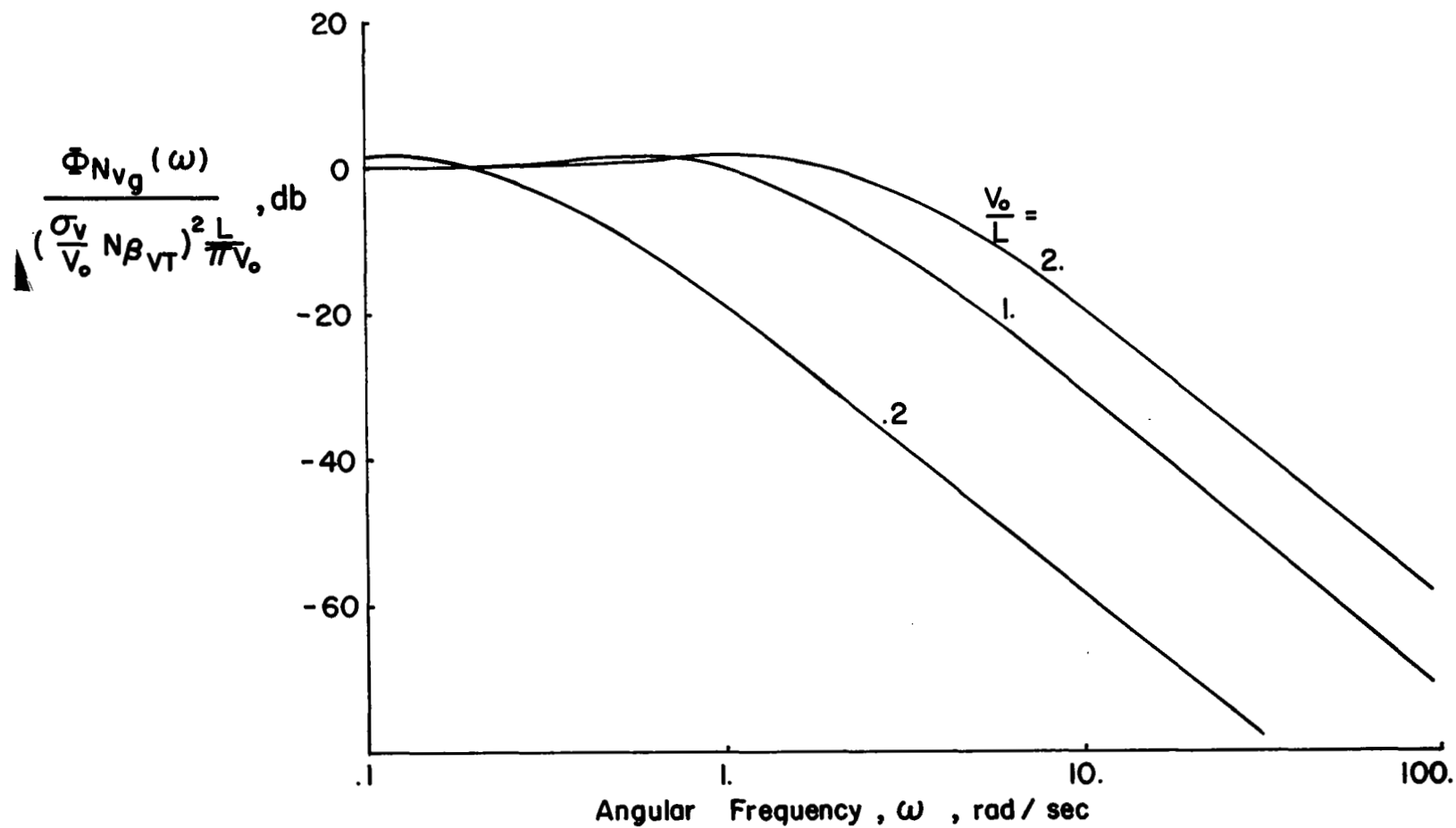
Figure 18.   Yawing Moment Spectra Due to Lateral Gusts

Approximation of Disturbance Spectra

To simplify the turbulence simulation to be used in the flight test program, it is desirable to obtain an approximate representation of the spectral density functions which retains the essential character of the spectra and the dependence on the parameters of interest. For example, consider the rolling moment spectrum due to vertical gusts, equation (44). The term $\Phi_{w_e}(\omega)$ in this equation given by equation (52) is of irrational form, and presents enough difficulties for an analytical study which requires the turbulence model. It is entirely unsuitable for mechanization in an experimental flight study. However, it is possible to devise a spectral model composed of a polynomial approximation of equation (44), where this polynomial may be factored as follows

$$\Phi_{L_{w_g}}(\omega) \doteq \frac{\Phi_{L_{w_g}}(0)}{(a_n \omega^{2n} + a_{n-1} \omega^{2(n-1)} + \cdots + 1)}$$

$$\doteq \frac{\Phi_{L_{w_g}}(0)}{(T_1^2 \omega^2 + 1)(T_2^2 \omega^2 + 1) \cdots (T_n^2 \omega^2 + 1)} \tag{61}$$

The polynomial factors shown here are representative of a filter network composed of a series of n first order linear filters. The time constants T_1, T_2, $\cdots T_n$ are chosen to provide an asymptotic approximation to equation (44) over a suitable range of frequency.

Consider the rolling moment spectra plotted as functions of frequency in Figure 19. For high frequency, the spectra attenuate as functions of ω^{-4}. This behavior suggests a spectral approximation of the form

$$\frac{\Phi_{L_{w_g}}(\omega)}{(\frac{\sigma_w}{V_o} L_p)^2 \frac{V_o}{\pi L}} \text{, db}$$

Angular Frequency, ω, rad / sec
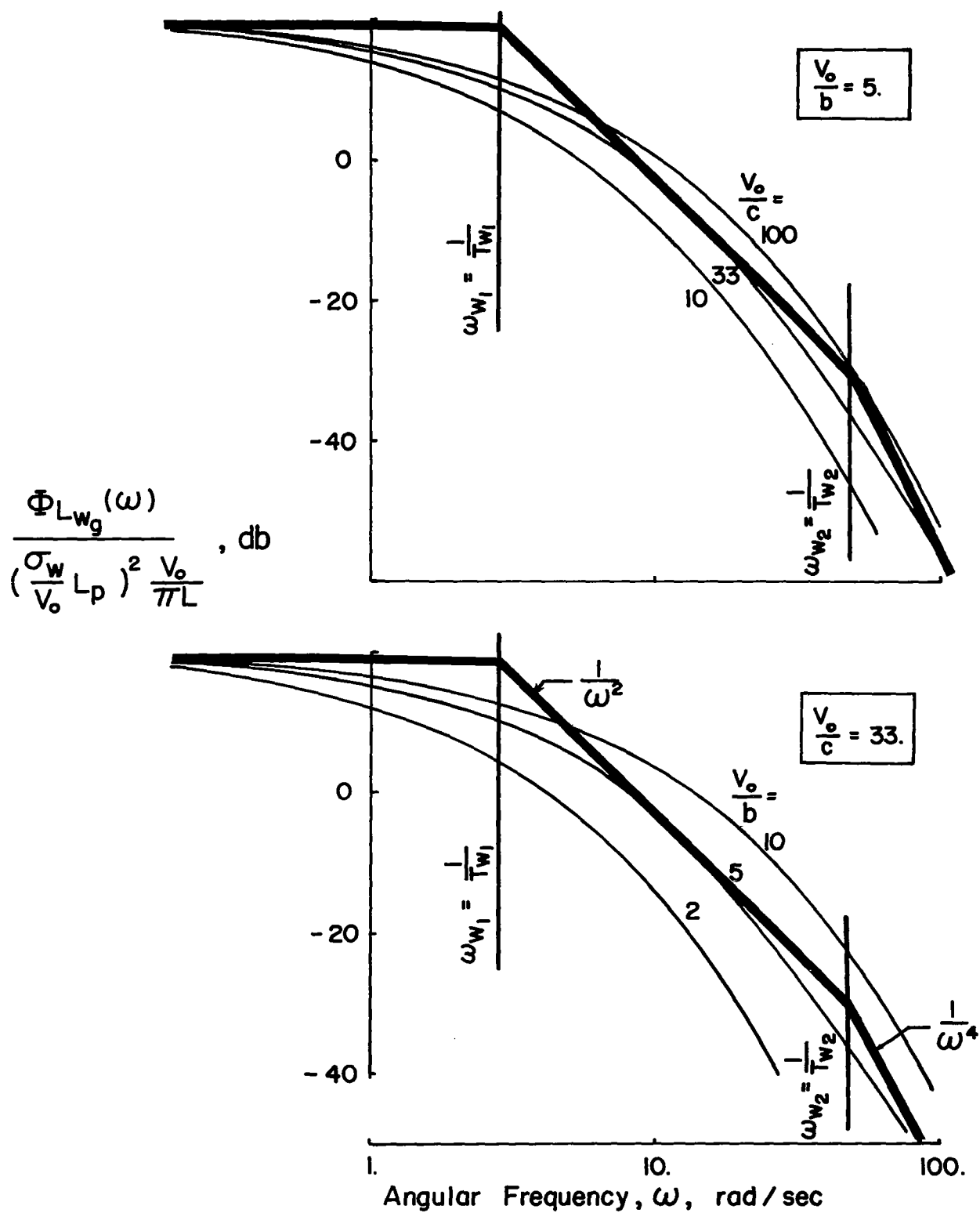
Figure 19. Asymptotic Approximation of Rolling Moment Spectra Due to Vertical Gusts

52

$$\Phi_{L_{w_g}}(\omega) \doteq \frac{\Phi_{L_{w_g}}(0)}{(T_{w_1}{}^2 \omega^2 + 1)(T_{w_2}{}^2 \omega^2 + 1)} \tag{62}$$

where the time constants T_{w_1} and T_{w_2} are functions of V_o/b and V_o/c reflecting the behavior of the actual spectra. If the actual spectra and the asymptotes of equation (62) are to coincide at high frequency as shown in Figure 19, equations (44) and (62) must be equivalent for $\omega \gg 1$. That is,

$$(\frac{\sigma_w}{V_o} L_p)^2 \frac{V_o}{\pi L} [36(\frac{V_o}{b})^3(\frac{V_o}{c})] \frac{1}{\omega^4} = \frac{\Phi_{L_{w_g}}(0)}{T_{w_1}{}^2 T_{w_2}{}^2 \omega^4} \tag{63}$$

Thus

$$T_{w_1}{}^2 T_{w_2}{}^2 = \frac{\Phi_{L_{w_g}}(0)}{(\frac{\sigma_w}{V_o} L_p)^2 (\frac{V_o}{\pi L}) [36 (\frac{V_o}{b})^3 (\frac{V_o}{c})]} \tag{64}$$

Furthermore, if the spectra and the asymptotes of its approximation coincide in the mid frequency range, then T_{w_1} and T_{w_2} may be shown empirically to be related to V_o/b and V_o/c by

$$T_{w_1} = 2.85 (\frac{V_o}{b})^{-3/4} (\frac{V_o}{c})^{-1/4} \tag{65}$$

$$T_{w_2} = .18 (\frac{V_o}{b})^{-3/4} (\frac{V_o}{c})^{-1/4} \tag{66}$$

At low frequency, the relationship between equations (44) and (62) reduces to

$$\Phi_{L_{w_g}}(0) \doteq \frac{9}{\pi} \left(\frac{\sigma_w}{V_o} L_p\right)^2 \frac{V_o}{L} \tag{67}$$

The complete spectral approximation is

$$\Phi_{L_{w_g}}(\omega) \doteq \frac{\frac{9}{\pi} \left(\frac{\sigma_w}{V_o} L_p\right)^2 \frac{V_o}{L}}{\left(.1225 \left(\frac{V_o}{b}\right)^{3/2} \left(\frac{V_o}{c}\right)^{1/2} \omega^2 + 1\right)\left(32.5 \left(\frac{V_o}{b}\right)^{3/2} \left(\frac{V_o}{c}\right)^{1/2} \omega^2 + 1\right)} \tag{68}$$

Figure 20 compares the actual spectrum and the approximation of equation (68) for typical ranges of the parameters V_o/b and V_o/c. The difference between the two spectra corresponds to an error in rms rolling moment of less than ten percent for the examples shown in Figure 20.

Rolling moments due to lateral gusts are defined by

$$\Phi_{L_{w_g}}(\omega) = \left(\frac{\sigma_v}{V_o} L_\beta\right)^2 \frac{L}{\pi V_o} \left[\frac{1 + 3\left(\frac{L}{V_o}\right)^2 \omega^2}{\left(1 + \left(\frac{L}{V_o}\right)^2 \omega^2\right)^2 \left(1 + \pi \frac{c}{V_o} \omega\right)}\right] \tag{69}$$

The asymptotes of the spectra are shown in Figure 21. To be precise the spectra attenuate in proportion to ω^{-3} at high frequency. The break in the asymptotes at high frequency is associated with the streamwise penetration factor and is a function of V_o/c. For values of V_o/c typical of general aviation airplanes, this break occurs at high frequency and at spectral magnitudes small enough to be ignored. By making this assumption, the spectra are proportional to ω^{-2} at high frequency. A suitable approximation is
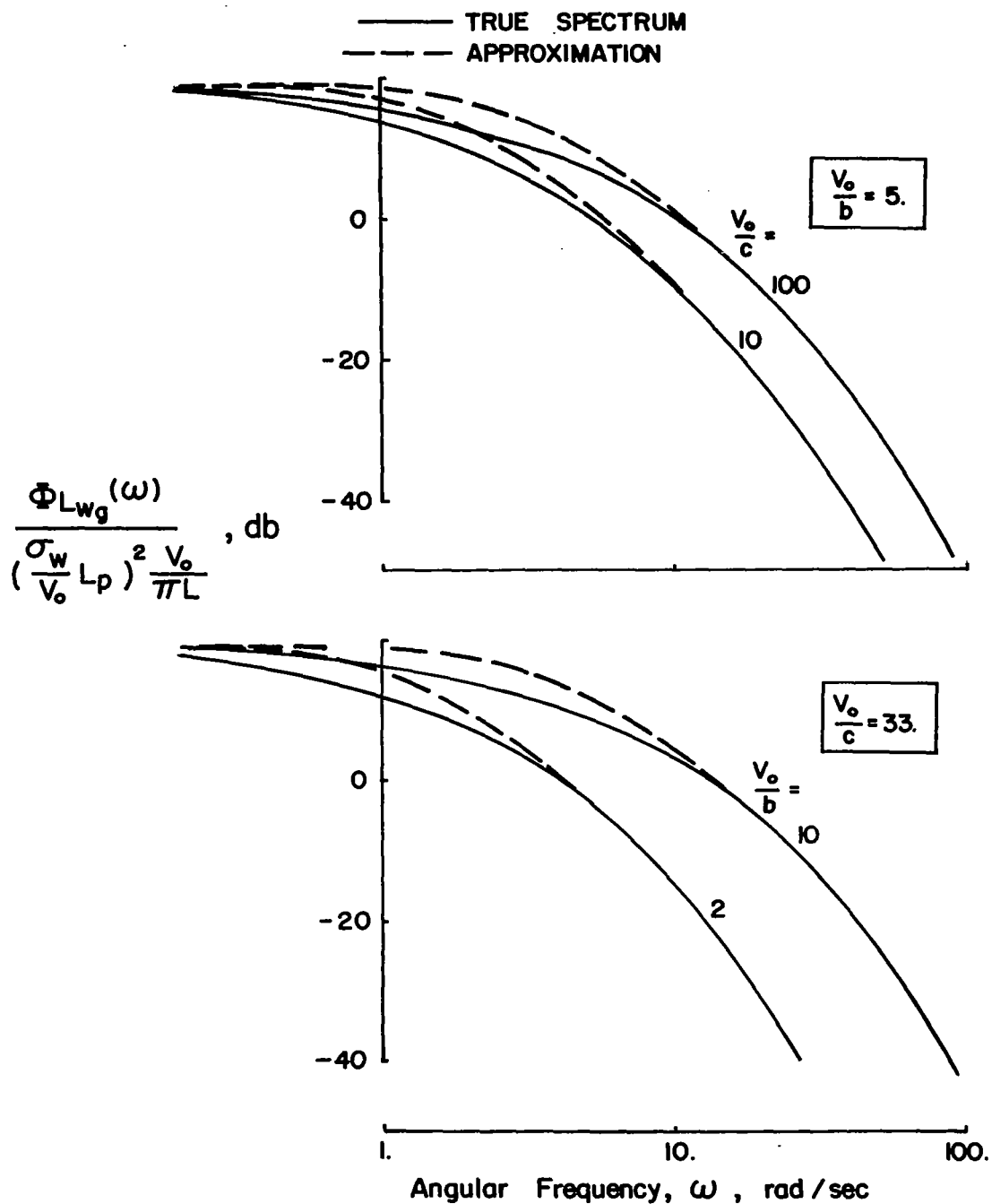
Figure 20. Comparison of Actual Rolling Moment Spectra With
Asymptotic Approximation - Vertical Gusts
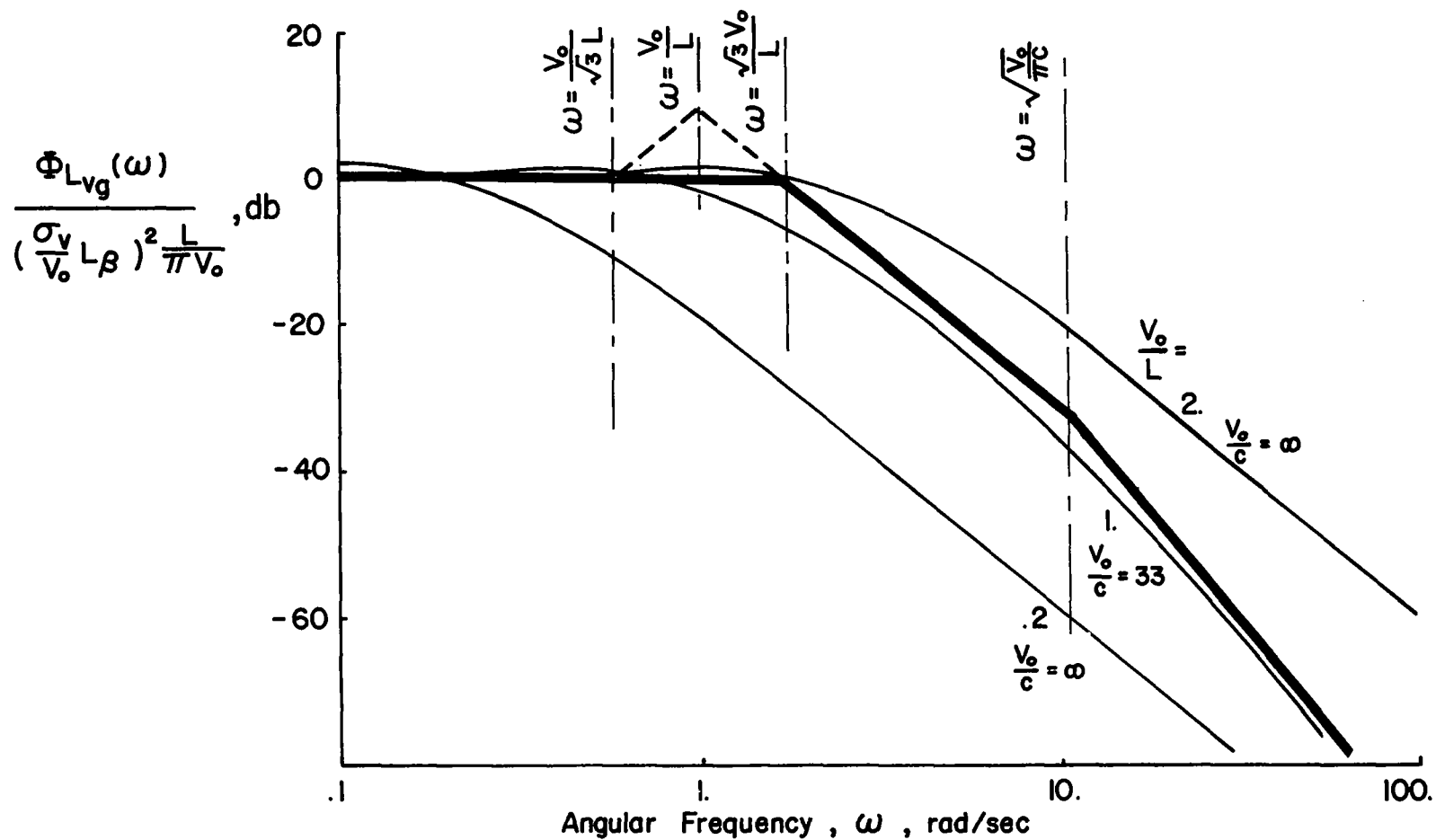
Figure 21. Approximation of Rolling Moment Spectra Due to Lateral Gusts

$$\Phi_{L_{v_g}}(\omega) \doteq \frac{\Phi_{L_{v_g}}(0)}{(T_{v_1}^2 \omega^2 + 1)} \qquad (70)$$

where T_{v_1} is defined by equating the two spectral expressions for $\omega \gg 1$.

$$T_{v_1} = \frac{L}{\sqrt{3}\, V_o} \qquad (71)$$

At low frequency, the approximation becomes

$$\Phi_{L_{v_g}}(0) = \left(\frac{\sigma_v}{V_o} L_\beta\right)^2 \frac{L}{\pi V_o} \qquad (72)$$

The resulting spectral approximation is

$$\Phi_{L_{v_g}}(\omega) = \frac{\left(\dfrac{\sigma_v}{V_o} L_\beta\right)^2 \dfrac{L}{\pi V_o}}{\left(\dfrac{L}{\sqrt{3}\, V_o}\right)^2 \omega^2 + 1} \qquad (73)$$

and is shown in relation to the actual spectra in Figure 22. A more precise representation of the spectra for frequencies in the neighborhood of $\sqrt{3}\, V_o/L$ could be provided using a lead filter $(T_{Lead} = \frac{\sqrt{3}\, L}{V_o})$ and a double lag filter $(T_{Lag} = \frac{L}{V_o})$ indicated by the dashed asymptotes in Figure 21; however, the small improvement in accuracy of the approximation does not justify the increased complication of the experimental simulation. The approximate spectrum has an rms level within five percent of the actual spectrum.

Representation of the yawing moment spectra due to lateral gusts follows much the same procedure as for the rolling moment spectra. Yawing moments are defined by
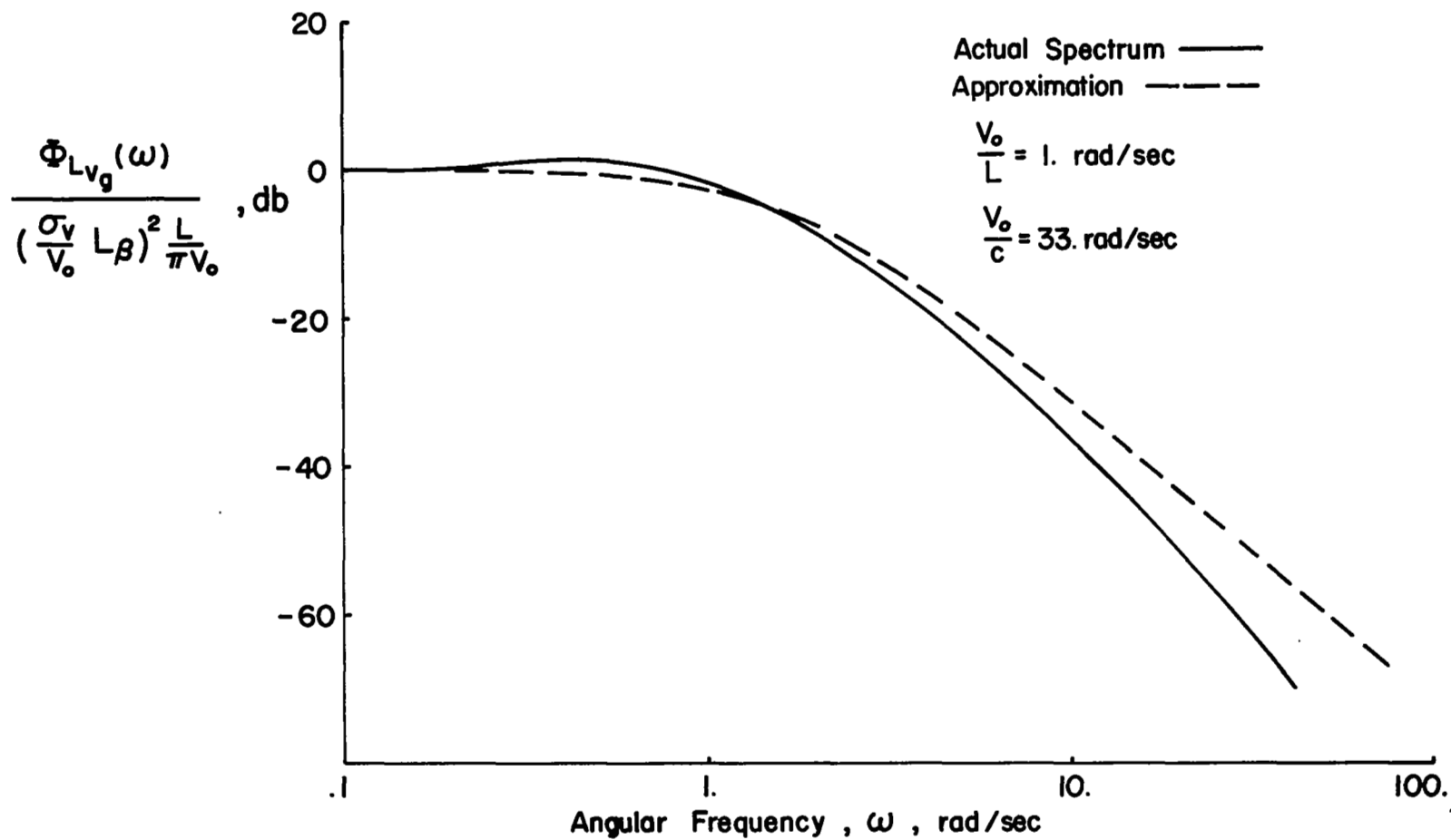
Figure 22. Comparison of Actual Rolling Moment Spectrum With
Asymptotic Approximation - Lateral Gusts

$$\Phi_{N_{v_g}}(\omega) = (\frac{\sigma_v}{V_o} N_{\beta_{VT}})^2 \frac{L}{\pi V_o} [\frac{1 + 3(\frac{L}{V_o})^2 \omega^2}{(1 + (\frac{L}{V_o})^2 \omega^2)^2}] \tag{74}$$

Simplifying this in the manner used for the L_{v_g} spectra gives

$$\Phi_{N_{v_g}}(\omega) \doteq \frac{(\frac{\sigma_v}{V_o} N_{\beta_{VT}})^2 \frac{L}{\pi V_o}}{(\frac{L}{\sqrt{3} V_o})^2 \omega^2 + 1} \tag{75}$$

Comparisons of this approximate spectrum with equation (74) are shown in Figure 23. In this case the rms level of the approximation is within eight percent of the rms of the actual spectrum. Assumptions permitting the streamwise penetration effects to be neglected are equally applicable in this case as for the rolling moment spectra.

The y-axis label reads:

$$\frac{\Phi_{N_{v_g}}(\omega)}{\left(\frac{\sigma_v}{V_o} N_{\beta_{VT}}\right)^2 \frac{L}{\pi V_o}} , db$$

Legend:

Actual Spectrum ———
Approximation — — —

$$\frac{V_o}{L} = 1. \text{ rad/sec}$$

x-axis values: .1, 1., 10., 100.

y-axis values: 20, 0, -20, -40, -60

Angular Frequency , ω , rad/sec
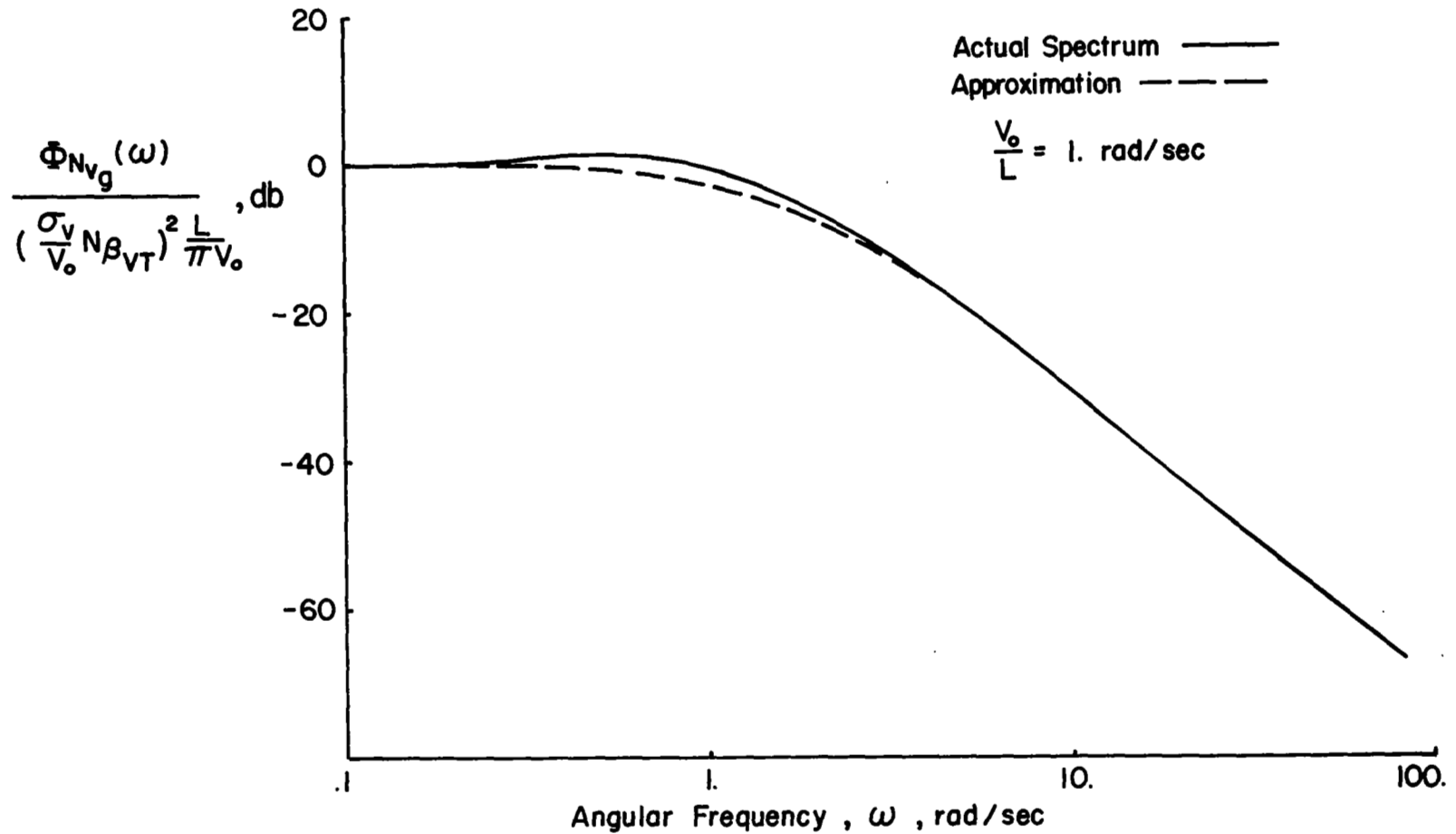
Figure 23. Comparison of Actual Yawing Moment Spectrum With
Asymptotic Approximation - Lateral Gusts

SECTION 4

DEFINITION OF TEST PROGRAM

Variations of the Turbulence Model

Numerous approaches to the variation of the turbulence model could be devised for the test program. However, the approach most suitable to the task at hand is to choose those characteristics of turbulence which represent the overall gust disturbances as the airplane encounters them and hence which represent the turbulence as the pilot sees it. In this regard, the overall magnitude of the roll and yaw disturbances, the correlation between the roll and yaw components, and the bandwidths of the disturbance spectra provide a suitable and complete description. These characteristics also suffice to statistically define the disturbances. They may be defined analytically as follows:

- Rms roll disturbance level represented by the rms angular acceleration in roll

$$\sigma_L = \sqrt{\sigma_{L_w}^2 + \sigma_{L_v}^2}$$

$$= \left[1.57 \left(\frac{\sigma_w}{V_o} L_p\right)^2 \frac{V_o}{L} \left(\frac{V_o}{b}\right)^{3/4} \left(\frac{V_o}{c}\right)^{1/4} + \frac{\sqrt{3}}{2} \left(\frac{\sigma_v}{V_o} L_\beta\right)^2 \right]^{1/2} \qquad (76)$$

which is a function of the rms level of turbulence and the magnitude of the roll damping and dihedral effect derivatives and the parameters V_o/L, V_o/b, and V_o/c. It is worth noting that since the rms gust velocities (σ_w and σ_v) and aerodynamic derivatives (L_p and L_β) occur as products, the separate influences of the gust velocities and derivatives will be indistinguishable to the pilot.

61

- Rms yaw disturbance level represented by the rms angular acceleration in yaw

$$\sigma_N = [\frac{\sqrt{3}}{2}(\frac{\sigma_v}{V_o} N_\beta)^2]^{1/2} \tag{77}$$

which is determined by the rms turbulence level and by the magnitude of directional stability.

- Correlation between the roll and yaw disturbances represented by the normalized cross correlation

$$\rho_{LN} = \frac{R_{LN}(0)}{\sigma_L \sigma_N}$$

$$= \frac{e^{-\sqrt{3}\frac{\ell_v}{L}}}{\sqrt{(\frac{\sigma_{L_w}}{\sigma_{L_v}})^2 + 1}} \tag{78}$$

which is related to the normalized tail length and to the relative amount of roll disturbance occurring from vertical and lateral gusts.

- Bandwidth of the disturbance spectrum which in the case of lateral gust contributions to roll and yaw disturbances is

$$\omega_{v_1} = \frac{1}{T_{v_1}} = \sqrt{3}\frac{V_o}{L} \tag{79}$$

and in the case of vertical gust contributions to roll disturbances is

$$T_{w_1} = 2.85 \left(\frac{V_o}{b}\right)^{-3/4} \left(\frac{V_o}{c}\right)^{-1/4} \tag{80}$$

$$T_{w_2} = .18 \left(\frac{V_o}{b}\right)^{-3/4} \left(\frac{V_o}{c}\right)^{-1/4} \tag{81}$$

Derivations of the parameters of equations (76)-(78) are presented in Appendix B. The bandwidth frequencies ω_{v_1}, ω_{w_1}, and ω_{w_2} are the same as derived in equations (71), (65), and (66) respectively of Section 3. Equation (3) in the Introduction, when expanded to show the influence of roll and yaw disturbances, reveals the separate influences of the aforementioned parameters. The error response of the closed loop pilot-airframe system in bank angle and heading to the given roll and yaw disturbances is

$$\varphi_\epsilon = -\left[\frac{N_{L_g}^\varphi}{\Delta'}\right] L_g - \left[\frac{N_{N_g}^\varphi}{\Delta'}\right] N_g \tag{82}$$

$$\psi_\epsilon = -\left[\frac{N'^\psi_{L_g}}{\Delta''}\right] L_g - \left[\frac{N'^\psi_{N_g}}{\Delta''}\right] N_g \tag{83}$$

In this case, the numerator terms represent the appropriate co-factor matrices of the complete response-disturbance matrix. The power spectral densities of bank angle and heading errors due to the external disturbance are

$$\Phi_{\varphi_\epsilon} = \left|\frac{N_{L_g}^\varphi}{\Delta'}\right|^2 \{\Phi_{L_{w_g}} + \Phi_{L_{v_g}}\} + \left|\frac{N_{N_g}^\varphi}{\Delta'}\right|^2 \Phi_{N_{v_g}}$$

$$+ 2R_e \left\{\left[\frac{N_{L_g}^\varphi}{\Delta'}\right]\left[\frac{N_{N_g}^\varphi}{\Delta'}\right]^* \Phi_{L_{v_g}N_{v_g}}\right\} \tag{84}$$

63

and

$$\Phi_{\psi_{\epsilon}} = \left|\frac{N'^{\psi}_{L_g}}{\Delta''}\right|^2 \{\Phi_{L_{w_g}} + \Phi_{L_{v_g}}\} + \left|\frac{N'^{\psi}_{N_g}}{\Delta''}\right|^2 \Phi_{N_{v_g}}$$

$$+ 2R_e \left\{\left[\frac{N'^{\psi}_{L_g}}{\Delta''}\right]\left[\frac{N'^{\psi}_{N_g}}{\Delta''}\right]^* \Phi_{L_{v_g}N_{v_g}}\right\} \qquad (85)$$

where it is understood that $\Phi_{L_{v_g}L_{w_g}} = \Phi_{L_{w_g}N_{v_g}} = 0$ based on the properties of isotropic turbulence. The turbulence spectra terms appearing in equations (84) and (85) have their counterparts in the previously defined disturbance parameters.

$$\Phi_{L_{w_g}} + \Phi_{L_{v_g}} \rightarrow \sigma_L = \sqrt{\sigma_{L_w}^2 + \sigma_{L_v}^2}$$

$$\text{and } \omega_{v_1}, \omega_{w_1}, \omega_{w_2}$$

$$\Phi_{N_{v_g}} \rightarrow \sigma_N \text{ and } \omega_{v_1}$$

$$\Phi_{L_{v_g}N_{v_g}} \rightarrow \rho_{LN}$$

Whether the problem is considered in terms of closed loop response, or in terms of the characteristics of the disturbances, the same contributions of turbulence appear.

The various influences of turbulence characteristics and airplane flight condition, geometry, and stability derivatives on the turbulence model parameters which have just been discussed are illustrated in Figure 24. For example, the contributions of the rms level of the lateral gust velocity and the magnitude of the airplane's dihedral effect to rms roll disturbances are noted in Figure 24a. These curves indicate the tradeoff between the gust

64
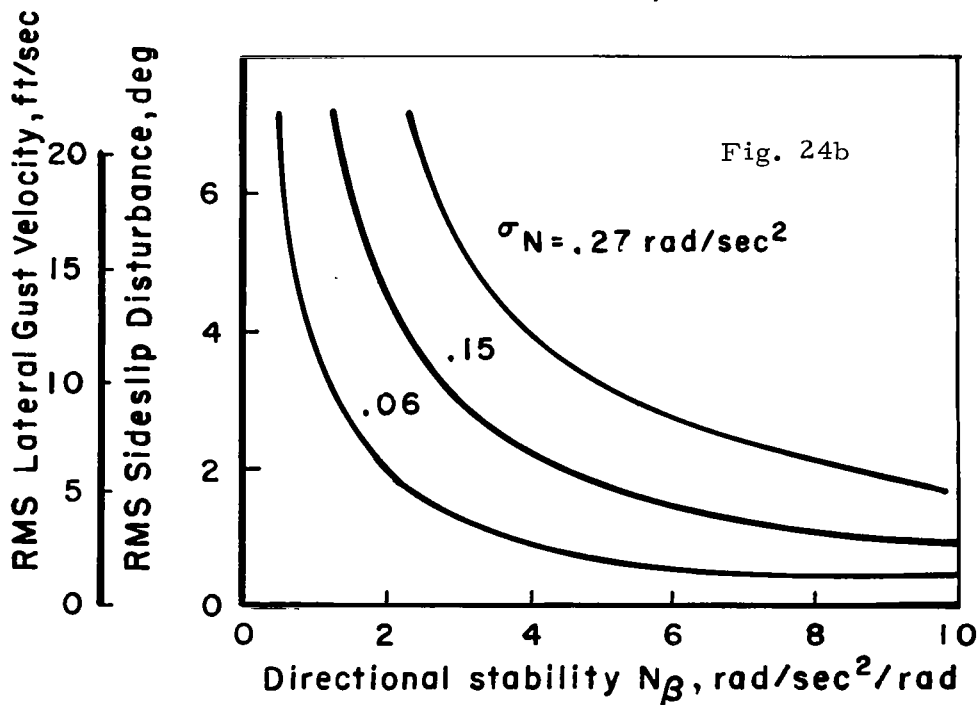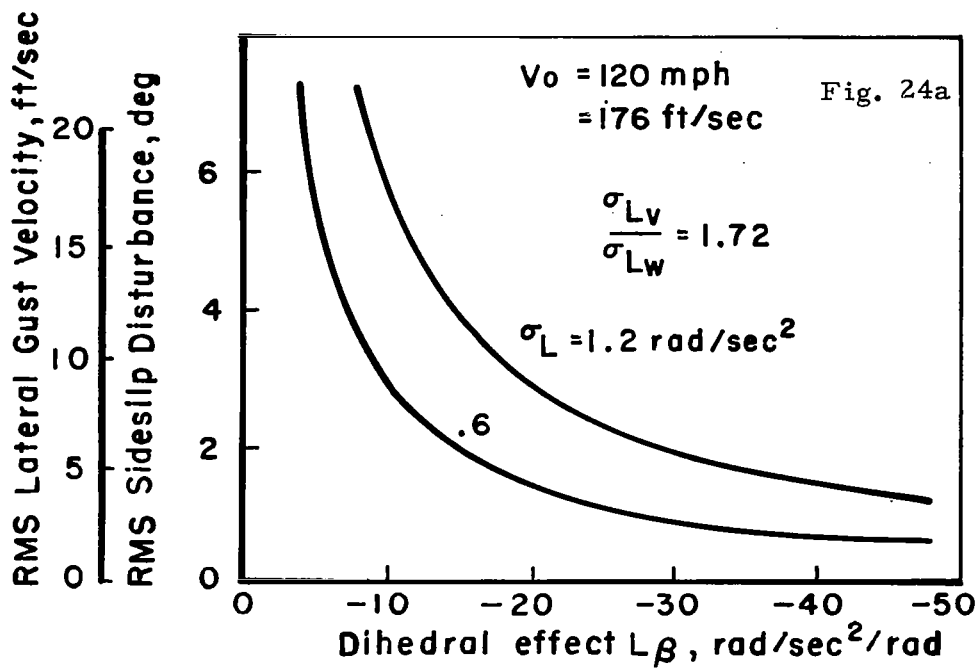
Figure 24. Contributions to the Turbulence Model Parameters

Fig. 24c

Fig. 24d

Fig. 24e

66
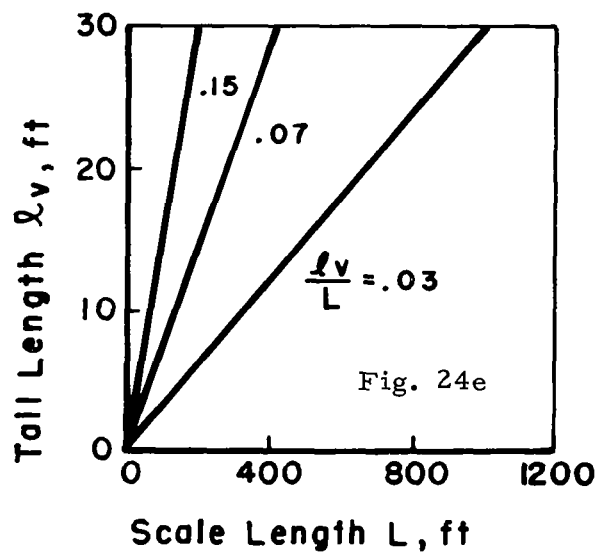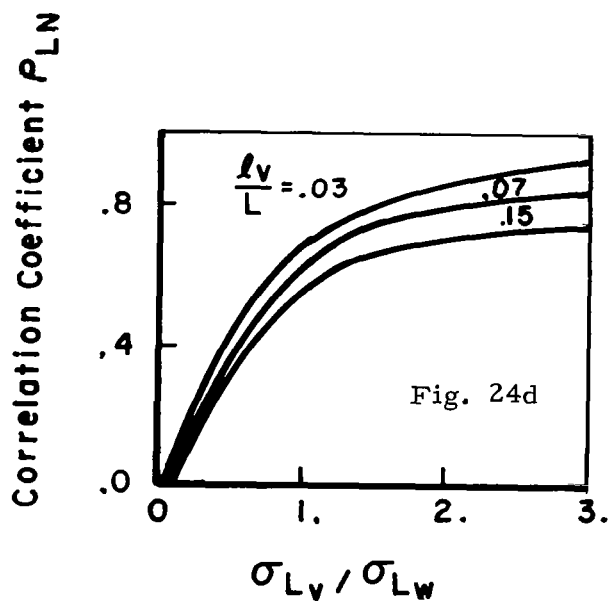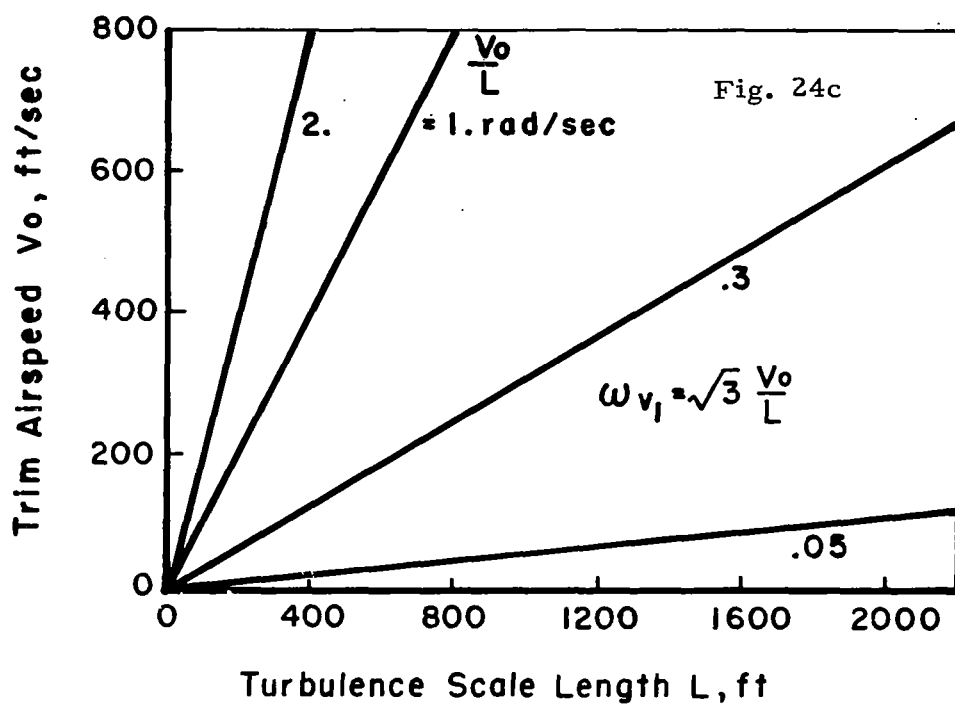
intensity and the airplane's lateral turbulence sensitivity (L_β) for several levels of roll disturbance. Since the relative contribution to roll disturbances of vertical and lateral gusts is constant for this figure ($\sigma_{L_v}/\sigma_{L_w} = 1.72$), referring to equation (76) it is also possible to determine the vertical gust intensity and the level of roll damping corresponding to a given value of rms roll disturbance (note that $\sigma_w = \sigma_v$ for isotropic turbulence). As a matter of interest, the Navion's dihedral effect for the airspeed and nominal gross weight of the test program is $L_\beta = -12.5$ radians/second^2/radian. The rms turbulence magnitude is indicated either in terms of an rms sideslip angle or an rms lateral gust velocity, the two measures being related by the airplane's trim airspeed ($\sigma_\beta = \sigma_v/V_o$, where for the test program $V_o = 120$ mph).

A similar illustration of the contributions to rms yaw disturbances is shown in Figure 24b. In this case the tradeoff is between the rms lateral gust velocity and the airplane's directional stability. The Navion's directional stability for the flight-loading conditions of the test program is $N_\beta = 6.0$ radians/second^2/radian.

To put the range of rms gust velocities in perspective, the probability of occurrence of rms gust velocities ranging from 1.0 to 10.0 feet/second is on the order of 90 percent to .007 percent according to Reference 40 (Section 3.7.3, Figure 2). A correlation between rms gust velocities and maximum derived gust velocities experienced during thunderstorm penetration is presented in Reference 31. The following examples of this correlation are excerpted from that report.

σ_u	$u_{d_{e_{max}}}$
1 foot/second	4 feet/second (eas)
10 feet/second	40 feet/second (eas)

The base test configuration of this program (Configuration 1) has the following values of aerodynamic derivatives pertinent to the turbulence disturbances:

$$L_\beta = -16.82 \ 1/\text{second}^2$$

$$L_p = -3.84 \ 1/\text{second}$$

$$N_\beta = 4.67 \ 1/\text{second}^2$$

If the derivatives in the turbulence equations are assumed to be equivalent to the above values, then the range of rms gust velocities which are associated with the range of rms roll and yaw disturbances tested is approximately $\sigma_w = \sigma_v = 5.0$ to 10.0 feet/second.

The range of the turbulence bandwidth parameter V_o/L which would be anticipated for typical ranges of trim airspeed and turbulence scale length is indicated in Figure 24c. For speeds from 100 to 500 feet/second and scale lengths of a few hundred to a few thousand feet, the corresponding variation in the bandwidth parameter is of the order .05 to 2.5 radians/second. This variation in V_o/L is somewhat broader than might be anticipated for realistic flight situations. The upper left corner of the diagram corresponds to high speed, low altitude flight conditions while the lower right corner represents low speed, high altitude operation, neither of which are particularly typical of general aviation airplane operation. A somewhat more constricted range of V_o/L was chosen for the test program ($V_o/L = .3$ to 2. radians/second), corresponding to actual spectral bandwidths ($\omega_{v_1} = \sqrt{3} \ V_o/L$) of .52 to 3.46 radians/second.

Contributions to the normalized roll-yaw correlation are shown in Figure 24d. The ratio of roll disturbances arising from vertical and lateral gusts can conceivably cover a considerable range ($\sigma_{L_v}/\sigma_{L_w} = 0$ for $L_\beta = 0$ to $\sigma_{L_v}/\sigma_{L_w} \gg 1.0$ for low roll damping) and thus it has a much larger influence on the normalized correlation than does the tail length contribution. Figure 24e indicates ranges of the normalized tail length appropriate to the general aviation class of airplane and the turbulence scale length.

Dynamics Configurations

Influences of closed loop dynamics on the airplane's turbulence re-
sponse are also apparent in equations (84) and (85). Parameters of closed
loop dynamics are not readily definable or available for variation in an ex-
perimental program. However, the influence of open loop dynamics on the
eventual closed loop characteristics have been given extensive consideration
in numerous analytical studies and in ground based simulators and variable
stability airplanes. While in general the nature of all the characteristic
modes of motion and the magnitude of their excitation by control inputs and
turbulence could be considered relevant to a flying qualities evaluation, the
significant contributions can be appreciated by confining attention to the
characteristics of the roll mode, the Dutch roll mode, and the degree of
excitation of the Dutch roll in either rolling or yawing motions.

The roll mode is important insofar as it affects the pilot's ability to
make rapid and precise changes in the airplane's wing attitude. The para-
meter of this mode which is a suitable measure of the aforementioned charac-
teristics is the roll mode time constant, T_R. It is approximately inversely
proportional to the airplane's dimensional roll damping derivative, L_p. It
reflects on the pilot's ability to control bank angle with the ailerons in a closed
loop sense and it also is a factor in the magnitude of roll response to turbu-
lence.

Although the Dutch roll mode does not represent an airplane response
which the pilot purposely induces in order to maneuver the airplane (unlike
the roll mode or short period longitudinal mode which normally dominate the
airplane's roll and pitch response to the pilot's control commands) it can be
annoying and burdensome to the pilot if it becomes large enough to interfere
with his precise control of bank angle or heading. This mode in general ap-
pears as a coupled rolling, yawing, sideslipping oscillatory motion whose
characteristics are specified by the frequency of the oscillation, ω_d, and

69

by the rate of decay or damping of the oscillation, ζ_d. It is typical of small airplanes that the Dutch roll frequency be closely identified with the level of directional stability, N_β ($\omega_d^2 \sim N_\beta$), and that the damping ratio is strongly dependent on the yaw damping derivative, N_r. Both the frequency and damping of the motion are important to precision roll and heading control. Turbulence response is also dependent on both the frequency and damping factors.

Excitations of the Dutch roll by either aileron or rudder control are also prospects for consideration. While a systematic variation of rudder excitation parameters is not undertaken in this study, aileron excitation of the Dutch roll is considered in choosing the test configurations. Aileron induced Dutch roll response arises because of yawing moments contributed by the ailerons themselves ($N_{\delta a}$) or from yawing moments due to the ensuing roll response (N_p). Furthermore, some sideslipping occurs as the airplane rolls from a wings level attitude as a result of the ensuing lateral force unbalance. A measure of the magnitude of Dutch roll excitation in the airplane's roll response which was suggested in Reference 2 is the parameter K_d / K_{ss}. This parameter provides some indication of the added difficulty in controlling wing attitude due to the Dutch roll oscillation.

Another element of roll control with ailerons is the stability of the closed loop system. This behavior is significantly influenced by the relative position of the Dutch roll pole and the zero of the bank angle to aileron transfer function. The parameter $\omega_\varphi / \omega_d$, which was first suggested in Reference 41 as a significant lateral handling qualities parameter and which has been considered in numerous experimental programs (References 2, 6, and 32 for example), and the K_d / K_{ss} factor together specify this pole-zero orientation and thus are a basis for inferring the likely behavior in the closed loop case.

The dynamics parameters included in the test matrix and their ranges of variation are given in Table 3.

TABLE 3

LATERAL-DIRECTIONAL DYNAMICS PARAMETERS

Parameter	Range
T_R	.1 to .5 seconds
ω_d	1.3 to 3. radians/second
ζ_d	.1 to .4
ω_φ/ω_d	.76 to 1.4
K_d/K_{ss}	.05 to .7

Test Matrix

Tables 4 and 5 list the turbulence configurations and open loop dynamic characteristics which were included in the test program. Specific combinations of turbulence and dynamics which were evaluated in flight are given in Table 6. These particular combinations were chosen for the purpose of

- obtaining a complete study of the several effects of turbulence for a given set of good dynamics - Configuration 1, and for a set of relatively poor dynamics - Configuration 6,

- evaluating the effects of roll time constant (roll damping) for a selected variation in the turbulence matrix, emphasizing rms roll disturbances and bandwidth; Dutch roll frequency and damping ratio are constant - Configurations 4 and 5,

- evaluating the effects of Dutch roll frequency (directional stability) for selected variations in turbulence which emphasize variations in rms yaw disturbances, bandwidth, and roll-yaw correlation; roll time constant and Dutch roll damping ratio are constant - Configurations 2 and 3,

- evaluating the effects of closed loop roll control characteristics (ω_φ/ω_d and K_d/K_{ss}) for selected variations in turbulence emphasizing rms roll disturbances; for a high and a low level of Dutch roll frequency corresponding to high and low levels of roll damping and for constant damping ratio - Configurations 9 through 14,

- evaluating the effects of Dutch roll damping ratio for variations in turbulence emphasizing rms yaw disturbances for high and low levels of Dutch roll frequency and for a fixed roll time constant - Configurations 7 and 8.

A neutral spiral mode was maintained for all test configurations except the high Dutch roll damping case, Configuration 7 and for Configurations 9 and 12. Imposing the neutral spiral requirement in these cases requires an unrealistically large value of the derivative L_r in order for the factor ($L_\beta N_r - N_\beta L_r$) to vanish. An airplane with such a large magnitude of L_r would be unusually sensitive in roll to the rudder and would also require the pilot to hold aileron against a turn. It was felt that such behavior might be objectionable to the pilot and hence the neutral spiral requirement was relaxed for these configurations. Instead, a value of L_r typical of many light airplanes was used (L_r = 2.0), resulting in a stable spiral condition with time constants as shown in Table 5. Based on the results of an exploratory study into the effects of a stable spiral mode on flying qualities conducted at Princeton which are described in Reference 33 and based on the results of Reference 34, this level of spiral stability was not found to change the pilot's evaluation in comparison to the neutral spiral condition.

In the cases where closed loop roll control is not under evaluation, the zeros of the bank angle to aileron transfer function were positioned with respect to the Dutch roll pole so as to minimize the effects of Dutch roll excitation on the pilot's evaluation.

TABLE 4

TURBULENCE CONFIGURATIONS

Configuration	σ_L	$\dfrac{\sigma_{L_w}}{\sigma_{L_v}}$	σ_N	ρ_{LN}	$\dfrac{V_o}{L}$	ω_{w_1}	ω_{w_2}
1	.6	.58	.06	.8	.314	1.5	∞
2	.6	.58	.15	.8	.314	1.5	∞
3	.6	.58	.27	.8	.314	1.5	∞
4	.9	.58	.09	.8	.314	1.5	∞
5	.9	.58	.27	.8	.314	1.5	∞
6	1.2	.58	.06	.8	.314	1.5	∞
7	1.2	.58	.15	.8	.314	1.5	∞
8	1.2	.58	.27	.8	.314	1.5	∞
9	1.2	.58	.15	.86	.314	1.5	∞
10	1.2	.58	.27	.86	.314	1.5	∞
11	.6	.58	.27	.86	.314	1.5	∞
12	.6	.19	.15	.9	.314	1.5	∞
13	1.2	.19	.27	.9	.314	1.5	∞
14	1.2	.19	.15	.95	.314	1.5	∞
15	.6	.19	.15	.95	.314	1.5	∞
16	.9	1.15	.18	.6	.314	1.5	∞
17	.9	1.15	.18	.6	.314	6.	∞
18	.9	1.15	.18	.6	.314	6.	12.5

TABLE 4 (continued)

Configuration	σ_L	$\dfrac{\sigma_{L_w}}{\sigma_{L_v}}$	σ_N	ρ_{LN}	$\dfrac{V_o}{L}$	ω_{w_1}	ω_{w_2}
19	.6	∞	.18	0.	.314	1.5	∞
20	.6	.58	.06	.77	1.	1.5	∞
21	.6	.58	.15	.77	1.	1.5	∞
22	.6	.58	.27	.77	1.	1.5	∞
23	.9	.58	.09	.77	1.	1.5	∞
24	.9	.58	.27	.77	1.	1.5	∞
25	1.2	.58	.06	.77	1.	1.5	∞
26	1.2	.58	.15	.77	1.	1.5	∞
27	1.2	.58	.27	.77	1.	1.5	∞
28	.6	.58	.15	.68	1.	1.5	∞
29	.6	.58	.27	.68	1.	1.5	∞
30	1.2	.58	.15	.68	1.	1.5	∞
31	1.2	.58	.27	.68	1.	1.5	∞
32	.6	.58	.15	.83	1.	1.5	∞
33	.6	.58	.27	.83	1.	1.5	∞
34	1.2	.58	.15	.83	1.	1.5	∞
35	1.2	.58	.27	.83	1.	1.5	∞
36	2.2	.58	.49	.83	1.	1.5	∞
37	3.1	.58	.7	.83	2.	1.5	∞
38	2.2	.58	.49	.83	2.	1.5	∞

TABLE 4 (continued)

Configuration	σ_L	$\dfrac{\sigma_{L_w}}{\sigma_{L_v}}$	σ_N	ρ_{LN}	$\dfrac{V_o}{L}$	ω_{w_1}	ω_{w_2}
39	.6	.5	.15	.85	1.	1.7	∞
40	.6	1.	.15	.68	1.	1.7	∞
41	.6	2.	.15	.43	1.	1.7	∞
42	.6	∞	.15	0	1.	1.7	∞
43	1.2	.5	.15	.85	1.	1.7	∞
44	1.2	2.	.15	.43	1.	1.7	∞
45	1.2	1.	.15	.68	1.	3.4	∞
46	1.2	1.	.15	.44	2.	1.7	∞
47	1.2	1.	.15	.68	1.	1.7	∞
48	1.2	1.	.15	.68	1.	1.7	12.5
49	.6	.58	.15	.77	2.	1.5	∞
50	.6	.58	.27	.77	2.	1.5	∞
51	1.2	.58	.15	.77	2.	1.5	∞
52	1.2	.58	.27	.77	2.	1.5	∞
53	1.2	.58	.15	.68	2.	1.5	∞
54	1.2	.58	.27	.68	2.	1.5	∞
55	.6	.58	.27	.68	2.	1.5	∞

TABLE 5

CONFIGURATION PARAMETER AND DERIVATIVE VALUES

Configuration	T_R	ζ_d	ω_d	L_β	L_p	L_r	N_β	N_r	N_p	$L_{\delta a}$	$N_{\delta a}/L_{\delta a}$	$N_{\delta r}$
1	.25	.1	2.3	-16.82	-3.84	1.32	4.67	-.37	.01	1.8	.0	-.8
2	.25	.1	1.3	-16.37	-3.92	.94	1.50	-.09	.13	1.8	.0	-.8
3	.25	.1	3.0	-17.6	-3.90	.91	8.62	-.45	.07	1.8	.0	-.8
4	.50	.1	2.3	-16.02	-1.70	1.66	4.87	-.51	.05	1.3	.0	-.8
5	.10	.1	2.3	-15.97	-9.97	.75	4.97	-.23	.01	2.3	.0	-.8
6	.50	.1	1.3	-15.97	-1.76	2.41	1.63	-.25	.15	1.3	.0	-.8
7*	.25	.4	1.3	-16.30	-3.87	2.00	1.73	-1.45	.07	1.8	.0	-.8
8	.25	.4	3.0	-15.8	-3.80	4.54	8.17	-2.35	.01	1.8	.0	-.8
9*	.25	.1	2.3	-16.0	-3.47	2.00	2.35	-.81	-.60	1.8	.174	-.8
10	.25	.1	2.3	-15.93	-3.81	1.41	4.48	-.40	-.05	1.8	-.078	-.8
11	.25	.1	2.3	-15.83	-4.12	.25	5.77	-.09	.35	1.8	.112	-.8
12*	.50	.1	1.3	-16.0	-1.74	2.00	1.54	-.73	.09	1.3	-.002	-.8
13	.50	.1	1.3	-15.96	-1.76	2.41	1.63	-.25	.15	1.3	-.043	-.8
14	.50	.1	1.3	-16.77	-1.90	1.06	1.68	-.11	.17	1.3	.095	-.8

*Spiral mode time constant

7 T_S = 1.84 sec
9 T_S = 14.1 sec
12 T_S = 2.16 sec

$\dfrac{Y_\beta}{V}$ = -.254 per second

$\dfrac{Y_{\delta r}}{V}$ = .01 per in•sec

V_o = 176 feet/second

I_{xz} = 0

TABLE 6

COMBINATIONS OF TURBULENCE AND DYNAMICS CONFIGURATIONS

Dynamics Configurations	Turbulence Configurations
1	Complete set of configurations
4, 5	2, 3, 7, 8, 21, 22, 23, 24, 26, 27, 30, 31, 16, 17, 51, 52
2, 3	2, 3, 7, 8, 20, 21, 22, 25, 26, 27, 29, 30, 31, 34, 35, 49, 50, 51, 52
9-14	8, 21, 26, 27, 31, 52 (14-52 combination not tested)
7, 8	2, 3, 7, 8, 21, 22, 26, 27, 30, 31, 50, 51, 52
6	2, 3, 7, 8, 21, 22, 26, 27, 29, 30, 31, 16, 17, 50, 51, 52

Aileron and rudder control effectiveness were optimized for a given set of dynamics and for flight in calm air based on the evaluation pilot's rating and commentary. The control effectiveness chosen was consistent among the pilots of this program and was also found to correspond to values of control effectiveness giving good flying qualities for general aviation airplanes noted in Reference 35. Control effectiveness was kept at this level for subsequent turbulence configurations and the same set of dynamics.

Evaluation Task

Flight evaluations of the test configurations were obtained from pilots performing a cruise flight IFR heading control task. Qualitative evaluations were obtained with the objective of determining the appropriate pilot opinion rating and corresponding commentary elaborating on the acceptable and deficient characteristics of a given combination of dynamics and turbulence disturbances. The pilot was instructed to hold constant heading and to make small heading changes on command of the safety pilot. This task can be illustrated pictorially by specializing the block diagram of Figure 1 to the heading control case (Figure 25). Heading control with both ailerons and rudder is provided. Roll control is performed to achieve equalization for the heading loops, as a means of making heading corrections with the ailerons, and to reduce the roll excursions due to turbulence to an acceptable level. Roll excursions were expected to influence the pilot's rating only to the extent that they prevented him from achieving the desired control over heading or otherwise proved disconcerting or distracting.

To establish an objective for the evaluation pilot, a desired level of performance was considered to be control of the airplane's mean heading within two degrees of some specified or commanded azimuth. This objective should be distinguished from control of excursions about the mean heading due to gust upsets. The diagram of Figure 26 should help to clarify the
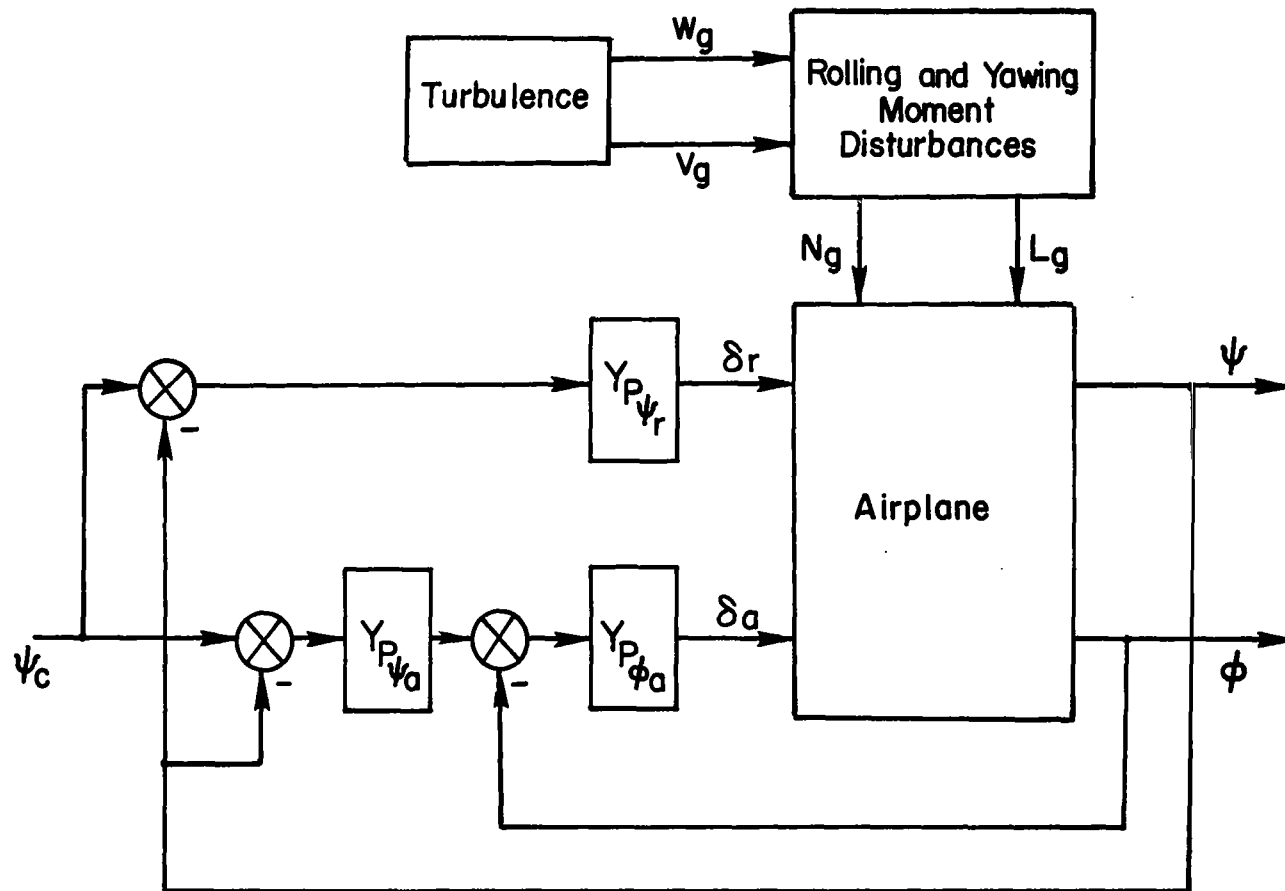
Figure 25.   Block Diagram of Heading Control Process in Turbulence
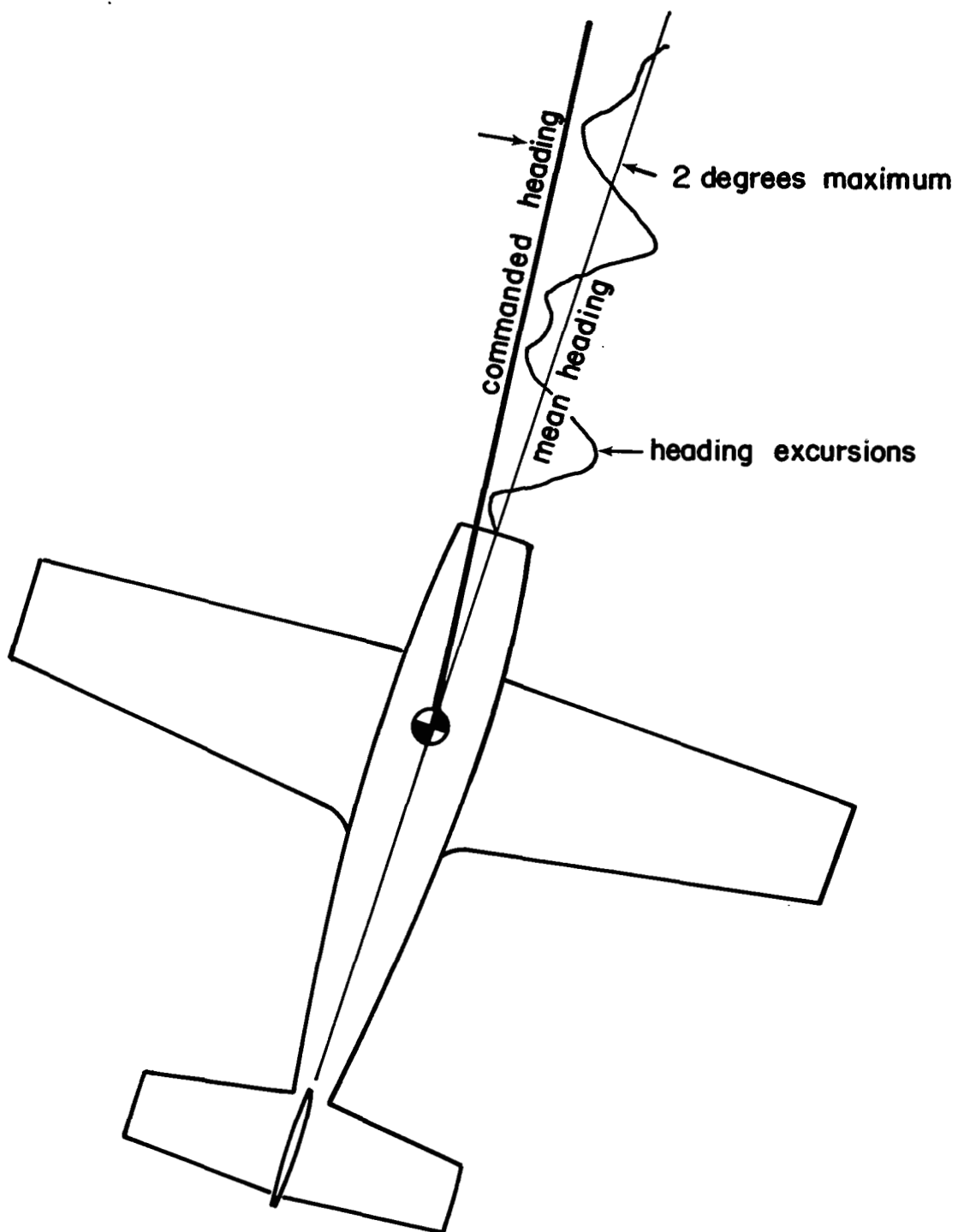
Figure 26. Pictorial Description of the Heading Tracking Task

flight task. While the pilots were not instructed to keep the rms heading excursions within specified limits, it is interesting to note in the flight test data that rms heading was maintained around 1.5 to 2.0 degrees. The degree of precision represented by this task was considered by the evaluation pilots to be comparable to the precision required for landing approach GCA vector tracking or for maintaining close formation flight.

The heading tracking task represents a realistic but demanding task of the pilot. As interpreted here it is a complete flight task in itself. It may also be a subtask of other flight phases such as the ILS approach and is important there inasmuch as good heading control is important to good localizer control. This task was chosen for the test program because it was felt that the level of pilot-airplane performance required was sufficiently demanding to permit a reasonably sensitive distinction to be made between good and bad combinations of airplane dynamics and turbulence disturbances. A less exacting task such as enroute navigation using VOR would not be likely to produce significant results. In the opposite sense, while the ILS approach places considerable demands on the pilot-airplane combination and would be worthy of study, it was rejected as an evaluation task for two considerations. First, the instrument approach is not a time stationary process since the sensitivity of one of the prime navigational aids, the localizer display, is time varying (becoming more sensitive to lateral offset as the airplane approaches the ILS transmitter). Such behavior renders any statistical analysis of performance data, founded on the assumption of stationarity, invalid. Second, the added complication of controlling lateral deviation serves to obscure the interaction between the pilot and basic airplane as it responds to gust upsets. The additional control loop activated for lateral displacement is of relatively low bandwidth. The significant pilot-airplane transfer function characteristics and the influences of turbulence on the closed loop system exist at higher frequencies and can best be studied by considering the inner control loops of the ILS task, namely the heading and bank angle control loops.

IFR heading control provides the opportunity for studying the pilot airplane dynamics while presenting the pilot with a realistic flight task. In several instances the problem was simplified another degree by requiring the pilot to control only bank angle in response to turbulence. While this task is not meaningful in itself to the pilot, it is important as a form of inner loop compensation as the pilot attempts to control heading with the ailerons. Analysis of performance data for the simple bank angle control task can provide insight to the extent of compensation required of the pilot to achieve satisfactory control over roll attitude.

A nominal longitudinal flight task was also performed by the pilot. Airspeed was held to within ±5 knots of 105 knots and essentially constant altitude was maintained in the presence of light turbulence. The basic Navion longitudinal dynamics which are quite satisfactory and easy to fly were used in this program in conjunction with simulated light pitch and heave turbulence. The pilot was instructed to not permit the longitudinal task to infringe on the lateral-directional evaluation process.

A typical sequence of events in the evaluation process consisted of the following items. First, the pilot was given the lateral dynamics configuration of interest and permitted to feel it out to his satisfaction in smooth air. During this interval, he would select what he felt to be his optimum aileron and rudder control sensitivities. Next, with turbulence turned on he continued to feel out the airplane's response and to settle on a desirable control technique, e.g., whether to use rudder in heading control, how effective aileron was in heading control, etc. He then performed his formal evaluation run for the turbulence and dynamics combination of interest. The subsequent evaluation was based on the duration of the test run. No attempt was made by the pilot to extrapolate his evaluation to factor fatigue or exposure time into his rating. The pilot also made note whenever his longitudinal control situation detracted from the lateral-directional evaluation. At the conclusion of the

evaluation, the pilot would radio his rating and commentary to the ground controller for tape recording and further study. The pilot was also requested to provide a set of data suitable for quantitative measurement of heading tracking performance. Under these circumstances, the task became one of holding constant heading over a period of time with the same performance objectives adopted for the qualitative evaluation. The pilot was instructed to pay strict attention to heading control for the duration of the run, with no diversions permitted for navigation or communication or even for anything but cursory attention to the longitudinal (air speed and altitude) situation.

The pilot's qualitative evaluation of a configuration consisted of assigning an appropriate pilot opinion rating and providing detailed pilot commentary on several itemized factors for that configuration. Pilot ratings were based on the revised Cooper-Harper scale described in Reference 36 and reproduced in Table 7. Factors covered in the commentary are:

- Heading control - how good in terms of performance and workload? Do excursions detract from ability to hold or change heading to desired accuracy?
- Roll control - how good in terms of performance and workload? Do excursions degrade heading performance?
- Magnitude of sideslip - do excursions degrade heading performance?
- Level of turbulence in roll and yaw.
- Frequency content of turbulence.

Quantitative flight data were obtained in the form of on-line chart recorded time histories of

                                roll attitude excursions

                                lateral control motion

                                yaw rate

                                heading excursions

                                sideslip

                                rudder control motion

ADEQUACY FOR SELECTED TASK OR REQUIRED OPERATION	AIRCRAFT CHARACTERISTICS	DEMANDS ON THE PILOT IN SELECTED TASK OR REQUIRED OPERATION	PILOT RATING
	Excellent Highly desirable	Pilot compensation not a factor for desired performance	1
	Good Negligible deficiencies	Pilot compensation not a factor for desired performance	2
	Fair — some mildly unpleasant deficiencies	Minimal pilot compensation required for desired performance	3
	Minor but annoying deficiencies	Desired performance requires moderate pilot compensation	4
	Moderately objectionable deficiencies	Adequate performance requires considerable pilot compensation	5
	Very objectionable but tolerable deficiencies	Adequate performance requires extensive pilot compensation	6
	Major deficiencies	Adequate performance not attainable with maximum tolerable pilot compensation. Controllability not in question	7
	Major deficiencies	Considerable pilot compensation is required for control	8
	Major deficiencies	Intense pilot compensation is required to retain control	9
	Major deficiencies	Control will be lost during some portion of required operation	10

Flowchart (left column):

Yes — Is it satisfactory without improvement → No → Deficiencies warrant improvement

Yes — Is adequate performance attainable with a tolerable pilot workload → No → Deficiencies require improvement

Yes — Is it controllable → No → Improvement mandatory

PILOT DECISIONS

84
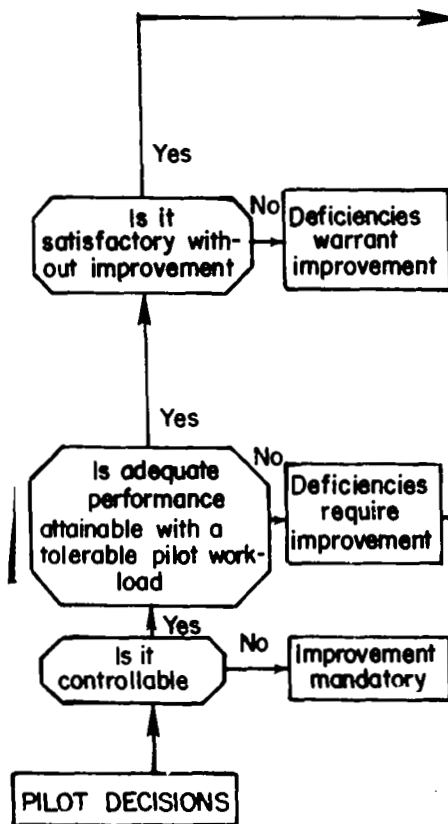
TABLE 7   PILOT OPINION RATING SCALE

Tape recorded time histories were made for all the above variables and in addition for

> roll rate
>
> bank angle
>
> roll turbulence
>
> yaw turbulence
>
> airspeed

Test Facilities

Flight evaluations were made using Princeton University's in-flight simulator shown in Figure 27. This vehicle consists of a basic North American Navion airframe modified to achieve a variable stability and control capability. While the original simulator configuration was described in detail in Reference 2, a considerable number of modifications and improvements have been made to the system in recent years which make a more thorough description of the machine necessary.

A variable stability capability is achieved in this airplane using the response feedback technique illustrated in general in Figure 28. Angle of attack, pitch rate, and airspeed are fed back to the elevator and flap to alter the basic airplane's longitudinal dynamics. A more recent modification permits angle of attack and airspeed to be fed into a throttle control system to gain control over the airplane's longitudinal force characteristics. Angle of sideslip and angular rates in roll and yaw are fed back to the ailerons and rudder in order to vary lateral-directional dynamics. No variation in side force characteristics from those of the basic airplane is possible.

Variable control is provided through adjustable gains for the cockpit control displacement to control surface deflection. This capability exists for the same five axes as does the variable stability system. Elevator, flap, throttle,
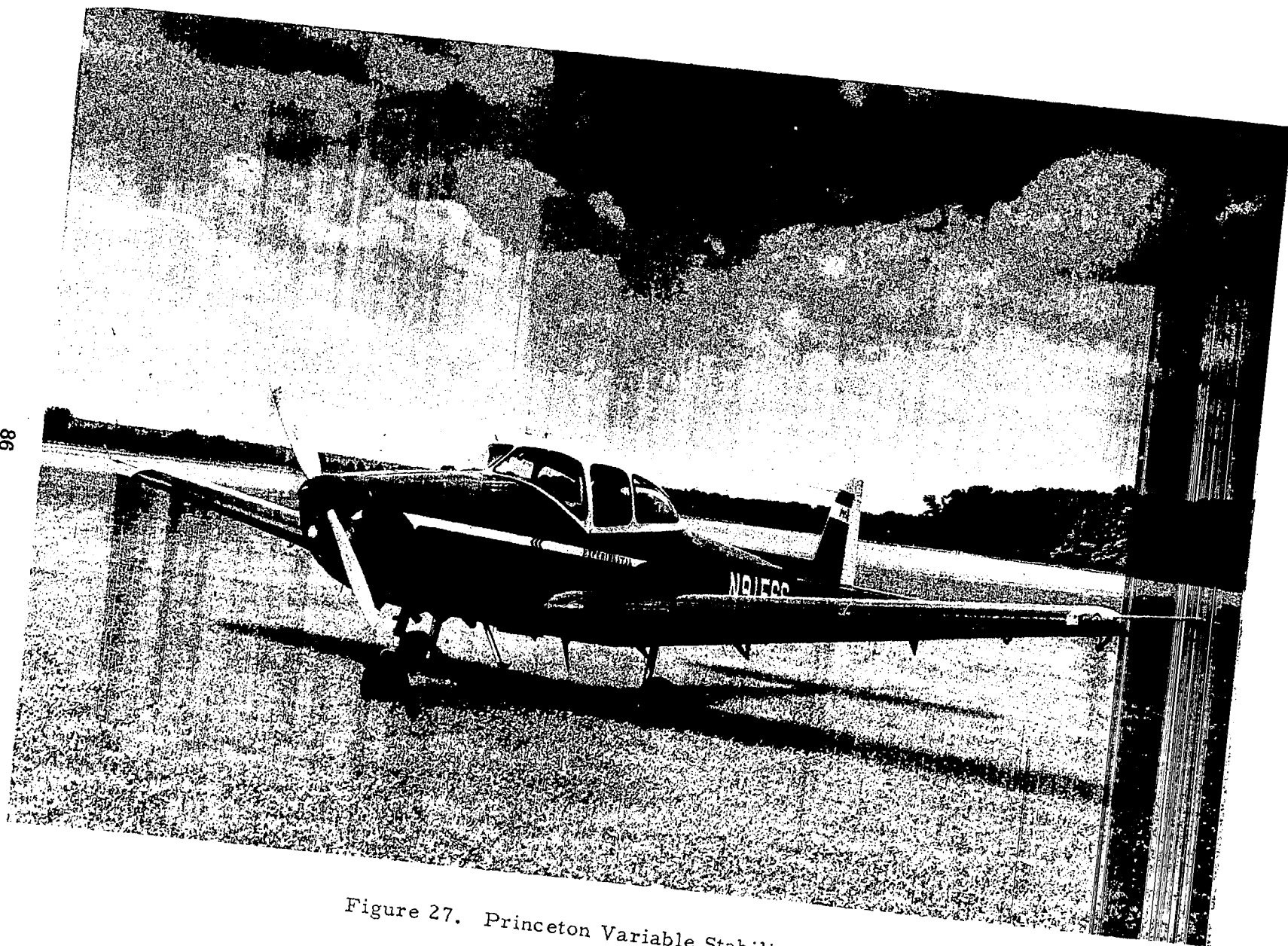
Figure 27. Princeton Variable Stability Navion
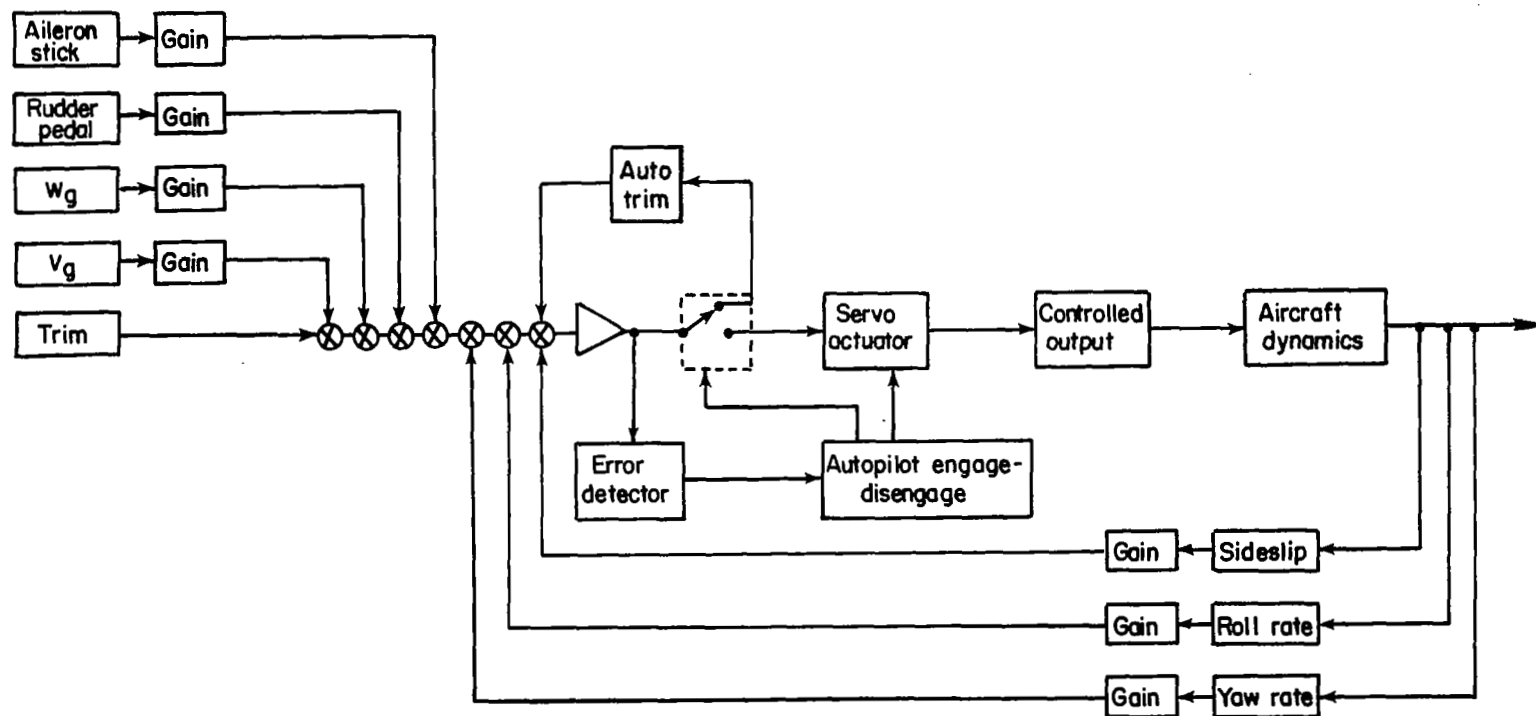
Figure 28.   Typical Variable Stability Control System Channel -
Lateral Directional Mode

aileron, and rudder control response characteristics may be altered. The elevator, aileron, and rudder cockpit controls have fixed force-displacement gradients and are the same as shown in Figure 5 of Reference 2.

Electronic circuitry in the automatic control system has been modified to incorporate the state of the art in solid state and printed circuit technology. Bendix hydraulic control surface servo actuators have been installed to drive the elevator, flap, throttle, and rudder. Typical frequency response characteristics of these servo actuators are

amplitude ratio	2 degrees peak to peak
natural frequency	10 cycles per second
damping ratio	.7

The ailerons are driven by two electro-mechanical actuators located in the wing adjacent to the individual surface bell cranks. Frequency response characteristics of these servos is given in Reference 2.

Safety circuits which disengage the automatic control system are activated by excessive error signals to the servo summing amplifier, by elevator and aileron control surface limit switches, by an abrupt opposing force applied to any of the primary cockpit controls by the safety pilot, or by an autopilot cutoff button on the safety pilot's control wheel. A typical block diagram is shown in Figure 28 for one axis of the control system.

Analog matching was used to achieve a proper correspondence between the airplane's response characteristics and the desired response produced by an analog computer simulation of the test configuration. The procedure and results are essentially those described in Reference 2.

The turbulence simulation system incorporated in the original version of the in-flight simulator was completely redesigned for this program. The new system is illustrated in the block diagram of Figure 29. The essential elements are a seven channel Pemco FM tape recorder capable of remote
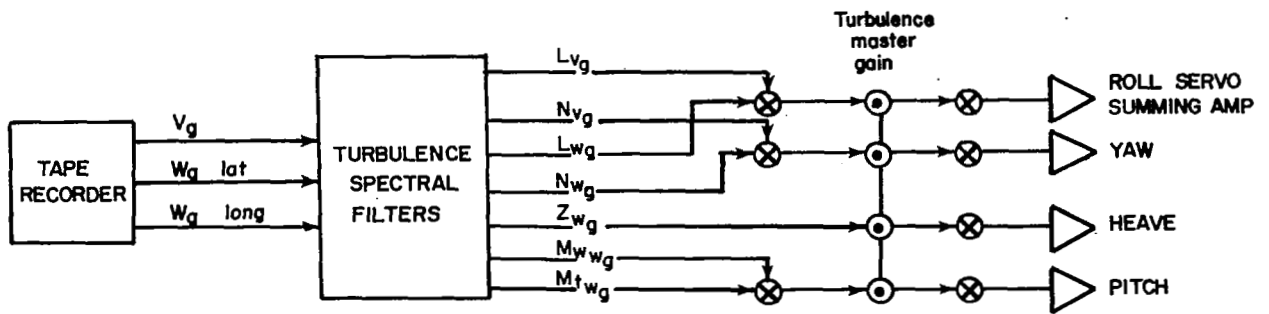
Figure 29.   Turbulence Simulation System
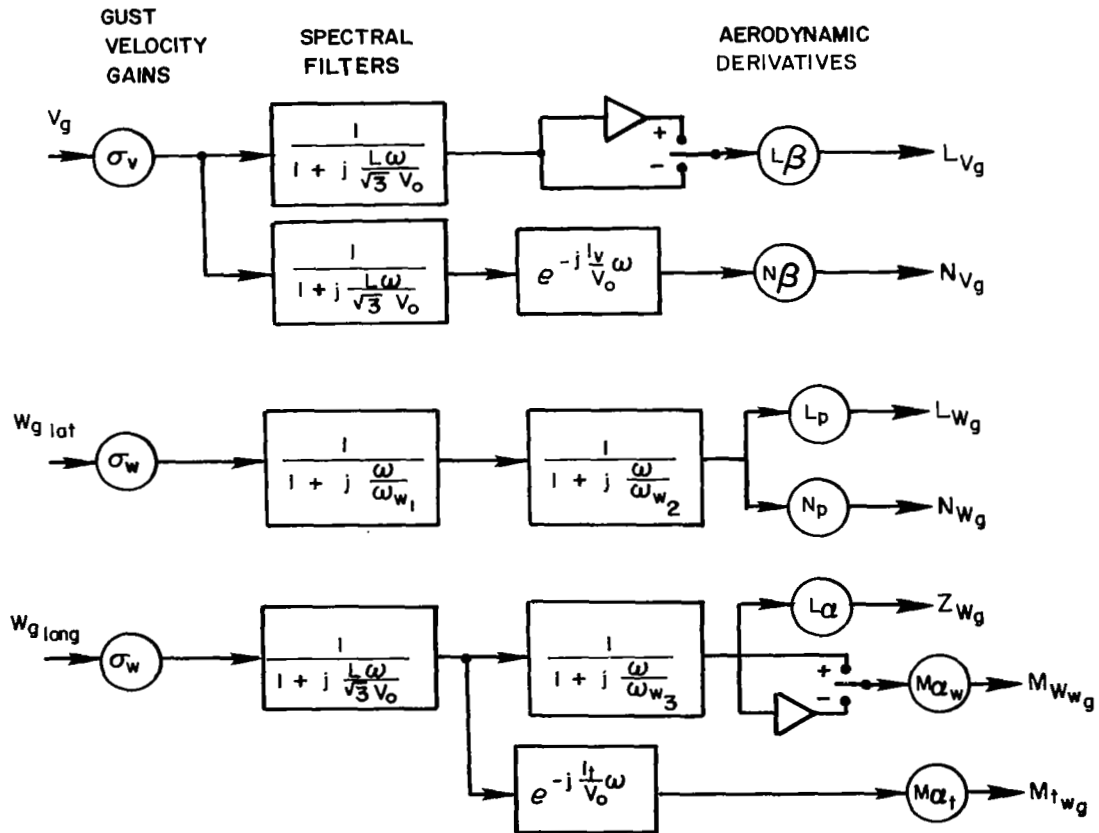
Figure 30.   Turbulence Spectrum Filter System

89

operation, and a set of linear first order lag filters and gain controls for the several components of turbulence. Prefiltered Gaussian white noise is recorded on three channels of the tape to represent the uncorrelated random gust components w_g (longitudinal), w_g (lateral), and v_g. The prefiltering consists of a 40 db/decade attenuation below .05 cps and a 20 db/decade attenuation above 4 cps for the longitudinal channel and above 2 cps for the two lateral channels. The low pass (2 or 4 cps) filtering was performed to reduce the high frequency excitation of the control servos. High pass filtering eliminated any steady state turbulence signals to exclude the possibility of control surface saturation as the airplane attempts to retrim for a change in the steady state gust velocity (wind direction) and to eliminate the steady sideslipped condition due to a steady lateral gust which occurs when the side-force component due to gusts is not simulated (Reference 2).

The three uncorrelated noise signals are then passed through the filter circuitry shown in detail in Figure 30. The appropriate spectral shaping is accomplished here by varying the filter break frequencies according to the simulation models of Section 3, and by adjusting the gains to match the appropriate amplitude characteristics associated with rms gust velocity and aerodynamic stability derivatives in the separate axes. A comparison of the simulated and actual turbulence spectra which illustrates the low and high frequency filtering is shown in Figure 31. First order Padé transport lag approximations are included to account for the separation of the horizontal and vertical tail surfaces from the wing. The performance of these lag filters is shown in the amplitude and phase plots of Figure 32. The perfect transport lag, represented by $e^{-j\omega\tau}$ in the frequency domain, is given for comparison. A list of the functions of the several controls for the turbulence model is given in Table 8.
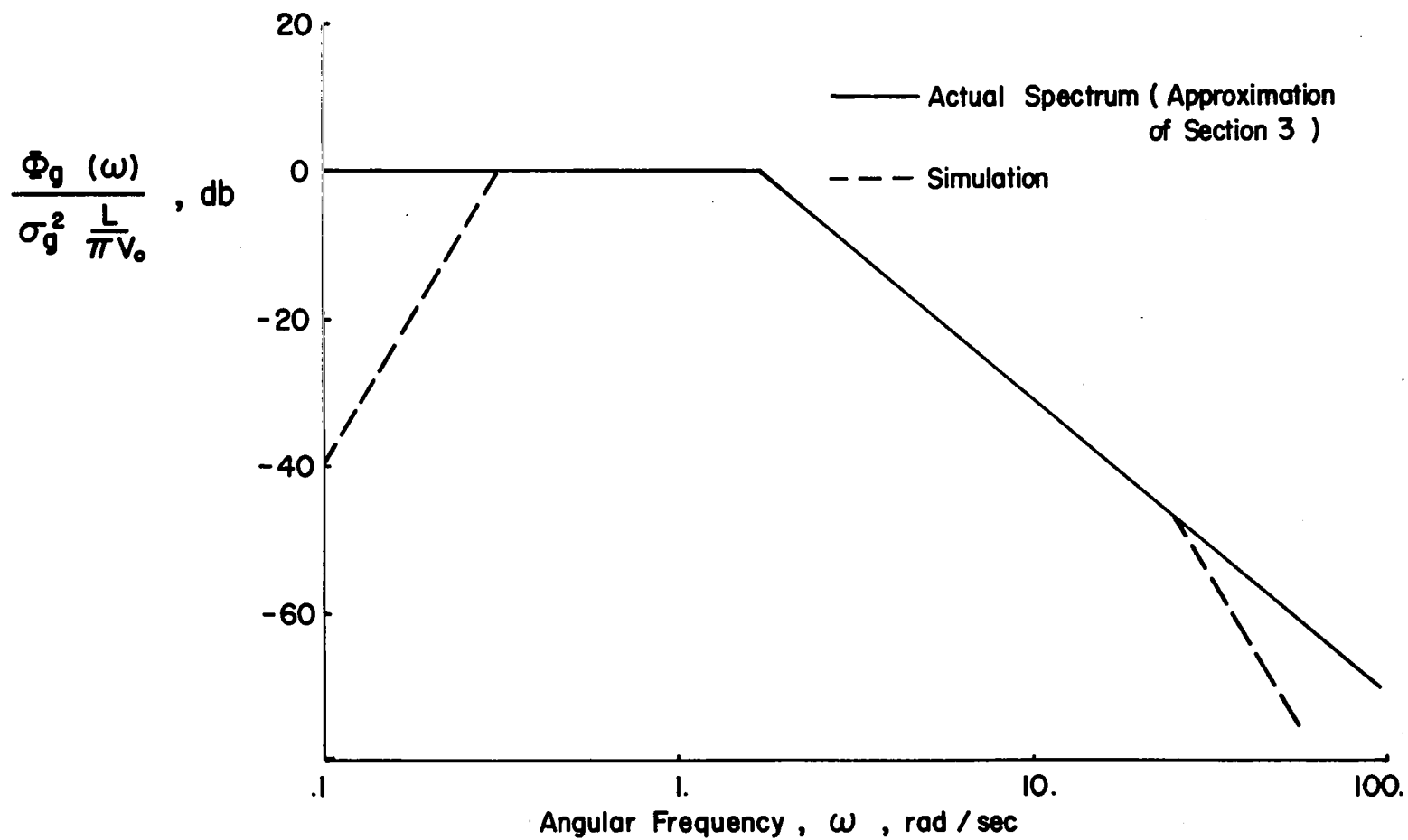
Figure 31. Asymptotes of Actual and Simulated Turbulence Spectra
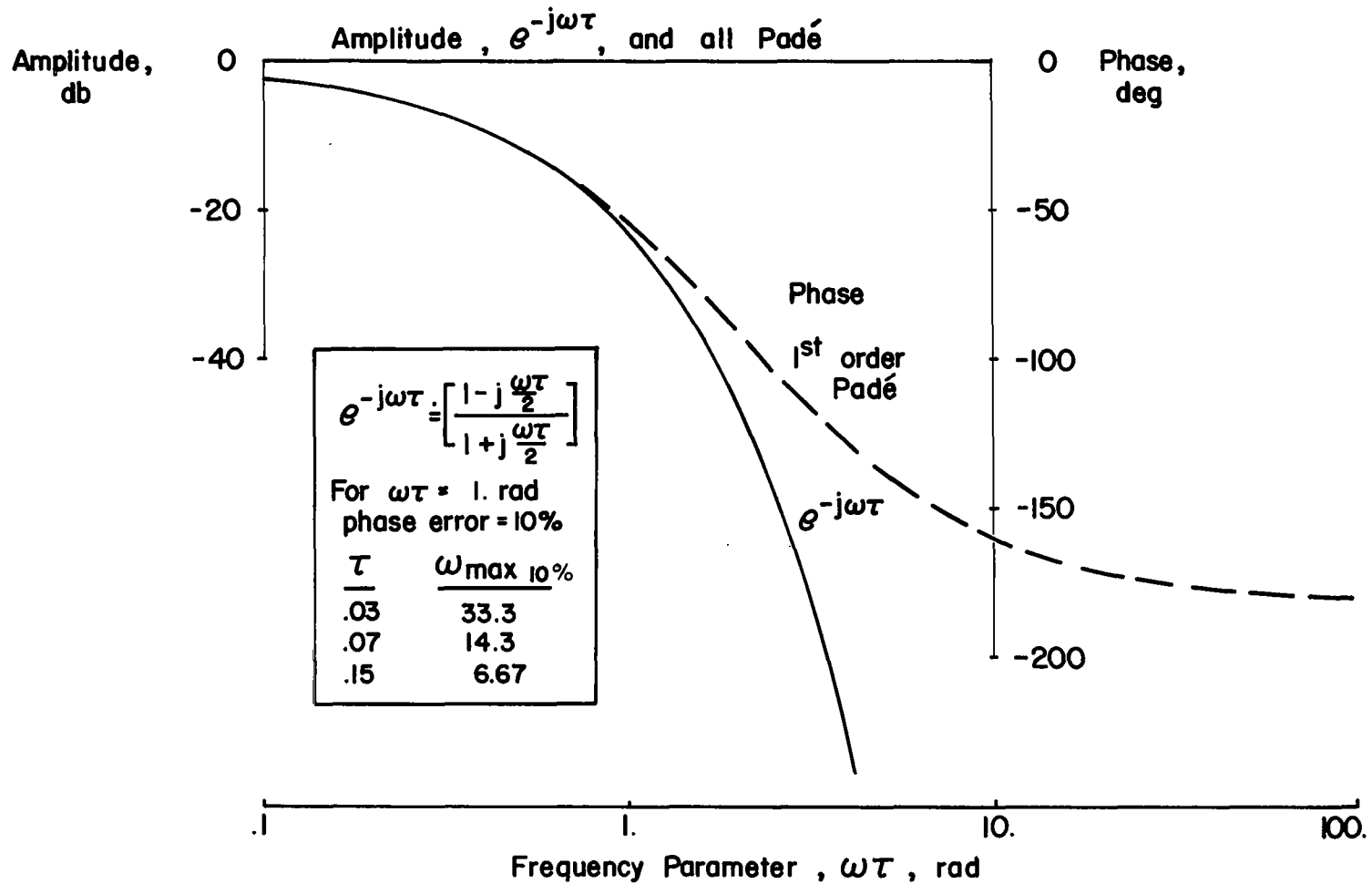
Figure 32. Comparison of Time Lag With First Order Padé
Approximation

TABLE 8

TURBULENCE SPECTRA CONTROLS
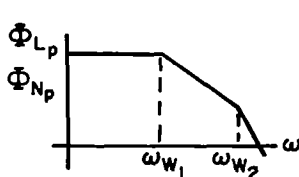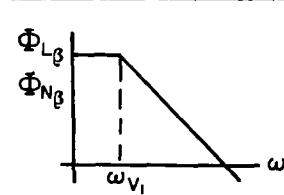
Pot	Parameter	Function	Spectra
$\sigma_{w_{lat}}$	$\sqrt{\dfrac{9}{\pi}\dfrac{V_o}{L}}\left(\dfrac{\sigma_w}{V_o}\right)$	Vary σ_w to jointly control σ_L and σ_N due to w_g; vary V_o/L consistent with ω_{w_1} and ω_{w_2} variations	
ω_{w_1}	$\omega_{w_1} = .35\left(\dfrac{V_o}{b}\right)^{3/4}\left(\dfrac{V_o}{c}\right)^{1/4}$	Vary low frequency break according to $\dfrac{V_o}{b}=\dfrac{V_o}{L}\cdot\dfrac{L}{b}$ and $\dfrac{V_o}{c}$	
ω_{w_2}	$\omega_{w_2} = 5.7\left(\dfrac{V_o}{b}\right)^{3/4}\left(\dfrac{V_o}{c}\right)^{1/4}$	Vary high frequency break	$\sigma_{L_w}^2 = 1.57\left(\dfrac{\sigma_w}{V_o}L_p\right)^2 \dfrac{V_o}{L}\left(\dfrac{V_o}{b}\right)^{3/4}\left(\dfrac{V_o}{c}\right)^{1/4}$
σ_v	$\sqrt{\dfrac{L}{\pi V_o}}\left(\dfrac{\sigma_v}{V_o}\right)$	Vary σ_v to jointly control σ_L and σ_N due to v_g; vary V_o/L to maintain constant σ as ω_1 changes	
ω_{v_1}	$\sqrt{3}\,\dfrac{V_o}{L}$	Vary low frequency break according to $\dfrac{V_o}{L}$ - roll and yaw channels	$\sigma_{L_v}^2 = \dfrac{\sqrt{3}}{2}\left(\dfrac{\sigma_v}{V_o}L_\beta\right)^2$
$\dfrac{\ell_v}{V_o}$	$e^{-\frac{\ell_v}{V_o}s} \doteq \dfrac{\left(1-j\frac{\ell_v}{2V_o}\omega\right)}{\left(1+j\frac{\ell_v}{2V_o}\omega\right)}$	Vary tail lag to control ρ_{LN}	$\sigma_N^2 = \dfrac{\sqrt{3}}{2}\left(\dfrac{\sigma_v}{V_o}N_\beta\right)^2$

TABLE 8 (continued)

Pot	Parameter	Function
L_p	L_p	Individual control over σ_{L_p}
N_p	N_p	Individual control over σ_{N_p}
L_β	L_β	Individual control over σ_{L_β}
N_β	N_β	Individual control over σ_{N_β}
M	Master gain	Control over σ_M, σ_Z, σ_L, σ_N

After the appropriate filtering is accomplished for each of the signals shown in Figure 30, these signals are fed to their respective control surface servos. A comparison of the side force, rolling moment, and yawing moment generated by the airplane's control surfaces with the force and moment disturbances encountered in actual turbulence is made below.

Actual Turbulence   Simulation

$$
\begin{Bmatrix} Y_{v_g} \\ L_{v_g} \\ N_{v_g} \end{Bmatrix} + \begin{Bmatrix} 0 \\ L_{w_g} \\ 0 \end{Bmatrix}
\qquad
\begin{Bmatrix} 0 \\ L_{\delta a} \\ N_{\delta a} \end{Bmatrix} \left\{ \frac{\delta a}{L_{v_g}} \frac{v_g}{V_o} + \frac{\delta a}{L_{w_g}} \frac{w_g}{V_o} \right\} + \begin{Bmatrix} \dfrac{Y_{\delta r}}{V_o} \\ L_{\delta r} \\ N_{\delta r} \end{Bmatrix} \left\{ \frac{\delta r}{N_{v_g}} \frac{v_g}{V_o} \right\}
$$

(assuming $Y_{w_g} \doteq N_{w_g} \doteq 0$)

$$
\frac{\delta a}{L_{v_g}} = \frac{L_{\beta_g}}{L_{\delta a}}, \quad \frac{\delta a}{L_{w_g}} = \frac{L_{P_g}}{L_{\delta a}}, \quad \frac{\delta r}{N_{v_g}} = \frac{N_{\beta_g}}{N_{\delta r}}
$$

Four anomalies appear in this comparison which deserve attention. First, the aileron yaw derivative results in yawing moments being produced in proportion to the amount of rolling moment (L_{v_g} and L_{w_g}) being simulated. Since the amplitude scaling and spectral shaping for yawing moments is accomplished in the rudder channel, in a strict sense the aileron yawing moments are a source of error in the simulated yaw disturbances. In reality, these errors are minimal due to the low level of aileron yaw of the Navion ($\frac{N_{\delta a}}{L_{\delta a}}$ = .007 for the basic airplane) and they are disregarded. Second, the rudder roll derivative could produce rolling moments in proportion to the magnitude of yawing moment being simulated (N_{v_g}). This problem is the converse of the aileron yaw problem just discussed. The error which would result in this case is eliminated by a rudder to aileron interconnect which is

95

used to cancel the $L_{\delta r}$ derivative. The third difficulty is concerned with the inability to simulate side forces in the proper proportion. This problem was discussed at some length at the beginning of Section 3. It was concluded that the error in side force simulation was tolerable since no errors of significance appear in the airplane's roll, yaw, sideslip, or lateral acceleration response to turbulence, at least so long as the low frequency turbulence components are removed. Finally, no attempt was made to account for the unsteady aerodynamic effects accompanying control deflection. It has been noted previously that turbulence signal inputs to the lateral-directional control system were attenuated above 2 cps. Transient aerodynamics associated with any of the Navion's control surfaces were expected to be present at frequencies in excess of this value for the flight condition used in the test program. Consequently, the simulated disturbance spectrum would not be influenced to any significant extent by unsteady aerodynamics. Of course the simulation itself departs from the turbulence model above approximately 1 cps due to the 2 cps low pass filter. Based on preliminary flight tests, this compromise in the simulation was found to be of little or no consequence to the pilot since the energy level at high frequency was low enough to hardly be apparent to him.

The cockpit environment of the Navion is shown in Figure 33. Panels containing the variable stability system controls and the tape recorder, portable control box and control pedestal for the turbulence system are indicated. The evaluation pilot is provided with a standard instrument display (gyro horizon, directional gyro, airspeed indicator, altimeter, instantaneous rate of climb indicator, and turn and bank instrument). A center stick control and conventional rudder pedals using linear springs to provide force sensing are provided. The stick geometry is also noted in Figure 33. Throttle control is at the pilot's left hand.

Since he is supposedly performing only perturbation flight maneuvers, no propeller pitch control (rpm) is used. In addition, a thumbwheel proportional controller regulating direct lift control through the flaps is also available to the pilot. This mode of control was not subject to evaluation and was not used in this program.

Analog data collection was achieved using an air to ground radio telemetry link. A total of 43 channels of data are mechanically sampled 20 times per second and multiplexed on a single carrier signal for transmission to the ground receiver. A sampling rate of 40 times per second can be obtained if an individual item of data is connected to two telemetry channels. The telemetered data are received in the ground station shown in Figure 34. Five separate channels of data can be immediately translated from the carrier signal and used as inputs to the analog computer for simulation or can be scaled on the computer and displayed on the chart recorder. The multiplexed signal may also be tape recorded for future evaluation.

The evaluation program was carried out primarily by two pilots. One pilot had a combined military and civil airplane background of some 3500 hours, of which approximately 1000 hours were logged in single and multi-engine civilian airplanes. He had a flight test engineering background with current experience as a flying qualities evaluation pilot and held commercial and instrument ratings. The other pilot had a total of 4500 hours in single and multi-engine airplanes and held an ATR rating. Both pilots participated in the qualitative evaluation and task performance phases of the test program. Some limited pilot rating data were also obtained from two additional pilots who were also professional flight test engineers and flying qualities evaluation pilots. These pilots were available to the test program on a limited basis. It was not possible under these circumstances to acquire a complete set of evaluation data from either of these pilots.

CONTROL STICK GEOMETRY
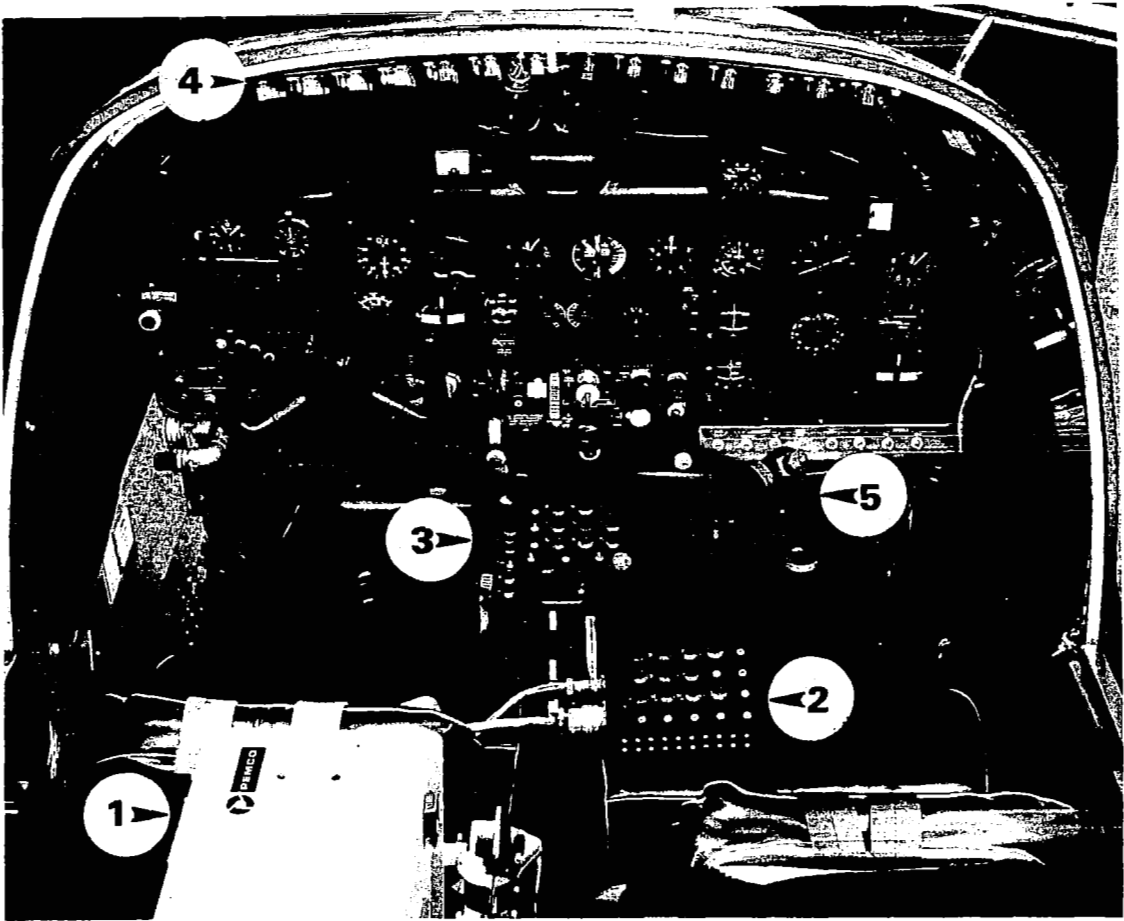
1. Tape Recorder
2. Turbulence Filter Circuitry
3. Individual Gain Controls
4. Variable Stability Feedback Gains
5. Control Stick (including DLC
   thumbwheel control)

center of hand grip

16.75"
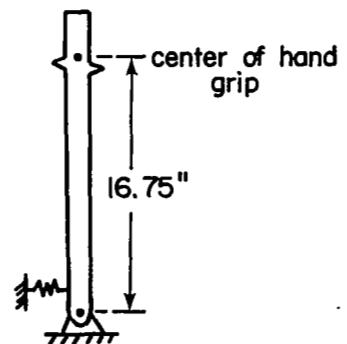
Lateral Force Gradient
4.0 lb/in. at hand grip

Figure 33. Cockpit Environment Including Control Stick Geometry

1. Telemetry Receiver
2. Telemetry Patch Panel and Decoder
3. FM Tape Recorder
4. EAI TR 48 Analog Computer
5. 6 Channel Pen Recorder
6. Communications Transceiver
7. Voice Tape Recorder
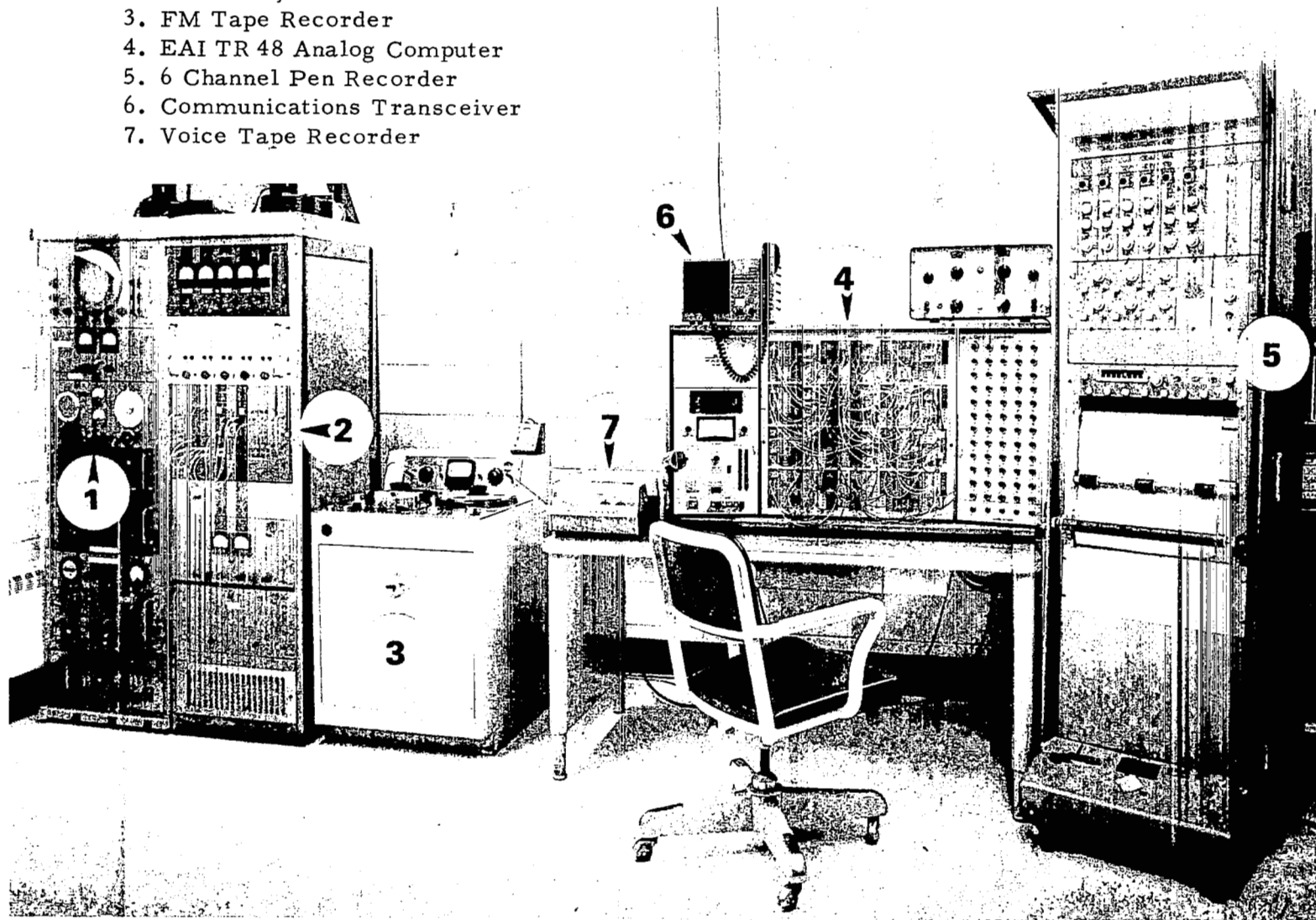
Figure 34. Telemetry Ground Station and Computer Facility

Data Analysis

Flight test data in the form of continuous time histories of the airplane's motion and the pilot's control activity in response to the simulated turbulence upsets were converted to discrete time samples and analyzed for measures of task performance and pilot workload and compensatory characteristics using a digital computer.

Conversion of the flight data from analog to digital form was accomplished with the equipment shown in Figure 35. A block diagram of the process is shown in Figure 36. The multiplexed signal on tape is first separated into individual data channels using a ground based telemetry decoder identical to the one in Figure 34. The channels selected for analysis are then connected to first order high pass filters which attenuate low frequency components of the signal and reduce the influence of any steady state or slowly varying bias on the data. Second order low pass filters (ω_n = 5 cps, ζ = .7) are then used to attenuate any high frequency noise. These filters are matched to preserve amplitude and phase relationships between the several channels for the frequency range of interest ($\omega > .5$ rad/sec). Next the data are passed through an analog-digital converter which digitizes the continuous time histories at a rate of 40 samples per second. The discrete data samples are then stored on tape for further processing.

The first step in the digital analysis procedure involves calibration of the individual data channels. At the beginning of each tape recording of digitized time histories, a reference data run was included which consisted of recording the zero and full scale reference signal of the telemetry unit. All subsequent data in the individual channels are compared to these reference signals and are then calibrated in terms of the full scale signal. Conversion to dimensional form can be made knowing the equivalence of the full scale telemetry signal to the physical dimensions involved.

1. FM Tape Recorder
2. Telemetry Decoder
3. Analog-Digital Converter
4. Digital Tape Recorder
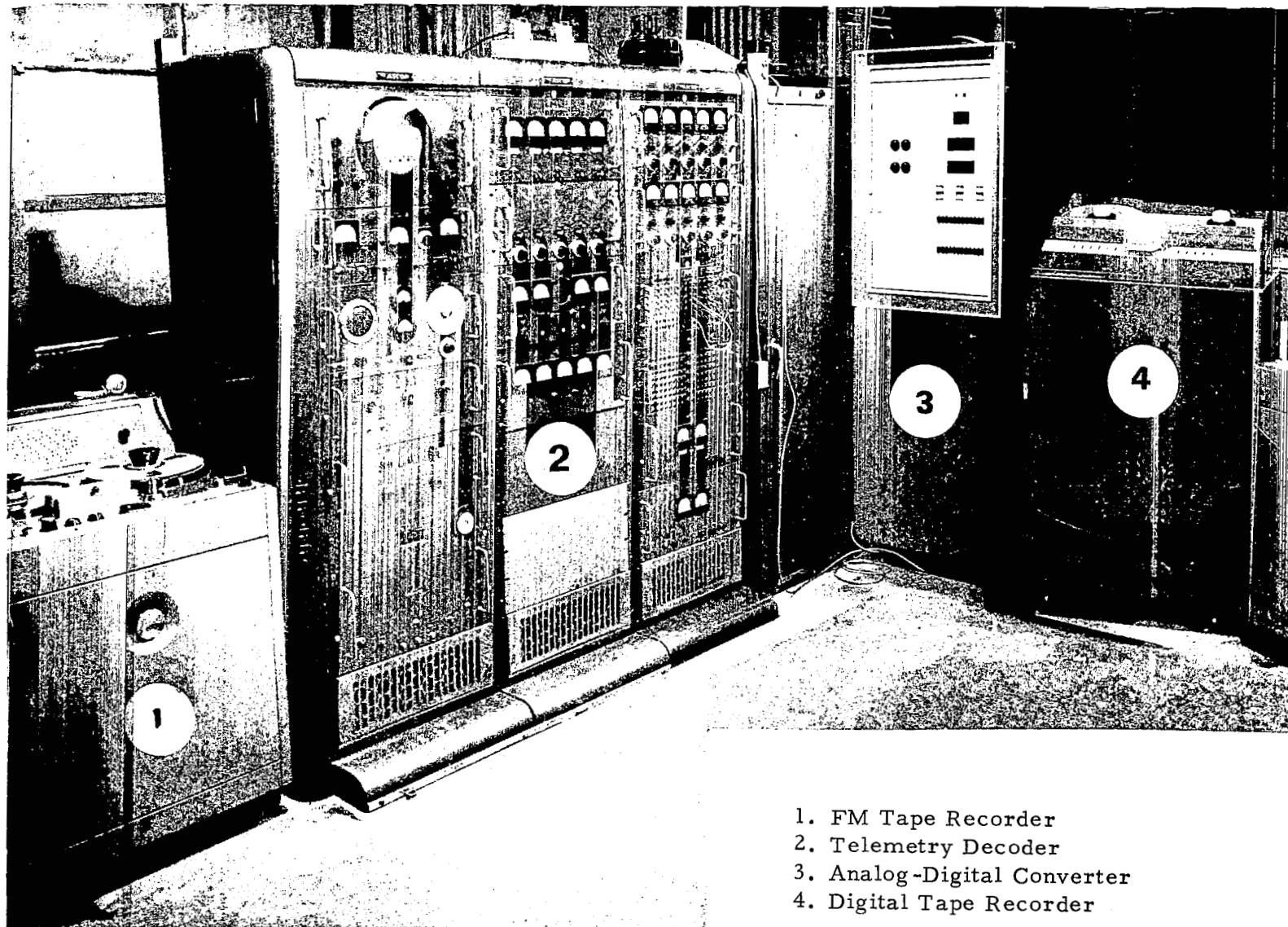
Figure 35. Analog-Digital Data Processing Equipment
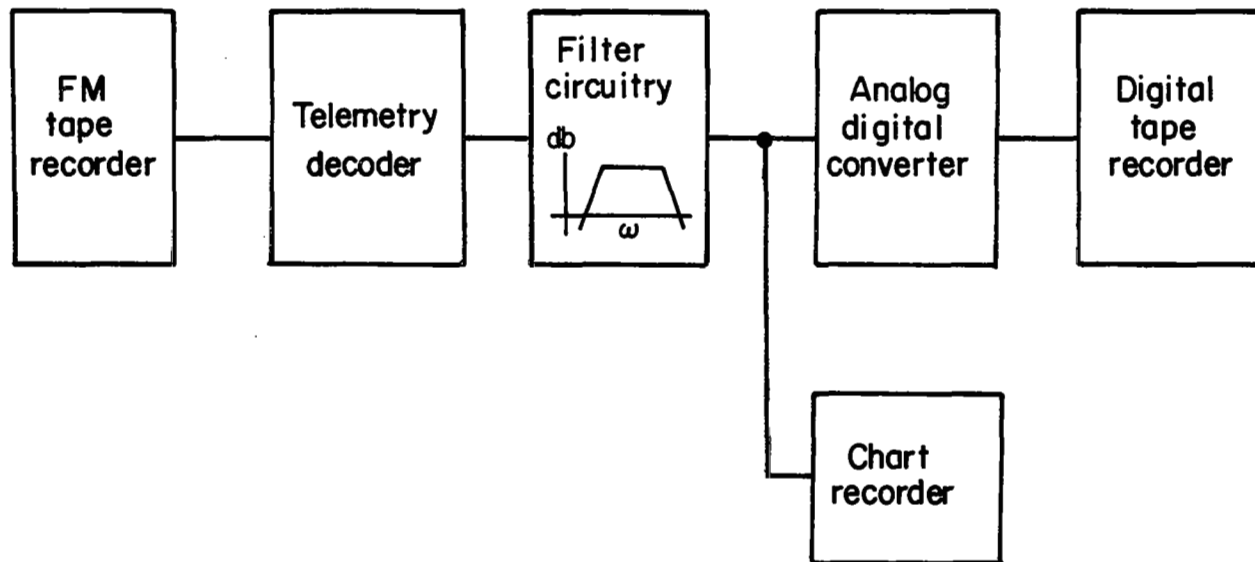
Figure 36. Analog-Digital Data Processing Procedure

Specific steps in the data analysis include measurement of the auto-correlation and cross-correlation functions and power and cross-spectral density functions for the variables of interest. The computer procedure for calculation of correlation functions is described by

$$R_{ij}(\tau) = \frac{1}{N} \sum_{n=1}^{N} x_i(n) \, x_j(n + \tau) \tag{86}$$

where

$i = j$ auto-correlation

$i \neq j$ cross-correlation

τ is an integer multiple of the sampling interval

When $\tau = 0$, the auto-correlation function is equivalent to the mean square value $\sigma_{x_i}^2$. The length of an individual test run typically was two minutes. Allowing for approximately fifteen seconds at the beginning of each run to eliminate the effects of transient behavior in the data reduction equipment, the usable data was on the order of 100 seconds. Time lags (τ) up to five seconds were used in the analysis, permitting the use of 3800 data points in the correlation computations.

Spectral densities were determined based on the relationship

$$\Phi_{ij}(\omega) = \frac{F_{x_i}(\omega) \, F_{x_j}^{*}(\omega)}{2T} \doteq \frac{\Delta t}{N+1} \left(\sum_{n=-N/2}^{N/2} x_i(n) e^{-j\omega n \Delta t} \right) \left(\sum_{m=-N/2}^{N/2} x_j(m) e^{+j\omega m \Delta t} \right) \tag{87}$$

using the computation procedure described in Reference 37. Transforms of the time domain data were obtained using a Fast Fourier Transform routine discussed in Reference 37 which was adapted for the IBM 360-30 computer.

103

While a spectral window of fixed bandwidth $(\Delta\omega = \frac{2\pi}{T})$ is used in this routine, provision was made for averaging over wider frequency bands. This permitted a suitable trade-off to be made between resolution on the frequency scale and accuracy of the transform computation.

SECTION 5

ANALYSIS OF RESULTS

Synopsis of the Discussion

A considerable amount of the data obtained in this test program is in the form of pilot opinion ratings and detailed commentary on the flying qualities of the individual configurations. Time history measurements of the airplane's motion, the pilot's control activity, and the simulated turbulence disturbances were also made for selected test runs during the program. These measurements permit the precision of task performance, the level of the pilot's control workload, and the extent of compensation required of him to be assessed for each configuration. The first part of this section is devoted to the presentation and interpretation of these results. The pilot opinion data and commentary are considered in the conventional manner by graphically displaying the pilot opinion ratings as functions of the pertinent test variables and by indicating the nature of the degradation in flying qualities through brief summaries of the pilot commentary compiled for each configuration. Measures of task performance, workload, and pilot compensation are compared with the pilot opinion data to provide quantitative support for the pilot opinion trends. The primary data in this regard are rms bank angle and heading excursions and rms aileron and rudder activity. Where these performance and workload data are inadequate to explain trends of pilot opinion, the nature of the pilots' compensation, depending on its availability from experimental measurements, are included in the interpretation. A complete tabulation of pilot opinion data and summaries of pilot commentary are included in Appendix E for each configuration.

It should be understood that the objective of this analysis is to identify the significant influences on lateral-directional flying qualities of the turbulence and dynamics parameters considered in this test program. This is an attempt to distinguish between important and unimportant effects, and not to establish absolute levels of flying qualities as functions of turbulence or dynamics. Neither the number of pilots nor the number of evaluations per pilot suffice to provide a set of data to which pilot opinion boundaries can be assigned with a high degree of confidence. However, it is reasonable to expect that a professional test pilot when presented with a number of test variables, each of which cover a wide range, can identify the important influences among these variables on his ability to perform an assigned task.

The second part of Section 5 involves an attempt to explain the results of the test program on the basis of closed loop pilot-vehicle systems theory. The underlying objective is to see whether these results can be understood analytically in a sufficiently general way to permit their extension to airplane configurations and turbulence environments not specifically examined in this program. It is also of interest to study the trends in closed loop performance and workload with the test program parameters which would be predicted by closed loop system theory. An analog computer simulation utilizing a transient analog representation of the gust input (described in Appendix C) was used to generate data on rms bank angle and heading excursions and rms aileron and rudder activity. The results of this study are used to assess

- the influence of pilot compensation on the trade-off between performance and workload for a given configuration and
- the influence of the parameters of turbulence and airplane dynamics on performance and workload.

106

Results of the Flight Test Program

Contribution of turbulence - Rms disturbance level

The effects of the rms magnitude of turbulence disturbances on pilot opinion rating are shown in Figure 37. The data of the upper diagram are for a given set of lateral-directional dynamics (Configuration 1, T_R = .25 seconds, ω_d = 2.3 radians/second, ζ_d = .1) and for a spectral bandwidth corresponding to $\frac{V_O}{L}$ = 1.0 radian/second. Average pilot opinion ratings for each pilot are noted adjacent to each test point. The primary evaluation pilot's rating is located at the right while the secondary pilots' ratings (if any) are found above and below the point. Iso-opinion contours are faired to the primary pilot's data. The consequences of increasing the rms turbulence level appear not too severe for the range of rms levels shown for this case of good lateral-directional dynamics. It is apparent that the pilot is more sensitive to yaw disturbances than to roll disturbances. For a satisfactory level of flying qualities, the magnitude of yaw disturbances which can be tolerated is on the order of 25 percent of the roll disturbance magnitude.

The trends described above are typical of the data for each pilot in the test program. The actual magnitudes of the pilot opinion ratings obtained from the different test subjects vary somewhat at the higher turbulence levels. This dispersion in ratings apparently is a result of the individual pilot's interpretation of the amount of yaw turbulence and of the degree of activity in the roll axis (both roll excursions and workload) which can be tolerated without degrading performance in the heading tracking task. The primary evaluation pilot's ratings were intermediate to those of the secondary pilots (indicated separately) in nearly every instance.

Pilots' commentary indicates that the degradation with increasing turbulence level is due to the increase in bank angle and heading excursions. Furthermore, the pilots seem to be able to judge the magnitude of the actual disturbances
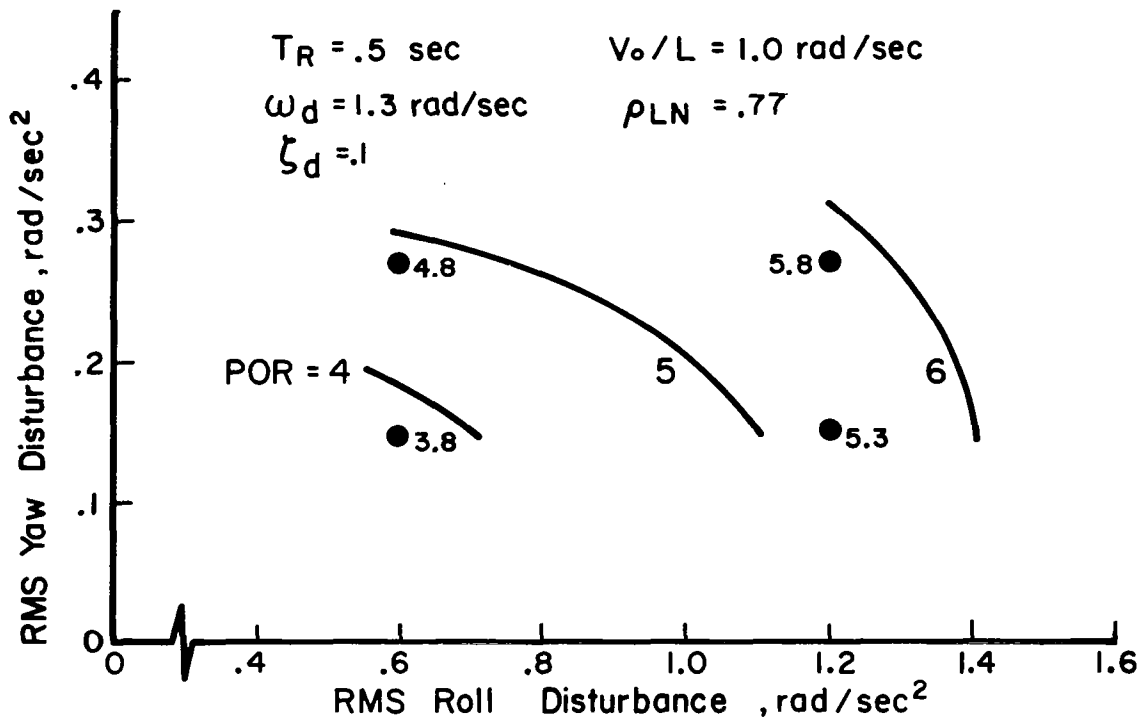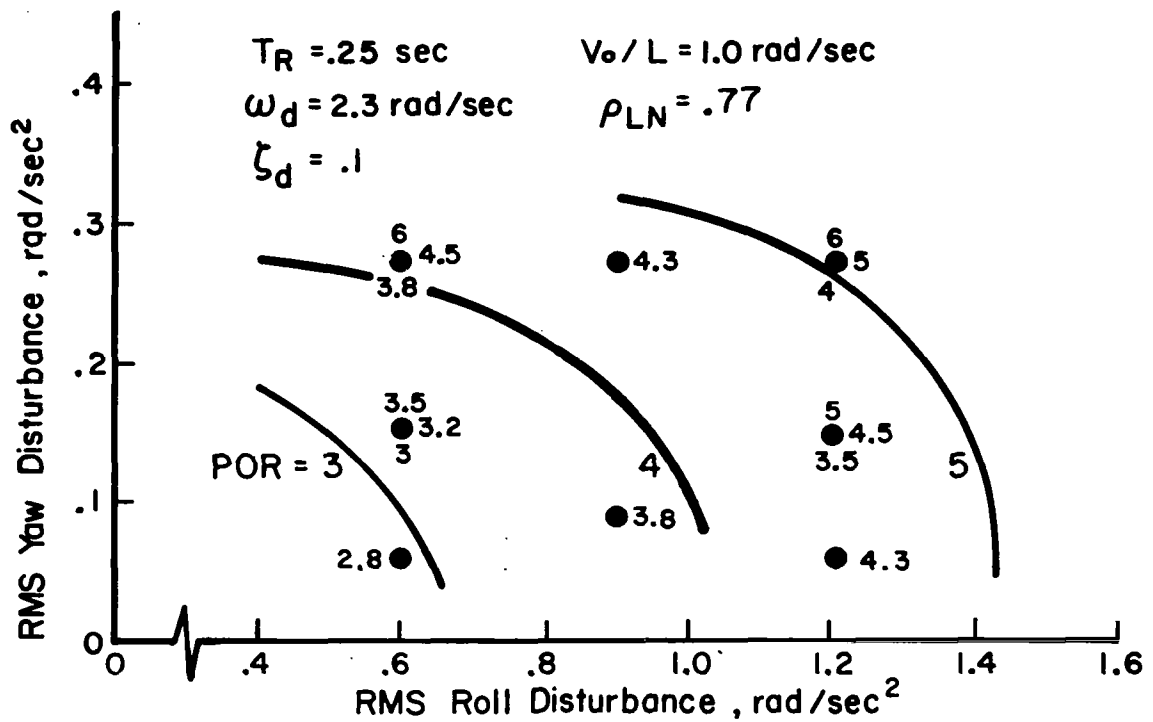
Figure 37. Effect of RMS Roll and Yaw Disturbances on Pilot Opinion
Ratings

by sensing the initial acceleration associated with the disturbance, although this does not appear to be the predominant basis for their ratings. This sensing of the turbulence appears to provide a cue to alert the pilots to the general level of the turbulence and may, because of the poor ride characteristics and the anxiety associated with the larger disturbances, have a partial influence on the opinion rating. However, the dominant reason given during the flights and in post flight debriefings for the degradation in ratings is the magnitude of the airplane's excursions in rough air or, conversely, the effort required of the pilot to maintain a desired level of task performance regardless of the magnitude of turbulence. For the case of large yaw disturbances, the pilot was forced to use the rudder to control heading excursions. While slower, low frequency heading changes were still made through bank angle commands to the ailerons, it was absolutely necessary to resort to the rudder for control of higher frequency yawing motions. Some note was also taken of increasing sideslip accompanying the large yaw disturbances and the distracting influence this had on the heading tracking task.

For the configuration having unsatisfactory flying qualities, shown in the lower diagram of Figure 37 (Configuration 6, T_R = .5 seconds, ω_d = 1.3 radians/second, ζ_d = .1), the trends in pilot ratings with turbulence magnitude in roll and yaw appear to be similar to those of Configuration 1. While the overall ratings are worse for the case of poor dynamics, the increments in pilot ratings with increasing turbulence are generally the same as for Configuration 1. Pilot commentary emphasizes the reduced roll damping and directional stability and the corresponding problems with bank angle and heading control. Excursions in roll and heading are observed to be large when the pilot does not maintain tight control and more effort is required of the pilot to achieve the desired level of task performance than for the case of good dynamics.

Variation in the precision of task performance and workload with the turbulence disturbance level are shown in Figures 38, 39, and 40. Task

$T_R = .25$ sec $\qquad V_o/L = 1.0$ rad/sec
$\omega_d = 2.3$ rad/sec $\qquad \sigma_N = .15$ rad/sec^2
$\zeta_d = .1$

○ δa_S
□ ϕ

○ primary pilot
● secondary pilot

RMS Stick Force , lb
RMS Aileron Stick, in.
RMS Bank Angle , deg
RMS Roll Disturbance , rad/sec^2

○ δr_p
□ ψ

RMS Pedal Force , lb
RMS Rudder Pedal, in.
RMS Heading, deg
RMS Roll Disturbance , rad/sec^2
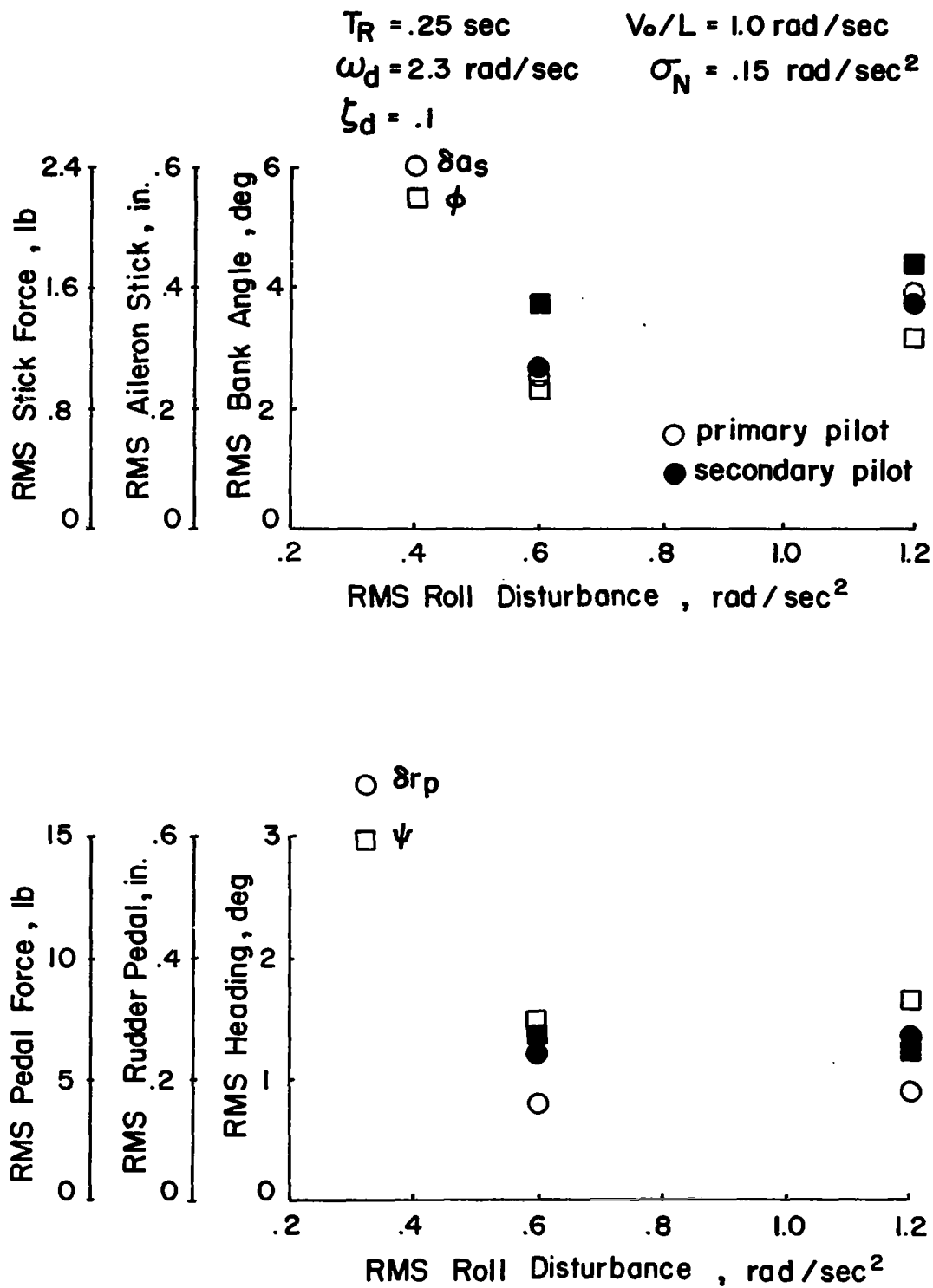
Figure 38. Trends of Task Performance and Pilot Workload with Roll Turbulence-Configuration 1

110
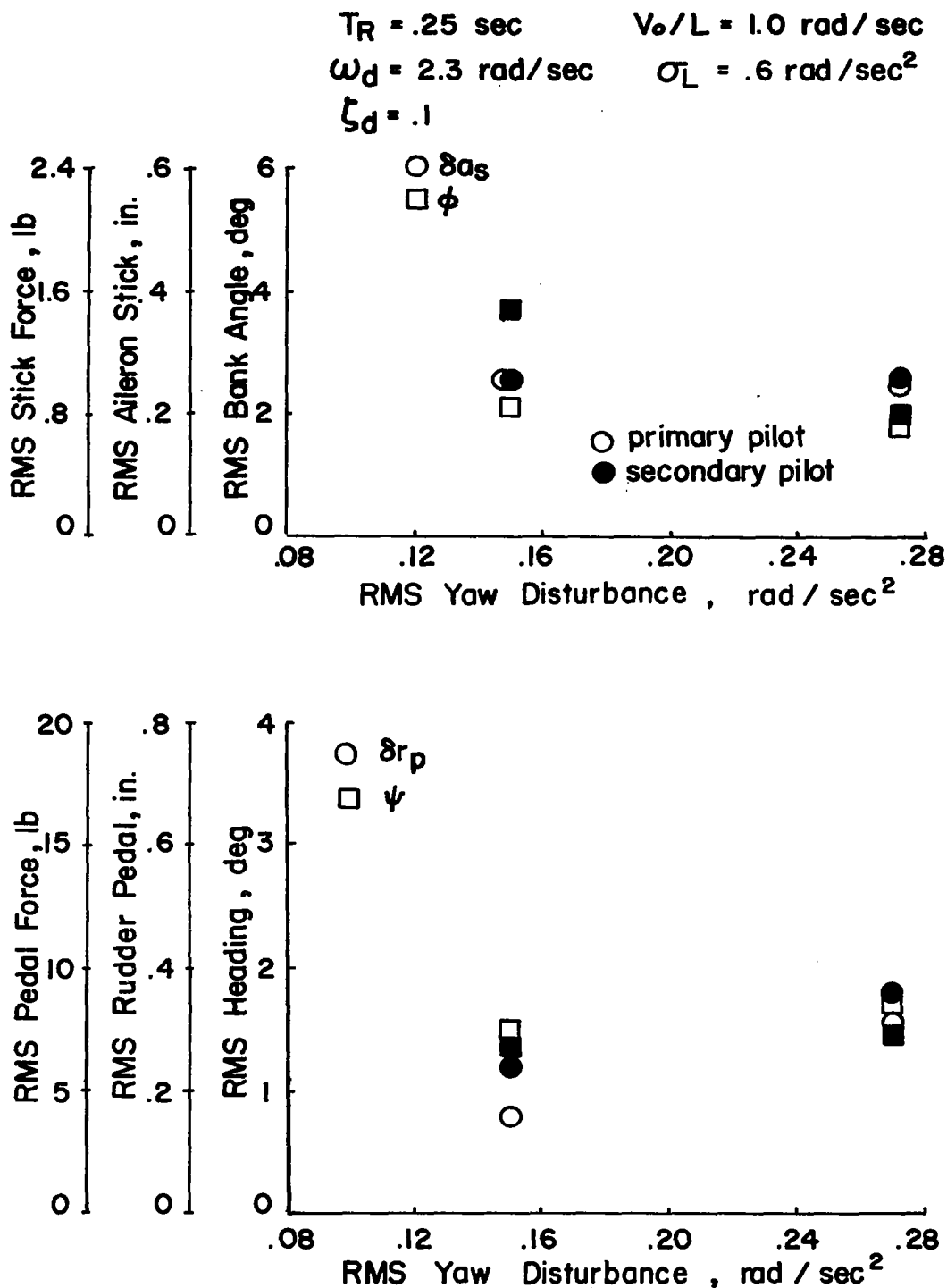
Figure 39. Trends of Task Performance and Pilot Workload with Yaw Turbulence-Configuration 1

$T_R = .5$ sec $\qquad V_o/L = 1.0$ rad/sec

$\omega_d = 1.3$ rad/sec $\qquad \sigma_N = .27$ rad/sec^2

$\zeta_d = .1$

$\sigma_L = 1.2$ rad/sec^2
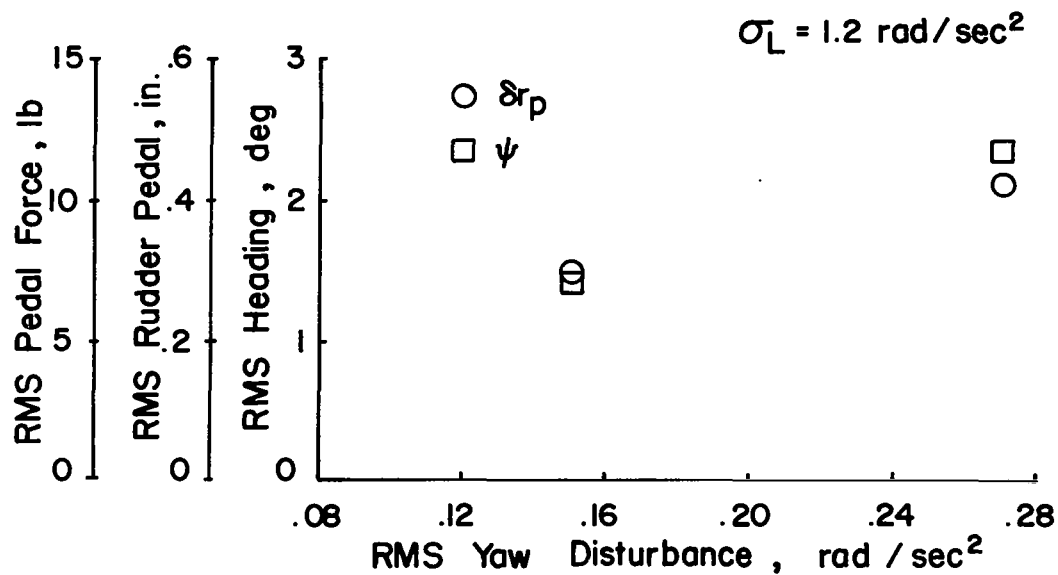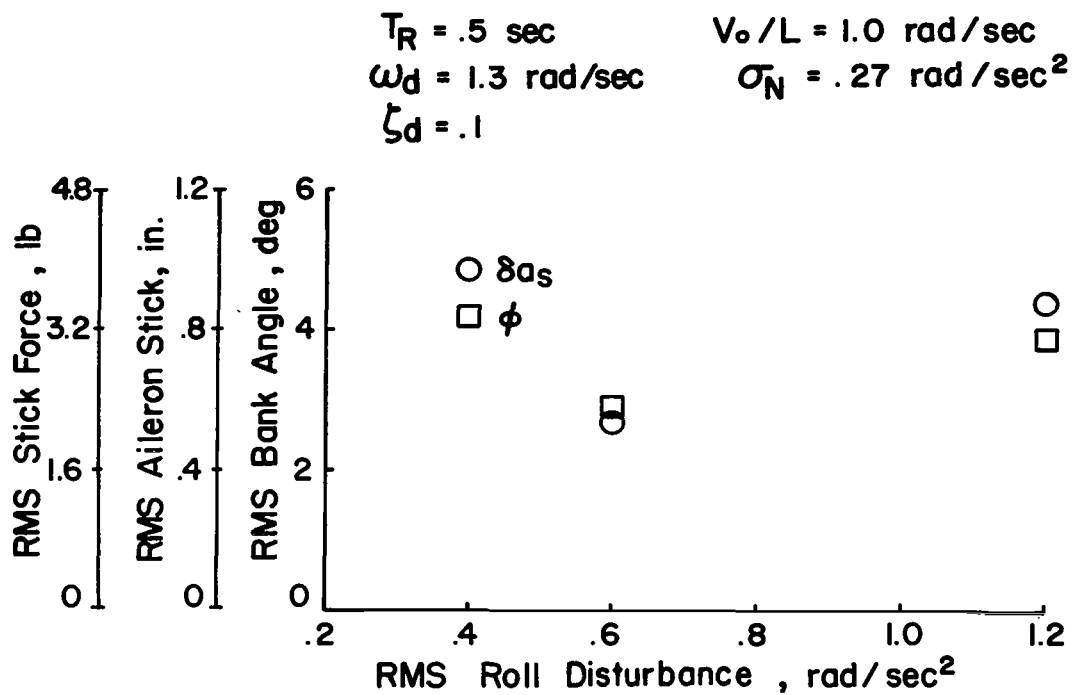
Figure 40.   Trends of Task Performance and Pilot Workload with
Roll and Yaw Turbulence - Configuration 6

performance is measured in terms of rms bank angle and heading excursions. Control workload is measured either in terms of rms aileron stick and rudder pedal displacement or rms stick and pedal force. In general, it can be stated that the degradation in pilot ratings with increasing turbulence level is accompanied by increases in pilot workload and by degradation in task performance. For Configuration 1 and for a bandwidth of 1.0 radian/second (Figure 38), the adverse effect of larger roll disturbances appears to be both an increased roll workload and larger excursions in bank angle. No significant changes in heading performance or rudder workload are apparent. An increase in the level of yaw disturbances, shown in Figure 39, primarily seems to increase rudder workload. Roll excursions and aileron control activity remain essentially unchanged. These data, shown as open symbols (O), are for the primary evaluation pilot and are substantially supported by the secondary test pilot's results indicated by solid symbols, ($\bullet$). Although the level of roll activity might be expected to increase for the larger yaw disturbances because of the coupling between roll and yaw provided by dihedral, this effect is apparently cancelled because the pilot is able to keep the level of yaw activity constant as the turbulence is increased.

Trends in workload and performance for Configuration 6 are shown in Figure 40 and are generally the same as shown for Configuration 1.

Contribution of turbulence – Spectral bandwidth

Trends of pilot opinion ratings with turbulence spectral bandwidth are shown in Figure 41. The data are presented for the case of good lateral dynamics (Configuration 1) and are given in terms of the equivalent rms sideslip disturbance and the spectral break frequency, $\frac{V_o}{L}$. For a given cruise speed (in this case, 120 mph) the sideslip disturbance may be interpreted as a specific lateral gust velocity. Furthermore, while the data are presented for various levels of rms sideslip for a specific magnitude of dihedral and directional stability ($L_{\beta_g} = -16.$, $N_{\beta_g} = 5.$) the results can be considered equally well in terms of increasing L_{β_g} and N_{β_g} for a constant rms sideslip disturbance.
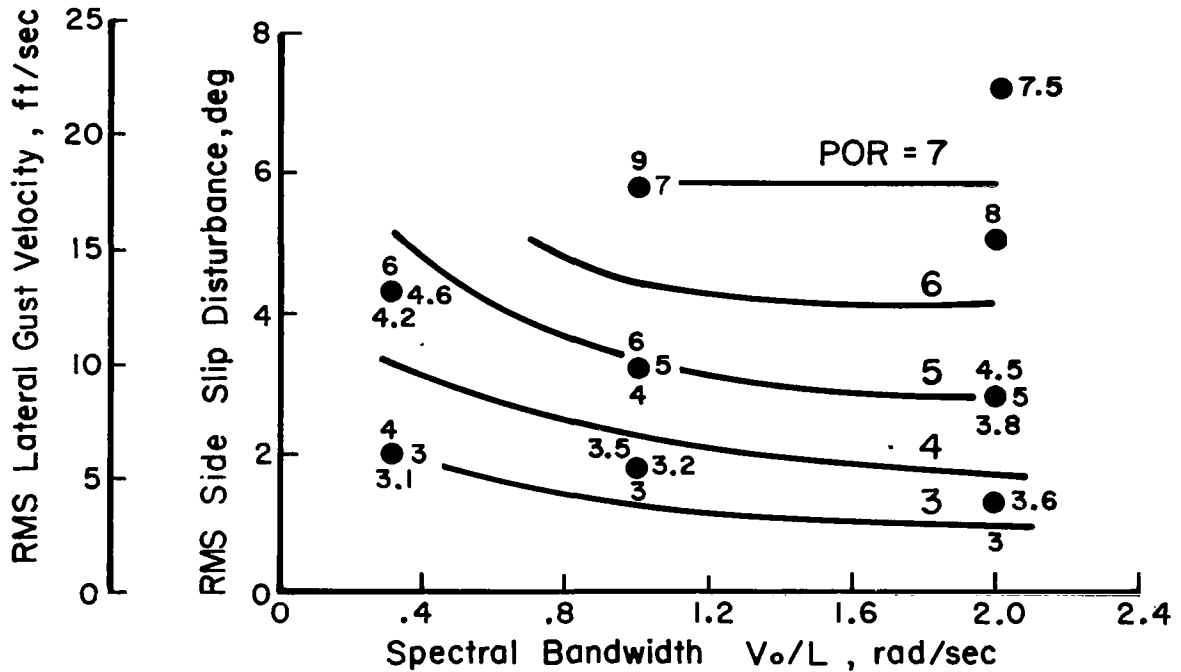
Figure 41. Influence of Spectral Bandwidth on Pilot Opinion Ratings - Configuration 1

A moderate influence of spectral bandwidth is observed in the pilot opinion data of Figure 41. Most of the degradation in flying qualities is noted with increasing bandwidth up to $\frac{V_o}{L} \doteq 1.0$ radian/second. However, the dominant influence in this set of data is still the rms level of the turbulence. The same behavior is noted when the variation in turbulence magnitude is considered for the roll and yaw axes separately, shown in Figure 42. Individual increases in either the rms roll or yaw disturbance level had a greater effect on pilot ratings than variations in bandwidth. Pilot commentary reveals no direct influence of the frequency content of the turbulence on the flight task. While the pilots were able to detect gross changes in frequency content, their typical comments mention an apparent decrease in the overall magnitude of the turbulence when higher frequencies are present. This observation reflects the reduction in amplitude of the low frequency components of turbulence as bandwidth increases in order to maintain a constant rms turbulence level. Furthermore, the pilots typically chose to ignore the highest frequency disturbances and excursions. They felt the effort required to track these motions would not be reflected in a commensurate improvement in performance. It was generally possible to live with the high frequency motion and still discern the average heading to the desired accuracy.

It should also be mentioned that pilot ratings and commentary are not affected by variations in frequency content of the roll disturbances due to vertical gusts. Furthermore, any higher frequency attenuation in the L_{w_g} spectrum associated with the second break frequency (ω_{w_2}) was not apparent to the pilots.

Pilot opinion data for the case of unsatisfactory lateral dynamics (Configuration 6) shown in Figure 43 seems to be somewhat more affected by the turbulence bandwidth than for the case of Configuration 1. While the rms magnitude of the turbulence is still the dominant influence, pilot opinion
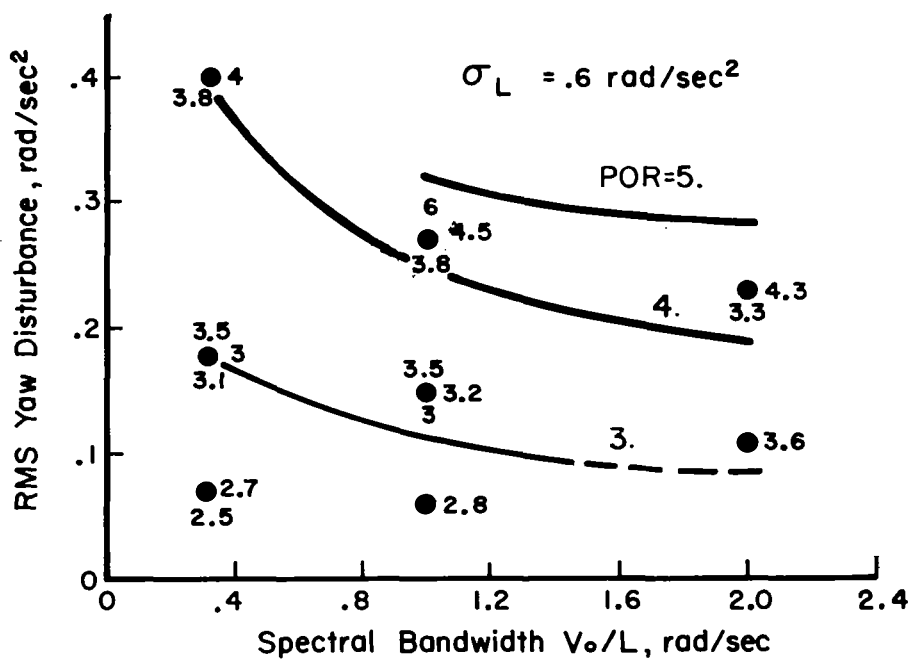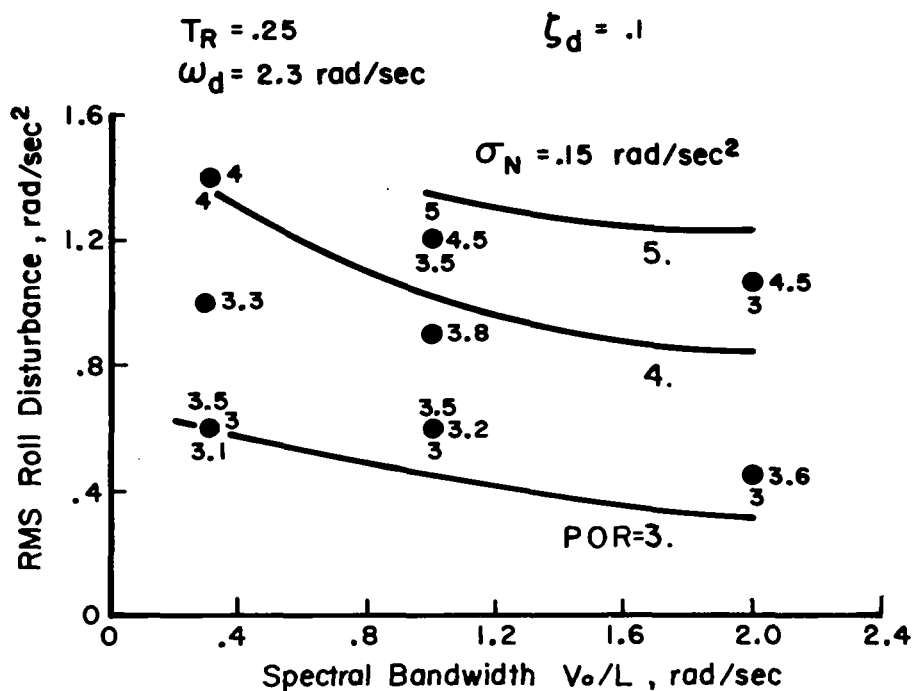
Figure 42.   Combined Effects of Spectral Bandwidth, Roll and Yaw
Disturbances on Pilot Opinion Rating - Configuration 1
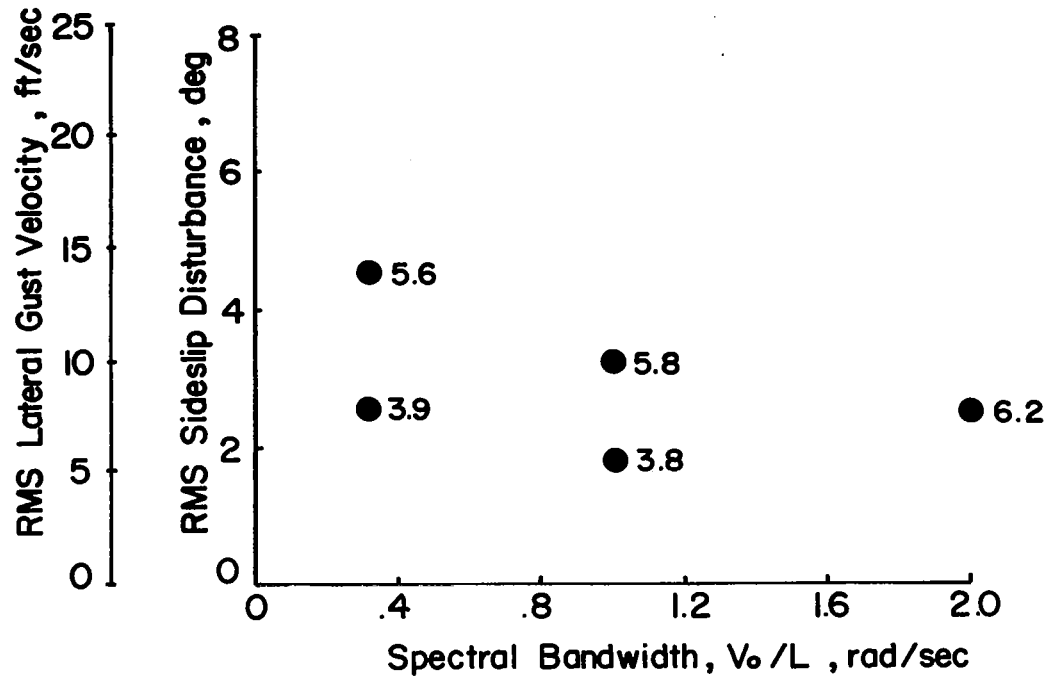
Figure 43. Influence of Spectral Bandwidth on Pilot Opinion Ratings - Configuration 6

deteriorates by approximately two rating units over the range of bandwidth tested. Essentially the same behavior is evident for the separate cases of large roll disturbances or large yaw disturbances shown in Figure 44.

Task performance and workload measures from flight test data are presented for Configurations 1 and 6 in Figures 45 and 46. These data relate to the pilot rating results of Figures 42 and 44. It may be noted in either Figure 42 or 44 that the different turbulence bandwidth test conditions are not at constant rms disturbance levels. (For example, the large roll disturbance test configurations at the top of Figure 42 have values of σ_L of approximately 1.4, 1.2, and 1.0 rad/sec^2 for $\frac{V_o}{L}$ of .314, 1.0, and 2.0 rad/sec respectively.) For the purpose of determining the independent influence of bandwidth on the performance-workload data, it is desirable to compare data having a common rms disturbance magnitude. To make this comparison the performance-workload data were adjusted to values corresponding to an rms level common to all of the bandwidths tested. This adjustment was made using a linear interpolation or extrapolation (as circumstances demanded) of the rms performance and workload data for two disturbance levels. The accompanying sketch graphically illustrates this technique for the case of σ_φ and $\sigma_{\delta a}$.
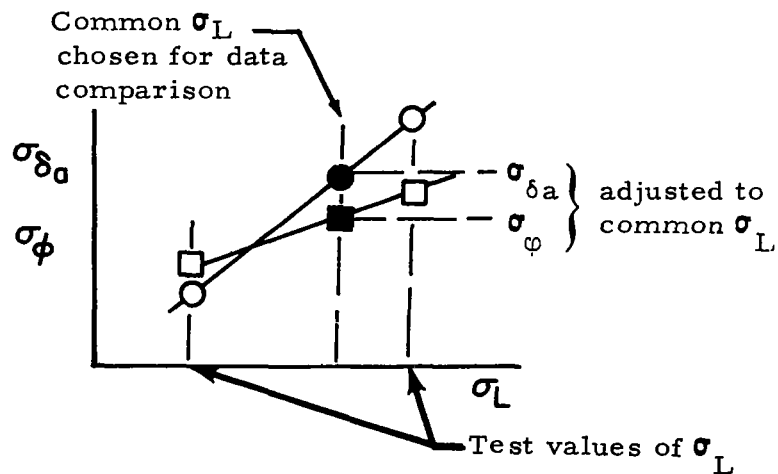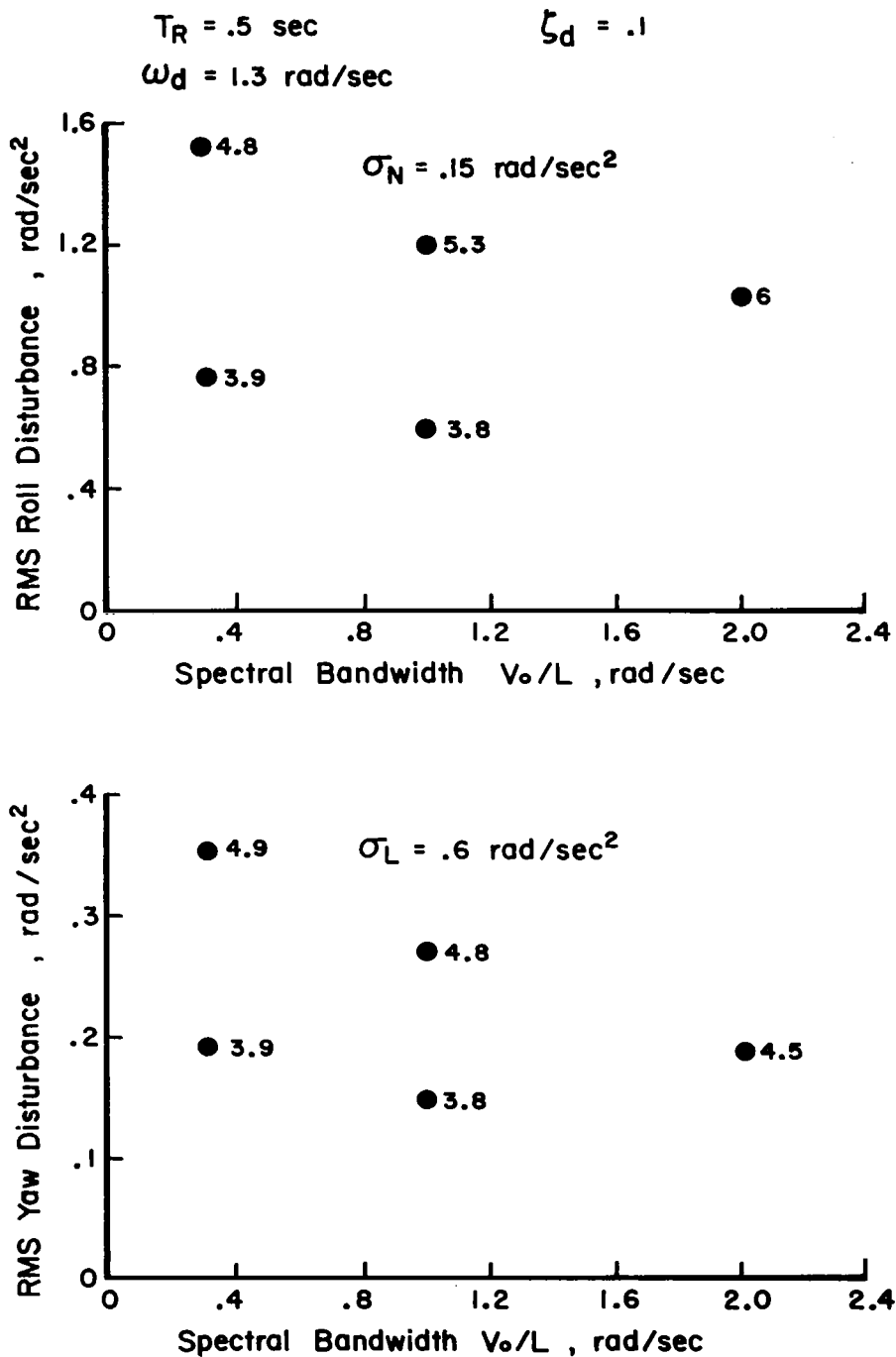
Figure 44.   Combined Effects of Spectral Bandwidth, Roll and Yaw
Disturbances on Pilot Opinion Rating – Configuration 6
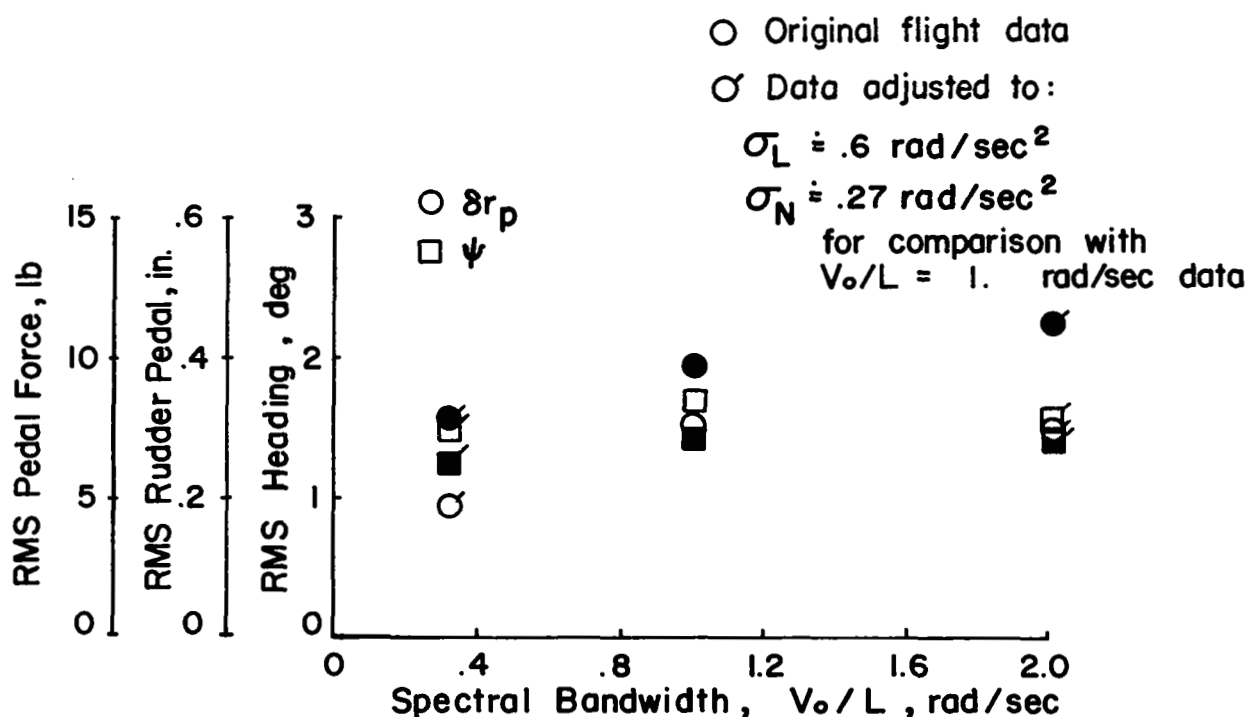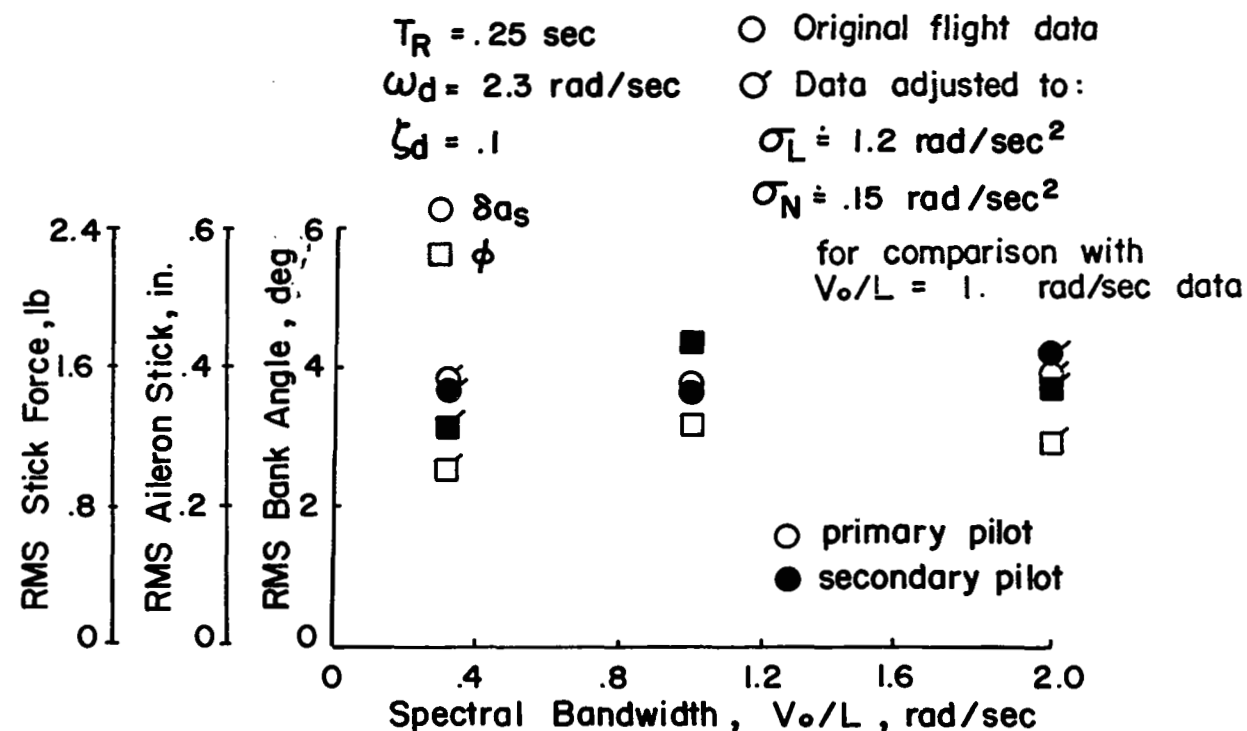
Figure 45.   Influence of Spectral Bandwidth on Task Performance
and Workload – Configuration 1

120
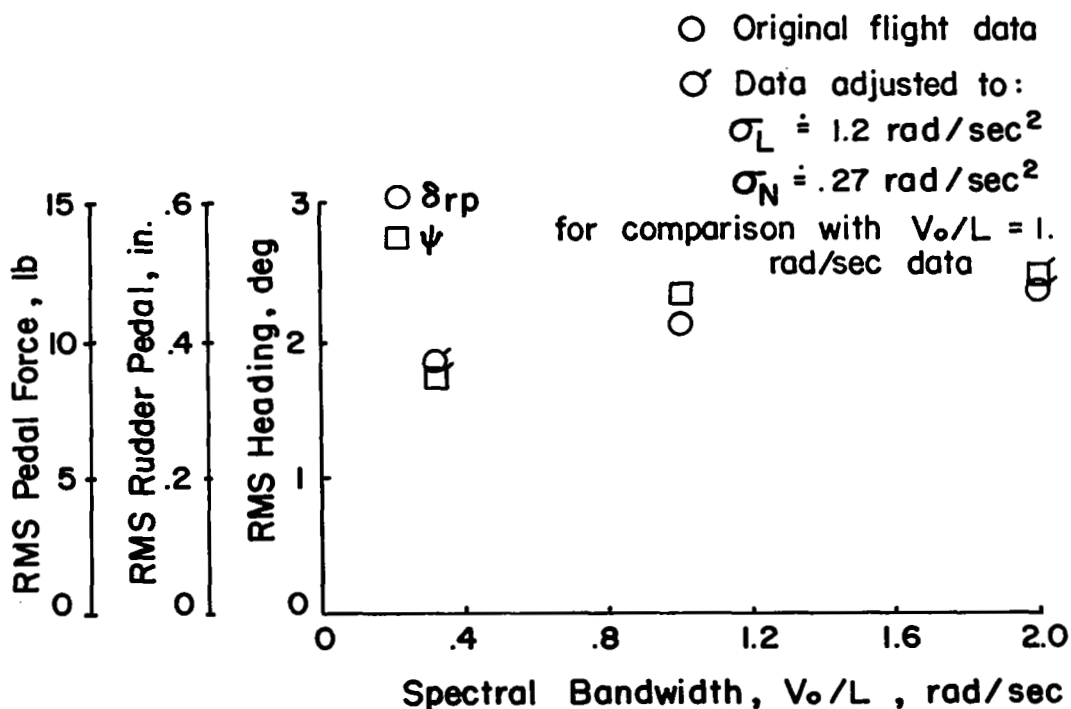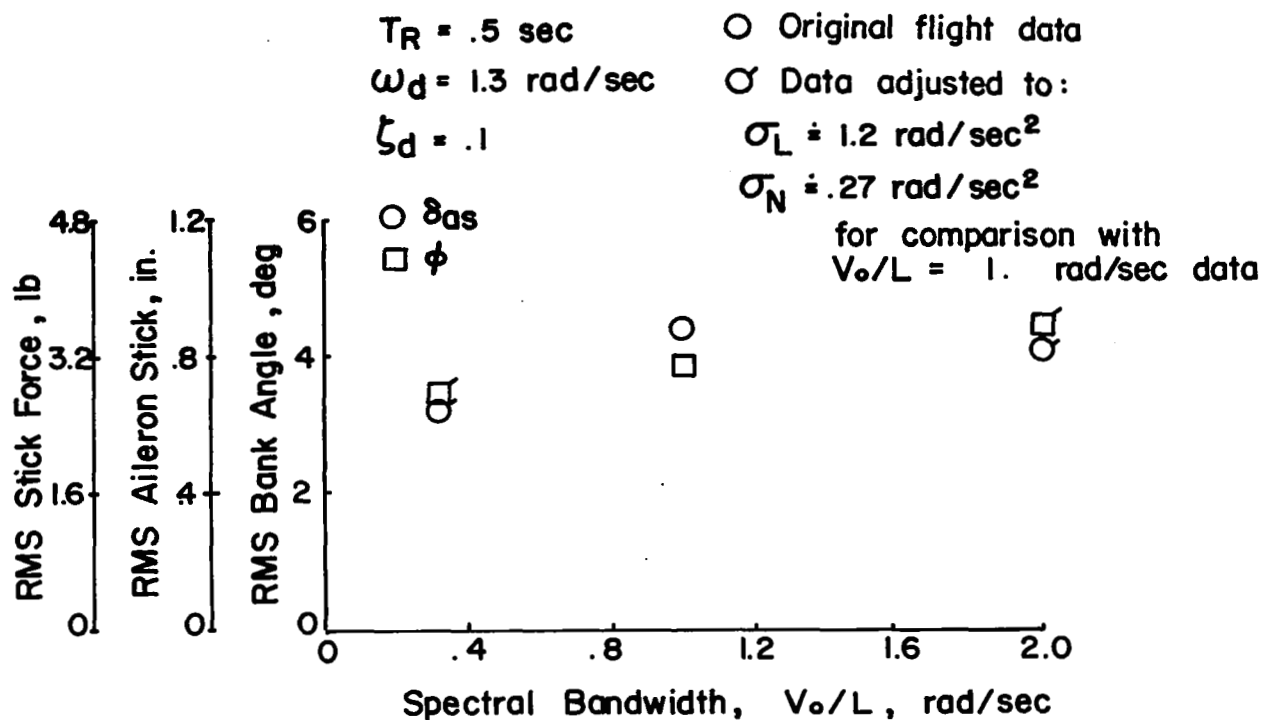
Figure 46. Influence of Spectral Bandwidth on Task Performance and Workload - Configuration 6

In Figure 45, the $\frac{V_o}{L}$ = .314 and 2.0 radians/ second data were adjusted to values of σ_L and σ_N corresponding to the levels of roll and yaw disturbances for the $\frac{V_o}{L}$ = 1.0 radian/ second condition.

For good lateral dynamics (Figure 45) the roll axis data, shown for a high level of roll disturbance, indicate a reasonably constant aileron workload and a modest increase in rms bank angle excursions in the low to intermediate frequency range. For the case of large yaw disturbances, the heading tracking performance is nearly constant over the range of bandwidths while rudder workload increases for bandwidths up to $\frac{V_o}{L}$ = 1.0 radian/ second. From the pilots' commentary, it is apparently these degradations in task performance or increases in control workload which influence his rating of the airplane in turbulence, rather than the frequency content of the turbulence as such.

Considering the poorer lateral dynamics (Figure 46), for either the roll or yaw axes airplane excursions and control workloads tend to increase with increasing bandwidth, again predominantly in the low to intermediate bandwidth range. The data are shown for the case of large roll and yaw disturbances. The observed trends in task performance and control workload provide a basis for the pilot rating data of Figure 43.

Effect of correlation between roll and yaw disturbances

Roll-yaw correlation was considered in this investigation for two reasons. It can be shown to have some contribution to the magnitude of the airplane's turbulence response. Furthermore, it was considered possible that some helpful (or hindering) cues as to the nature of the turbulence might be available to the pilot, depending on the correlation between the two disturbances. It was noted in Section 4 that separate contributions to the correlation coefficient arise from the relative amounts of roll disturbances due to

vertical and lateral gusts, $\dfrac{\sigma_{L_v}}{\sigma_{L_w}}$, and from the normalized tail length, $\dfrac{\ell_v}{L}$.

The influence of roll-yaw correlation on pilot ratings is shown in Figures 47 and 48 for good lateral dynamics and for a bandwidth, $\dfrac{V_o}{L} = 1.0$ radian/second. The individual contributions to the correlation of roll and yaw are considered separately.

Roll-yaw correlation, as determined by the relative amounts of L_{w_g} and L_{v_g} disturbances, is of no consequence to the pilot. This part of the data set is presented in Figure 47. Correlation coefficients ranging from 0. to .87 were evaluated for a low level of roll disturbance ($\sigma_L \doteq .6$ radians/second^2) and a range of .44 to .87 was evaluated for larger roll disturbances ($\sigma_L \doteq 1.2$ radians/second^2). No significant variation in pilot rating is observed.

When the variation in correlation is obtained by altering the tail length, some effect on pilot opinion is noted. This part of the data set is given in Figures 48 and 49 for two levels of roll disturbance. The trend indicated is a slight degradation in pilot ratings with reduced correlation (increasing tail length). Considerable change in tail length is required to cause a deterioration in flying qualities of any consequence for the case of good dynamics (Figure 48) or poor dynamics (Figure 49).

Pilot commentary suggests that the deterioration in flying qualities for the larger tail lengths is a result of a slight increase in the level of yaw excursions. Considering the last term in equation (85), it is apparent that the cross-correlation between roll and yaw disturbances contributes to the magnitude of the closed loop heading response. However, it can be shown that the net effect of the cross-correlation influence is small compared to the direct influence of the yaw disturbance itself. This result applies whether the correlation is varied by the tail length or by the roll distur-bance ratio, $\dfrac{\sigma_{L_v}}{\sigma_{L_w}}$. Pilots were occasionally able to detect when nearly
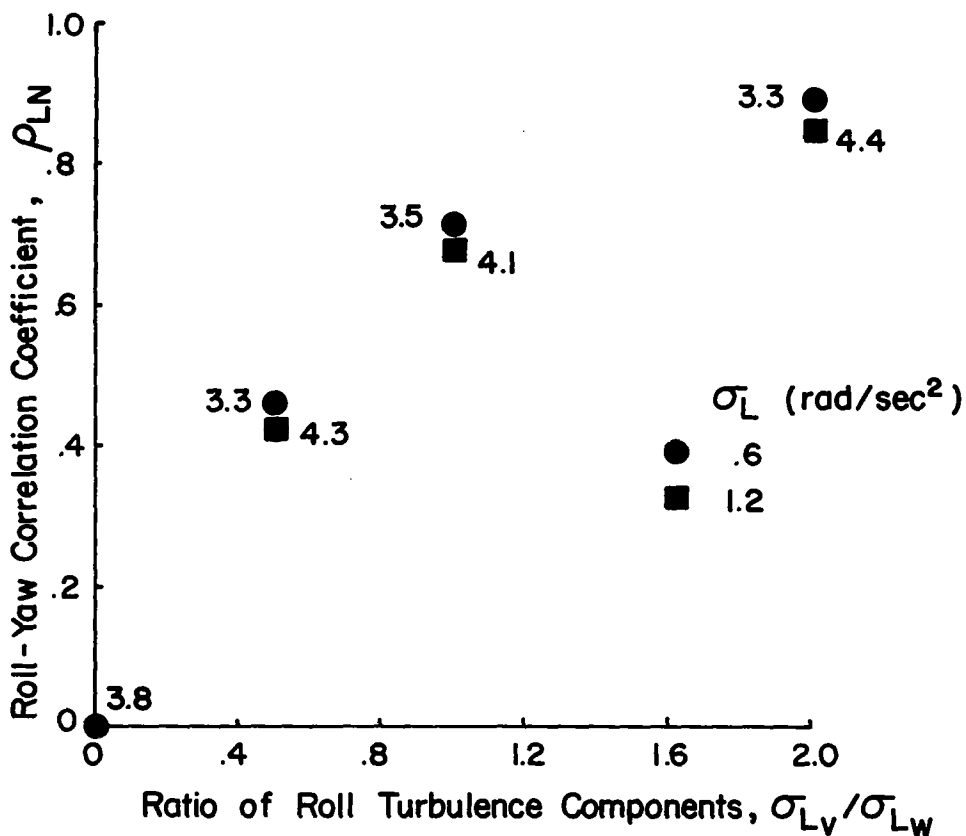
Figure 47. Effect of Roll-Yaw Disturbance Correlation on Pilot Opinion Rating - Contribution of Roll Turbulence Components
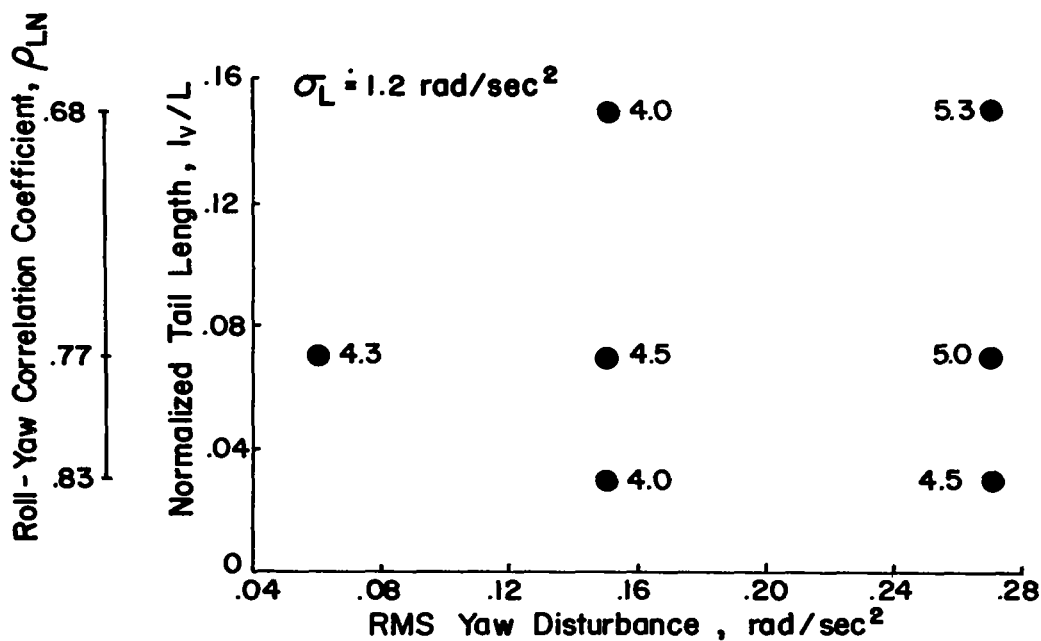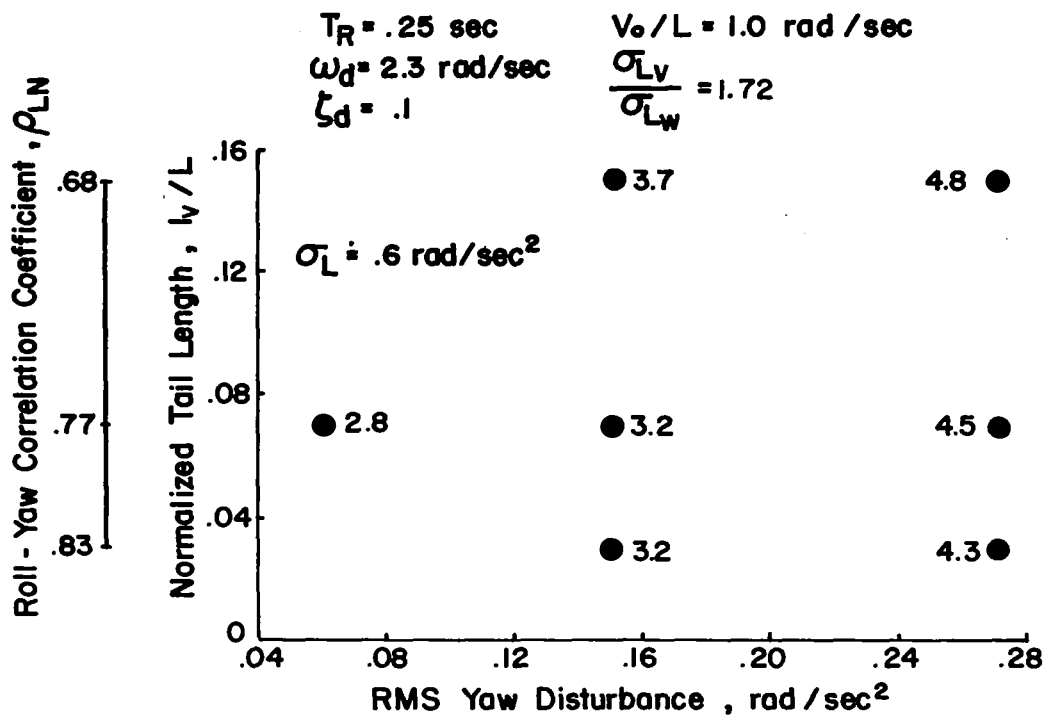
Figure 48.   Effect of Roll-Yaw Disturbance Correlation on Pilot
             Opinion Rating - Contribution of Tail Length,
             Configuration 1

125
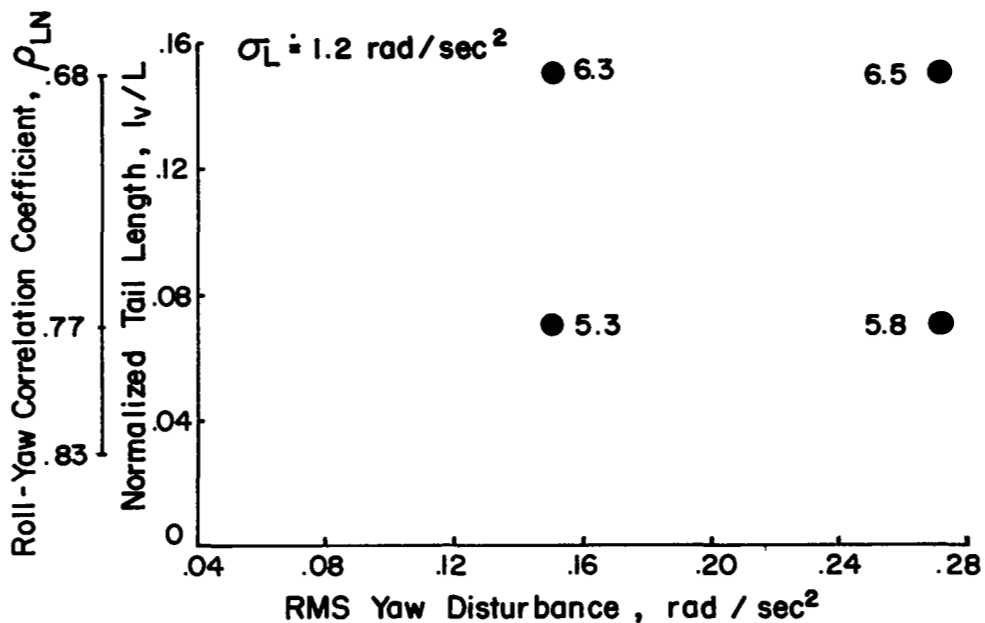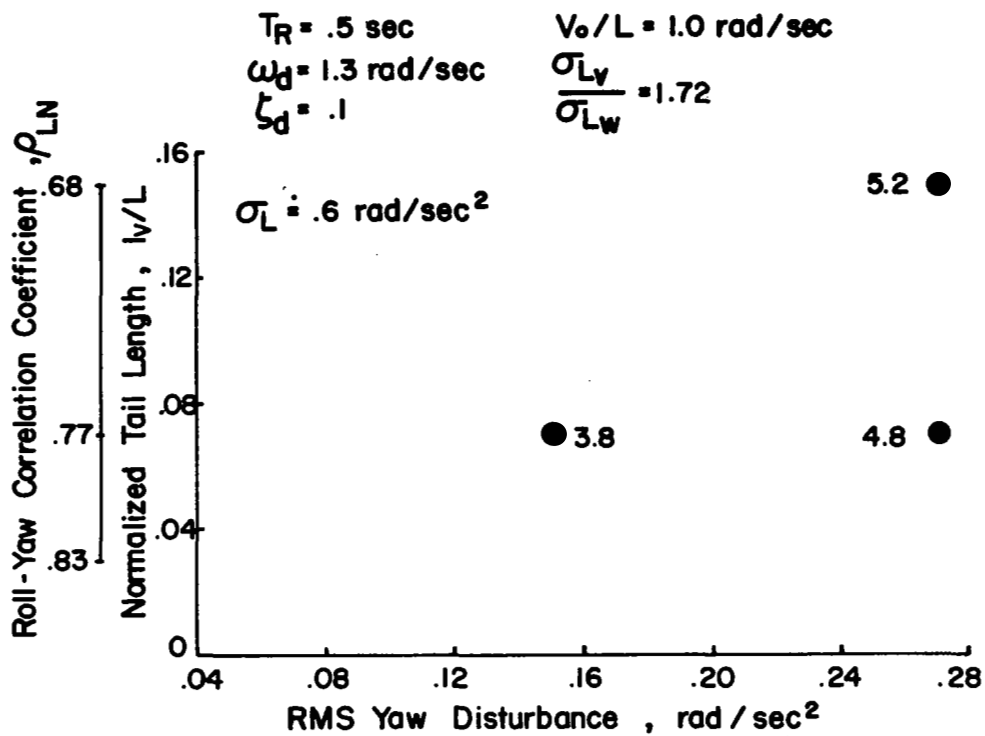
Figure 49. Effect of Roll-Yaw Disturbance Correlation on Pilot
Opinion Rating - Contribution of Tail Length,
Configuration 6

126

perfect correlation existed between roll and yaw disturbances ($l_v \doteq 0$, and $\dfrac{\sigma_{L_v}}{\sigma_{L_w}}$ large). However, this characteristic of the turbulence proved to be of no value to the pilot in performing the heading tracking task. Due to the continuous, random nature of the disturbances, anything other than near perfect correlation between roll and yaw appeared as essentially uncorrelated disturbances to the pilot.

Heading performance and workload data for Configurations 1 and 6 are shown in Figure 50. No trends of any consequence appear in heading excursions or rudder activity for either good or poor dynamics as the tail length is increased.

Contribution of roll damping (T_R)

The combined effects of roll damping (or roll mode time constant) with rms roll disturbance level are shown in Figure 51. These data are presented for constant Dutch roll frequency and damping ratio ($\omega_d = 2.3$ radians/second, $\zeta_d = .1$) and for a low level of yaw disturbance ($\sigma_N \doteq .15$ radians/second^2).

Variations in roll damping along with variations in the roll disturbance level for a constant bandwidth ($\dfrac{V_o}{L} = 1.0$ radian/second) indicate that reductions in roll damping or increases in roll disturbances or both degrade flying qualities. Furthermore, it is apparent that higher levels of roll damping (lower T_R) are desired with increasing roll disturbance magnitude. At the lowest level of roll damping ($T_R = .5$ seconds), pilot commentary emphasizes the increasing magnitude of roll excursions and the difficulty in controlling bank angle to reduce roll excursions to a level which does not distract from the heading tracking task.
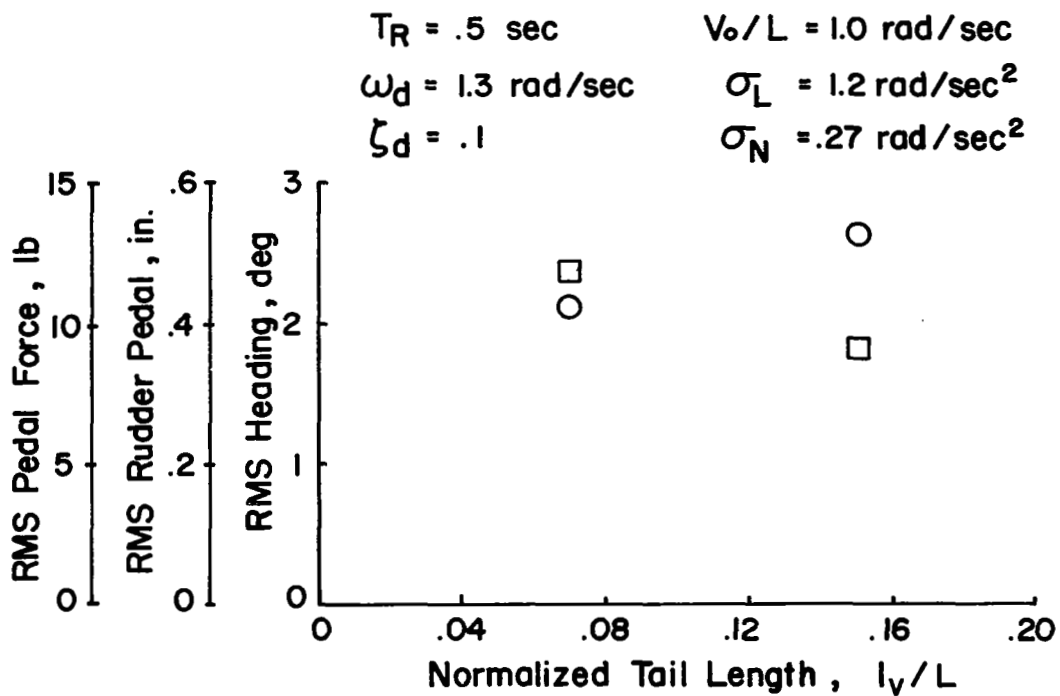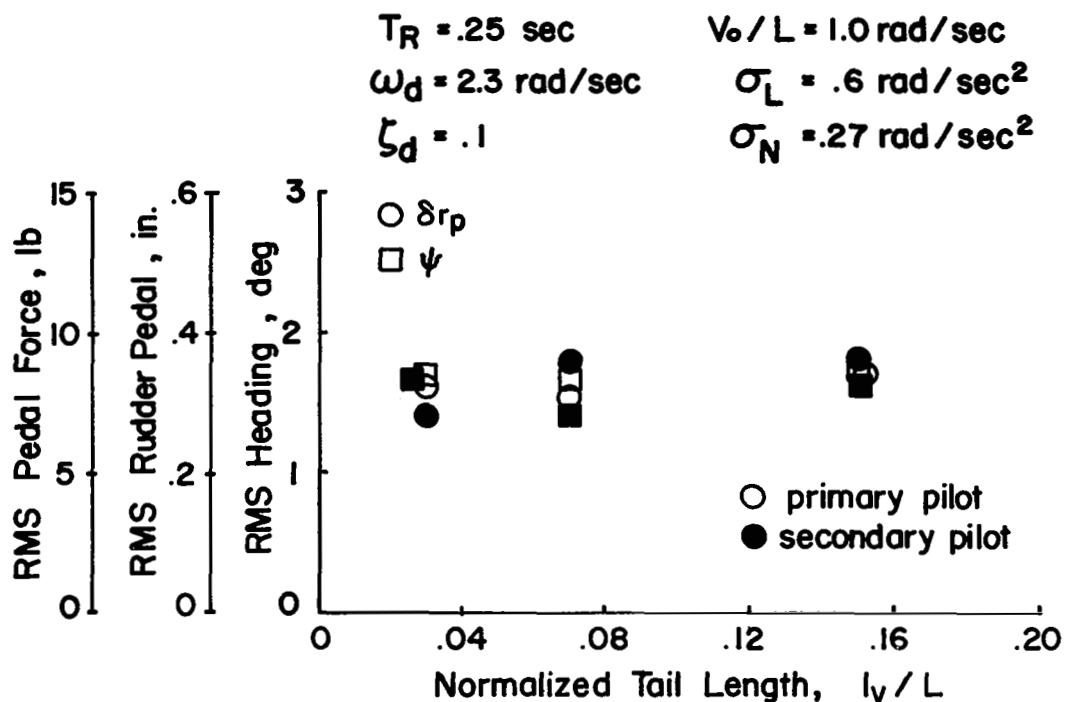
Figure 50. Variation in Heading Performance and Rudder Workload with Roll-Yaw Correlation - Tail Length Contribution, Configurations 1 and 6

128
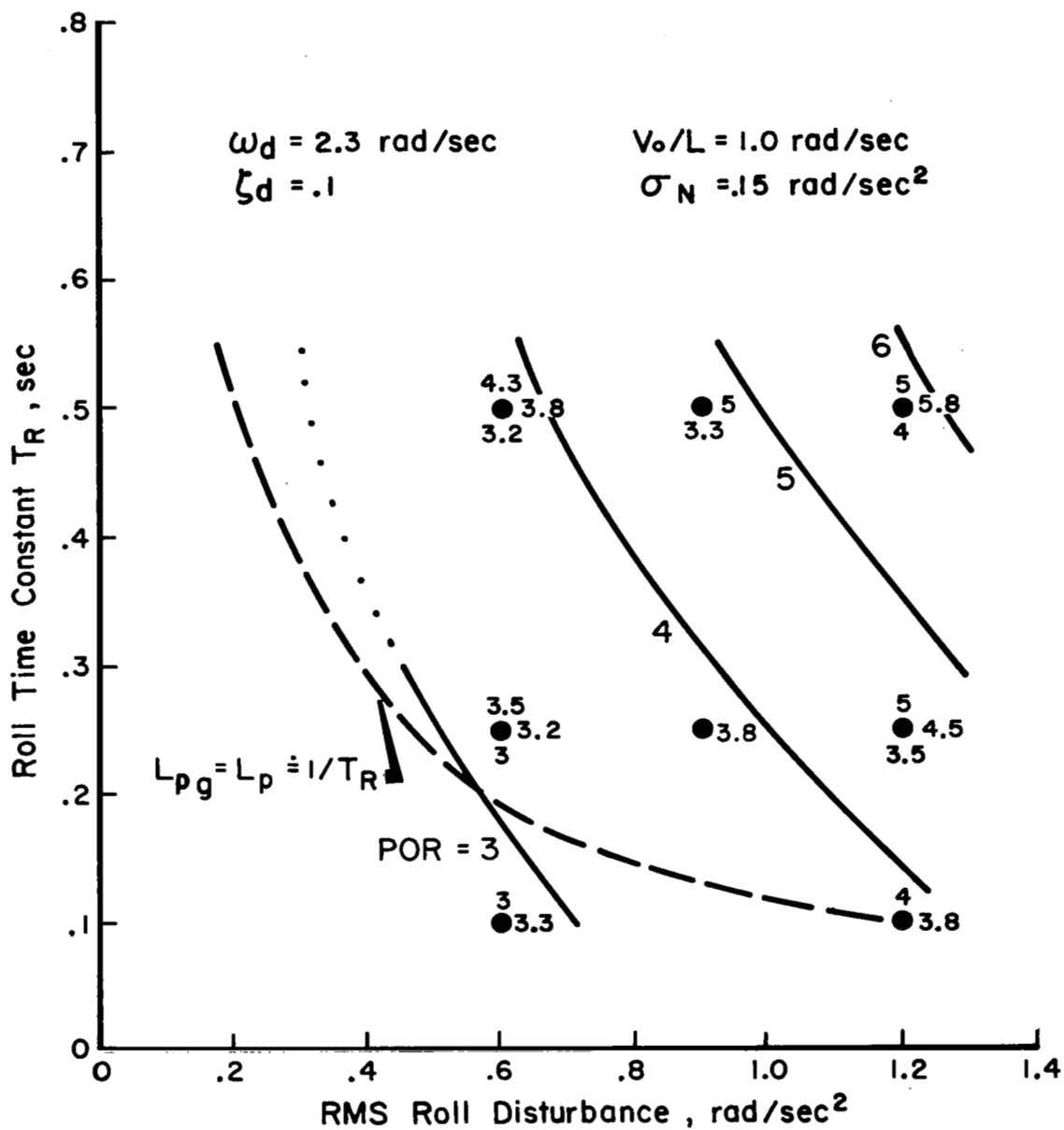
Figure 51. Trends of Pilot Opinion Rating with Roll Damping and
Roll Disturbance

It should be re-emphasized that the data points of Figure 51 represent independent variations of roll damping and roll disturbance magnitude. Thus, T_R and σ_L are not in general interrelated for the configurations of Figure 51. As a matter of interest, the conditions where T_R and σ_L would be interrelated, that is where T_R is determined entirely by aerodynamic roll damping ($T_R \doteq -\frac{1}{L_p}$ and $L_p = L_{p_g}$), are indicated by the dashed line. The relation of this dashed line to the POR contours permits an assessment to be made of the effect of a combined variation in roll damping and roll turbulence due to L_p on the pilot's rating. In the range corresponding to the lowest values of L_p tested (high T_R, low σ_L) an increase in roll damping causes no change in pilot rating, apparently because the improvement in roll control characteristics is counteracted by the increase in roll turbulence. However, further increases in L_p corresponding to $T_R = .25$ sec and less begin to degrade pilot ratings because the severity of the roll disturbances now overrides the accompanying improvement in roll dynamics. On the other hand, if changes in T_R are accomplished using inertial roll damping (where roll rate sensed by a rate gyro is fed back to the ailerons through a servo control system) then variations in T_R may be made without correspondingly changing the level of roll disturbances. As Figure 51 indicates, reducing T_R in this manner (increasing inertial roll damping) generally improves pilot rating.

The influence of turbulence bandwidth on pilot rating is re-evaluated for levels of roll damping above and below the nominal value of Configuration 1. Trends of pilot rating with turbulence bandwidth and rms roll disturbance are shown in Figure 52 for roll damping corresponding to $T_R = .1$ and $.5$ seconds. These data reveal the degrading effect of increasing

bandwidth for either the high or low level of roll damping, with the predominant change in pilot rating for $\frac{V_o}{L}$ between .314 and 1.0 radian/ second. As noted previously for Configuration 1, pilot commentary reveals no explicit influence of the frequency content of the turbulence on pilot ratings. Airplane excur- . sions in response to turbulence and the control activity required to perform the task still dominate the pilots' remarks.

Flight test bank angle excursion and aileron workload data are shown in Figures 53 and 54. The results are presented in a manner to compare the separate effects of roll damping, roll disturbance level, and spectral bandwidth on performance and workload. The influence of roll damping alone is shown in Figure 53 for low levels of roll and yaw disturbances. The consequence of reduced roll damping which is reflected in pilot ratings is the increase in both roll excursions and aileron workload. In the upper diagram of Figure 54 the combined effects of roll damping and roll disturbance variations are indicated. The increase in roll excursions and aileron workload with increasing roll disturbances is somewhat more pronounced for the lower value of roll damping. This confirms the impression gained from pilot rating trends that less in the way of roll disturbances can be tolerated at the lower levels of roll damping. To evaluate the contribution of turbulence bandwidth, data for the three levels of roll damping and for the bandwidths tested were adjusted to a common rms roll turbulence for comparison. The results are shown in the lower diagram of Figure 54. An increase in bandwidth over the low to intermediate frequency range generally degrades the precision of roll control and increases the control workload. The adverse influence of bandwidth in this frequency range is slightly more pronounced for the lower levels of roll damping.

$$\omega_d = 2.3 \text{ rad/sec} \qquad \sigma_N \doteq .15 \text{ rad/sec}^2$$
$$\zeta_d = .1$$

$T_R = .1$ sec

$T_R = .5$ sec
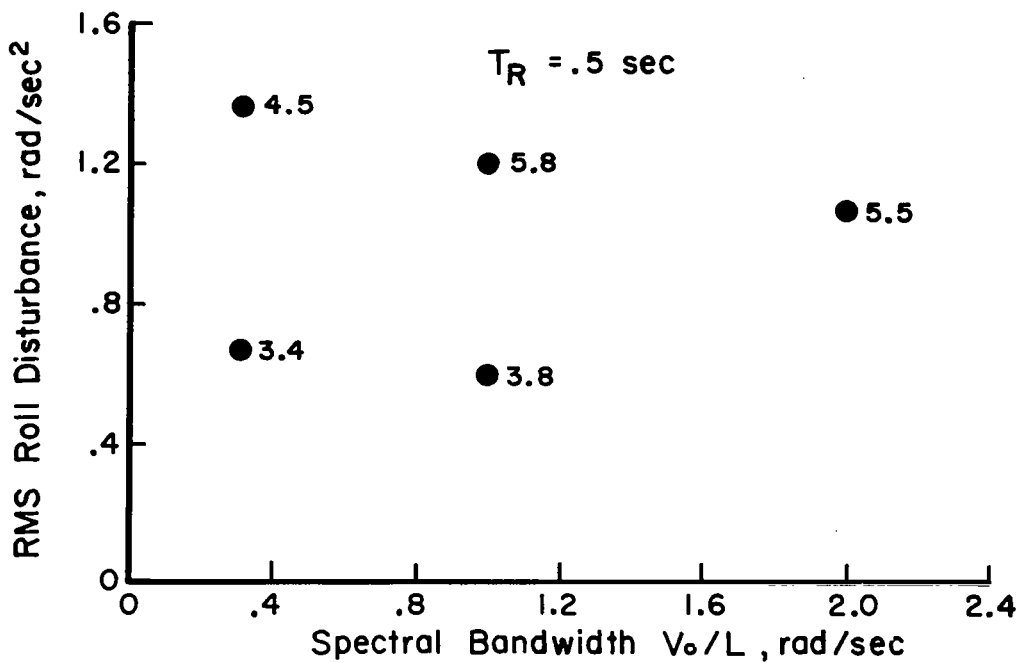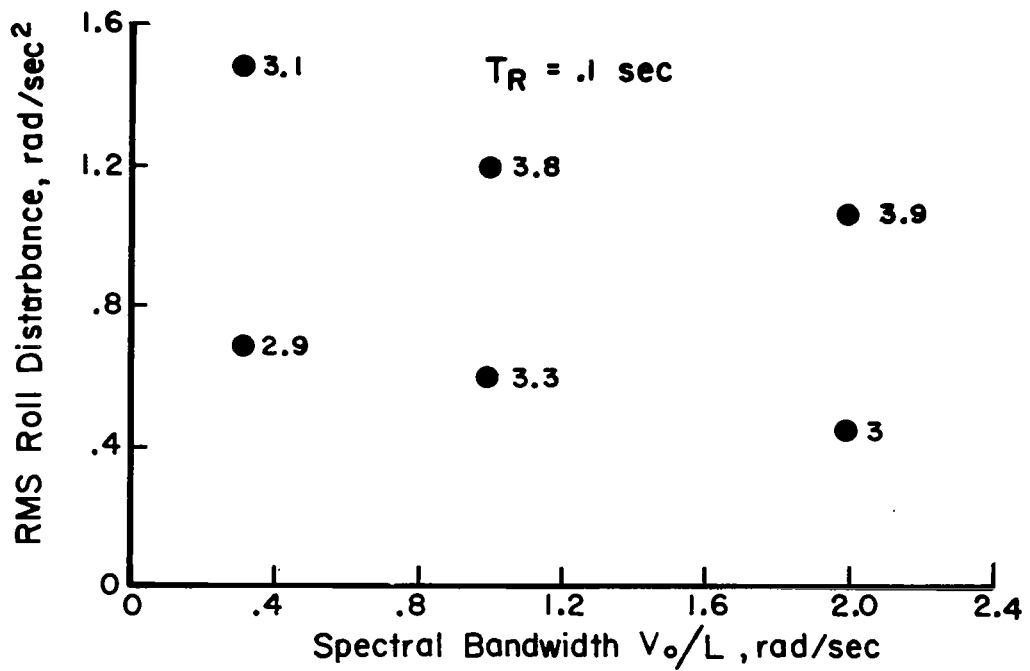
Figure 52. Trends of Pilot Opinion Rating with Spectral Bandwidth
- High and Low Roll Damping

132
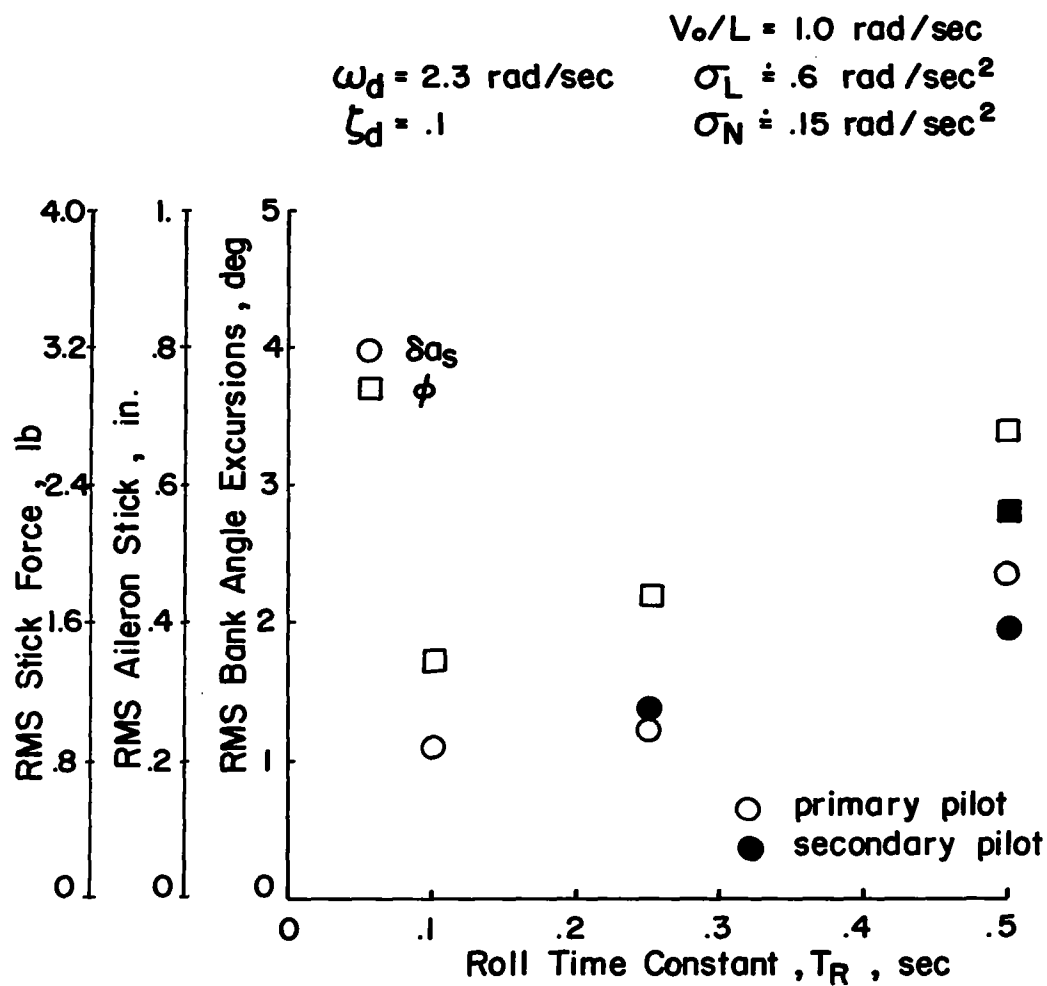
Figure 53. Influence of Roll Damping (T_R) on Bank Angle Performance and Aileron Workload
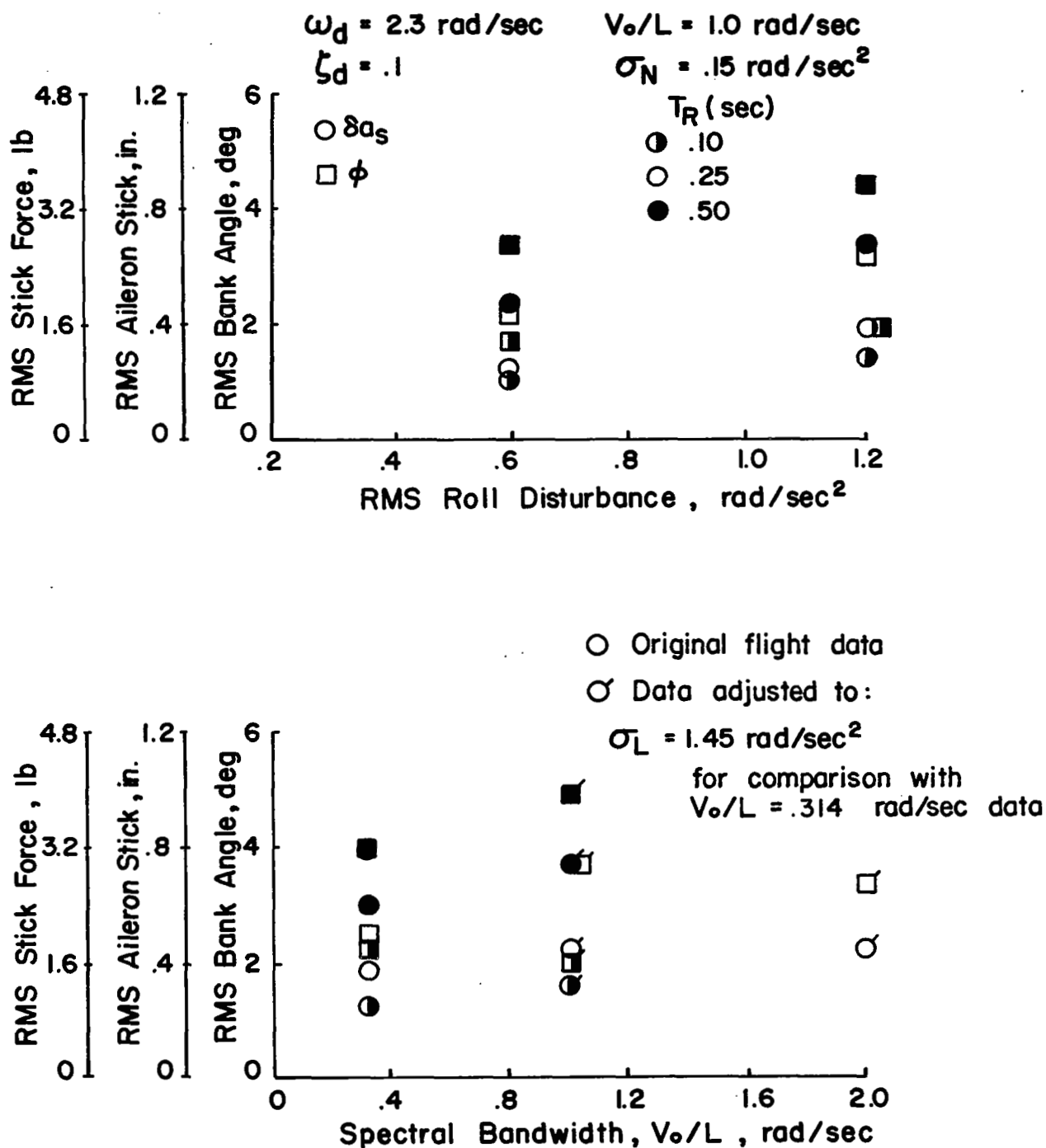
Figure 54. Combined Effects of Roll Damping, Roll Disturbance and Bandwidth on Bank Angle Performance and Aileron Workload

134

Contribution of directional stability (ω_d)

The combined effects of directional stability (or Dutch roll frequency) with rms yaw disturbance level are shown in Figure 55. These data are presented for constant values of roll damping, Dutch roll damping ratio, and spectral bandwidth (T_R = .25 seconds, ζ_d = .1, $\dfrac{V_o}{L}$ = 1.0 radian/second) and for high and low levels of roll disturbances.

Considering the primary evaluation pilot's data it is apparent that reducing the airplane's directional stability or increasing the level of turbulence upsets in yaw both degrade flying qualities in the heading task. The trends of pilot opinion also show that higher levels of directional stability are desired as yaw disturbance magnitude increases. The previous comments apply for both levels of roll disturbance shown in Figure 55. Pilot commentary emphasizes the difficulty in performing the heading tracking task with a reasonable rudder workload when the directional stability is low. Complaints of occasional very large excursions in heading (10 degrees or more) were made for several test runs. Large yaw disturbances serve to further complicate an already difficult problem. The low directional stiffness associated with the lowest frequency configurations permits large sideslip excursions to occur, particularly at the higher levels of yaw disturbances. Pilot commentary indicates that these side-slipping motions were particularly disconcerting to the heading tracking task and were occasionally uncomfortable as well. They eventually reach a level which forces the pilot to take compensatory action to eliminate them. He does this by including the turn and bank in his instrument scan and applying correcting control by "stepping on the ball" in the pilots' idiom. While the lateral acceleration accompanying the sideslip provides some clue to its onset, and most of the discomfort in the ride as well, the pilots concurred that they did not use this cue in a compensatory sense while performing the task. However, their comments indicate that angular accelerations in yaw may well have provided them with useable cues for closed loop heading control.
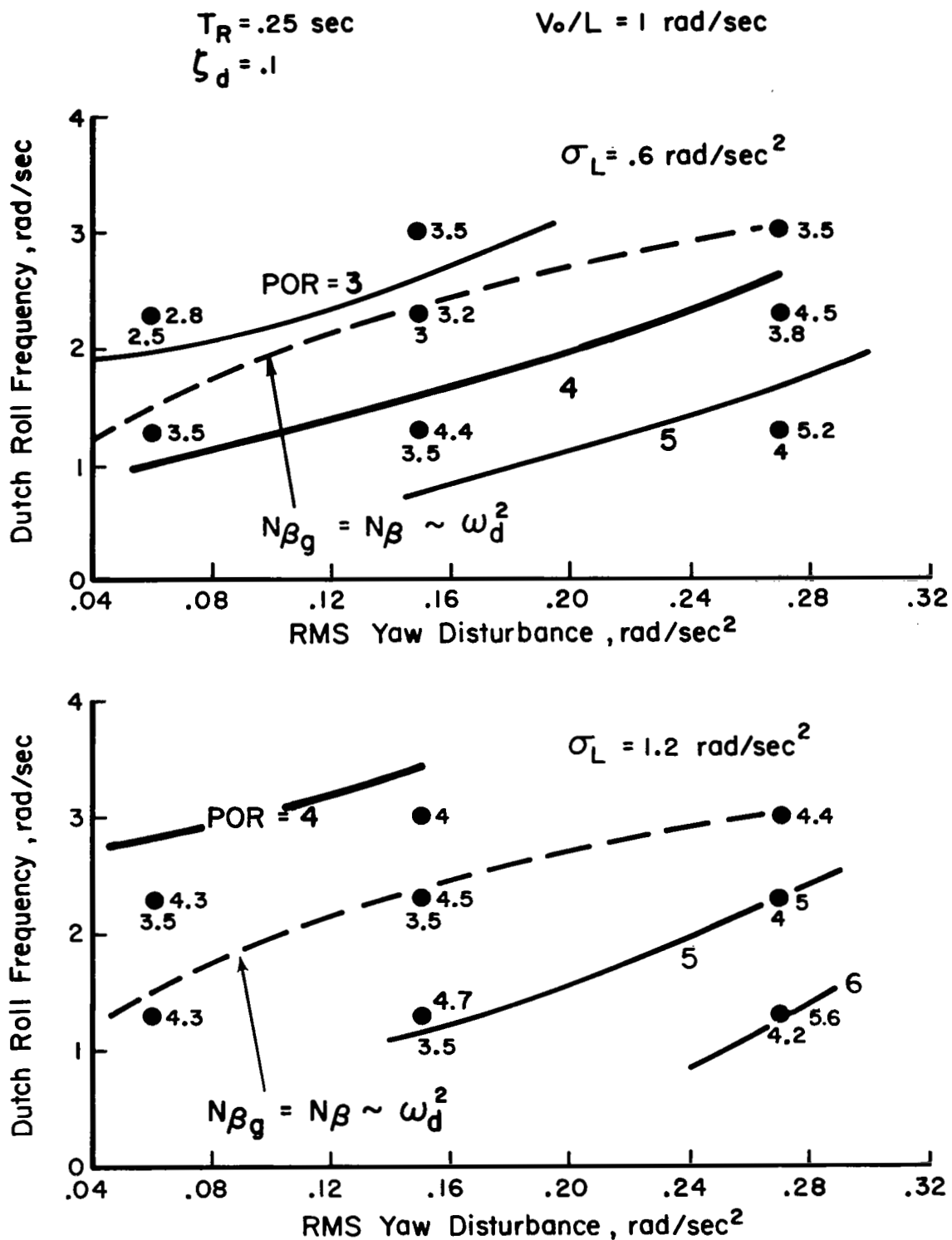
Figure 55.   Trends of Pilot Opinion Rating with Directional Stability
and Yaw Disturbance

Occasionally, the sideslip excursions would become large enough to distract the pilots' attention from the heading task to a considerable degree. In one instance, one of the secondary evaluation pilots noted that he completely disregarded heading and the primary task to track sideslip exclusively in order to return the airplane to a generally symmetrical attitude.

It again should be emphasized that the flight test program was designed to explore the effects of lateral-directional dynamics and turbulence disturbances separately. While the Dutch roll frequency and the magnitude of yaw disturbances can normally be interrelated by the airplane's directional stability $(\omega_d \sim \sqrt{N_\beta},\ \sigma_N \sim N_\beta)$, the test configurations corresponding to the data points of Figure 55 represent independent variations in ω_d and rms yaw disturbance magnitude. Thus, in general, N_β (which determines ω_d) and the yawing moment due to lateral gusts are not related in Figure 55. To evaluate the combined effects of dynamics and turbulence, it is of interest to consider the case where ω_d and σ_N are related by $N_\beta = N_{\beta g}$. Configurations in the test program to which this applies are indicated by the dashed line of Figure 55. Over the range of configurations tested the dashed line generally follows the iso-opinion contours and in this region the trade-off between directional stability (ω_d) and yaw turbulence magnitude tend to counteract each other. However, at the higher levels of directional stability in the neighborhood of $\omega_d = 3.0$ radians/second, further increases in directional stability apparently begin to degrade pilot rating. This behavior is most likely the result of an unacceptable increase in the yaw disturbance level for which the increase in directional stability (and improved heading control) does not fully compensate.

The effect of turbulence bandwidth on the heading tracking task is reconsidered in Figure 56 for levels of directional stability above and below that of Configuration 1. Trends of pilot rating with bandwidth and with rms yaw

137
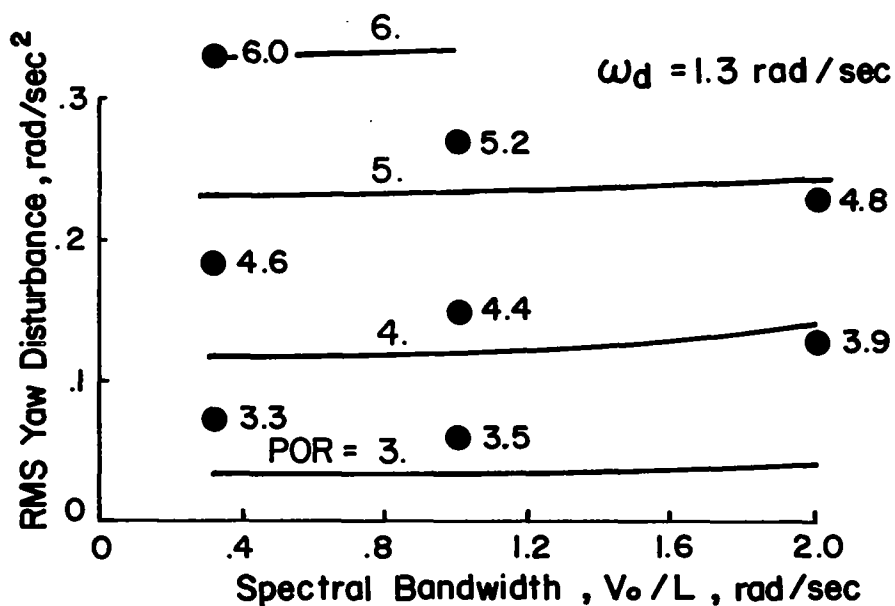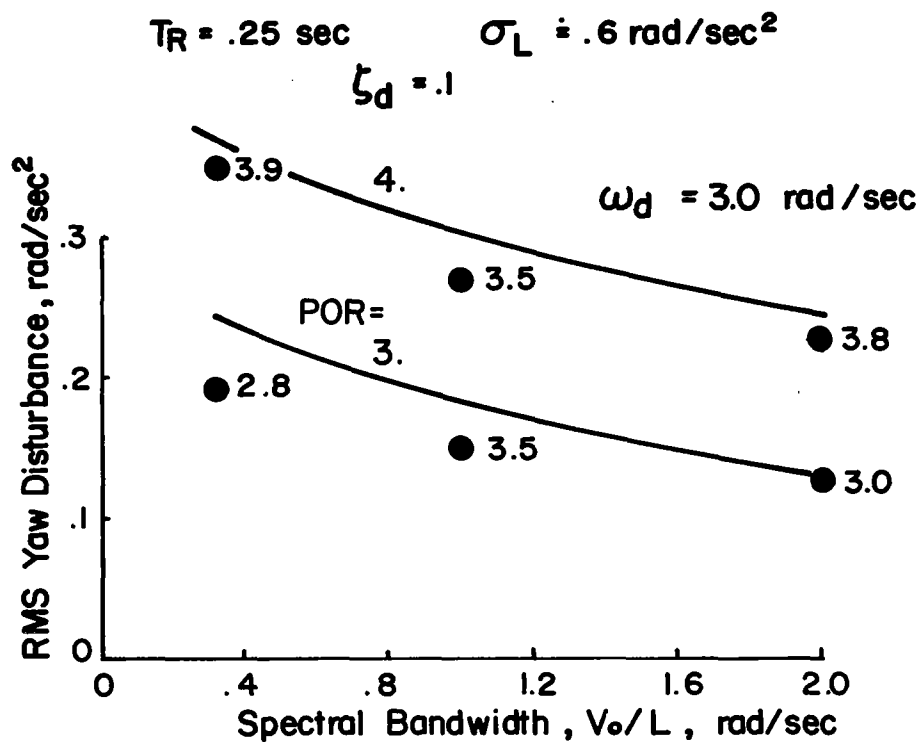
Figure 56. Trends of Pilot Opinion Rating with Spectral Bandwidth
- High and Low Directional Stability

disturbance are shown for directional stability corresponding to ω_d = 1.3 and
3.0 rad/sec. It may be concluded from these data along with the data of
Figure 42 that increasing bandwidth over the range of $\frac{V_o}{L}$ = .3 to 1.0 radian/
second degrades flying qualities at the intermediate and high levels of direc-
tional stability tested (ω_d = 2.3 and 3.0 radians/second). This adverse affect
of increasing bandwidth is not apparent at low directional stability (ω_d = 1.3
radians/second). The only noteworthy distinction in the pilot commentary
which has not been mentioned previously is the existence of large low fre-
quency heading excursions for the low directional stability, low bandwidth
case.

Effects on task performance and workload for both the roll and yaw
axes are shown in Figure 57 as a function of Dutch roll frequency (directional
stability). The data, for the combination of low roll and high yaw disturbance
levels, show little or no trend in roll excursions or aileron workload with ω_d.
Heading excursions are also held to a virtually constant level. The penalty for
reducing ω_d appears as a substantial increase in rudder activity. This trend
in control workload is the basis for the adverse pilot ratings for low directional
stability configurations.

Variations in performance-workload data with rms yaw disturbance and
spectral bandwidth are presented in Figure 58. Essentially no change in head-
ing excursions occurs with increased turbulence level for either of the values
of ω_d shown (upper diagram). Rudder workload shows somewhat more of an
increase with yaw disturbance for the low frequency configuration than for the
intermediate frequency case. This result helps to justify the trend in pilot
rating noted in Figure 55. To evaluate the influence of turbulence bandwidth,
data for two levels of directional stability were converted to a common rms
yaw turbulence magnitude. The results are shown in the lower diagram of
Figure 58. The general impression from these data is that increasing

139
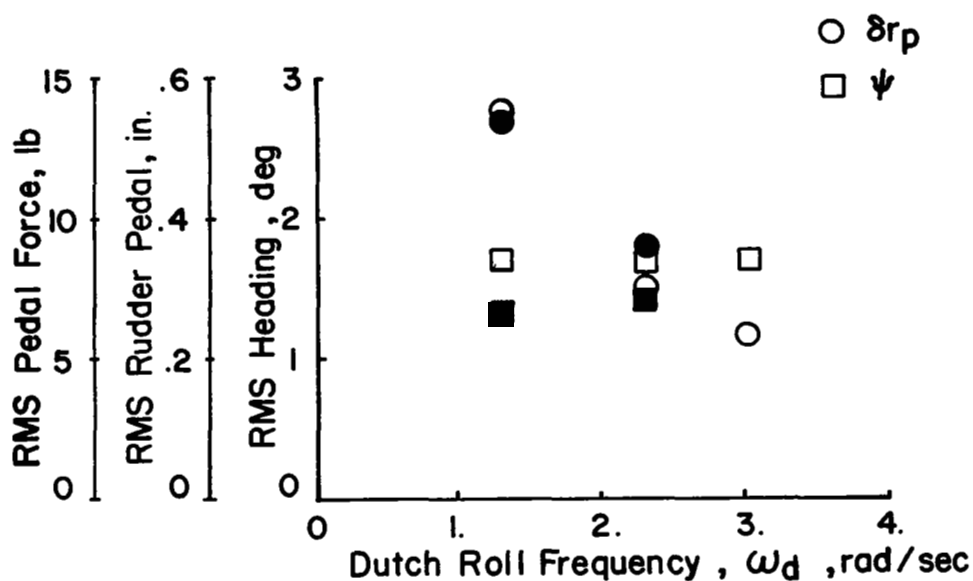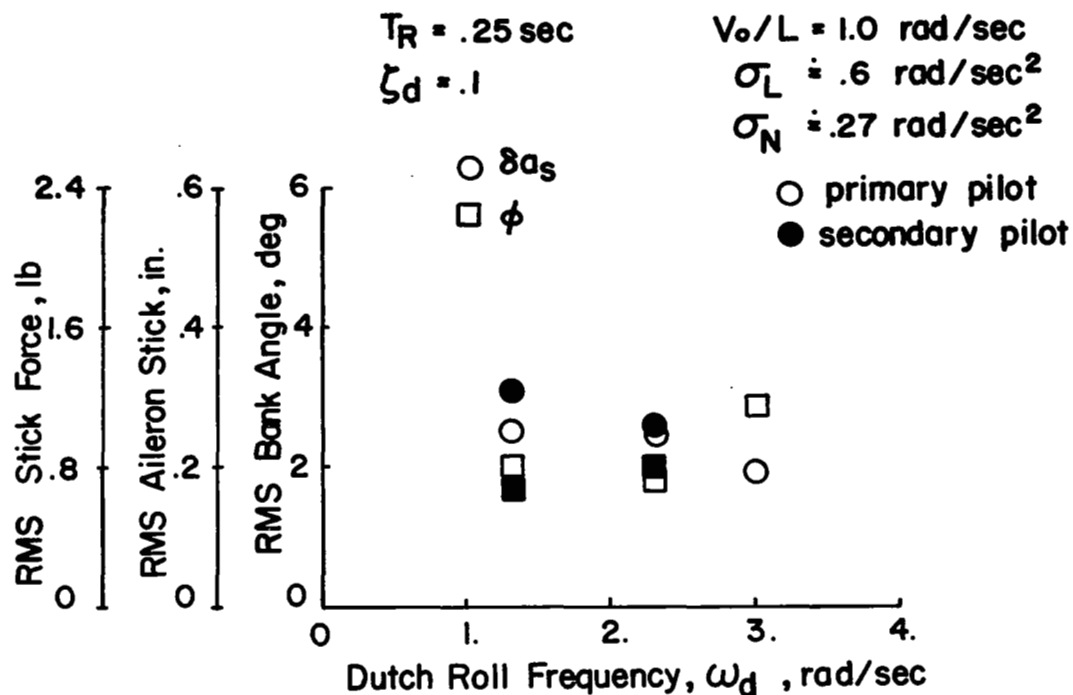
Figure 57.   Effects of Directional Stability (ω_d) on Task Performance and Workload

140
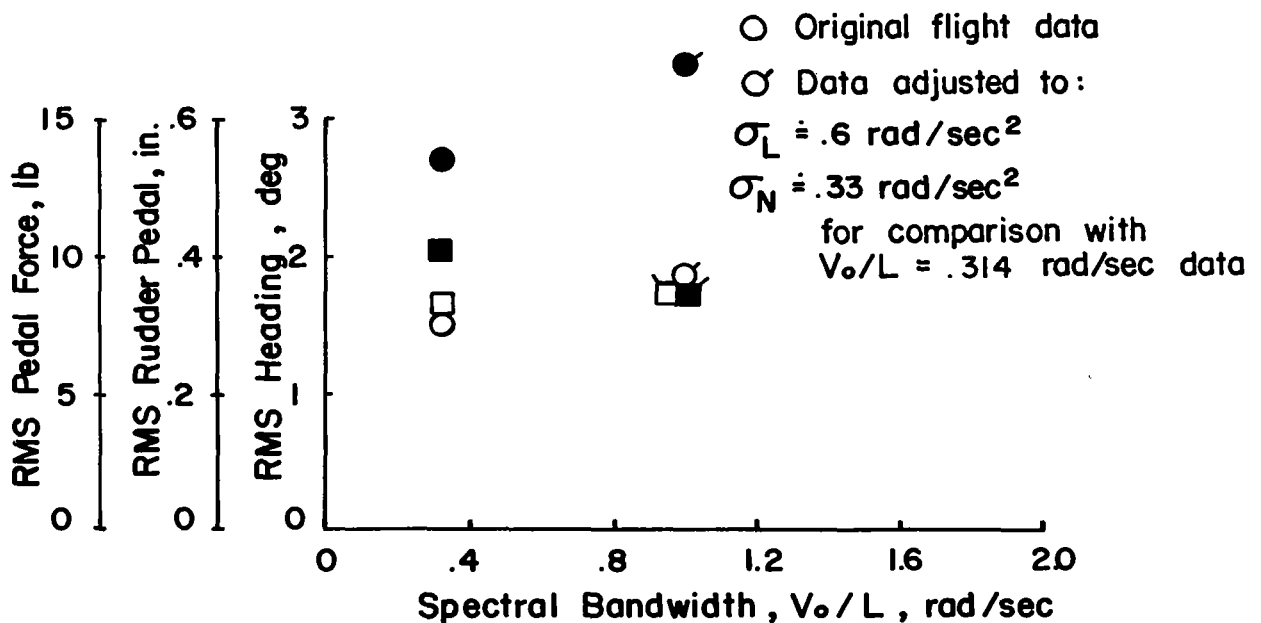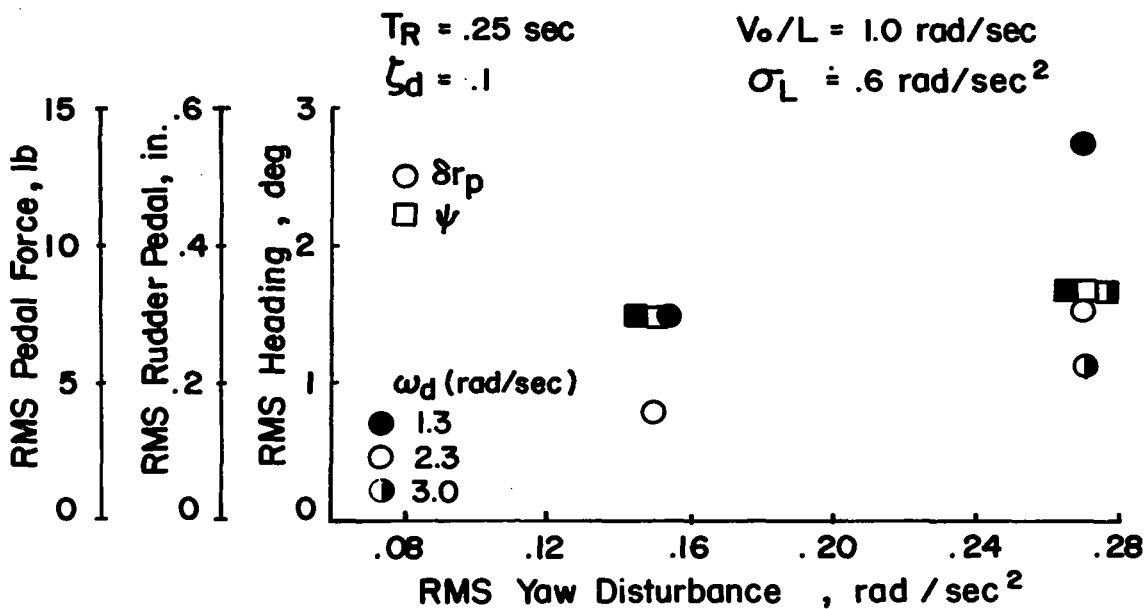
Figure 58.   Combined Influence of Directional Stability, Yaw Dis-
turbances and Bandwidth on Heading Performance and
Rudder Workload

141

bandwidth from $\frac{V_o}{L}$ = .314 to 1.0 radian/ second degrades workload with little change in heading performance for ω_d = 2.3 radians/ second and a slight improvement in performance for ω_d = 1.3 radians/ second. While the higher ω_d performance-workload data confirms pilot rating trends, the ω_d = 1.3 workload data suggest an influence of bandwidth on flying qualities which is absent in the pilot ratings of the lower diagram of Figure 56. For low ω_d, the pilots' objection to large, low frequency heading excursions stands as the likely explanation for the lack of improvement in pilot ratings when bandwidth was reduced.

Contribution of Dutch roll damping ratio

For the lowest Dutch roll frequency tested, increasing the Dutch roll damping ratio offers an improvement in flying qualities for the heading tracking task. The combined effects of Dutch roll damping ratio and yaw disturbances on pilot rating are shown in Figure 59. Data for both low and high levels of roll disturbance, for a roll time constant, T_R = .25 seconds, Dutch roll frequency, ω_d = 1.3 radians/ second, and bandwidth $\frac{V_o}{L}$ = 1.0 radian/ second are given in the figure. Improvements in pilot rating on the order of a full rating unit are observed for an increase in damping ratio from ζ_d = .1 to .4, regardless of the level of roll or yaw disturbances. Although no data are shown for other dynamics configurations, some brief evaluations indicated little or no improvement in rating for the same increment in ζ_d at the highest Dutch roll frequency, ω_d = 3.0 radians/ second.

Flight test data reveal a reduction in the rudder workload for the case of large roll and yaw disturbances when the damping ratio is increased from ζ_d = .1 to .4. These results are shown in Figure 60 for T_R = .25 seconds, ω_d = 1.3 radians/ second, $\frac{V_o}{L}$ = 1.0 radian/ second. No change in the magnitude of heading excursions is noted for the large disturbance case, nor does there seem to be any effect of damping ratio on bank angle excursions or aileron workload. Since the level of yaw excursions is essentially the same

$T_R = .25$ sec $V_o/L = 1.0$ rad/sec
$\omega_d = 1.3$ rad/sec

$\sigma_L \doteq .6$ rad/sec^2

Dutch Roll Damping Ratio, ζ_d

RMS Yaw Disturbance, rad/sec^2

$\sigma_L \doteq 1.2$ rad/sec^2
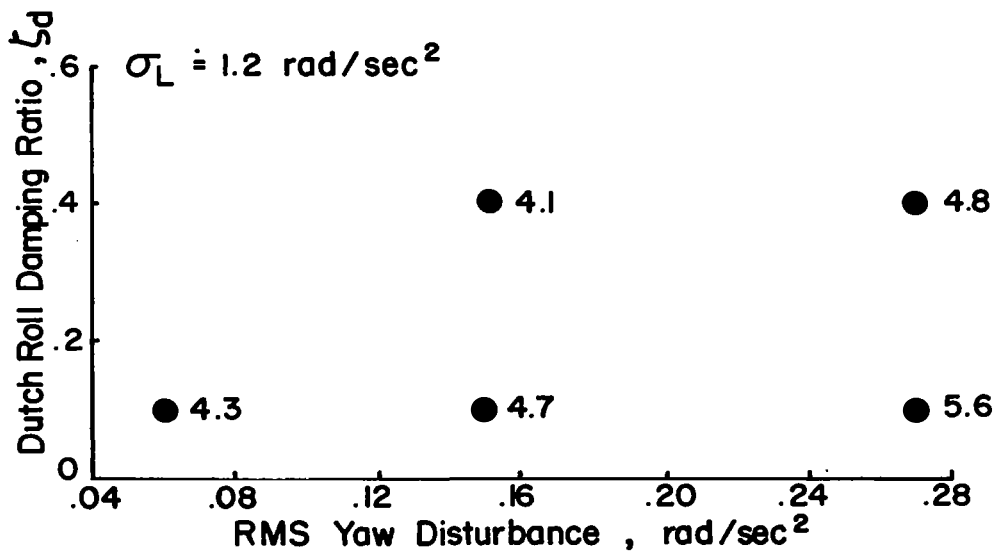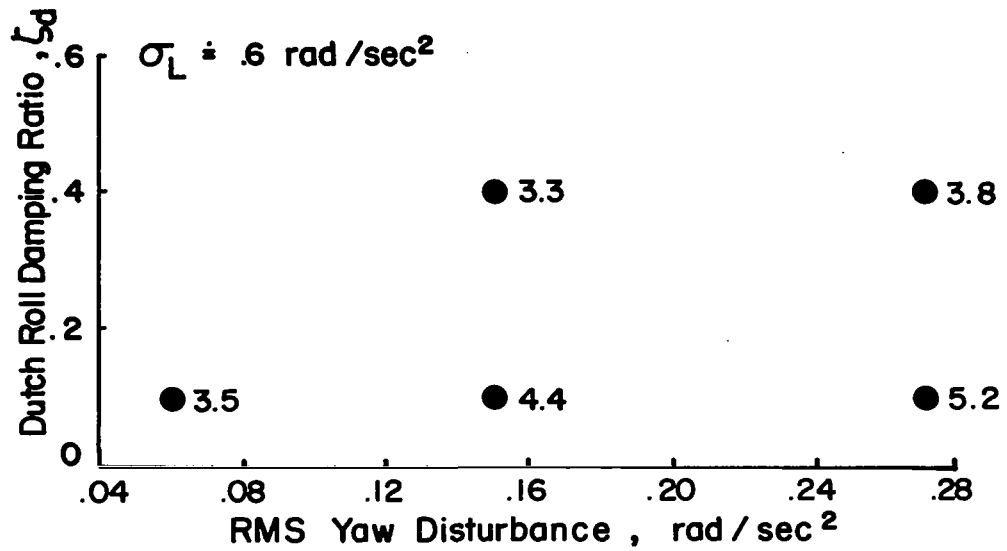
Figure 59.   Effect of Dutch Roll Damping Ratio on Pilot Opinion

$T_R = .25$ sec $V_o/L = 1.0$ rad/sec
$\omega_d = 1.3$ rad/sec $\sigma_L \doteq 1.2$ rad/sec^2
$\sigma_N = .27$ rad/sec^2
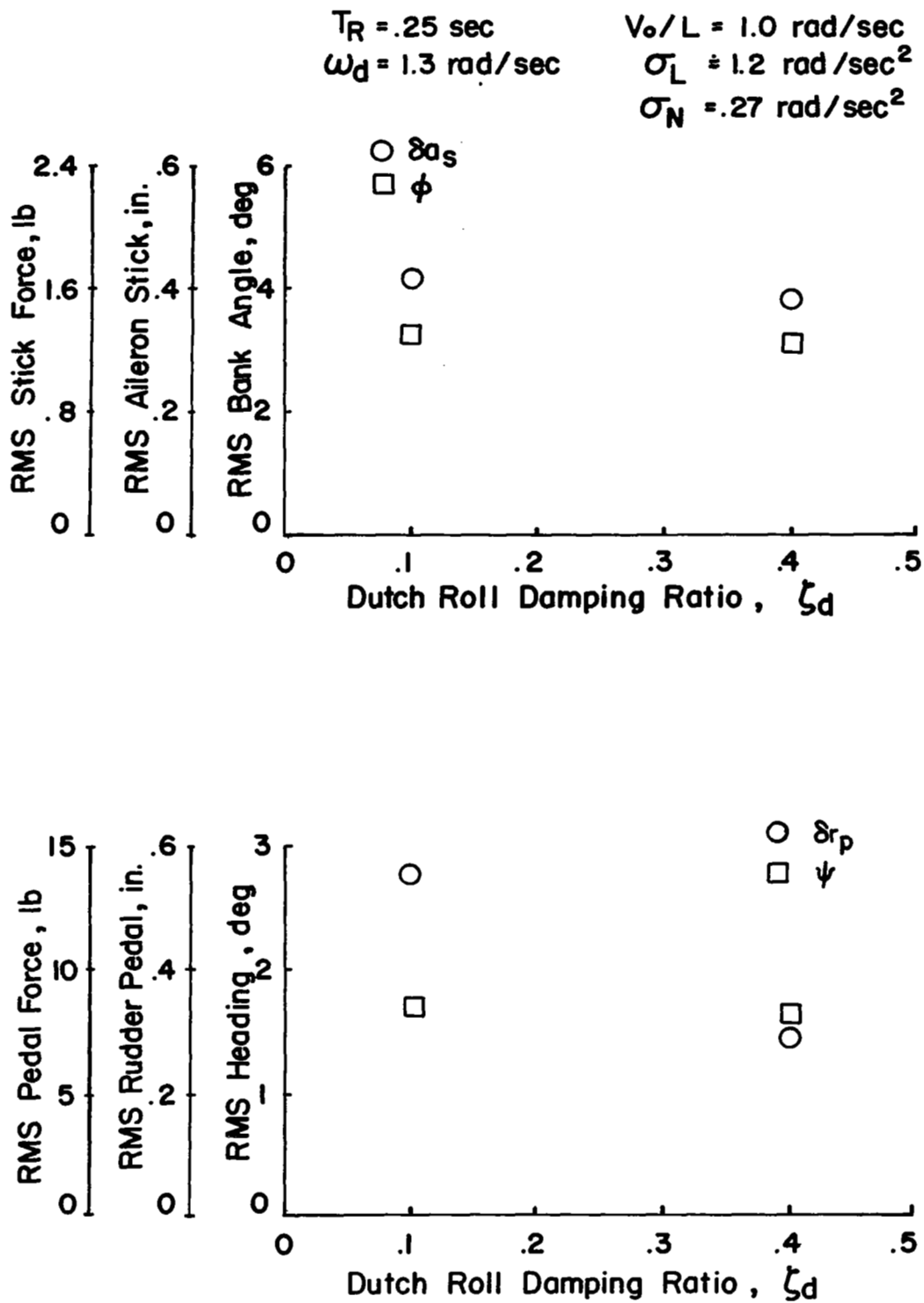
Figure 60.   Effect of Dutch Roll Damping Ratio on Task Performance and Workload

144

for the two values of damping ratio, the effect of yaw coupling into roll is similar in both instances, hence the activity in the roll channel would be expected to stay the same. At the lowest roll and yaw disturbance level (not shown) no changes in performance or workload for either roll or yaw are apparent as the damping ratio is increased.

Contribution of aileron yaw ($N_{\delta a}$ or $\frac{\omega_\varphi}{\omega_d}$)

Considering the primary evaluation pilot's data (shown to the right of the test points) no significant trends in POR are observed for variations in the airplane's aileron yaw characteristics. Figure 61 shows the aileron yaw configurations tested along with variations in the level of roll and yaw disturbances for an otherwise good combination of lateral dynamics ($T_R = .25$ seconds, $\omega_d = 2.3$ radians/second, $\zeta_d = .1$, $\frac{V_o}{L} = 1.0$ radian/second). It is intriguing to note the case for large roll and small yaw disturbances where vigorous lateral control activity might be anticipated as the pilot attempts to reduce the bank angle excursions. Even large amounts of adverse and favorable yaw do not produce degraded pilot ratings. Furthermore, increasing the yaw disturbance level has no more degrading effect on the pilot's ratings for large amounts of aileron yaw than in the absence of aileron yaw. Essentially the same conclusions may be drawn for the unsatisfactory lateral dynamics configuration. Data for this case ($T_R = .5$ seconds, $\omega_d = 1.3$ radians/second, $\zeta_d = .1$, $\frac{V_o}{L} = 1.0$ radian/second) is shown in Figure 62. The maximum spread in pilot rating shown, Δ POR $= .4$, is hardly significant considering the ranges of aileron yaw and of the $\frac{\omega_\varphi}{\omega_d}$ parameter which were tested.

Data obtained from two other evaluation pilots for variations in aileron yaw characteristics are also shown in Figures 61 and 62 above and below the test point. It is apparent for either of these pilots that favorable yaw has an undesirable effect on pilot ratings for the heading control task. This observation particularly applies for the case of large roll disturbances and for the airplane with the poorer lateral-directional dynamics shown in Figure 62. The
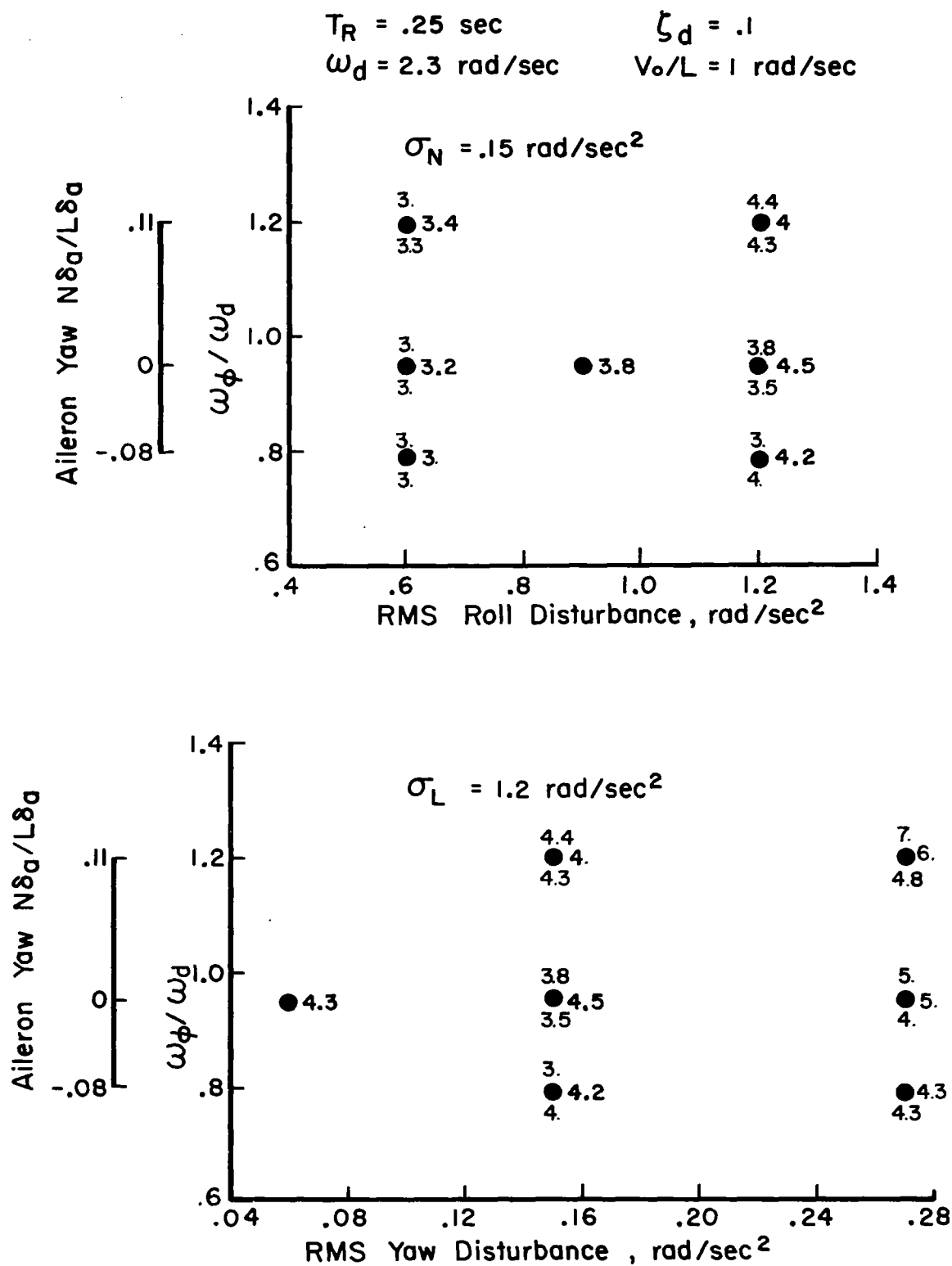
Figure 61. Effect of Aileron Yaw on Pilot Opinion Rating - High Roll
Damping and Directional Stability

146

$T_R = .5$ sec $\zeta_d = .1$
$\omega_d = 1.3$ rad/sec $V_o/L = 1$ rad/sec

$\sigma_N = .15$ rad/sec^2

$\sigma_L = 1.2$ rad/sec^2
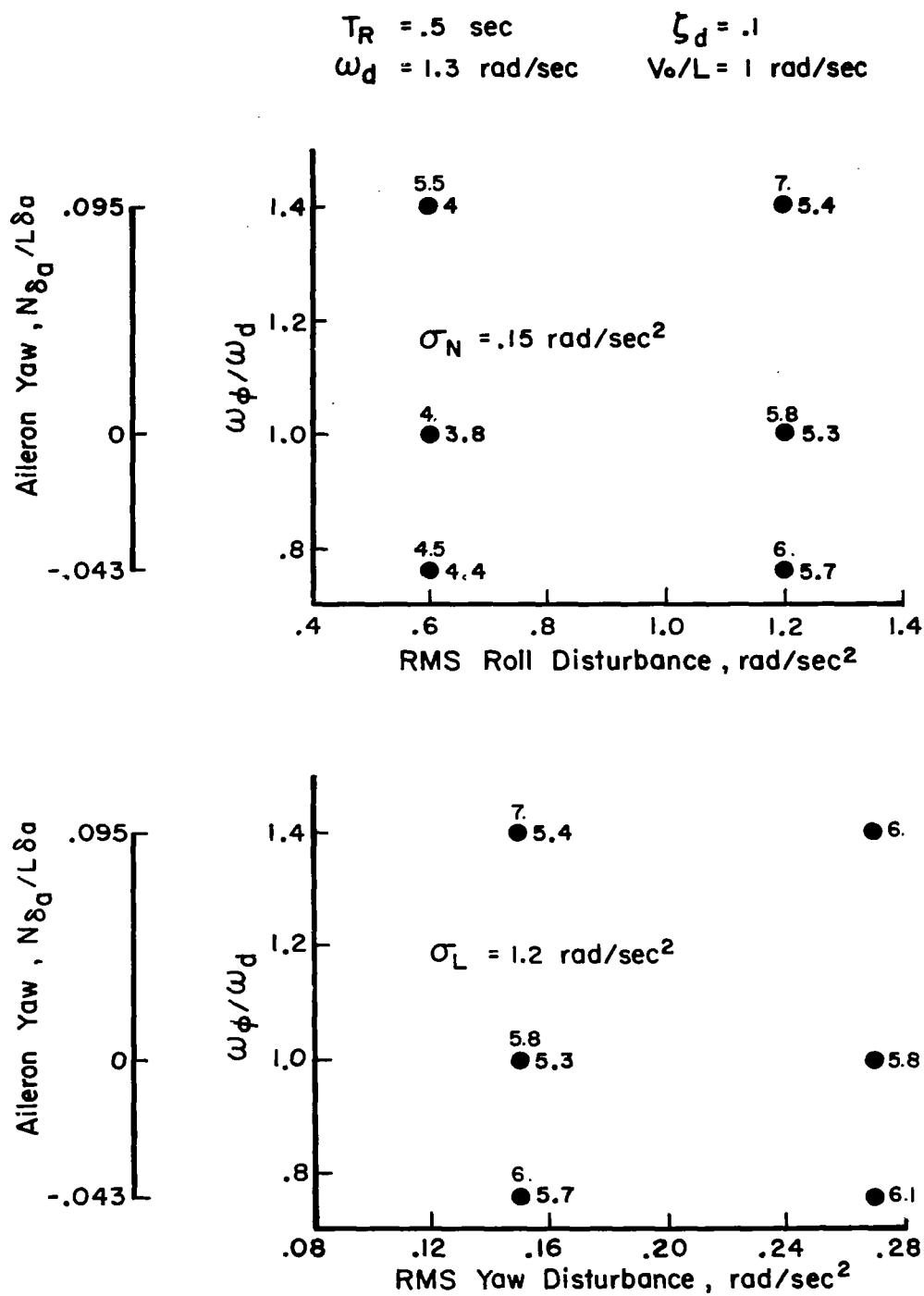
Figure 62. Effect of Aileron Yaw on Pilot Opinion Rating – Low Roll
Damping and Directional Stability
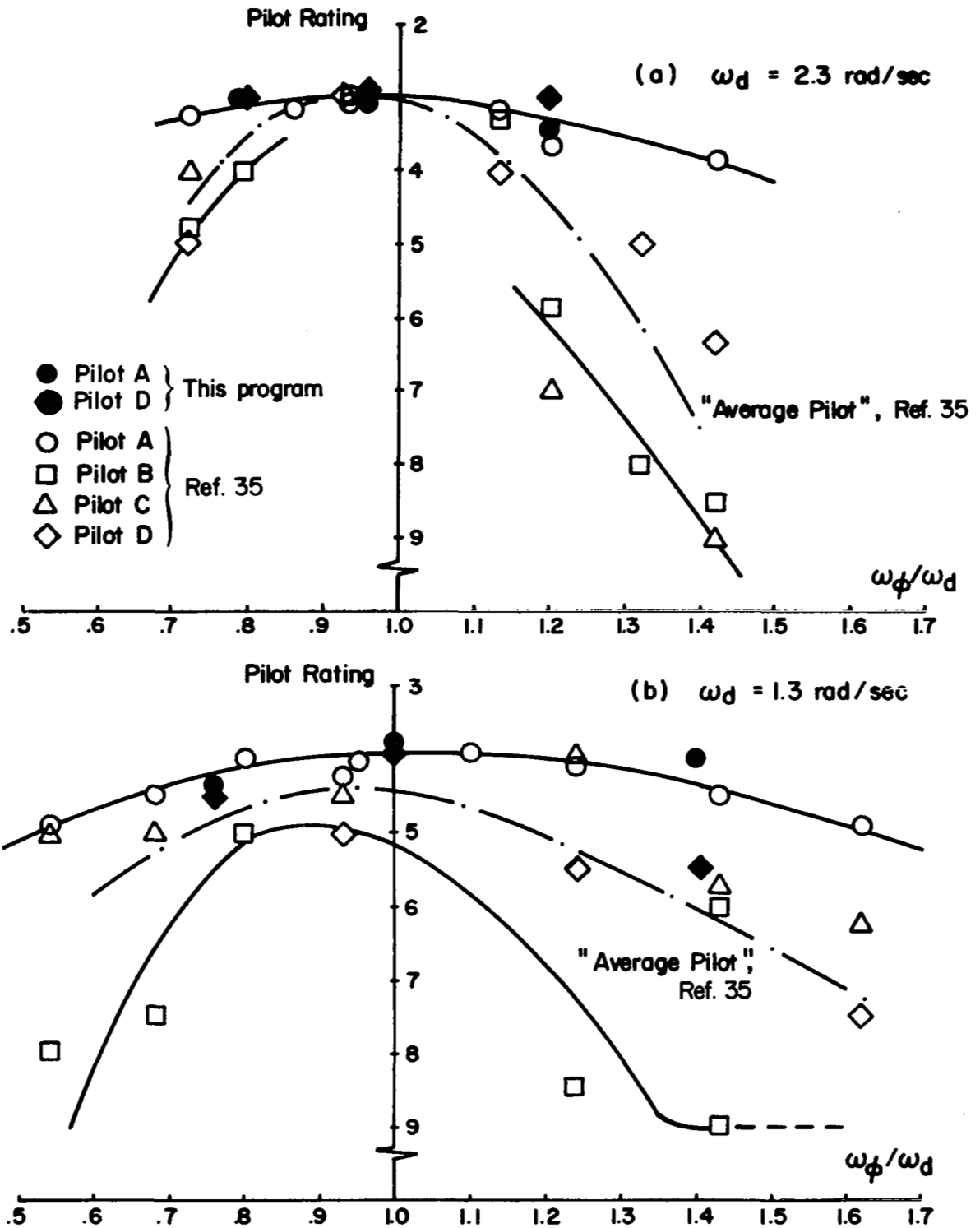
Figure 63.   Comparison of POR Trends with Aileron Yaw with
Reference 35 Data

148

influence of adverse yaw is not so pronounced. While it appears that pilot ratings may be degraded in the presence of adverse yaw compared to the case when aileron yaw is absent, this trend is not clear cut. The influence of aileron yaw on the heading control task for the range of $-N_{\delta a}$ tested may equally well be considered negligible.

Pilot commentary reveals an awareness of the presence of aileron yaw and its sign even though a degradation in rating was not always reported accordingly. Favorable yaw was particularly easy for the pilot to detect and remarks which have come to be expected for tight roll attitude control under these circumstances were noted, i.e., "Dutch roll is apparent," "poorly damped," "seem to be feeding it with my lateral control," etc. However, the primary evaluation pilot while registering many of these complaints did not correspondingly downgrade the airplane's flying qualities. The ability and willingness of the pilot to use the rudder under circumstances such as these seems to have some bearing on the results. The primary pilot was obviously willing to use the rudder vigorously when directional control got out of hand, and he apparently could use it to good advantage. When specifically questioned in this regard, one of his comments worthy of note could be paraphrased-----I would not downgrade a configuration just because I had to use the rudder in addition to the ailerons to maintain satisfactory control. It depends on how well I can use the rudder in a given instance and how hard I have to work to get the performance I want-----. Furthermore, his remarks indicate that he was using the rudder and ailerons as separate controls, without attempting to work the rudder in a coordinated manner with the ailerons. He apparently adopted this technique because the airplane's roll and heading response to turbulence appeared to him as two distinct and uncorrelated motions.

The apparent insensitivity of the primary evaluation pilot to favorable aileron yaw is worthy of further discussion. This pilot's comments suggest that his ability to skillfully use the rudder to counteract heading disturbances

due to aileron activity may account for the absence of a trend of his ratings with aileron yaw. However, as is subsequently indicated, neither rudder workload data or the closed loop analysis of the heading control task support this insensitivity to favorable yaw. Furthermore, considerable data exists in the flying qualities literature (References 2, 6, 32, 40, and 41 are examples) which demonstrate a degrading influence of favorable yaw on closed loop roll control with ailerons. Therefore, it is reasonable to consider whether this pilot's data provides a representative indication of the effects of aileron yaw on the heading control task.

A series of tests were conducted at Princeton during another flying qualities study which evaluated the influence of aileron yaw (or $\omega_\varphi / \omega_d$) on the ILS task. The results of that program are reported in Reference 35 and some data pertinent to the dilemma at hand are reproduced from that report in Figure 63. The data shown apply to two sets of dynamics which are:

(a)	(b)
$\omega_d = 2.3$ rad/sec	$\omega_d = 1.3$ rad/sec
$\zeta_d = .1$	$\zeta_d = .1$
$T_R = .25$ sec	$T_R = .25$ sec

It is apparent that a wide range of opinion existed about the influence of favorable aileron yaw. While the trend of POR for the "average pilot" indicates a decidedly undesirable effect of favorable yaw, the upper bounds of these data show a trend with aileron yaw comparable to the primary pilot's ratings of the current program. Data from Figures 61 and 62 are included among the Reference 35 results in Figure 63 for sake of comparison. Test conditions in the top (a) diagram correspond exactly for the two sets of data so far as dynamics and simulated turbulence disturbances are concerned. In the bottom (b) diagram the following differences in test conditions between this program and those of Reference 35 should be noted:

Current program   Reference 35

$T_R = .5$ sec $T_R = .25$ sec

$\sigma_N = .15$ rad/sec^2 $\sigma_N = .06$ rad/sec^2

For both (a) and (b) the Reference 35 data were obtained from an ILS approach terminated by a VFR alignment maneuver. Although the data for the $\omega_d = 1.3$ radian/second configuration from the two programs were not obtained for identical test conditions, it is still interesting to compare their trends of POR with ω_φ/ω_d.

As has just been noted in the foregoing discussion, the primary pilot's data (O) for cases (a) and (b) shows essentially the same variation with ω_φ/ω_d as the upper boundary of the Reference 35 results. This agreement between the pilot ratings of the two programs is unlikely to be coincidental since the same pilot produced both sets of data. One of the secondary pilots ($\Diamond$) also participated in both programs and it is interesting to note, particularly for $\omega_d = 1.3$ radians/second, that the trends of his ratings with ω_φ/ω_d were also reasonably consistent for the two sets of data. This pilot's ratings indicate a degrading influence of favorable aileron yaw comparable to the so-called "average pilot" of Reference 35.

The point of the foregoing discussion is to suggest the likelihood of a degrading influence of favorable aileron yaw on the heading control task, such as is not apparent in the primary evaluation pilot's data of this program. The explanation of this divergence between the different pilots' impressions of favorable yaw may possibly be related to the respective pilots' willingness to use the rudder for control of heading excursions and their ability to use it skillfully and independently of the lateral control. The same conclusion is reached in Reference 35. In both programs it is apparent that the primary pilot was quite adept at using the rudder for heading control while it was not so clear that the other pilots could perform as well with their feet. At any rate, data obtained in this program are not sufficient to definitively establish the trend of pilot rating with aileron yaw. A larger sampling of pilots is required to define the influence of aileron yaw to a satisfactory degree of confidence.

Performance-workload data for the primary and one of the secondary evaluation pilots are shown in Figure 64 for otherwise good lateral dynamics and for the high level of roll disturbance. The primary evaluation pilot's results show no significant trends in bank angle excursions or aileron workload with aileron yaw. Degradation in rudder workload is observed for the favorable yaw configuration. The secondary pilot's data show some increase in roll workload with aileron yaw. Yaw axis performance data remain essentially constant with aileron yaw, while workload increases somewhat with favorable aileron yaw.

For the case of unsatisfactory lateral dynamics, shown in Figure 65, the primary pilot's bank angle excursion and aileron workload improve somewhat for favorable yaw. Heading performance is constant over the range of aileron yaw tested; however the rudder workload increases with aileron yaw, particularly in the favorable sense. The secondary pilot's roll attitude performance deteriorates some with aileron yaw while his workload remains the same. While heading excursions are nearly constant regardless of the amount of aileron yaw, the rudder workload increases substantially with favorable yaw.

The performance and workload data obtained for both pilots offer some support of their individual pilot ratings. Exceptions to this general conclusion are the higher than nominal rudder workloads for the favorable yaw cases of Configurations 11 and 14. No corresponding deterioration was noted in the primary pilot's ratings to accompany these workload trends.
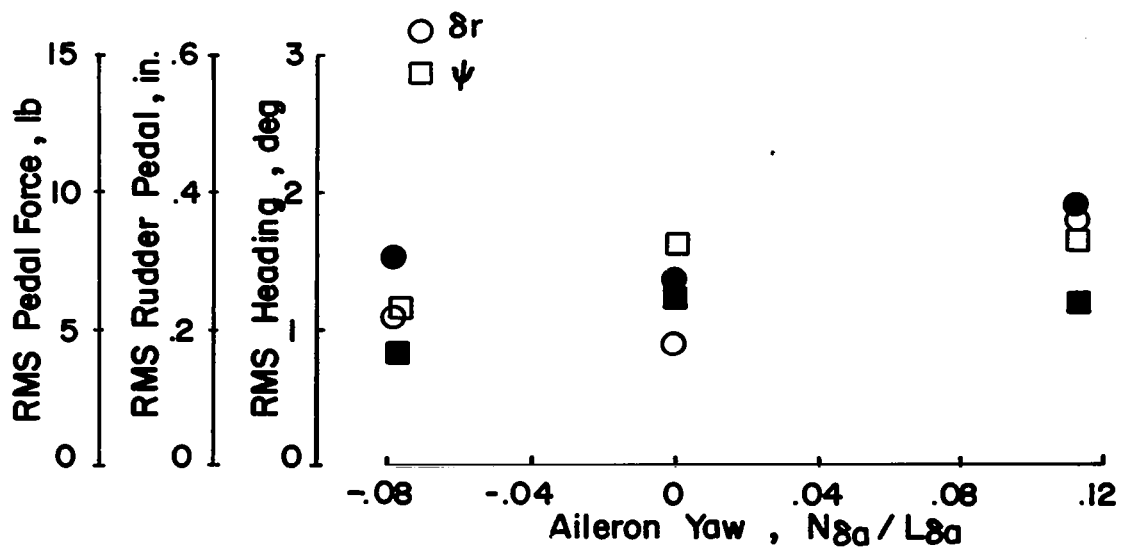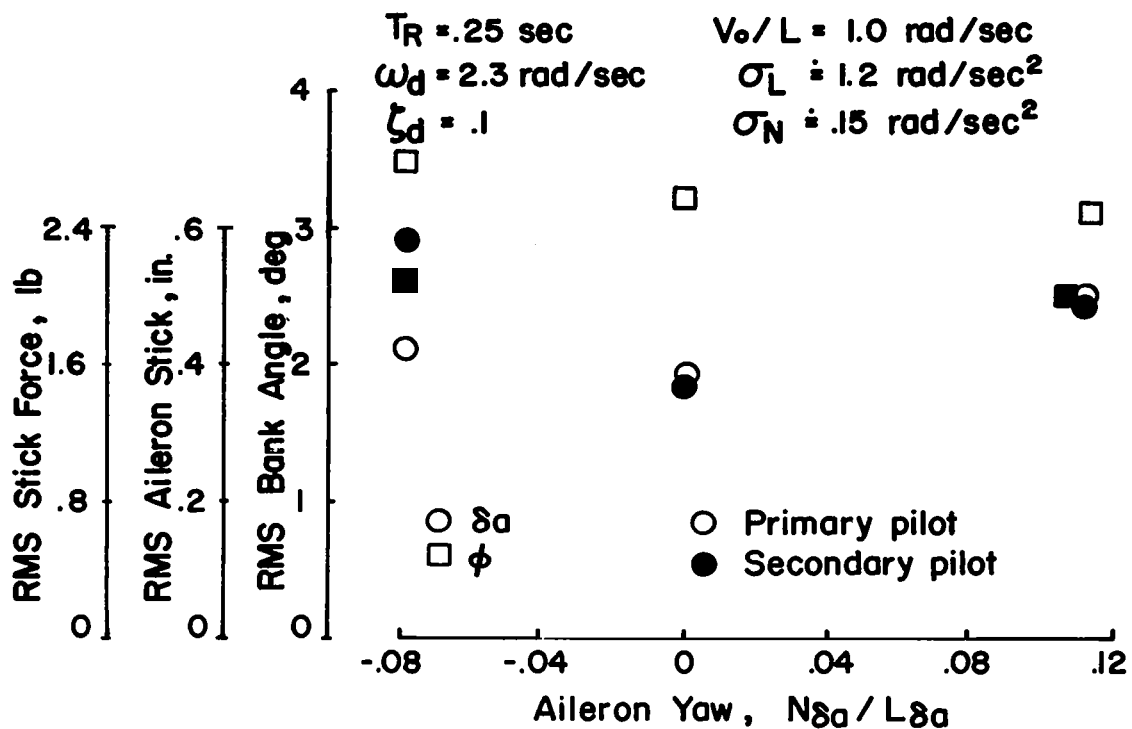
Figure 64. Effect of Aileron Yaw on Task Performance and Work-
load - Good Roll Damping, Good Directional Stability

153
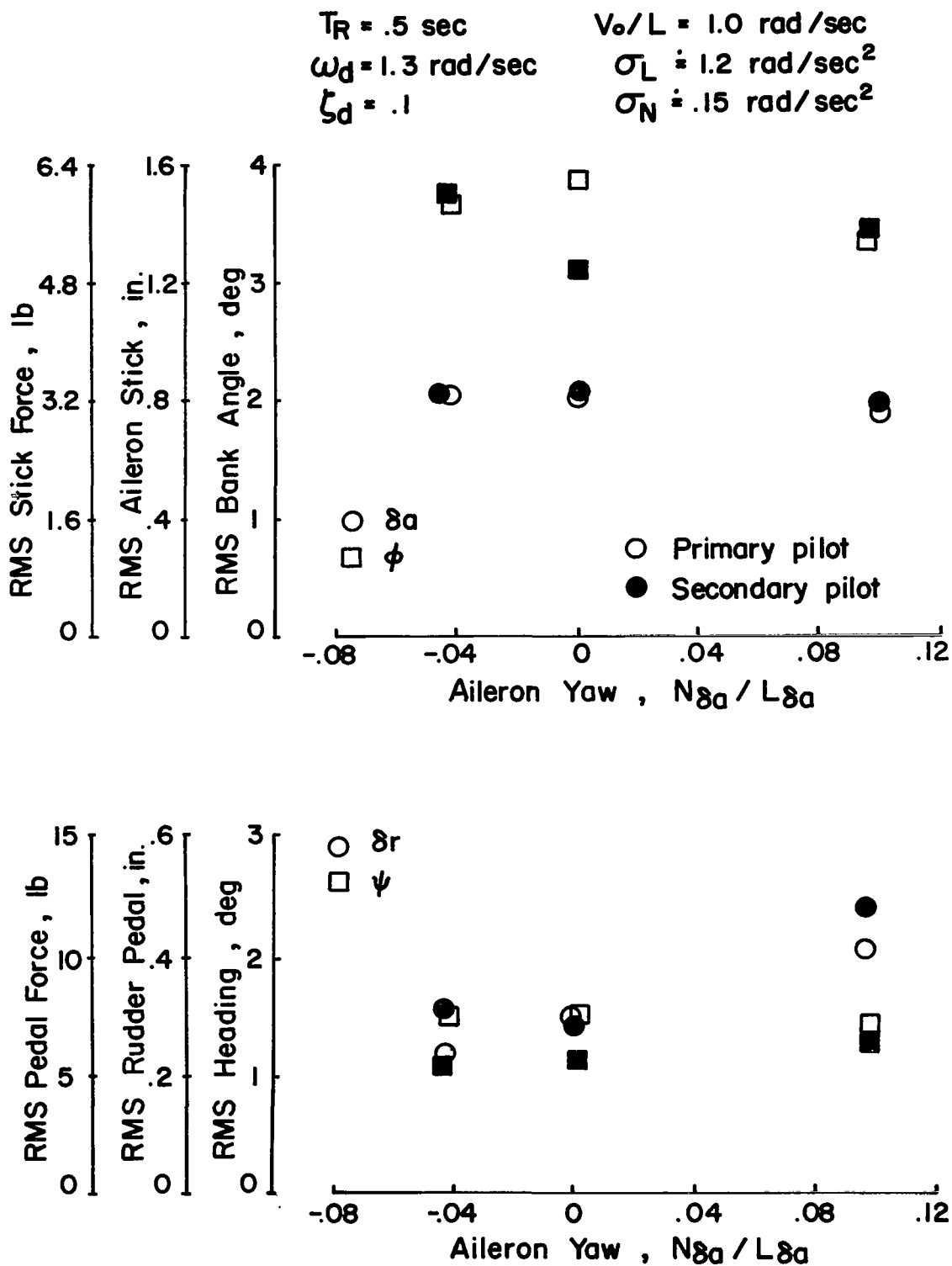
Figure 65.   Effect of Aileron Yaw on Task Performance and Work-
load - Poor Roll Damping, Poor Directional Stability

154

Pilot-Vehicle Systems Analysis

Background

The foregoing discussion has presented the results of the flight test program in terms of pilot opinion ratings and commentary, and has attempted to substantiate these results with measures of the precision of task performance and pilot control workload. The following text presents a closed loop systems analysis of the control of the airplane in turbulence with the purpose of identifying deficiencies of pertinent control loops and predicting trends in task performance and control workload with variations in turbulence and airplane dynamics.

The problem of closed loop control of the airplane in turbulence is stated analytically in equation (4) of Section 1 as

$$\Phi_{\epsilon\epsilon} = \left| \frac{Y_G}{1 + Y_A Y_p} \right|^2 \Phi_{ff}$$

neglecting command inputs.

Specializing this to the cases of roll and heading excursions gives

$$\Phi_{\varphi_\epsilon} = \frac{\left| \dfrac{N^\varphi_{w_g}}{\Delta} \right|^2 \Phi_{w_g} + \left| \dfrac{N^\varphi_{v_g}}{\Delta} \right|^2 \Phi_{v_g}}{\left| 1 + Y_{P_{\delta a}} \dfrac{N^\varphi_{\delta a}}{\Delta} \right|^2} \tag{88}$$

for the bank angle spectral density for roll control with ailerons only and

$$\Phi_{\psi_{\epsilon}} = \frac{|\dfrac{N'^{\psi}_{w_g}}{\Delta'}|^2 \, \Phi_{w_g} + |\dfrac{N'^{\psi}_{v_g}}{\Delta'}|^2 \, \Phi_{v_g}}{|\, 1 + Y_{p_{\delta r}} \dfrac{N'^{\psi}_{\delta r}}{\Delta'}|^2} \tag{89}$$

for the spectral density of heading excursions for heading controlled with the rudder and bank angle controlled with the ailerons. In the case of either bank angle or heading, the closed loop turbulence response spectra can be interpreted as the airplane's open loop response spectra divided by the square of the absolute magnitude of the closed loop characteristic roots for the pertinent control loop. This statement may be analytically expressed by rewriting equation (4) as

$$\Phi_{\epsilon\epsilon} = |\frac{Y_G}{1 + Y_A Y_p}|^2 \, \Phi_{ff} = \frac{\Phi_{O.L.}}{|\, 1 + Y_A Y_p|^2}$$

This statement is correct for bank angle response but it is not precise for the case of heading response. The so-called open loop heading response in the numerator of equation (89) actually represents heading response with a bank angle to aileron loop closed. However, for the analysis to follow where the bank angle loop is closed at high gain, it is sufficiently accurate to represent the numerator of (89) by open loop heading response to turbulence. Furthermore, if yaw disturbances due to vertical gusts are much less than yaw disturbances due to lateral gusts (as will be the case when $N_{p_g} \ll N_{\beta_g}$) then the open loop heading response is approximately that due to lateral gusts. Thus the numerator of (89) may be written

$$\Phi_{\psi_{O.L.}} \doteq |\frac{N'^{\psi}_{v_g}}{\Delta}|^2 \, \Phi_{v_g} \doteq |\frac{N'^{\psi}_{w_g}}{\Delta'}|^2 \, \Phi_{w_g} + |\frac{N'^{\psi}_{v_g}}{\Delta'}|^2 \Phi_{v_g}$$

If the closed loop turbulence response is to be considered in terms of these two elements, that is open loop response and closed loop control characteristics, it is first necessary to set forth a criteria for specifying the pilot's role in the control loops of interest. To obtain desirable closed loop response it has been pointed out in Reference 38 that the pilot will try to achieve the following results

- $Y_A Y_p \gg 1$ for $\omega \ll \omega_c$ in order to suppress the effects of the turbulence disturbances and other undesirable inputs, and to follow command inputs over a sufficient bandwidth, where ω_c, the crossover frequency, is the frequency for which $|Y_A Y_p| = 1.0$

- $Y_A Y_p \ll 1$ for $\omega \gg \omega_c$

- $Y_A Y_p$ in the crossover region of the form $\dfrac{\omega_c \, e^{-j\omega \tau_e}}{j\omega}$, with bandwidth to exceed the input bandwidth, $\omega_c \gg \omega_f$, and with sufficient stability margin to avoid a poorly damped dominant mode.

In pursuit of these objectives, the pilot can increase his own gain, observing the constraints imposed by excessive workload and stability considerations. For cases where the vehicle may be approximated by one of a few simple single loop transfer functions, Reference 38 has shown that the pilot, in attempting to follow a command input with minimum error, will maintain an essentially constant open loop bandwidth for $Y_A Y_p$ (using gain to do so) and will provide sufficient stability margin either by generating a first order lead or by reducing his equivalent time lag. Consideration is given these principles in defining the loop closures best suited to achieving the desired closed loop response.

157

Bank angle control - Considering the case of bank angle control with the ailerons, the general form of the open loop transfer function relating bank angle to aileron inputs is

$$\frac{\varphi}{\delta a} = \frac{N^{\varphi}_{\delta a}}{\Delta} = \frac{L_{\delta a}(s^2 + 2\zeta_{\varphi}\omega_{\varphi}s + \omega_{\varphi}^2)}{(s + 1/T_S)(s + 1/T_R)(s^2 + 2\zeta_d\omega_d s + \omega_d^2)} \tag{90}$$

while the pilot may be represented by

$$Y_p = K_{\varphi} T_{L\varphi}(s + 1/T_{L\varphi})\left(\frac{1 - \dfrac{\tau_e}{2}s}{1 + \dfrac{\tau_e}{2}s}\right) \tag{91}$$

Lead compensation is provided by the term $s + 1/T_{L\varphi}$ while the pilot's transport delay and neuromuscular lags are approximated by the first order Padé expression $\left(\dfrac{1 - \dfrac{\tau_e}{2}s}{1 + \dfrac{\tau_e}{2}s}\right)$. The time constant is a composite of the transport delay and muscular lag factors $\tau_e \doteq \tau_p + T_N + \dfrac{2\zeta_N}{\omega_N}$ and is on the order of $0.2 < \tau_e < 0.4$ seconds. This simplified representation of the transport delay provides reasonably accurate information of the amplitude and phase characteristics of the more complete pilot model of Reference 38 over the range of frequencies of interest in this problem.

The closed loop characteristic equation may now be written

$$1 + \frac{L_{\delta a} K_{\varphi} T_{L\varphi}(s + 1/T_{L\varphi})(s^2 + 2\zeta_{\varphi}\omega_{\varphi}s + \omega_{\varphi}^2)(1 - \dfrac{\tau_e}{2}s)}{(s + 1/T_S)(s + 1/T_R)(s^2 + 2\zeta_d\omega_d s + \omega_d^2)(1 + \dfrac{\tau_e}{2}s)} \tag{92}$$

Since in the vicinity of crossover, the pilot's objective is to achieve a combined controller - controlled element which looks like

$$Y_p Y_A \doteq \frac{\omega_c}{s} e^{-\tau_e s}$$

he will tend to create enough lead to cancel the airplane's roll mode, $1/T_R$. Furthermore, if the amounts of aileron yaw, yaw due to roll, and dihedral effect are fairly small (or in suitable combination such that $\zeta_\varphi \omega_\varphi \doteq \zeta_d \omega_d$ and $\omega_\varphi \doteq \omega_d$) then the second order zero will cancel the Dutch roll pole. Finally, assuming a nearly neutral spiral mode, the closed loop characteristic equation may be simplified to

$$1 + \frac{L_{\delta a} K_\varphi T_{L\varphi}}{s} \left(\frac{1 - \frac{\tau_e}{2} s}{1 + \frac{\tau_e}{2} s} \right) \tag{93}$$

The bandwidth and closed loop stability achievable are indicated by rewriting the closed loop equation

$$s^2 + \frac{2}{\tau_e} \left(1 - \frac{\tau_e}{2} K_\varphi T_{L\varphi} L_{\delta a} \right) s + \frac{2}{\tau_e} K_\varphi T_{L\varphi} L_{\delta a} \tag{94}$$

The real damping $\zeta_{CL} \omega_{CL}$ and natural frequency ω_{CL} can be expressed in terms of the coefficients of (94)

$$\zeta_{CL} \omega_{CL} = \frac{1}{\tau_e} \left(1 - \frac{\tau_e}{2} K_\varphi T_{L\varphi} L_{\delta a} \right)$$

$$\omega^2_{CL} = \frac{2}{\tau_e} K_\varphi T_{L\varphi} L_{\delta a}$$

or with a little reorganization

$$\zeta_{CL} = \frac{1}{\tau_e \omega_{CL}} - \frac{\tau_e \omega_{CL}}{4} \qquad (95)$$

$$\omega_{CL} = \sqrt{\frac{2}{\tau_e} K_\varphi T_{L\varphi} L_{\delta a}} \qquad (96)$$

Hence, the bandwidth of the system can be related directly to the pilots gain and to his effective time lag, while the closed loop damping is dependent on the time lag and bandwidth. For neutral stability

$$\tau_e \omega_{CL} = 2.$$

and hence, for the range of time lags previously noted, the corresponding range of bandwidths associated with neutral stability is

$$5 < \omega_{CL} < 10 \text{ radians/second}$$

Since some stability margin is desirable, the actual permissible bandwidth in the bank angle loop will be somewhat less than this. Experimental results from Reference 38, where the pilot is attempting to minimize error in tracking a random command input, indicates a bandwidth of around 4.5 radians/second and time lags in the neighborhood of .2 seconds for a controlled element of the type $\frac{K_c}{s}$. These characteristics might reasonably be assumed as the best practicable for the roll loop indicated and will be used for upper bounds for the level of closed loop performance in the absence of more directly applicable evidence of pilot compensation.

When the roll axis can be represented in the aforementioned manner, the pilot should have little trouble in achieving satisfactory closed loop bandwidth and stability margin, at least so long as he has adequate control authority and effectiveness and is able to generate lead on the order of the roll mode time

160

constant. Evidence from roll tracking task data indicates that pilot opinion of the controlled element begins to deteriorate for roll time constants in excess of approximately .5 seconds. Recent landing approach studies at Princeton (References 2, 3, and 35) support this tendency as does the analysis of Reference 39 and the data collected in Reference 40. Hence difficulty with roll control and an associated deterioration in pilot rating would be anticipated for roll time constants in the neighborhood of .5 seconds or greater.

When the derivatives L_β, N_p, and $N_{\delta a}$ are not all small or in the proper combination to provide effective cancelling of the Dutch roll pole - zero pair the roll control situation is not so simply described. The relative orientation of the numerator roots with respect to the Dutch roll pole on the complex plane has a great deal to do with the closed loop bandwidth and stability margin which can be achieved as has been amply demonstrated analytically in Reference 41. In particular, if $\zeta_\varphi \omega_\varphi < \zeta_d \omega_d$, and especially if $\zeta_\varphi \omega_\varphi$ is negative or if $\omega_\varphi > \omega_d$, the ability to achieve a satisfactory bandwidth while retaining sufficient stability margin is severely compromised. Conversely, if $\zeta_\varphi \omega_\varphi > \zeta_d \omega_d$ and if $\omega_\varphi < \omega_d$, the Dutch roll does not tend to interfere with the achievement of good closed loop performance in the roll tracking task. All of what has just been stated can be demonstrated by the root locus - Bode diagram of Figure 66. The potential for closed loop instability and the limits on bandwidth when $\zeta_\varphi \omega_\varphi < \zeta_d \omega_d$ or $\omega_\varphi > \omega_d$ are apparent. Typical closed loop roots are shown for the case where $\zeta_\varphi \omega_\varphi \doteq \zeta_d \omega_d$, $\omega_\varphi \doteq \omega_d$. For this condition the closed loop Dutch roll remains in the near vicinity of the open loop Dutch roll, the roll mode is constrained at its open loop value, and the spiral-pilot time delay roots coalesce into a complex pair representing a well damped oscillatory mode (referred to as the roll-spiral pair).
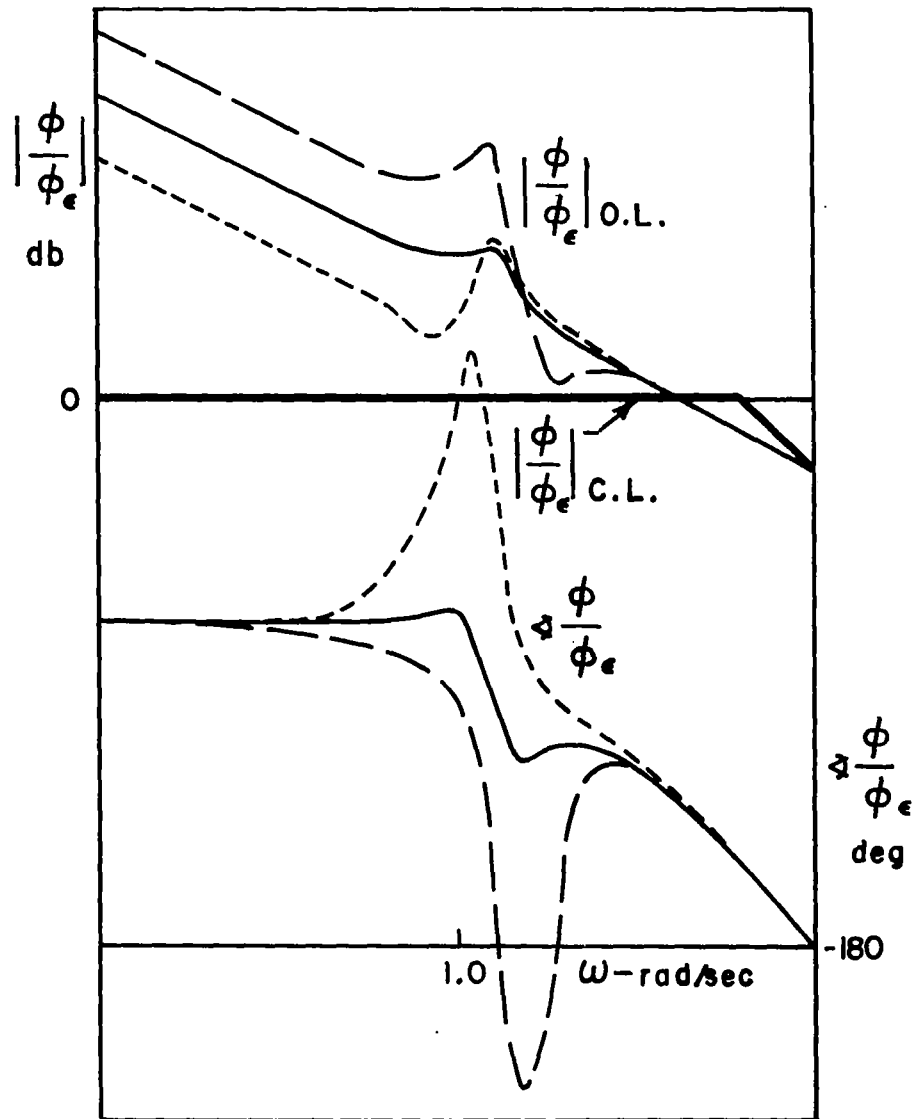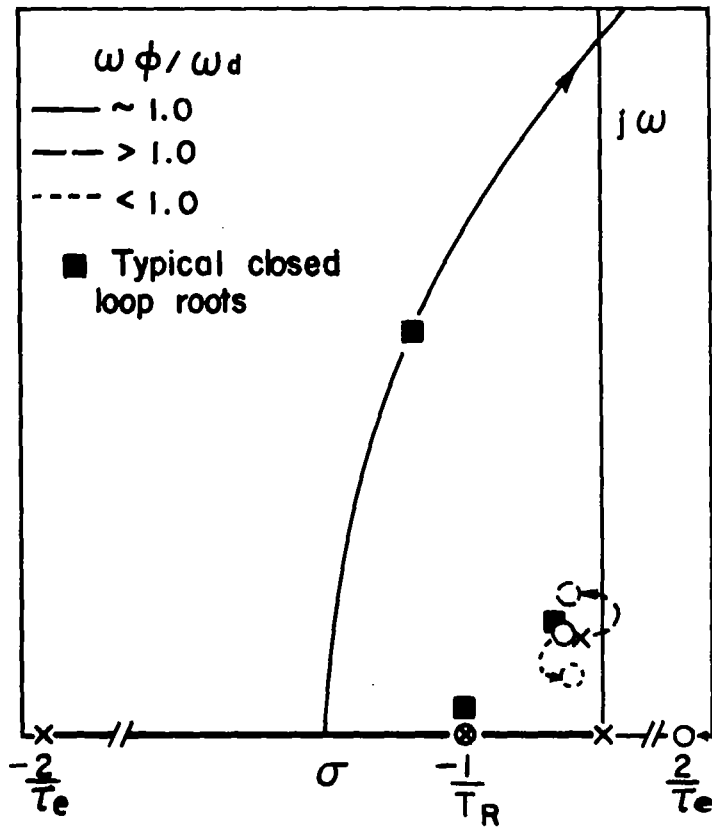
Figure 66. Characteristics of Closed Loop Bank Angle Control
with Ailerons

The foregoing discussion encompasses only part of the problem of roll turbulence response, namely the contribution associated with the denominator of equation (88). The numerator represents the airplane's open loop roll response to turbulence. To illustrate the contribution of lateral gusts to roll, the open loop roll response spectrum may be written as shown in Appendix D.

$$\Phi_{\varphi_{O.L.}}(\omega) = \left| \frac{\dfrac{L_\beta T_R}{\omega_d^2}(j\omega)}{(T_R j\omega + 1)\left(\dfrac{j\omega^2}{\omega_d^2} + \dfrac{2\zeta_d}{\omega_d}j\omega + 1\right)} \right|^2 \frac{\left(\dfrac{\sigma_v}{V_o}\right)^2 \dfrac{L}{\pi V_o}}{\left[\left(\dfrac{\omega L}{\sqrt{3}\,V_o}\right)^2 + 1\right]} \qquad (97)$$

for the case of a neutral spiral mode and for $L_\beta = L_{\beta_g}$.
The factors having an influence on the magnitude and frequency content of the roll excursions are

- magnitude $\quad \dfrac{L_\beta T_R}{\omega_d^2}$, $\left(\dfrac{\sigma_v}{V_o}\right)$, ζ_d , ω_d , T_R , $\dfrac{V_o}{L}$

- frequency content $\quad T_R$, ω_d , $\dfrac{V_o}{L}$

A typical roll spectrum appears in Figure 67. It is apparent that a dominant portion of the energy in the spectrum is in the immediate vicinity of the Dutch roll root.

Combining the open loop roll response to lateral gusts with the closed loop roots achieved by controlling bank angle with ailerons gives the closed loop roll response to lateral gusts. A graphical display of the two contributions to roll response is shown in Figure 68. To significantly improve the airplane's roll response, the pilot must achieve sufficient bandwidth to attenuate energy in the open loop spectrum in the vicinity of the
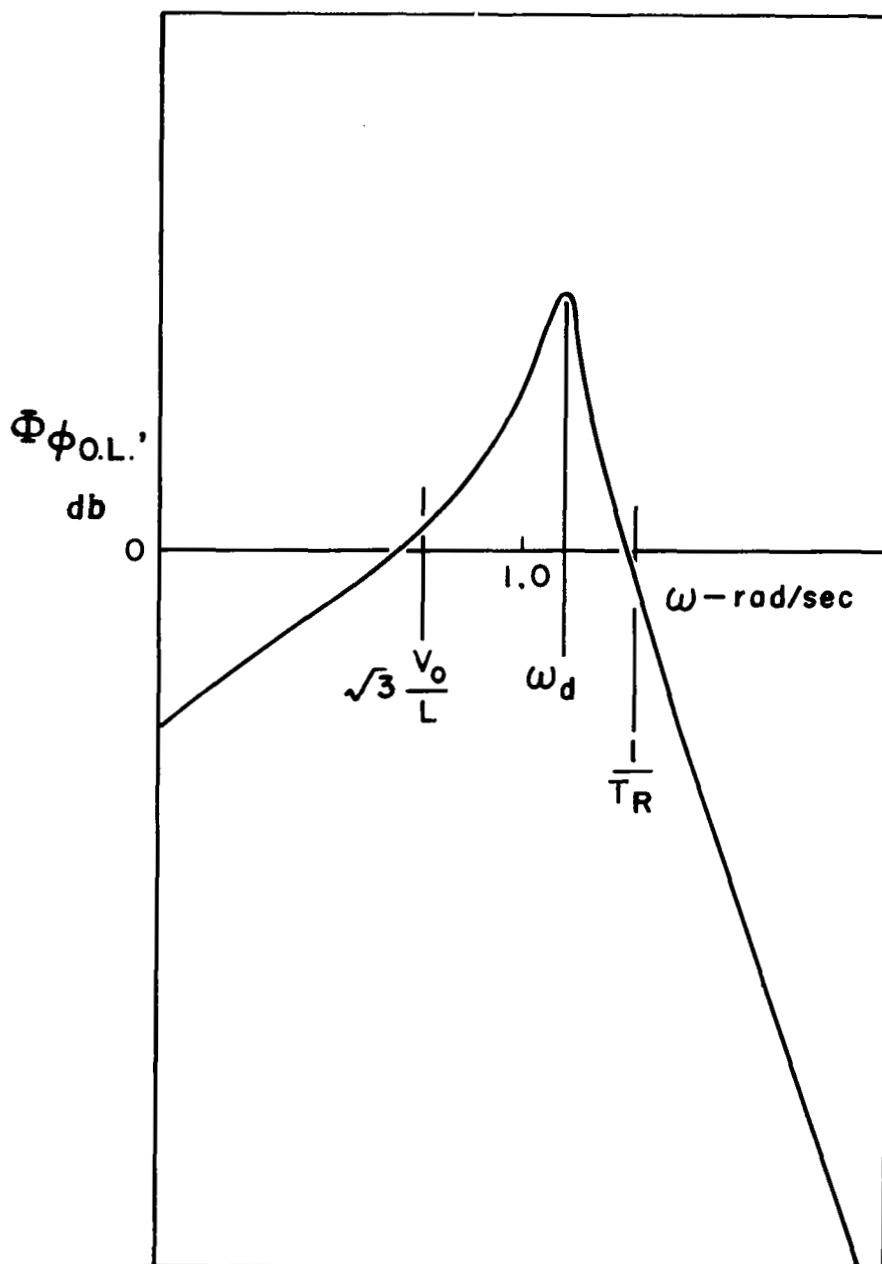
Figure 67. Typical Open Loop Roll Response Spectrum
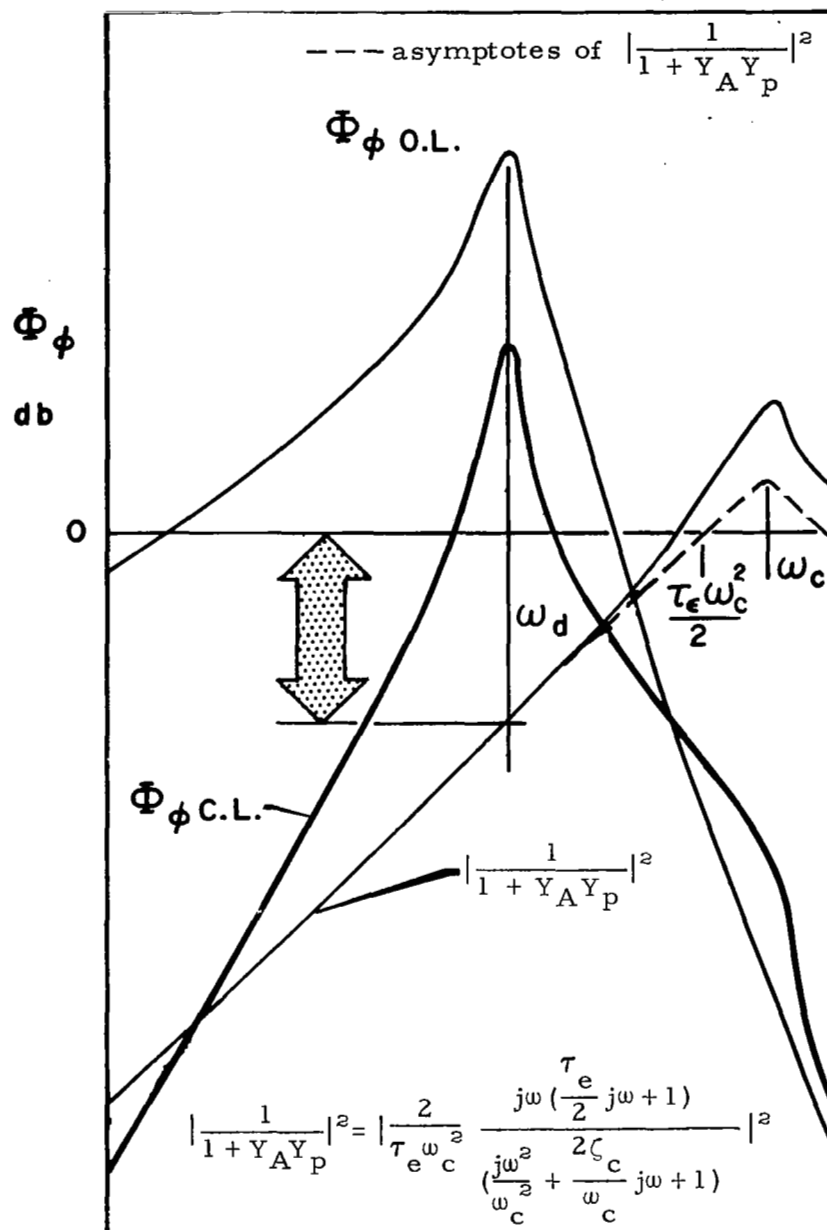
Figure 68. Closed Loop Bank Angle Response to Lateral Gusts

Dutch roll frequency. A grossly simplified estimation of the attenuation achievable in the open loop spectrum can be made by determining the attenuation provided by the closed loop pilot-airplane at the Dutch roll frequency (indicated by the arrow⤒). Considering the asymptotes of the closed loop equation, this attenuation may be expressed

$$\left[\frac{\Phi_{\varphi_{C.L.}}}{\Phi_{\varphi_{O.L.}}} \right]_{\omega=\omega_d} \doteq \left(\frac{\omega_d}{\frac{\tau_e}{2} \omega_c^2} \right)^2$$

$$\doteq \frac{\omega_d^2}{(K_\varphi T_{L\varphi} L_{\delta a})^2} \qquad (\text{for } \zeta_\varphi \omega_\varphi \doteq \zeta_d \omega_d$$

$$\omega_\varphi \doteq \omega_d)$$

(98)

The closed loop bank angle spectrum is indicated by the heavy solid line. The suppression of the Dutch roll provided by the pilot is apparent. Note that the contribution of the higher frequency closed loop roll-spiral mode to the response spectrum is insignificant and will remain so as long as it has sufficient damping.

Heading control - As the pilots indicate in their comments on configurations having heading control problems, they were forced to use the rudder as their primary heading control. The ailerons were useful in making corrections in the airplane's average heading on a long period basis. As will be seen later, the heading-aileron loop does not have sufficient bandwidth to attenuate higher frequency heading excursions.

The heading to rudder transfer function, assuming bank angle control by ailerons provides an inner loop form of equalization, may be represented by

$$\frac{\psi}{\delta r}\Big]_{\varphi \to \delta a} = \frac{N^{\psi}_{\delta r} + Y_{P_{\delta a}} N^{\psi \, \varphi}_{\delta r \, \delta a}}{\Delta + Y_{P_{\delta a}} N^{\varphi}_{\delta a}} = \frac{N'^{\psi}_{\delta r}}{\Delta'} \tag{99}$$

using the format for multiloop equations described in Reference 47. When the bank angle to aileron loop is closed at high gain consistent with band-widths noted in the previous discussion of roll control, and when $T_{L_{\varphi}} \doteq T_R$, then the heading to rudder transfer function may be expressed as

$$\frac{N'^{\psi}_{\delta r}}{\Delta'} = \frac{N_{\delta r}(s + 1/T_{\psi_1})(s + 1/T_R')(s^2 + 2\zeta_{\psi}\omega_{\psi}s + \omega_{\psi}^2)}{s(s^2 + 2\zeta_{SR}\omega_{SR}s + \omega_{SR}^2)(s + 1/T_R)(s^2 + 2\zeta_d'\omega_d's + \omega_d'^2)}$$

The numerator terms may be explained as follows

- $1/T_{\psi_1}$ - low frequency root largely determined by the magnitude of Y_v.

- $1/T_R'$ - approximately the magnitude of the roll mode or pilot time delay root resulting from the bank angle to aileron loop closure.

- $\zeta_{\psi}, \omega_{\psi}$ - approximately the frequency and damping ratio to cancel the oscillatory root resulting from the bank angle to aileron loop.

The denominator terms are the characteristic roots of the bank angle to aileron loop and are typically defined as

- $\dfrac{1}{T_R}$ — roll mode, which is exactly the open loop roll mode if $T_{L\varphi} = T_R$ in the bank angle to aileron loop.

- ζ_{SR}, ω_{SR} — referring to the oscillatory roots of the $\varphi \to \delta_a$ loop which are typically wide bandwidth and well damped.

- ζ_d', ω_d' — referring to the modified Dutch roll mode, which can either be well damped or poorly damped, based on the open loop Dutch roll roots and on the $\zeta_\varphi, \omega_\varphi$ zeros of the bank angle to aileron loop.

It is reasonable to simplify the heading to rudder transfer function, based on the approximate cancellations noted, to the form

$$\frac{N_{\delta r}^{\psi'}}{\Delta'} \doteq \frac{N_{\delta r}(s + 1/T_{\psi_1})}{s(s^2 + 2\zeta_d' \omega_d' s + \omega_d'^2)} \tag{100}$$

Combining (100) with a pilot model of the same form as equation (91) produces a closed loop heading to rudder equation

$$1 + \frac{K_\psi T_{L\psi} N_{\delta r}(s + 1/T_{L\psi})(s + 1/T_{\psi_1})(\frac{2}{\tau_e} - s)}{s(s^2 + 2\zeta_d' \omega_d' s + \omega_d'^2)(\frac{2}{\tau_e} + s)} \tag{101}$$

The bandwidth of this loop is strongly dependent on ω_d' and on ζ_d', $T_{L\psi}$, τ_e, and T_{ψ_1} as well. Damping of the modified Dutch roll is a strong influence on the achievable bandwidth. The amount of lead the pilot can generate when tracking heading and his effective time lag have a bearing on the stability margin which can be maintained with increasing bandwidth.

A typical representation of these characteristics is shown in Figure 69. In particular, the closed loop Bode asymptote (heavy solid line) reveals a so-called "mid frequency droop" which is referred to in Reference 42. Note that if the modified Dutch roll is poorly damped (dashed line), the effective band-width of this loop can be on the order of the $1/T_{\psi_1}$ root or less. Furthermore, if $1/T_{\psi_1}$ is very small, there will be a wide frequency range over which the pilot has a limited ability to attenuate unwanted disturbances.

It has been stated that the modified heading response numerator of equation (89) is essentially the same as the airplane's open loop heading response to lateral gusts (p. 156). In cases where this observation is sufficiently pre-cise, namely when aileron yaw $(N_{\delta a})$ and yaw due to roll (N_p) are small such that the following approximations hold

$$\frac{N_{\delta a}}{L_{\delta a}} \ll \frac{N_\beta}{L_\beta}$$

$$\frac{N_p}{L_p} \ll \frac{N_\beta}{L_\beta}$$

then the numerator of equation (89) may be approximated as shown in Appendix D.

$$\Phi_\psi(\omega)_{O.L.} \doteq \left| \frac{\dfrac{N_\beta}{\omega_d^2}}{(\dfrac{j\omega^2}{\omega_d^2}) + \dfrac{2\zeta_d}{\omega_d} j\omega + 1)} \right|^2 \frac{(\dfrac{\sigma_v}{V_o})^2 \dfrac{L}{\pi V_o}}{[(\dfrac{\omega L}{\sqrt{3}\, V_o})^2 + 1]} \qquad (102)$$
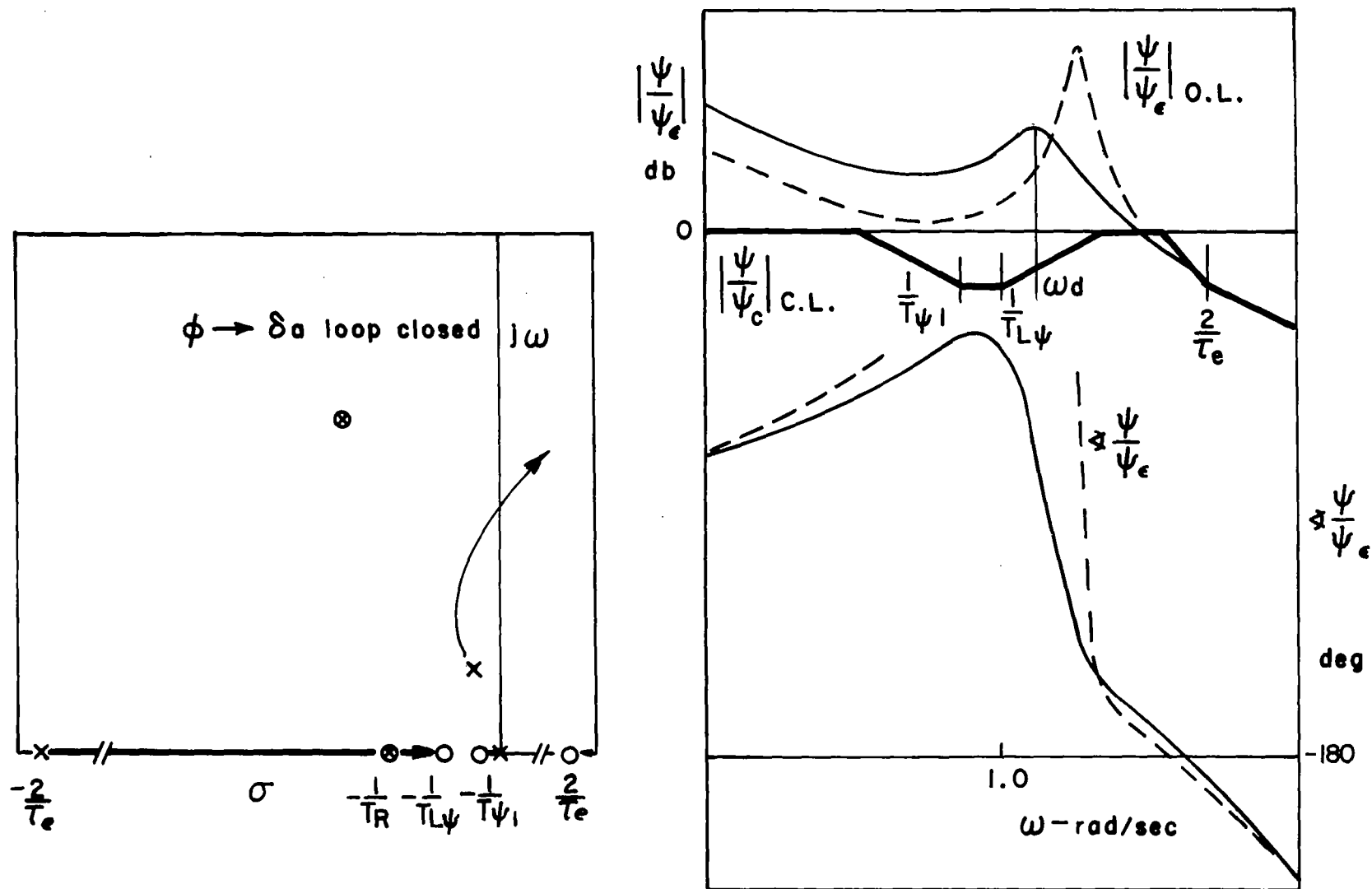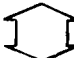
Figure 69.   Characteristics of Closed Loop Heading Control with
Rudder ($\phi \rightarrow \delta_a$ inner loop)

Magnitude and frequency content of the open loop heading response are determined by

- magnitude $\dfrac{N_\beta}{\omega_d^2}$, $\dfrac{\sigma_v}{V_o}$, ζ_d, ω_d, $\dfrac{V_o}{L}$

- frequency content ω_d, $\dfrac{V_o}{L}$

A typical heading spectrum appears in Figure 70. While the energy is spread across the frequency range up to the Dutch roll mode, if the open loop Dutch roll is at all poorly damped, a considerable portion of the total energy will be confined to the vicinity of ω_d.

Closed loop heading response to turbulence is determined by modifying the open loop response to account for the attenuation provided by the characteristic roots of the heading to rudder loop closure. The two components of closed loop heading response to lateral gusts are shown in Figure 71 along with the closed loop spectrum itself. The reduction in open loop response achievable by closing the heading to rudder loop appears to be largely dependent on the gain associated with the mid frequency asymptote indicated by the arrow ⟩⟨ . The attenuation associated with this gain may be shown to be

$$\left[\frac{\Phi_{\psi_{C.L.}}}{\Phi_{\psi_{O.L.}}} \right] \doteq \left(\frac{\tau_e' \, \omega_d'^2}{\tau_e \, \omega_d''^2} \right)^2 \tag{103}$$

The increase in bandwidth provided by the rudder loop closure (bandwidth increased approximately from ω_d' to ω_d'') provides the means for reducing the open loop response. A subtle influence on the adequacy of this loop, but a

171
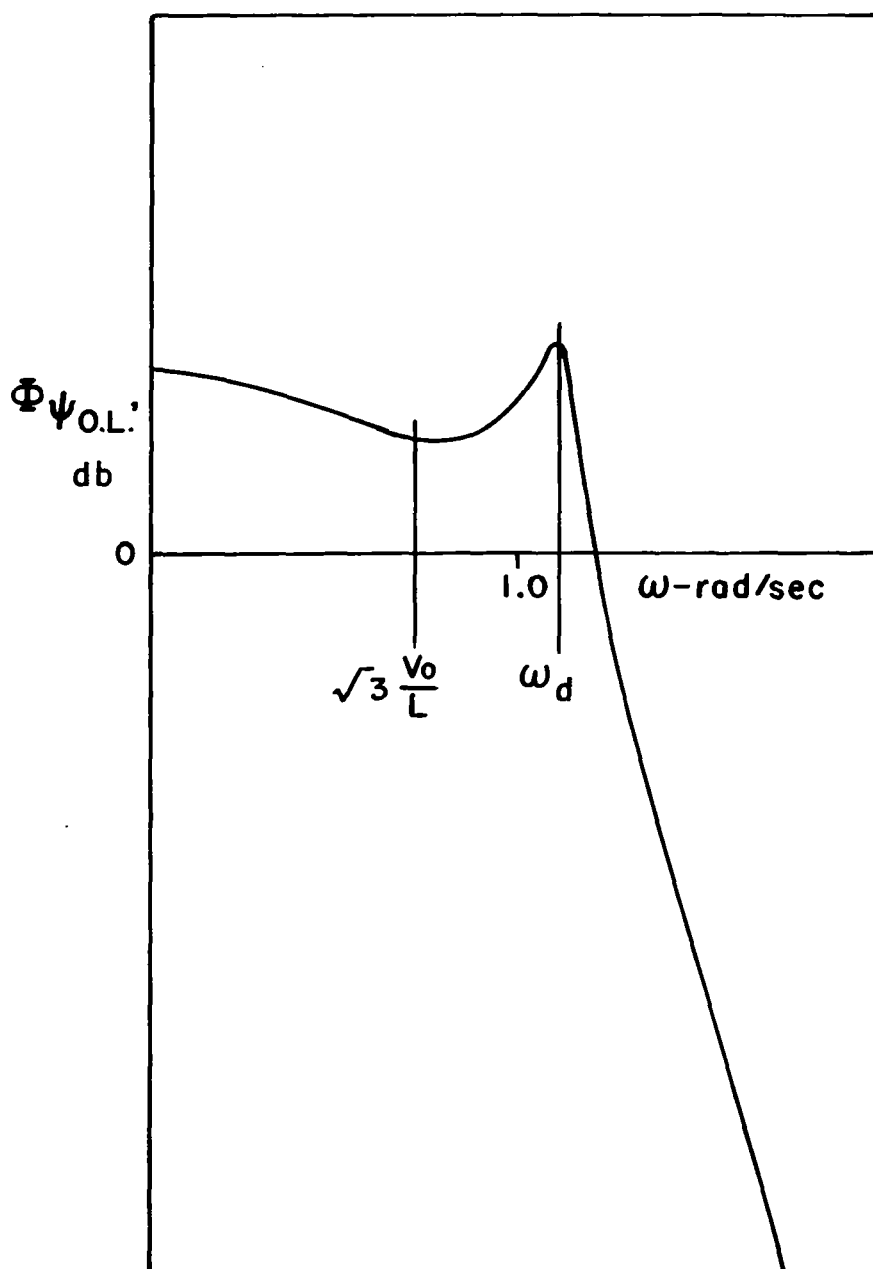
Figure 70. Typical Open Loop Heading Response Spectrum

172

potentially significant one, is the damping of the modified Dutch roll at ω_d''. The ability to attenuate open loop response may be compromised or even made impossible if a sufficient stability margin is not maintained at crossover or if the bandwidth of the modified Dutch roll is not made to exceed the open loop Dutch roll. Since attenuation of the open loop spectrum is of the order ω^{-6} for $\omega > \omega_d$, and if the bandwidth of the system is increased substantially, then no significant energy contribution should appear at the modified Dutch roll frequency, ω_d''. The degree of attenuation of the closed loop spectrum over the open loop case is apparent in Figure 71.

More specific consideration will be given to the characteristics of the bank angle to aileron and heading to rudder control loops for selected configurations from the test matrix. Root locus and frequency response (Bode) analyses are presented for the pilot-airplane combination of each of these configurations in the following discussion. Transfer functions of the system's closed loop response to turbulence are also shown. These configurations are chosen to demonstrate the effects of the same individual characteristics of turbulence and dynamics or combination of characteristics on which the flight test program focussed. To reiterate, these are

- contribution of turbulence - effects of rms roll and yaw disturbances, bandwidth, and roll-yaw correlation for satisfactory and unsatisfactory dynamics configurations,

- effect of roll damping combined with variations in rms roll disturbances and bandwidth,

- effect of directional stability combined with variations in rms yaw disturbances and bandwidth,

173

$- - -$ asymptotes of $\left|\dfrac{1}{1 + Y_A Y_p}\right|^2$

Φ_ψ O.L.

Φ_ψ db

Φ_ψ C.L.

ω_d''

O

$\dfrac{1}{T_{\psi_1}'}$

$\left[\dfrac{K}{T_{\psi_1}'}\right]^2$

ω_d'

$\dfrac{2}{\tau_e}$

$\left|\dfrac{1}{1 + Y_A Y_p}\right|^2$

$K = \dfrac{T_{\psi_1}' \, \tau_e' \, \omega_d'^{\,2}}{\tau_e \, \omega_d''^{\,2}}$

$$\left|\dfrac{1}{1 + Y_A Y_p}\right|^2 =$$

$$\left|\dfrac{K\,j\omega\left(\dfrac{j\omega^2}{\omega_d'^{\,2}} + \dfrac{2\zeta_d'}{\omega_d'}\,j\omega + 1\right)\left(\dfrac{\tau_e}{2}\,j\omega + 1\right)}{(T_{\psi_1}'\,j\omega + 1)\left(\dfrac{\tau_e}{2}\,j\omega + 1\right)\left(\dfrac{j\omega^2}{\omega_d''^{\,2}} + \dfrac{2\zeta_d''}{\omega_d''}\,j\omega + 1\right)}\right|^2$$
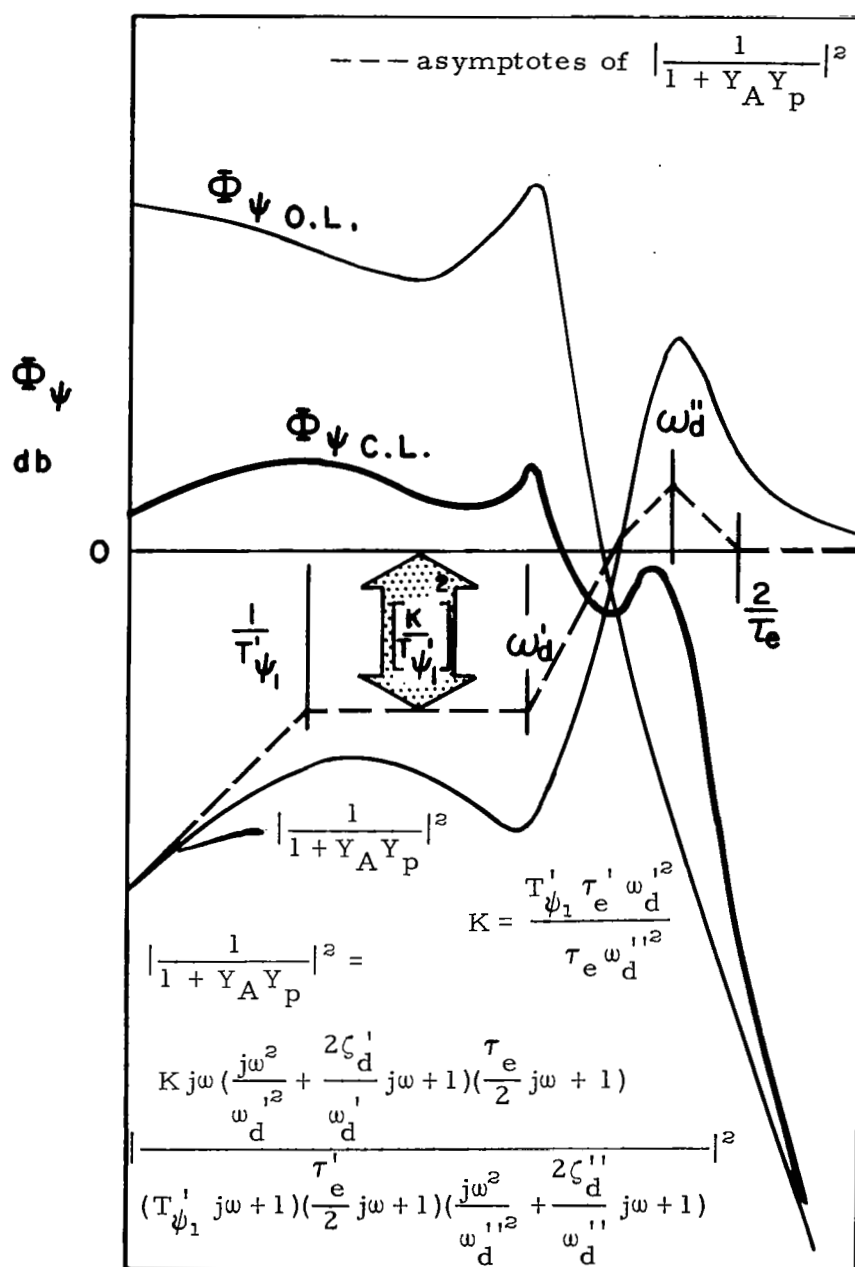
Figure 71. Closed Loop Heading Response to Lateral Gusts

174

- effect of Dutch roll damping combined with variations in rms yaw disturbances,

- effect of aileron yaw concentrating on the higher levels of roll disturbances.

Task performance and control workload - Considering the pilots' commentary throughout the test program, the level of task performance (measured in terms of rms excursions of the controlled variable, heading or bank angle) and control workload (rms rudder pedal or aileron stick activity) had a great deal to do with his eventual evaluation of the flying qualities of a configuration in turbulence. The pilot commentary and the correlation between pilot ratings and measured performance-workload data potentially give these performance and workload measures a unifying role in the explanation of flying qualities trends associated with the variety of parameters considered in the test program.

An indication of the overall variation of performance and workload for the entire test program is given in Figure 72. The data shown were obtained from the primary evaluation pilot and are a complete collection of his pilot rating and performance-workload data. The data presentation is separated into configurations primarily having heading control problems and configurations having roll control difficulties. The general impression gained from this figure is that the data predominantly reflect a variation in workload rather than performance. Rms heading excursions range from 1.1 to 2.5 degrees at either extreme with the bulk of the data concentrated between 1.4 and 2.0 degrees. Rudder pedal workload runs from .06 to .6 inches (1.5 to 15.0 pounds) and is rather evenly distributed throughout. Bank angle excursions and aileron stick workload are both evenly distributed over their ranges. Rms bank angles fall between 1.8 and 4.6 degrees while rms aileron stick runs from .18 to .94 inches (.75 to 3.7 pounds). For either the roll or yaw case the proportional increase in workload was greater than the proportional increase in bank angle or heading excursions.
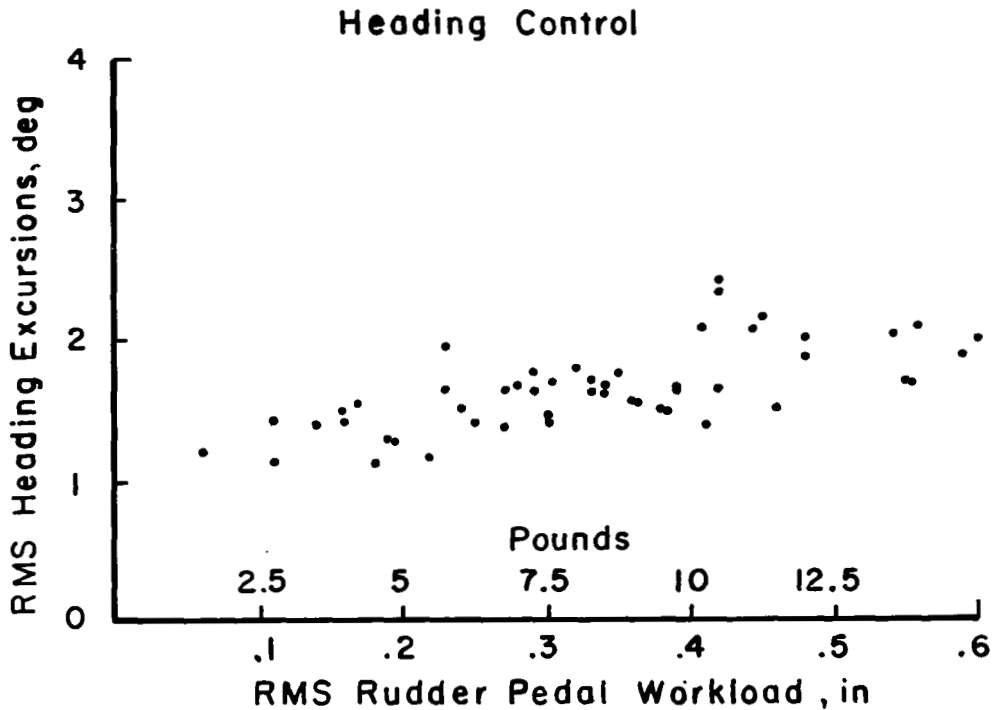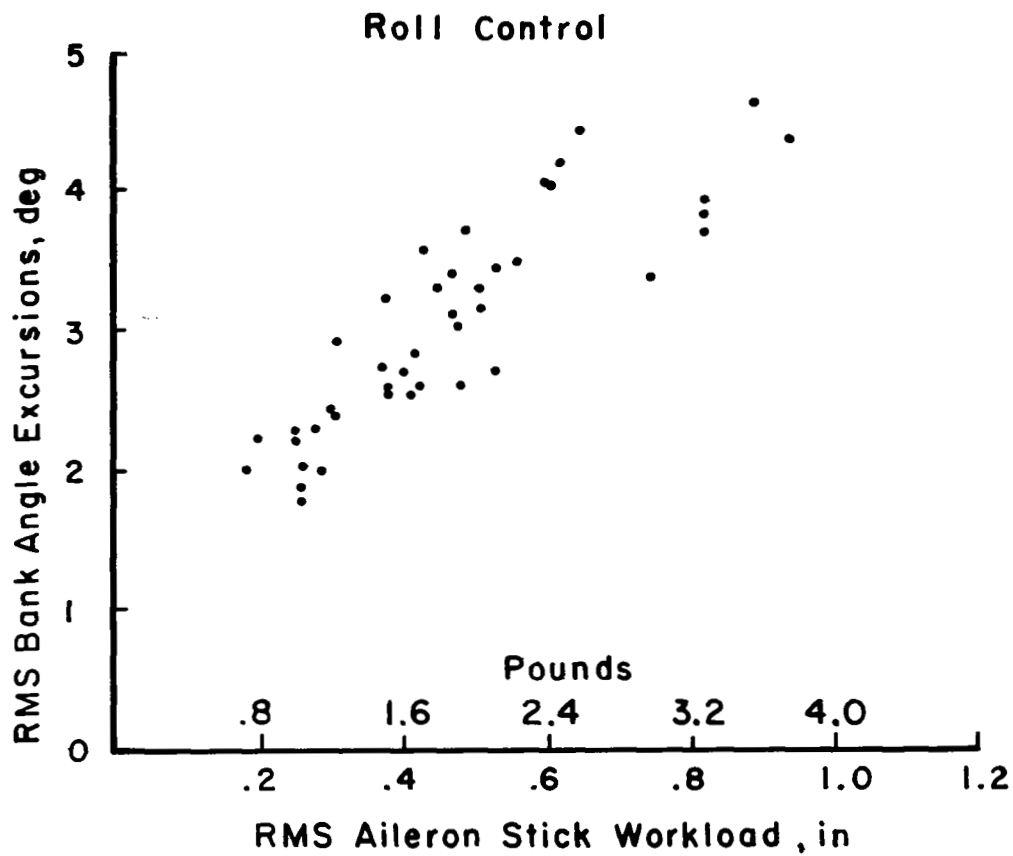
Figure 72. Trade Off Between Task Performance and Control
Workload - Primary Pilot

Pilot opinion ratings for these same configurations are shown in Figures 73 and 74. The pilot ratings are presented as functions of workload and performance separately. Considering the heading control data (Figure 73), a better correlation between pilot ratings and workload is apparent than between pilot ratings and heading excursions. Pilot rating scatter for the workload data is on the order of ±.5 rating units while the heading excursion data has a tolerance more on the order of ±1.0 unit. The scatter of one-half rating unit about a nominal value is quite acceptable and is within the limits of accuracy generally attributed to the rating scale.

Conclusions concerning the roll control data (Figure 74) are not as firm as for heading control. Pilot ratings appear to correlate to about the same degree with workload as with performance. Data scatter of ±.75 rating unit is typical for both cases.

Although the work put forth in the task and the performance achieved appear to have a great deal to do with the acceptability of a particular configuration in turbulence, they should not be considered the sole contributing factors. Another influence which is likely to be reflected in pilot ratings to some degree and which certainly affects the tradeoff between performance and workload is the degree of pilot compensation in either the roll or heading control loops. When the pilot is required to generate lead information to compensate for deficiencies in the airplane's dynamics, pilot rating is generally expected to degrade accordingly. References 39 and 43 offer evidence to this effect. Some lead compensation can be anticipated for some of the configurations in the test program particularly for the larger turbulence disturbances, and is often implicit in the related commentary, e.g., "I had to pay close attention to the task to get the desired level of performance," "high degree of concentration required." Some spectral measurements were made on selected data from the performance-workload flights and estimates were made of the lead time constant for the pilot in the heading-rudder loop. These results are introduced in the sub-section on system analysis for their respective configurations.

177
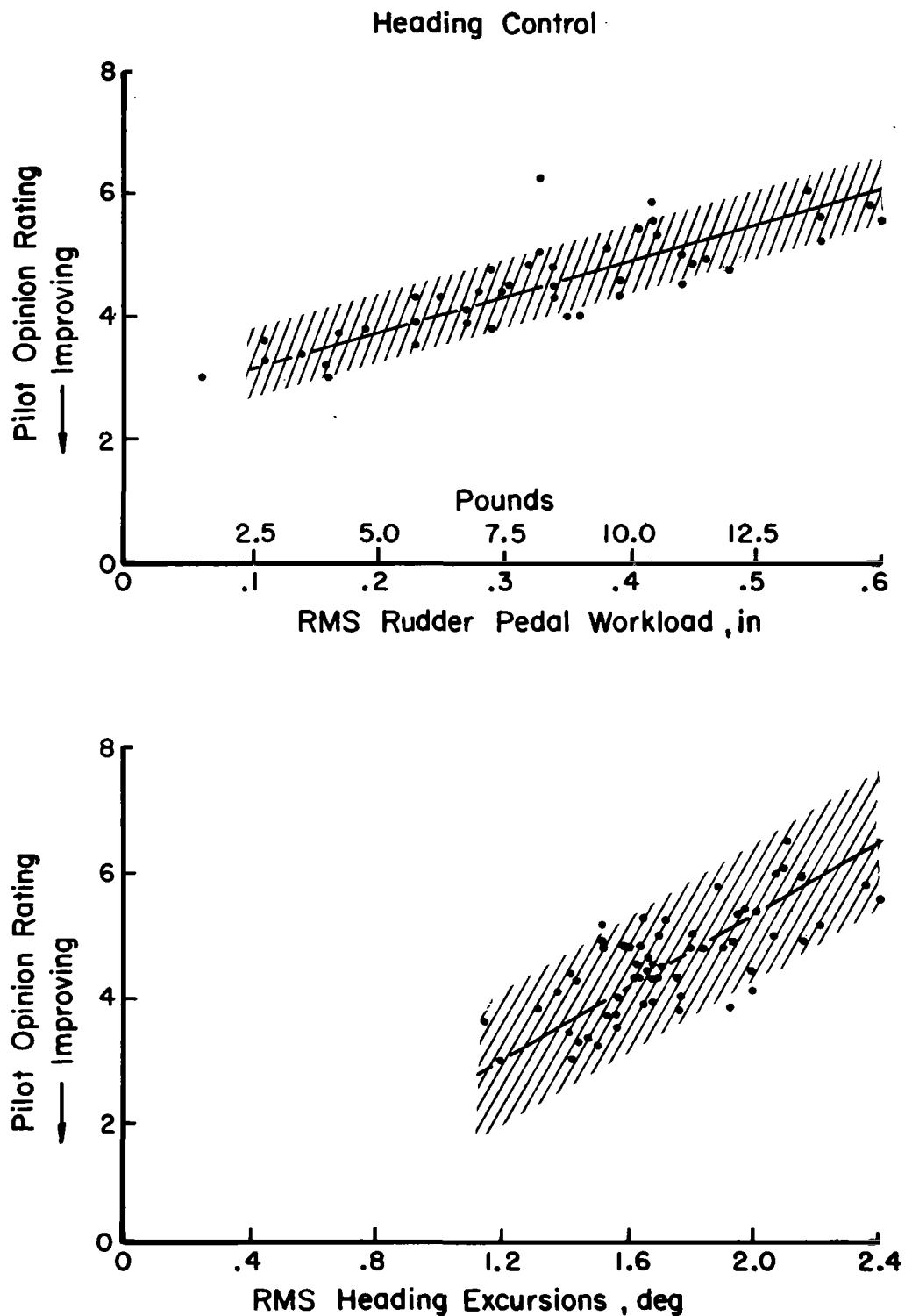
Figure 73.   Trends of Pilot Opinion Rating with Rudder Workload
and Heading Performance
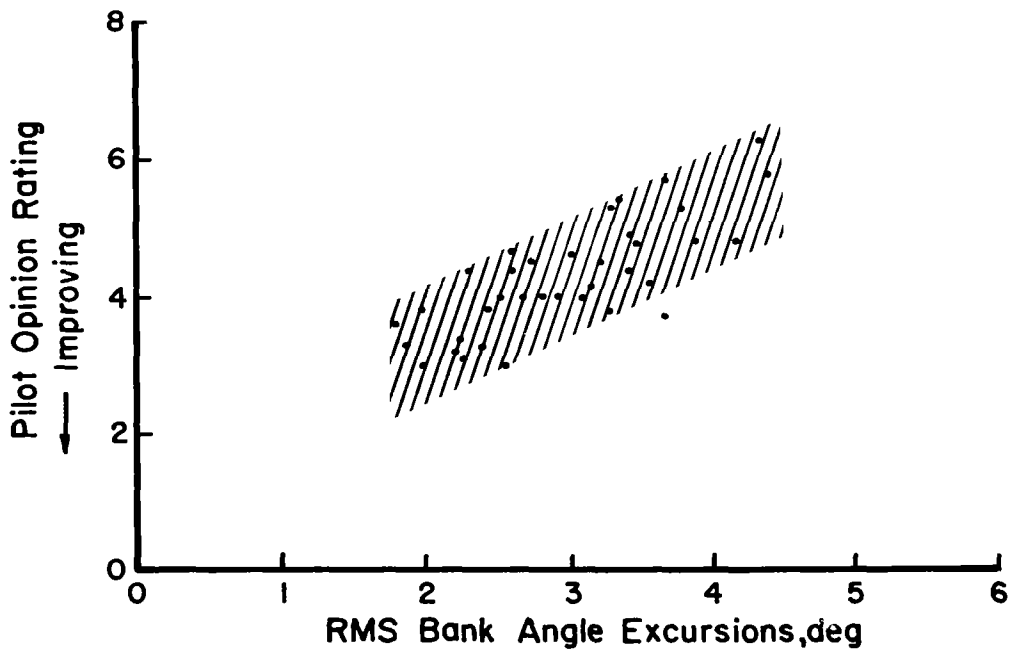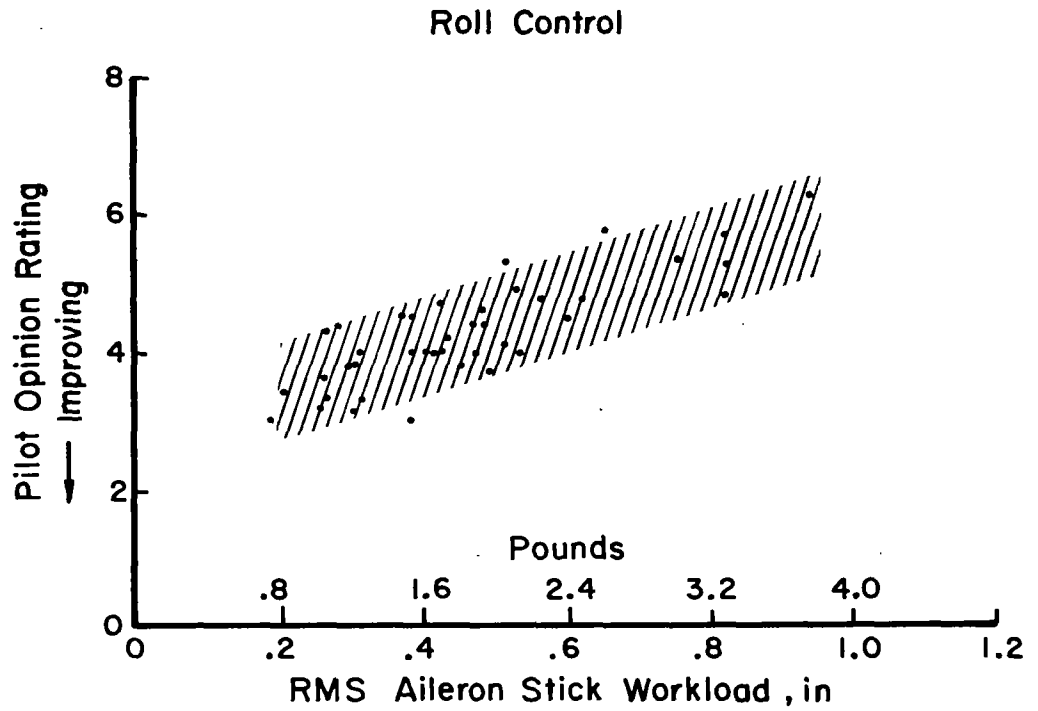
Figure 74. Trends of Pilot Opinion Rating with Aileron Workload and Bank Angle Performance

179

To gain an understanding of the relationships between performance, workload, compensation, and the test parameters of turbulence and dynamics, the results of an analog computer study are presented in the following discussion in conjunction with the root locus and Bode analyses. The analog simulation was programmed on an EAI TR48 computer and included the three degree of freedom lateral-directional equations of motion, pilot models for both aileron and rudder controls of the form of equation (91), and a transient analog representation of the turbulence disturbance (Appendix C). Raw data from the simulation are first plotted to show the tradeoff between performance and workload as a function of lead compensation for a single turbulence-dynamics configuration. An example of these data is shown in Figure 75. After compiling these data for all of the turbulence-dynamics combinations of interest, the data were cross-plotted to show the effects of turbulence and dynamics on performance and workload separately. In every case, the variation in workload to achieve the same level of performance over a range of turbulence or dynamics parameters is shown. In some instances the change in performance assuming a constant workload is also indicated. The workload and compensation required to attain a given level of performance is not unique as is apparent from Figure 75. The combination of $\sigma_{\delta r}$ and $T_{L\psi}$ chosen in a given instance was based on one of two criteria. The first objective was to create no more lead than necessary, and particularly to stay within the shaded region at the knee of the $\sigma_{\delta r}$, $T_{L\psi}$ curve shown in the inset diagram of Figure 75. This approach agrees with the philosophy that it is more difficult for the pilot to create lead than to raise his gain and it is felt that he would be unlikely to create a considerable amount of lead unless it was giving him a favorable tradeoff with workload. The tail of the $\sigma_{\delta r}$, $T_{L\psi}$ curve is not likely to be associated with a favorable tradeoff. The second objective, which was generally, but not exclusively observed, was to confine the pilot's gain and lead to levels which fell within 3 radian/second bandwidth and 10 degree phase

180
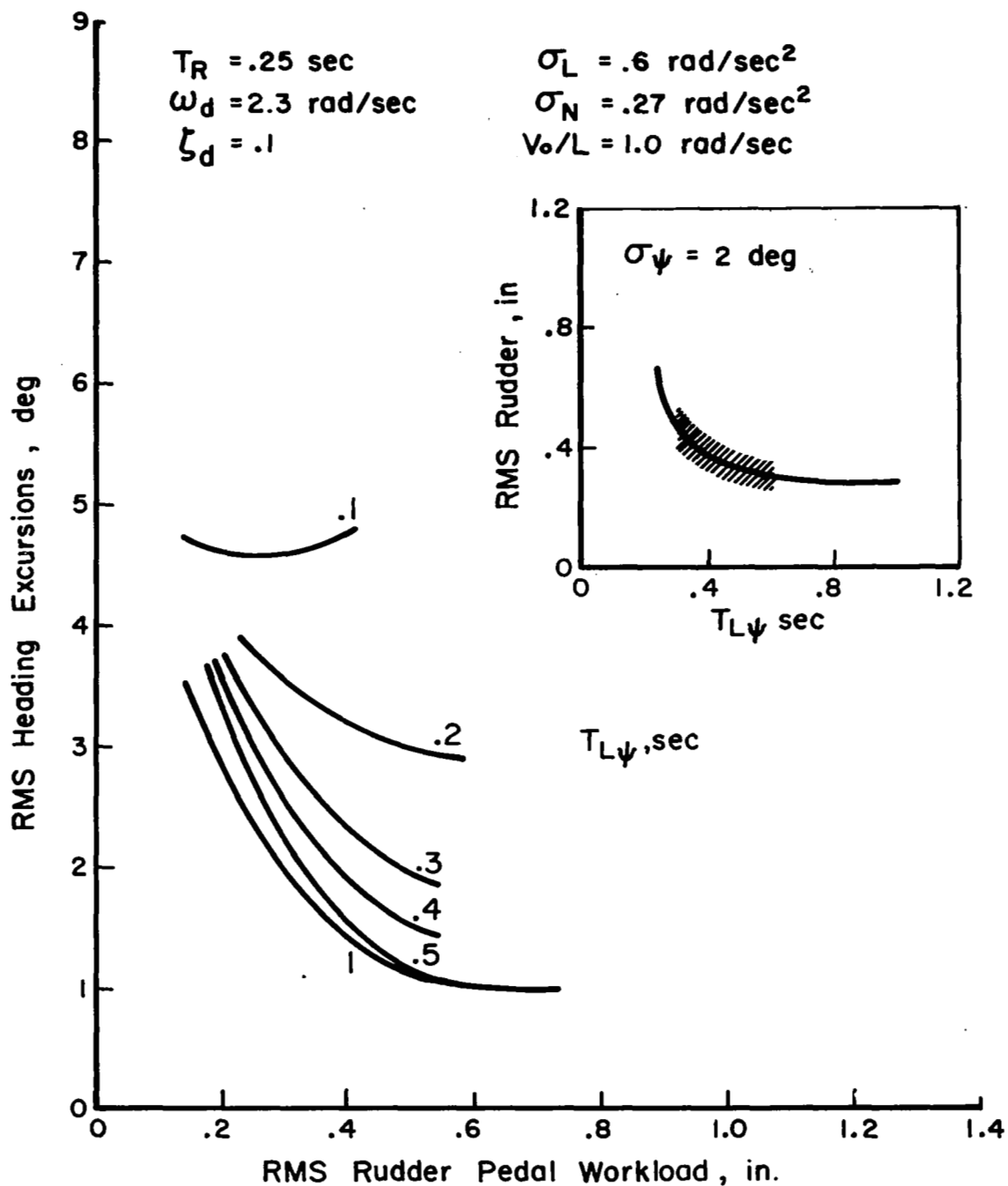
Figure 75. Trade Off Between Heading Performance and Rudder
Workload

181

margin boundaries. The bandwidth limitation was chosen on the hypothesis that the bandwidths observed for the appropriate controlled element of Reference 38 would be the best the pilot would choose to do. The phase margin limitation is arbitrary to an extent; however, much smaller phase margins would be unlikely due to the poorly damped dominant mode which would result.

For roll control, the desired performance level was permitted to vary depending on the difficulty of the control problem. In all cases the amount of lead was chosen so that $T_{L\varphi} \doteq T_R$ leaving but one choice for the corresponding workload. Roll loop closures to provide equalization in the heading to rudder loop were made for a gain which produced a bandwidth on the order of 4.5 radians/second at crossover.

Contribution of turbulence - Configuration 1

The favorable roll control characteristics of this configuration are apparent in the root locus and Bode diagrams shown in Figure 76. The more interesting parts of the loci away from the real axis are shown. The various loci are not all included along the real axis since their overlap would only add confusion to the plot. Instead one typical locus is shown completely and the numerator roots for the pilot lead term $(T_{L\varphi})$ are indicated for the other loci. Adequate bandwidth and stability margins are achievable at low levels of lead compensation. In particular, for $T_{L\varphi} = .2$ seconds and for a gain $K_{\varphi} = .214$ inches/degree the observed bandwidth is 4.75 radians/second with a 30 degree phase margin and 6 db gain margin. The level of gain K_{φ} was chosen to produce a crossover frequency $(\omega_{co} = \omega_{db=0})$ for $T_{L\varphi} \doteq T_R$ which complied with the bandwidth of the appropriate controlled element $(\frac{K}{s})$ in Reference 38. The effective pilot time lag is also in agreement with the Reference 38 data for a $\frac{K}{s}$ system. Dutch roll damping is somewhat better than the open loop case and Dutch roll excitation in roll is small due to the close proximity of the pole-zero pair. The closed loop roots for the indicated gain are shown on the root locus diagram.
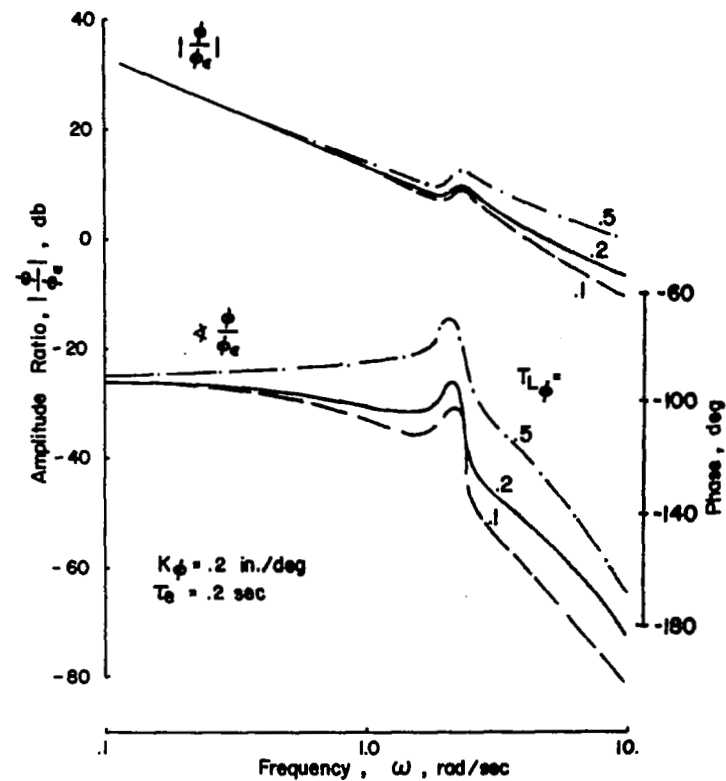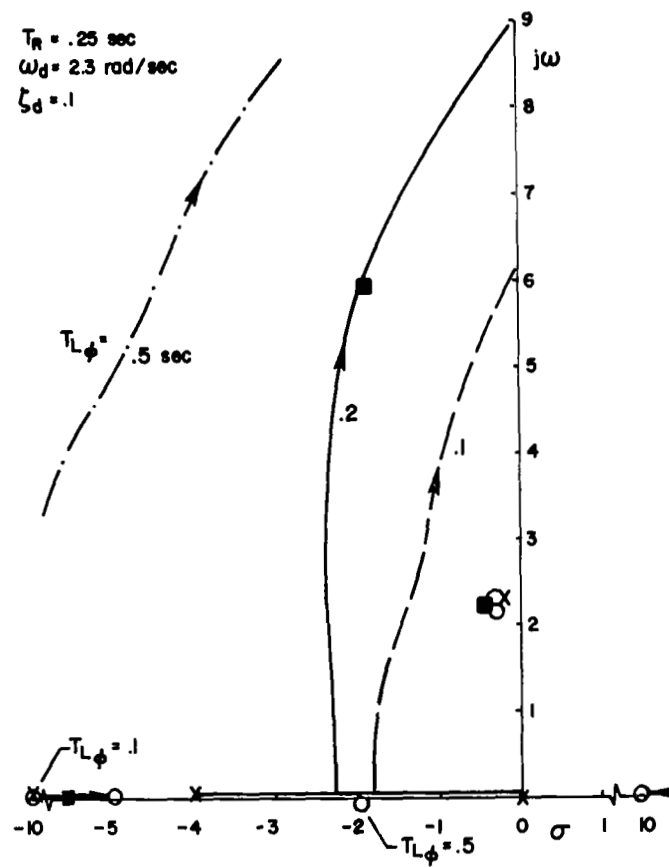
Figure 76. Bank Angle to Aileron Loop Closure - Configuration 1

183

The transfer function of closed loop bank angle response to lateral gusts, illustrating the effects of rms roll disturbance magnitude, is shown in Figure 77. Increasing rms roll disturbances raises the energy level of the bank angle spectrum as would be expected. The unusual character of the $|\frac{\varphi}{\beta_g}|^2$ transfer function for the large roll disturbance ($\sigma_L = 1.2$ rad/sec^2) deserves comment. While it might be expected that this transfer function would increase in direct proportion to σ_L for all frequencies, this is not the case in Figure 77. In fact, the $\sigma_L = 1.2$ transfer function dips below the $\sigma_L = .6$ case over a limited frequency band. This behavior stems from the fact that L_{β_g}, which scales the magnitude of roll disturbances, is not equivalent to the L_β of the characteristic matrix. In general $L_{\beta_g} \neq L_\beta$, $L_{p_g} \neq L_p$, and $N_{\beta_g} \neq N_\beta$ in order that variations of the turbulence disturbances may be made independently of the pilot-airplane dynamics. A complete discussion of this problem is presented in Appendix D. As is noted in the appendix, the numerator of the $|\frac{\varphi}{\beta_g}|$ transfer function may be written

$$N_{\beta_g}^{\varphi} = L_{\beta_g} (s^2 + a s + b) \tag{104}$$

If $L_{\beta_g} = L_\beta$ and $N_{\beta_g} = N_\beta$ and if the spiral mode is neutral so that $L_\beta N_r - L_r N_\beta = 0$, then the numerator reduces to

$$N_{\beta_g}^{\varphi} = L_{\beta_g} s^2 \tag{105}$$

It happens that equation (105) is a fair approximation for the $N_{\beta_g}^{\varphi}$ numerator of Configuration 1 when $\sigma_L = .6$, whereas the $\sigma_L = 1.2$ case requires the full second order representation of equation (104). Other ramifications of the inequality of the turbulence and dynamics derivatives are considered in Appendix D.
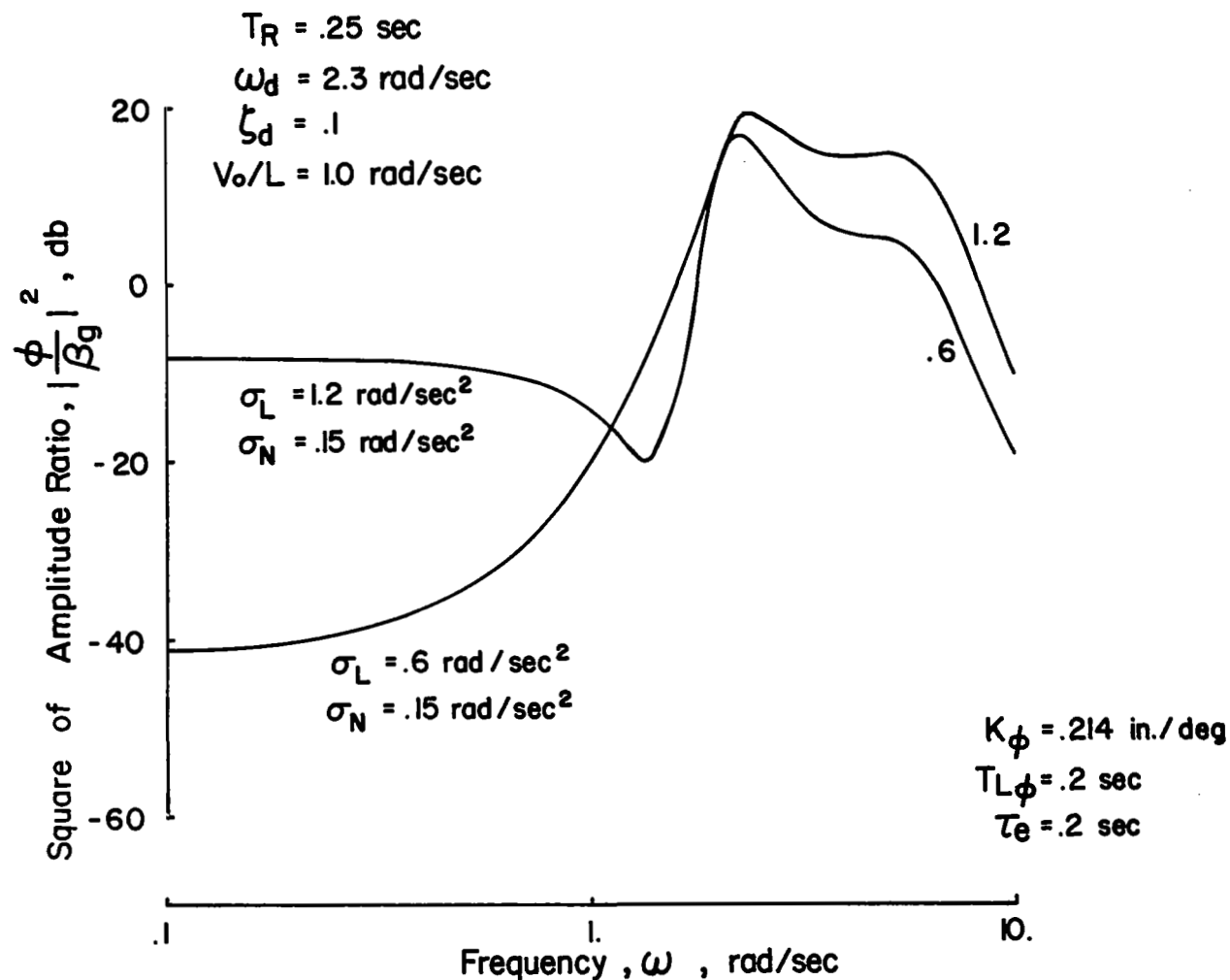
Figure 77.   Closed Loop Bank Angle Response to Lateral Gusts –
Effect of RMS Roll Turbulence

Increasing the disturbance bandwidth at a constant turbulence level changes the frequency content and magnitude of the response spectrum in the manner shown in Figure 78. Considering the increase in bandwidth, corresponding to $\frac{V_o}{L}$ = .314 to 2.0 radians/ second , the significant effect appears as an increase in roll response over the range $\frac{V_o}{L}$ = .314 to 1.0 radians/ second. Changes in the spectrum for $\frac{V_o}{L}$ above 1.0 radian/ second are much less by comparison.

The increase in aileron workload necessary to sustain a constant level of rms bank angle excursions (σ_φ = 2 degrees) with increasing roll disturbances is shown in Figure 79. The same lead time constant ($T_{L\varphi}$ = .2 seconds) is used throughout, while bandwidth is increased by increasing the pilot's gain to achieve a constant level of performance. Comparison of these data with the appropriate flight test results of Figure 38 reveals similar trends in the workload although the absolute magnitudes do not correspond. The lack of agreement in actual magnitudes of the predicted workload with flight test data can be at least partially attributed to the fact that the same level of bank angle excursions were not maintained in flight for the range of roll disturbances shown. Also, the rudder was used in flight to reduce yaw excursions and this would be expected to reduce roll excursions attributable to the coupling between roll and yaw (L_β = -16 radians/ second^2/ radian).

As a contrast to the trends in workload with turbulence level noted above, the penalty in roll excursions which result if the pilot maintains a constant workload as roll turbulence increases is also shown. The degradation in performance is somewhat more severe than for workload.

In the inset diagram of Figure 79, the tradeoff between workload and compensation required to keep rms roll excursions invariant is shown to support the choice of lead time constant. Increasing the amount of lead above that for $T_{L\varphi}$ = .2 seconds permits very little reduction in the workload while $T_{L\varphi}$ much less than .2 seconds increases the pilot's workload considerably. Although there is some latitude in the choice of $T_{L\varphi}$, it should satisfy $T_{L\varphi} \doteq T_R$ and hence a value $T_{L\varphi}$ = .2 seconds was selected.

Figure 78. Effect of Turbulence Bandwidth on Bank Angle Response – Configuration 1
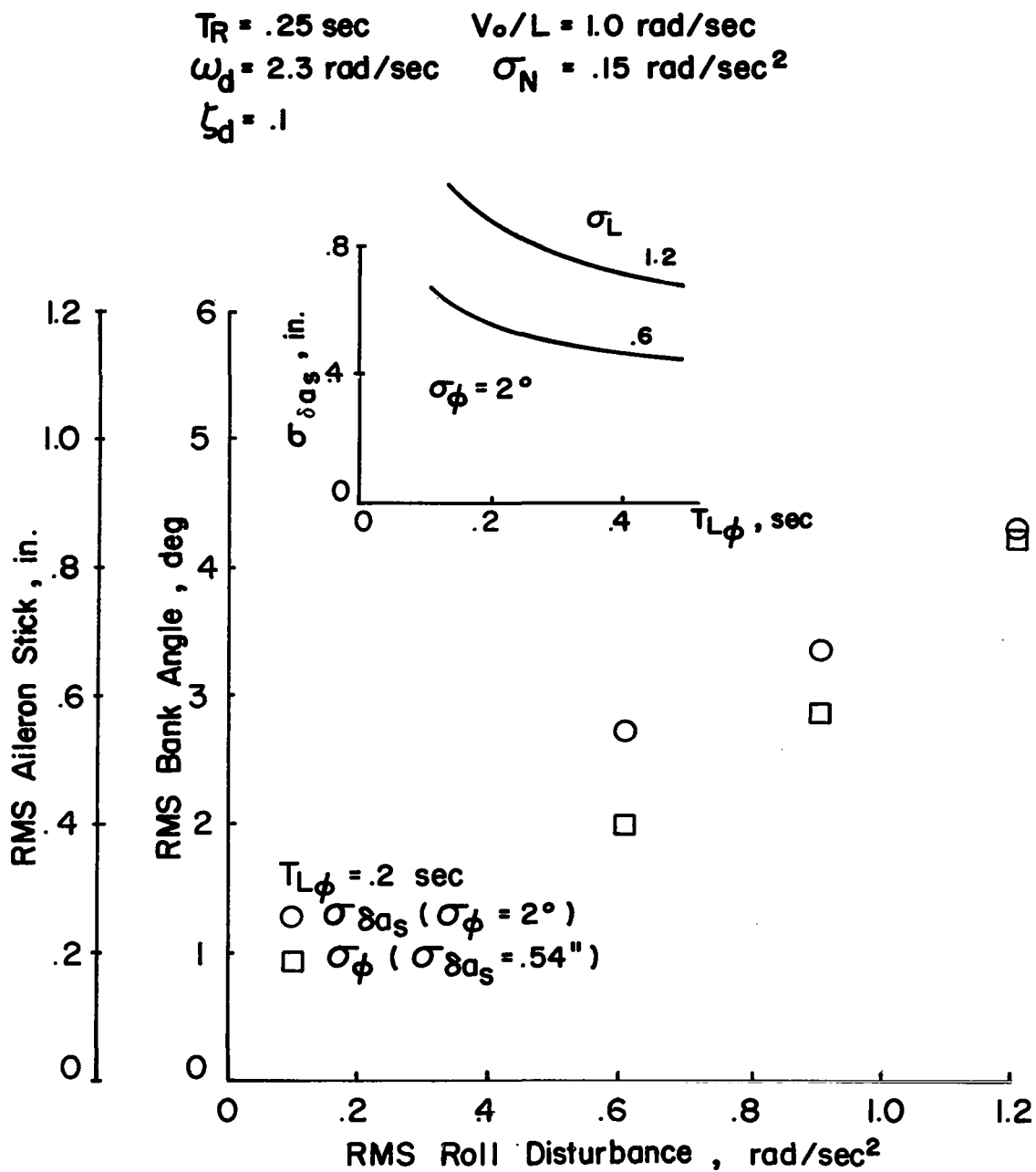
Figure 79. Effect of RMS Roll Disturbance on Roll Performance
and Aileron Workload - Configuration 1

Effects of turbulence bandwidth on workload and performance confirm the trends shown in the roll response spectra of Figure 78. As indicated in Figure 80, the aileron workload required to hold bank angle excursions at a constant rms value must increase for an increase in bandwidth corresponding to $\frac{V_o}{L}$ = .314 to 1.0 radians/second. Above $\frac{V_o}{L}$ = 1.0 radian/second the workload is essentially constant. While this trend agrees with the variation of pilot rating with bandwidth, the flight test measured performance-workload data show less variation than was obtained in the computer simulation.

Turning to consideration of heading control, it is immediately apparent from the root locus-Bode diagrams of Figure 81 that heading control with the ailerons can only be a low gain, low bandwidth proposition at best. If the gain is raised to the point of instability, the bandwidth is only on the order of .7 radians/second, and is less than the bandwidth of turbulence disturbances. Hence, the pilot will be unable to attenuate the turbulence induced heading excursions by use of the ailerons. Furthermore, it is difficult if not impossible to generate any reasonable and effective compensation in this loop. The reason for using the rudder is apparent in the root locus-Bode analysis of Figure 82. Much wider bandwidths and better stability margins are possible by using the rudder to control heading. However to achieve acceptable bandwidths it is still necessary to generate some lead compensation. To obtain the bandwidth measured for systems of the type $\frac{K}{s^2}$ in Reference 38 (approximately 3.0 radians/second) a lead time constant on the order of T_{L_ψ} = .2 seconds or greater is necessary for this configuration. The closed loop roots corresponding to a gain K_ψ = .09 inch/degree and T_{L_ψ} = .2 seconds are shown on the root locus diagram in Figure 82.

Since the criteria for the heading loop closure developed up to this point is somewhat tenuous, some information regarding the pilot's transfer function was sought from the flight data to provide substantiation of the hypothetical
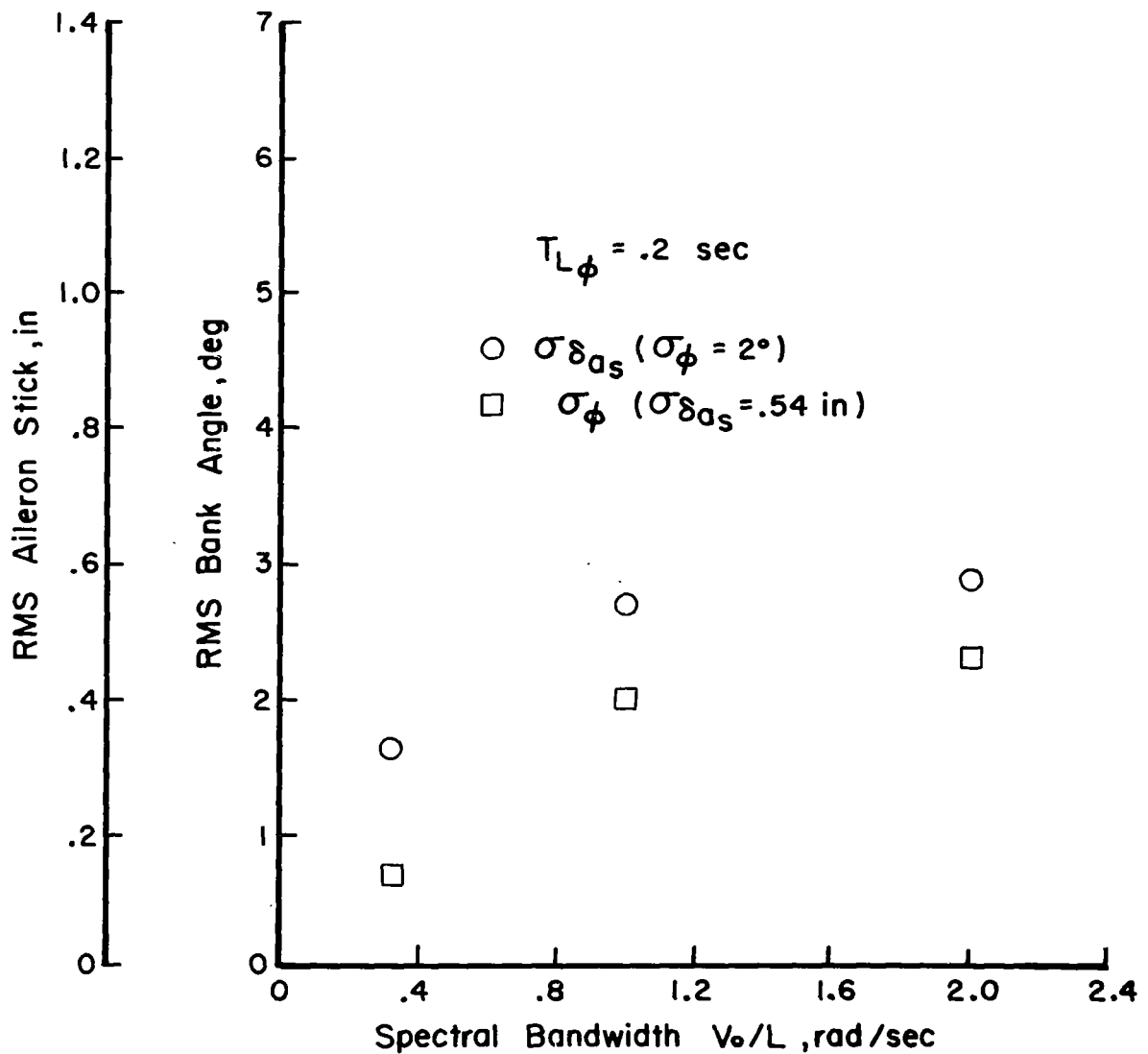
Figure 80. Effect of Turbulence Bandwidth on Roll Performance
and Aileron Workload - Configuration 1
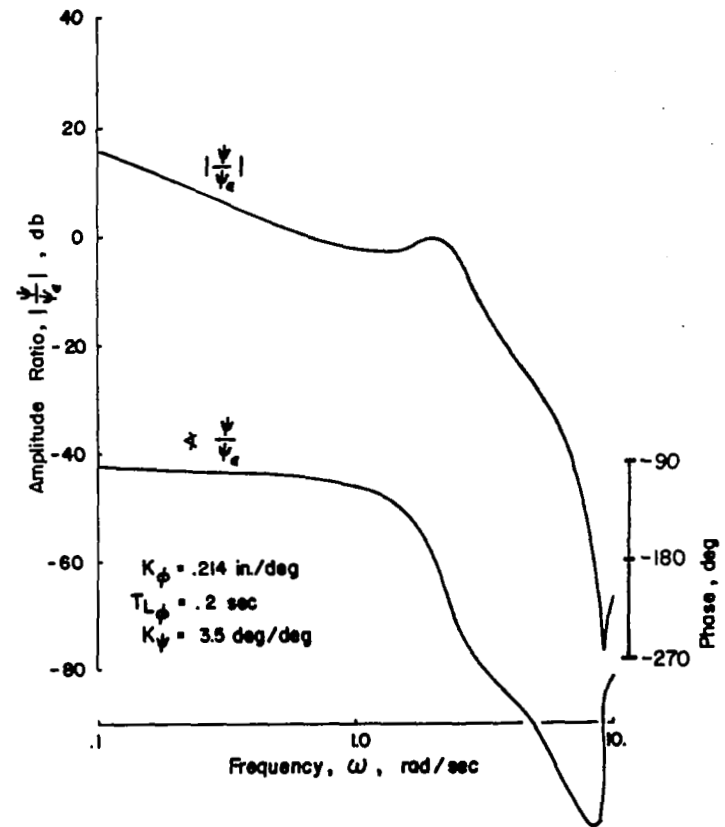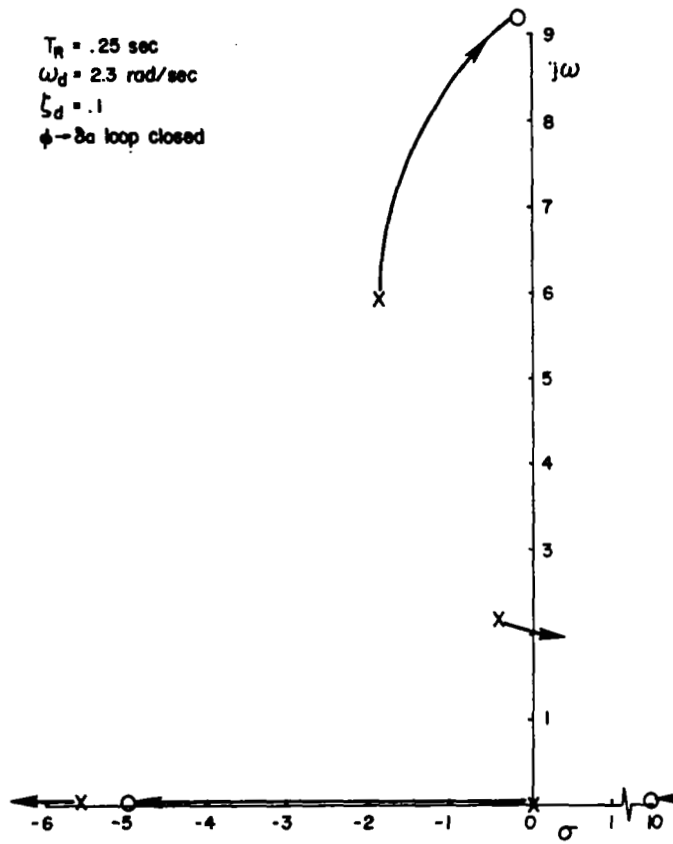
Figure 81. Heading to Aileron Loop Closure - Configuration 1

191
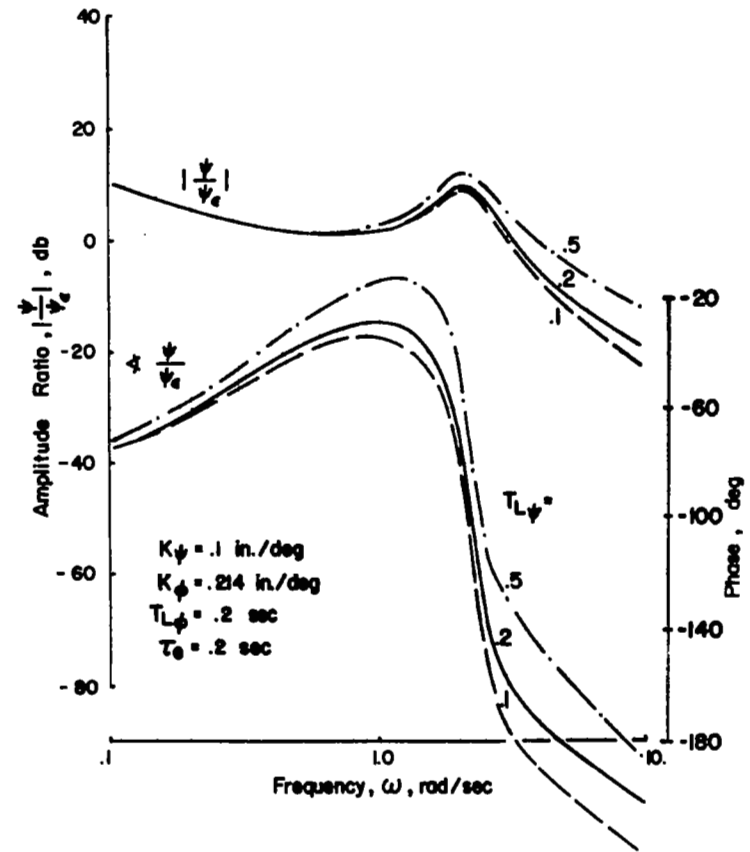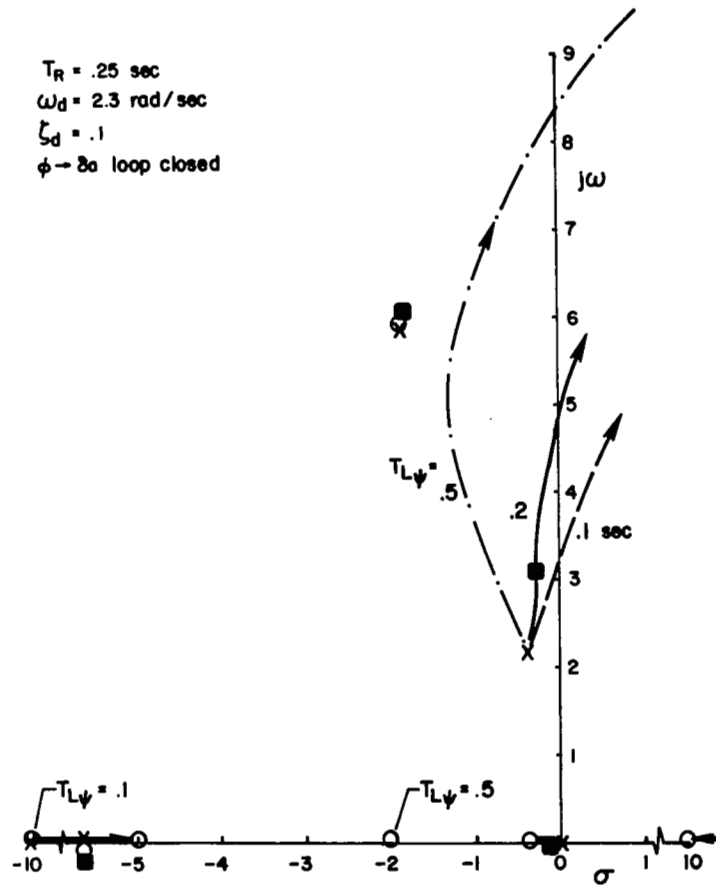
Figure 82. Heading to Rudder Loop Closure - Configuration 1

pilot model discussed heretofore. Digital processing of the time history data for rudder control, heading excursions, and yaw turbulence was performed to form the cross-spectral density functions necessary to define the pilot. The appropriate relationship for the pilot's rudder control transfer function based on the approach of Reference 11 is

$$Y_{P_{\delta r}} = \frac{\Phi_{\delta r} N_{v_g}}{\Phi_\psi N_{v_g}} \tag{106}$$

assuming independent use of ailerons and rudder for roll and yaw control respectively. Amplitude ratio data from this transfer function was combined with the airplane's open loop transfer function to form the pilot-airplane combination $Y_A Y_p (|\frac{\psi}{\psi_\epsilon}|)$. This result is compared to the behavior of the open loop system anticipated from crossover model theory, particularly to note the bandwidth and the slope of the amplitude data with frequency at crossover.

Data for Configuration 1 is shown in Figure 83. The magnitude and bandwidth of turbulence corresponding to one set of data is $\sigma_L = .6$ rad/sec^2, $\sigma_N = .27$ rad/sec^2, $\frac{V_o}{L} = 1.0$ rad/sec. An acceptable fit of these results is provided by the pilot-airplane combination with the pilot model characteristics

$$K_\psi = .1 \text{ inch/degree}$$

$$T_{L\psi} = .5 \text{ seconds}$$

particularly in the region of crossover. The bandwidth is noted to be 3.8 radians/second and the asymptotic slope of the transfer function at crossover is -20 db/decade, both of which conform to the characteristics anticipated by the crossover model. For the lower yaw disturbance level, $\sigma_N = .15$ rad/sec^2, the bandwidth is more on the order of 2.5 to 3.0 radians/second and a better fit is provided by the pilot model characteristics

$$K_\psi = .09 \text{ inch/degree}$$

$$T_{L\psi} = .3 \text{ seconds}$$
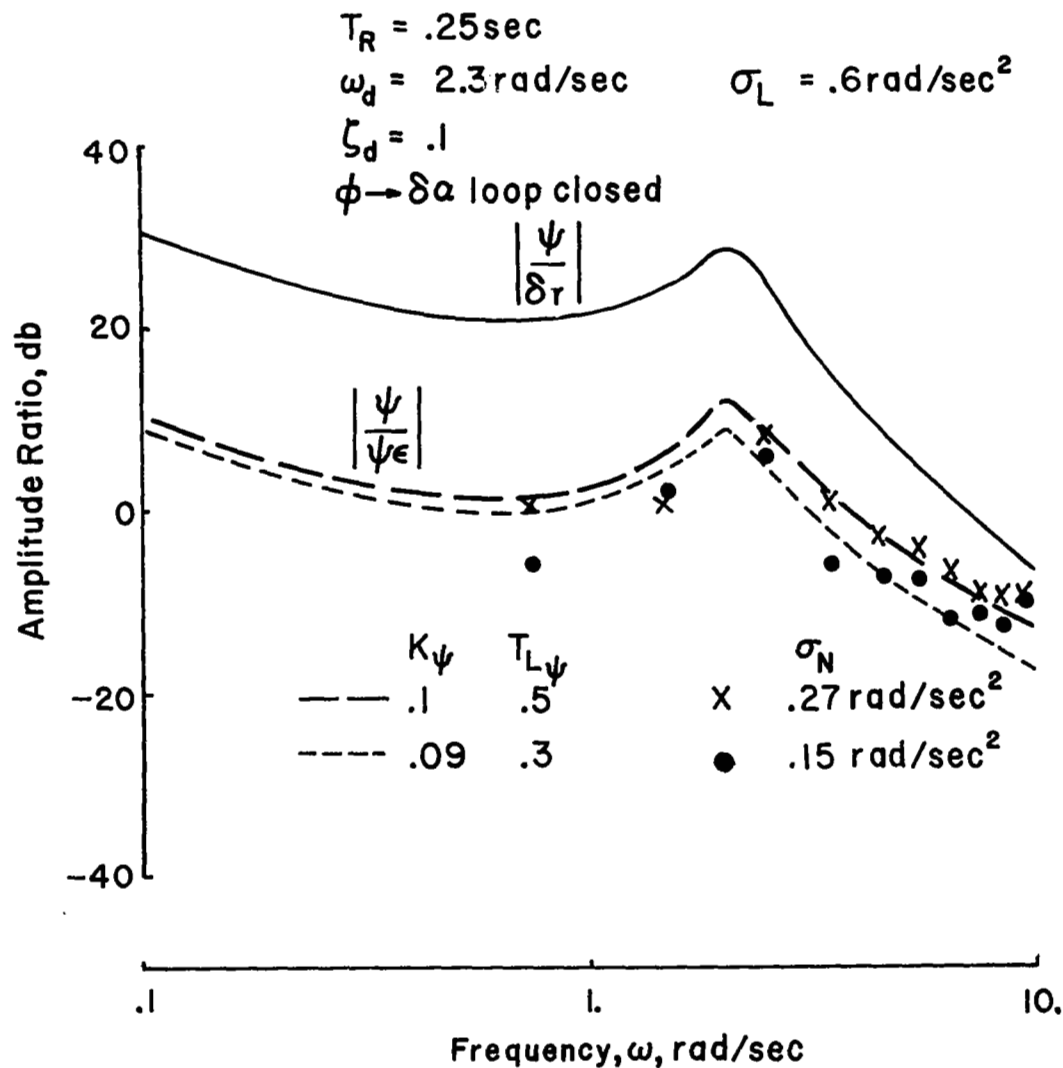
Figure 83. Flight Test Measured Pilot Compensation in Heading Control with Rudder - Configuration 1

Closed loop heading response transfer functions shown in Figure 84 indicate the effect of increasing rms yaw disturbances. The result is generally an increase in energy across the spectrum, independent of frequency. Similar to the roll spectra, a considerable amount of the energy in the airplane's heading response is located at frequencies in the vicinity of the modified Dutch roll mode. An interesting contrast can be made between heading response spectra for the cases of aileron and rudder control. This comparison is made for a lower level of yaw disturbance $(\sigma_N = .15$ radians/ second$^2)$. The large magnitude of heading response for the $\psi \rightarrow \delta a$ loop as compared to the $\psi \rightarrow \delta r$ loop reflects the fact that the pilot is unable to increase his gain appreciably in the aileron loop to attenuate the open loop response.

The predominant effects of turbulence bandwidth, shown in Figure 85, are to increase energy in the frequency range of interest as bandwidth increases from $\frac{V_O}{L} = .314$ to 1.0 radians/ second. The Dutch roll contribution is particularly emphasized. Little difference is noted between the spectra for $\frac{V_O}{L} = 1.0$ and 2.0 radians/ second.

Performance-workload data for heading control with the rudder are presented in Figures 86, 87, and 88. The first figure of this group illustrates the effect of yaw disturbance magnitude on the workload required to hold rms heading excursions to 2 degrees. A higher level of pilot lead compensation in the $\psi \rightarrow \delta r$ loop was assumed in the case of the larger disturbance and was justified by a favorable tradeoff between $\sigma_{\delta r}$ and T_{L_ψ} around the $T_{L_\psi} = .5$ second level and by the pilot describing function data. The trends in rudder workload agree with those obtained in flight. The level of aileron activity required to achieve the smallest rms heading excursions possible (in excess of 2 degrees in all cases) is also shown. While aileron and rudder workloads probably cannot be so directly related, the trend of aileron workload is much worse than for the rudder, and the level of performance is so inferior that the case for using the rudder is obvious.
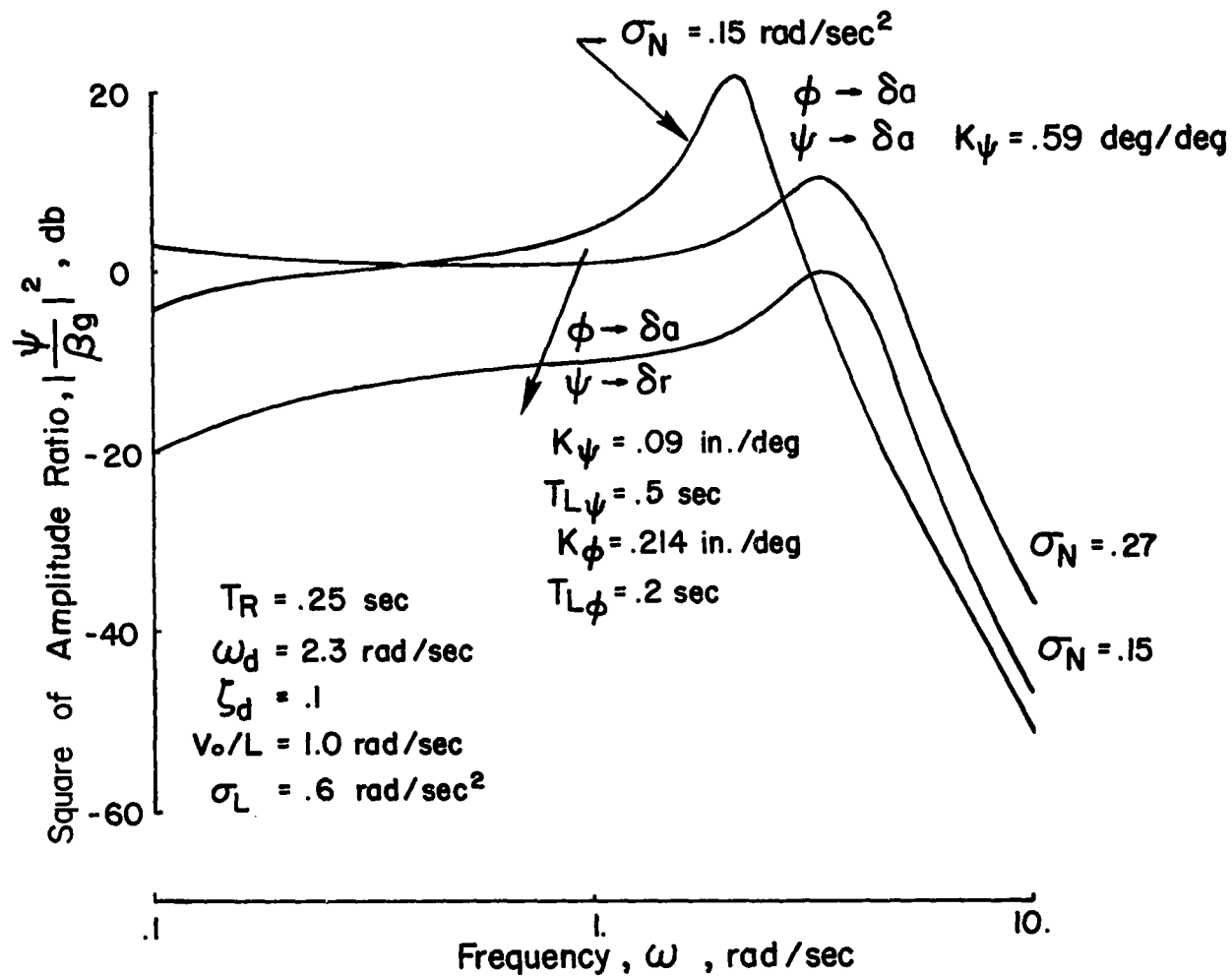
Figure 84. Closed Loop Heading Response to Lateral Gusts –
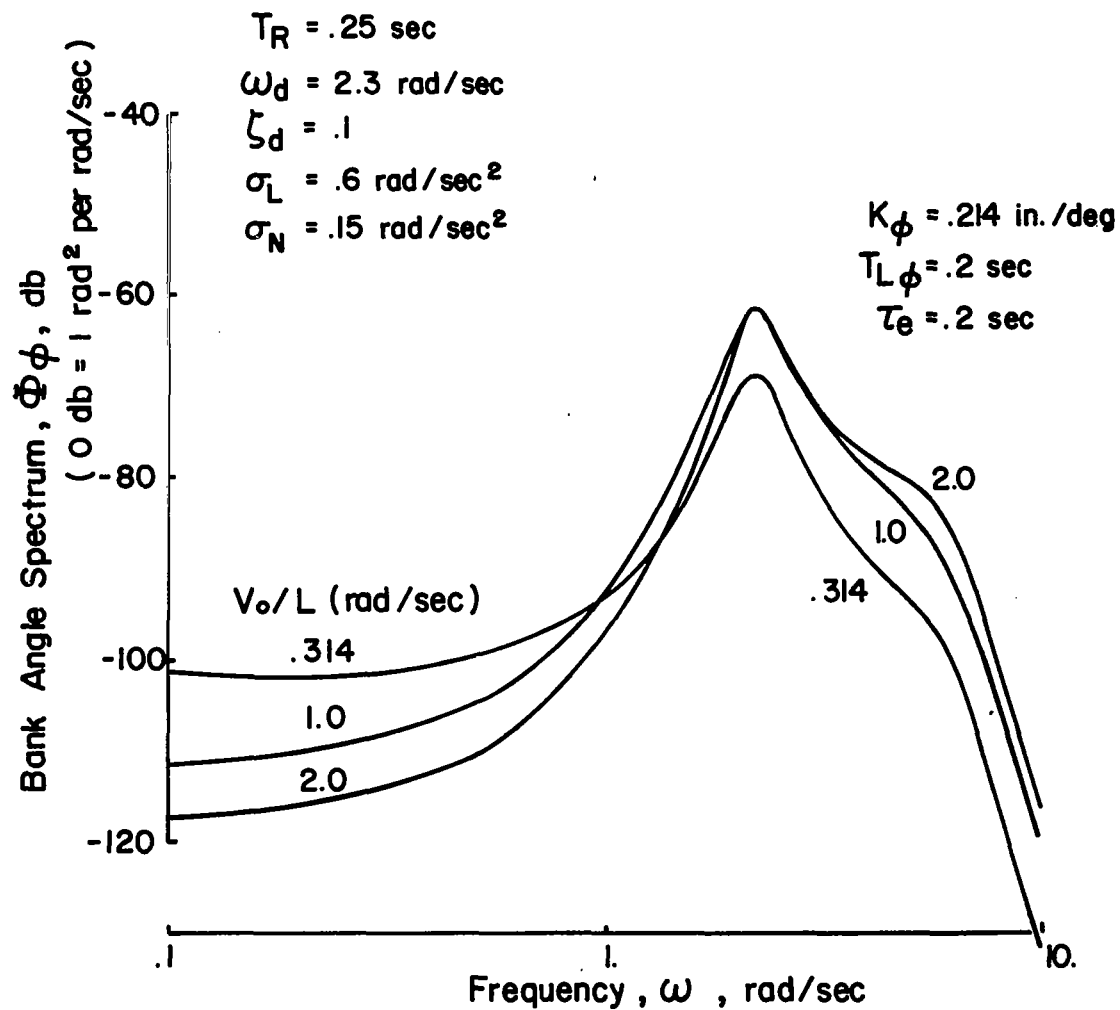Effect of RMS Yaw Turbulence
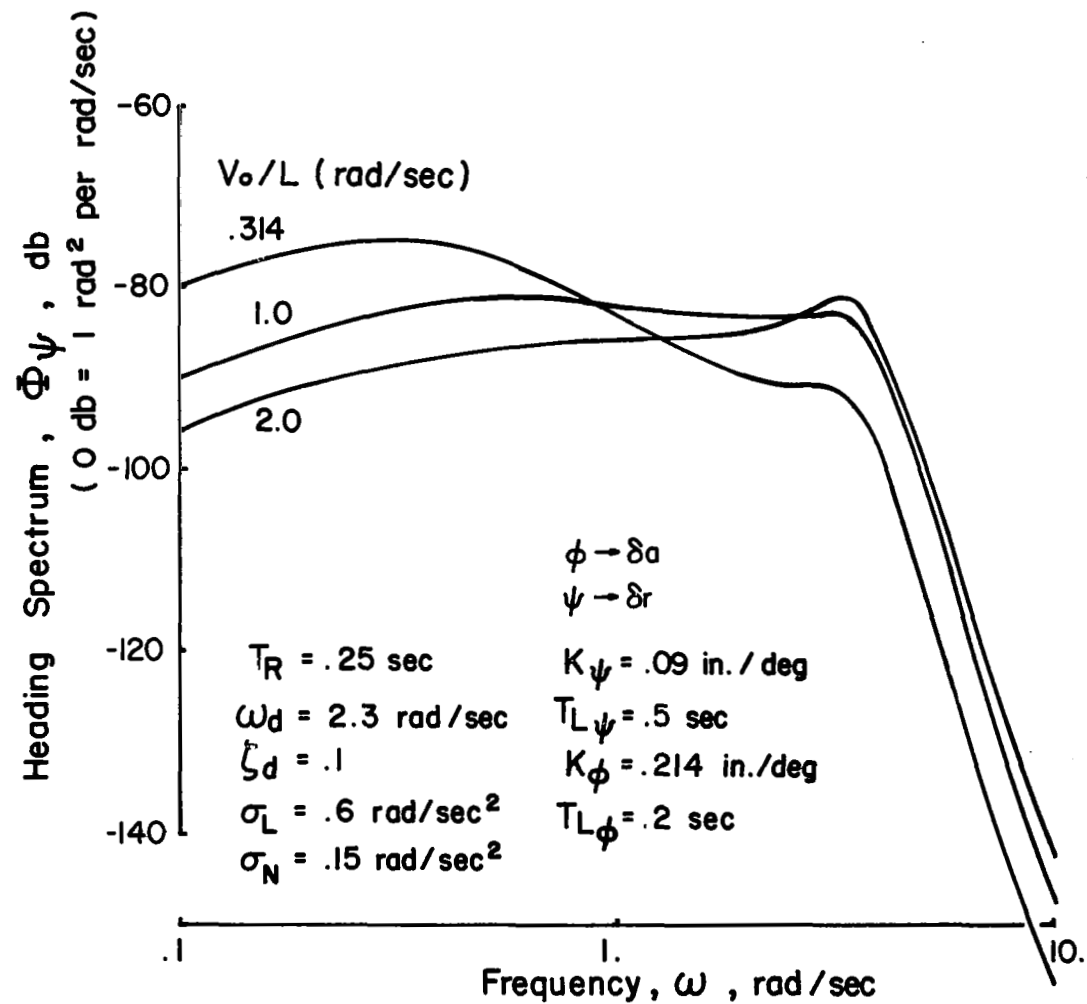
Figure 85. Effects of Turbulence Bandwidth on Heading Response
Configuration 1

Figure 86. Effect of RMS Yaw Disturbances on Heading Perform-
ance and Control Workload - Configuration 1
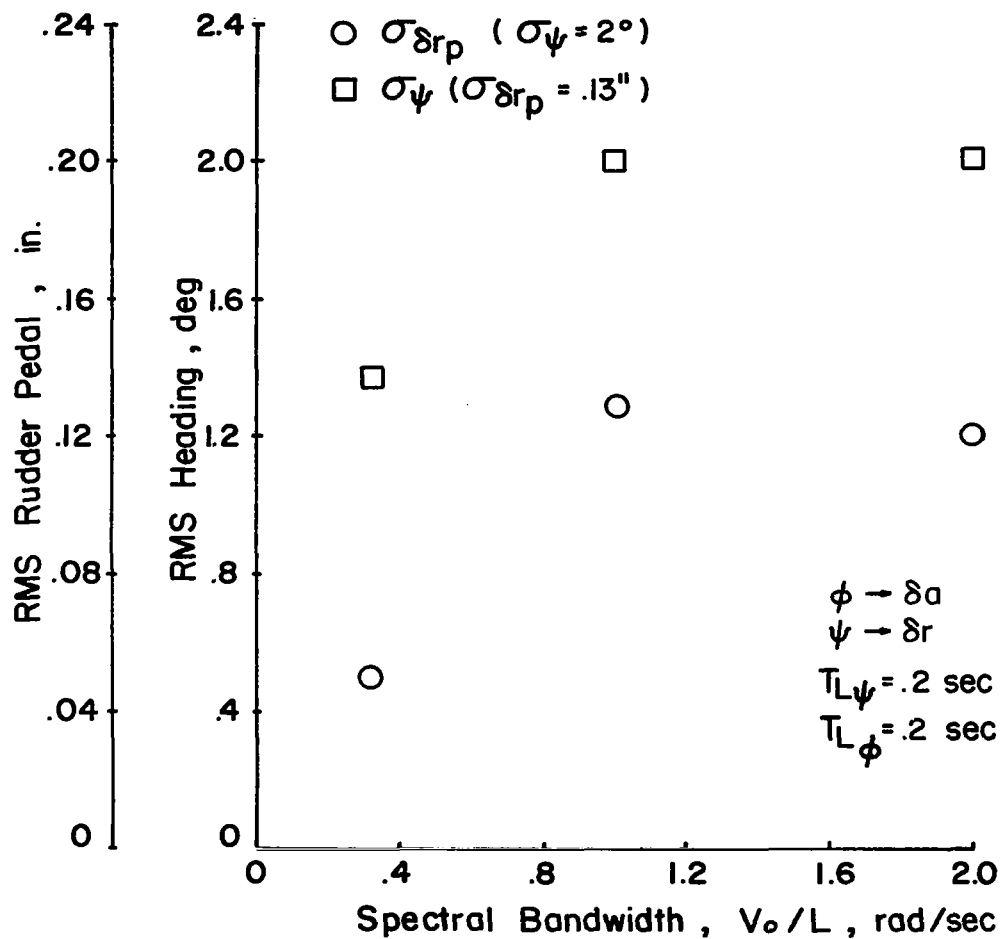
Figure 87.   Effect of Turbulence Bandwidth on Heading Perform-
ance and Rudder Workload - Configuration 1
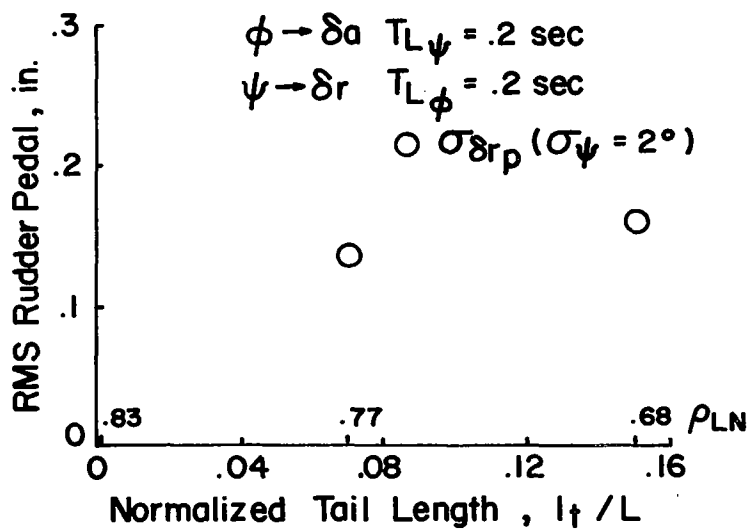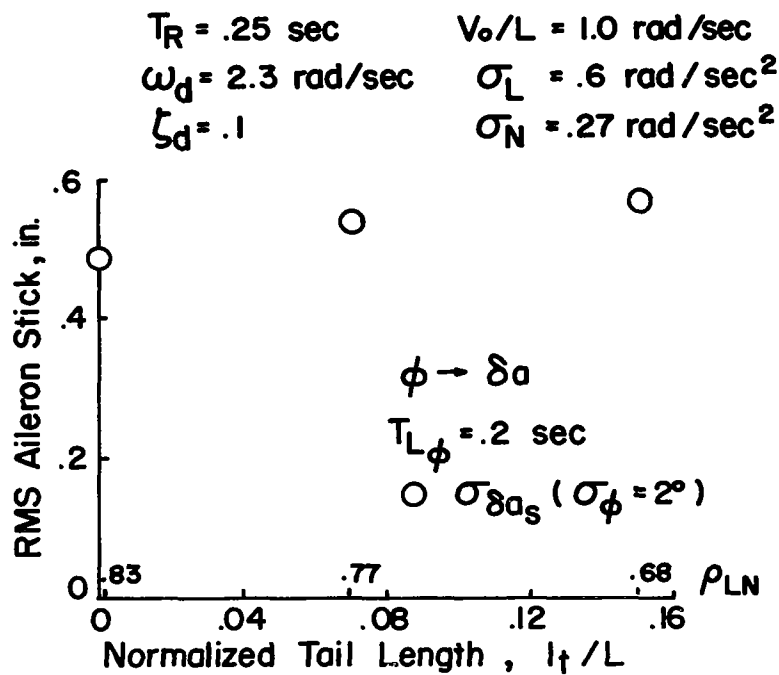
Figure 88. Effect of Roll-Yaw Correlation on Control Workload -
Configuration 1

It may be noted in Figure 87 that both the performance and workload increase moderately as bandwidth increases up to 1.0 radian/second. Above 1.0 radian/second, neither performance nor workload vary with increasing bandwidth. The flight data show a similar variation in workload and performance with bandwidth, and pilot ratings also reflect this trend.

Finally, to conclude the data for this group, the effect of correlation between the roll and yaw disturbances on aileron and rudder workload is shown in Figure 88. Correlation varies as a function of normalized tail length. For the aileron and rudder loop closures indicated, the effect of increasing tail length (decreasing correlation) is to slightly increase the workload required to achieve constant bank angle and heading performance. In comparison to the influence of other turbulence parameters, the effect of roll-yaw correlation can be considered to be negligible.

To summarize the contributions of turbulence for Configuration 1, both the flight test data and the pilot-airplane systems analysis indicate the dominant influence to be the magnitude of the turbulence itself, hardly a surprising discovery. Closed loop control of bank angle and heading are good, assuming the rudder is used for yaw control. In terms of the evaluation task used in this program, the degrading effects of the rms disturbance magnitude appeared to relate to increased rudder workload or degraded heading performance or both. Under circumstances where roll control or bank angle excursions were a problem, the aileron workload and roll performance entered into the evaluation. Pilot rating and performance-workload in the heading tracking task were much more sensitive to the level of yaw disturbances, hence increases in this component of turbulence were much less acceptable than were increases in roll disturbance of the same magnitude.

The effect of increasing turbulence bandwidth ($\frac{V_o}{L}$ = .314 to 2.0 radians/second) while maintaining constant levels of rms roll and yaw disturbances is revealed by the closed loop analysis to be a modest increase in the airplane's

closed loop bank angle and heading excursions and in control workload. These degradations in performance and workload predominate for the lower range of frequencies tested, namely below about $\frac{V_o}{L}$ = 1.0 radian/second, and are primarily a result of the change in turbulence energy at frequencies in the vicinity of the Dutch roll. Pilot opinion ratings reflect these trends in performance and workload with bandwidth by showing some improvement at low frequencies. While the pilots could generally discern the frequency content of the disturbance, their ratings and comments never pointed to frequency specifically as the problem. They did indicate that they generally ignored the highest frequency components of the disturbances for the highest bandwidth tested ($\frac{V_o}{L}$ = 2.0 radians/second) and tracked only disturbances over a bandwidth for which they could achieve adequate stability margins. This form of high frequency attenuation of the pilot's performance, generally known as bandwidth regression, has been identified in the experimental results of Reference 38. Higher order break frequencies of the disturbance spectrum have no effect on pilot rating or on task performance and workload. Energy attenuation above the first break frequency of the spectrum is rapid enough to render the higher frequency attenuation meaningless.

Correlation between the roll and yaw disturbances (whether contributed by tail length or $\sigma_{L_W}/\sigma_{L_V}$ effects) has little influence on the task performance or control workload. This behavior is reflected in the pilot opinion ratings and performance-workload data which show trends of little consequence with the correlation coefficient.

Contribution of turbulence - Configuration 6

As a result of the lower level of roll damping for this configuration compared to Configuration 1 (T_R = .5 seconds compared to T_R = .25 seconds) more lead compensation is required of the pilot in the bank angle to aileron loop to achieve a satisfactory bandwidth. Adopting a lead time constant T_{L_φ} = .5 seconds allows the gain to be increased to produce a bandwidth and stability

margin comparable to Configuration 1. The bandwidth and phase margin for the value of gain indicated in Figure 89 are 4.5 radians/second and 39 degrees respectively. The Dutch roll pole-zero pair are in close enough proximity that aileron excitation of the Dutch roll will not be objectionable. However, damping of the Dutch roll is still light and this, in combination with the low frequency (low directional stability), will result in larger bank angle excursions in response to turbulence. The closed loop roots for the specified value of pilot gain are shown on the root locus diagram.

The closed loop transfer functions for bank angle due to lateral gusts shown in Figure 90 reveal the increased magnitude of roll response to a unit lateral gust in comparison to the response characteristics of Configuration 1 (Figure 77). Transmission of energy at frequencies near the Dutch roll is particularly pronounced. Increasing the level of roll disturbances has the effect of increasing the transmission of energy toward the higher frequency region of the spectrum. The fact that the low frequency asymptote for $\sigma_L = .6$ is larger in magnitude than the $\sigma_L = 1.2$ asymptote is attributable to the fact that $L_{\beta_g} \neq L_\beta$ as discussed previously on page 184 and in Appendix D.

Increasing turbulence bandwidth for a constant rms roll disturbance level serves to increase spectral energy for $\frac{V_o}{L}$ up to 1.0 radian/second. As indicated in Figure 91, the increment in spectral energy occurs primarily for frequencies near the Dutch roll and above. No significant changes are noted in the spectra with an increase in bandwidth from $\frac{V_o}{L} = 1.0$ to 2.0 radians/second. This behavior substantiates the flight test variation in roll excursions. Pilot rating data are also in agreement although they would suggest a continued degradation for $\frac{V_o}{L}$ up to 2.0 radians/second.

Trends in aileron workload with increasing roll disturbances are shown in Figure 92. The magnitude of roll excursions noted ($\sigma_\varphi = 7$ degrees) is nearly the best performance achievable by closing the bank angle loop alone. Substantially better roll performance is possible if rudder is used to reduce yaw
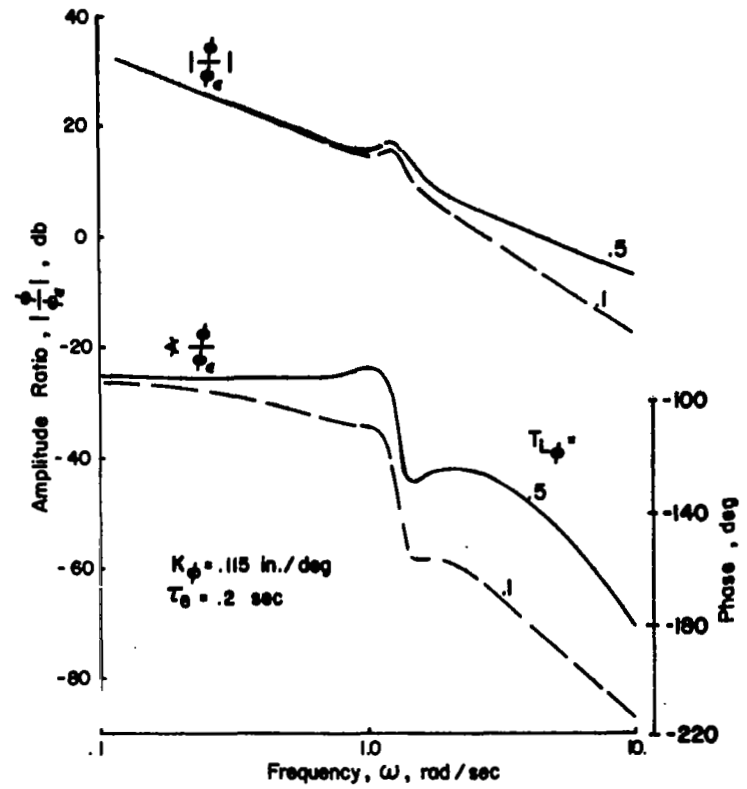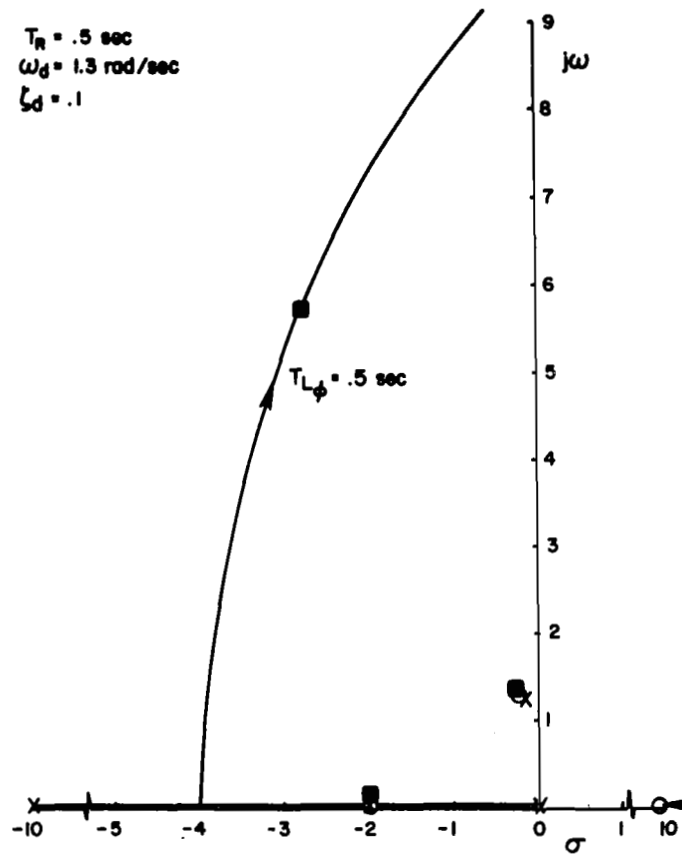
Figure 89. Bank Angle to Aileron Closure - Configuration 6
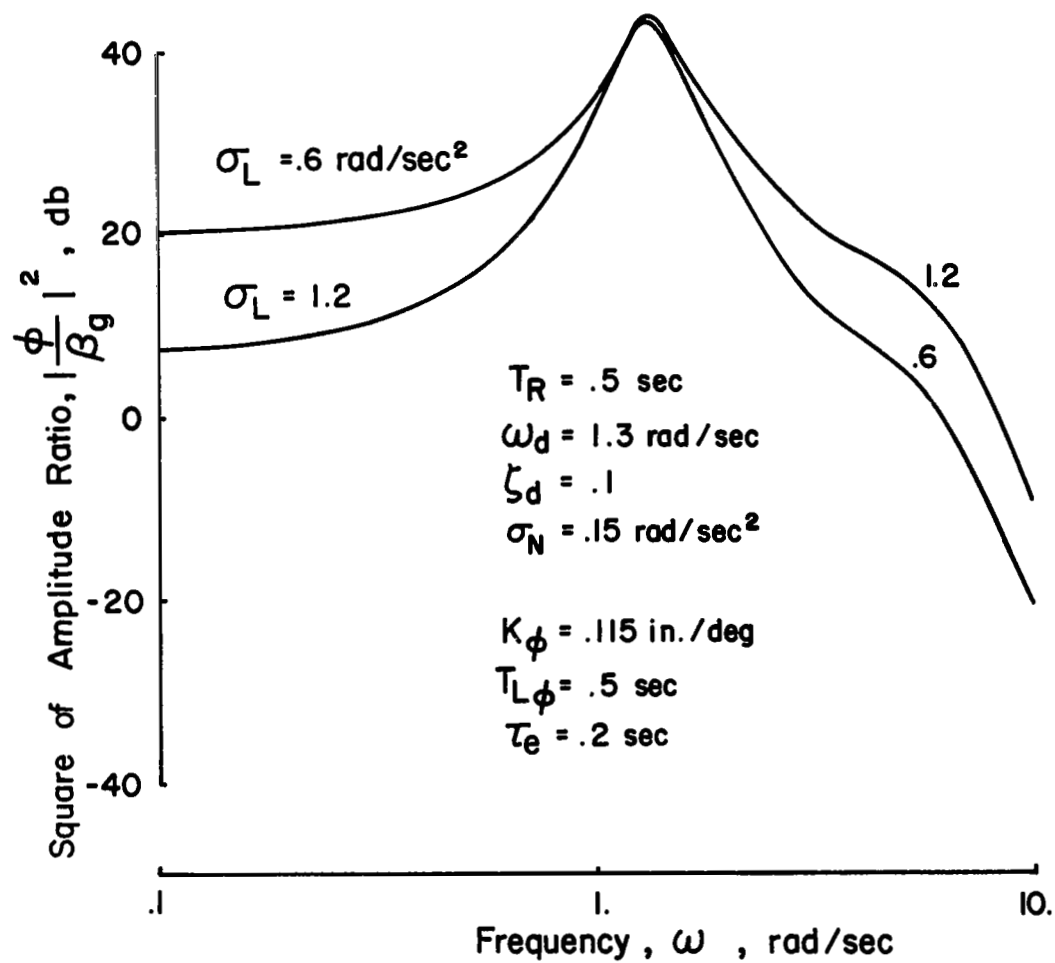
Figure 90.   Closed Loop Bank Angle Response to Lateral Gusts –
Effect of RMS Roll Turbulence

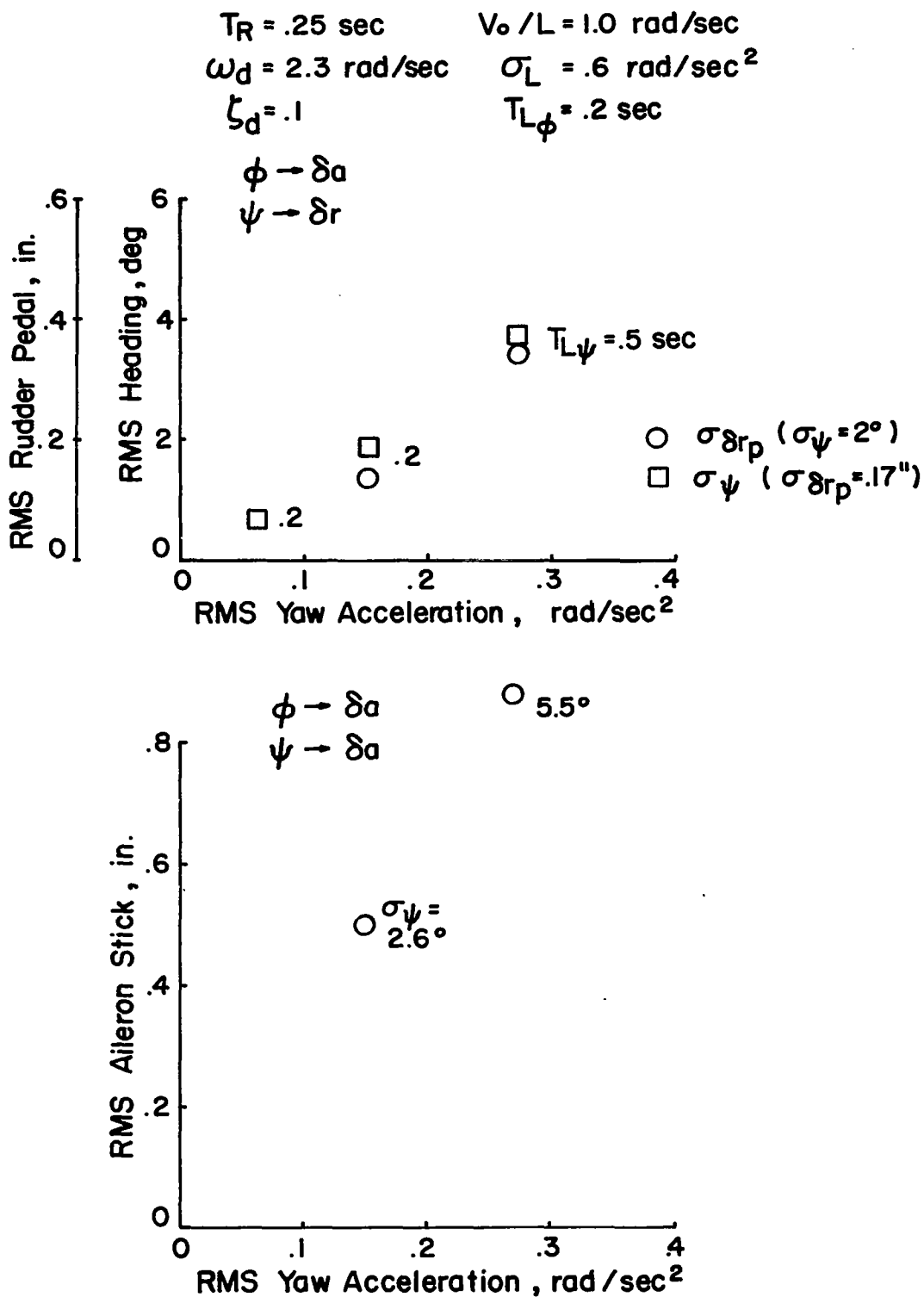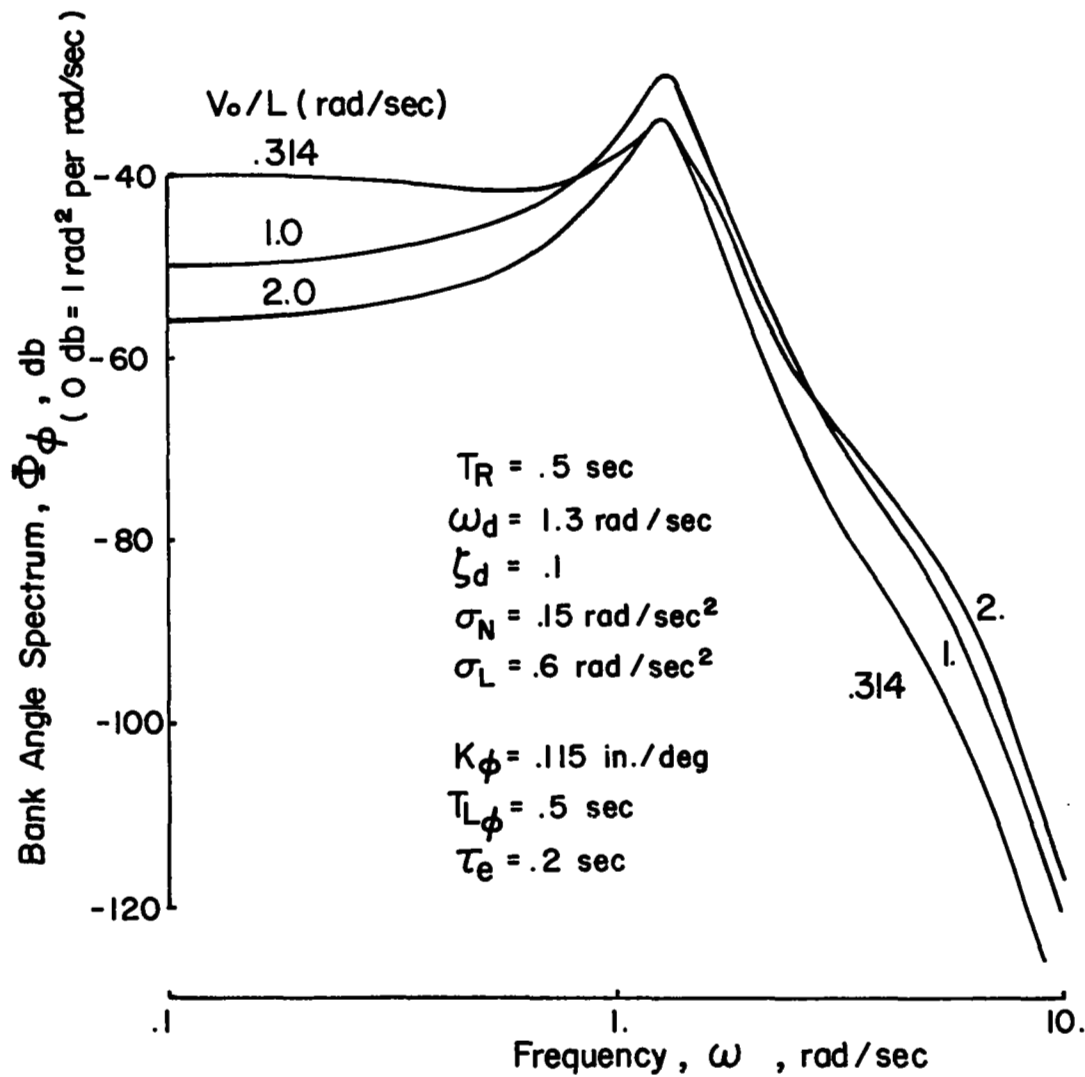Figure 91. Effects of Turbulence Bandwidth on Roll Response -
Configuration 6
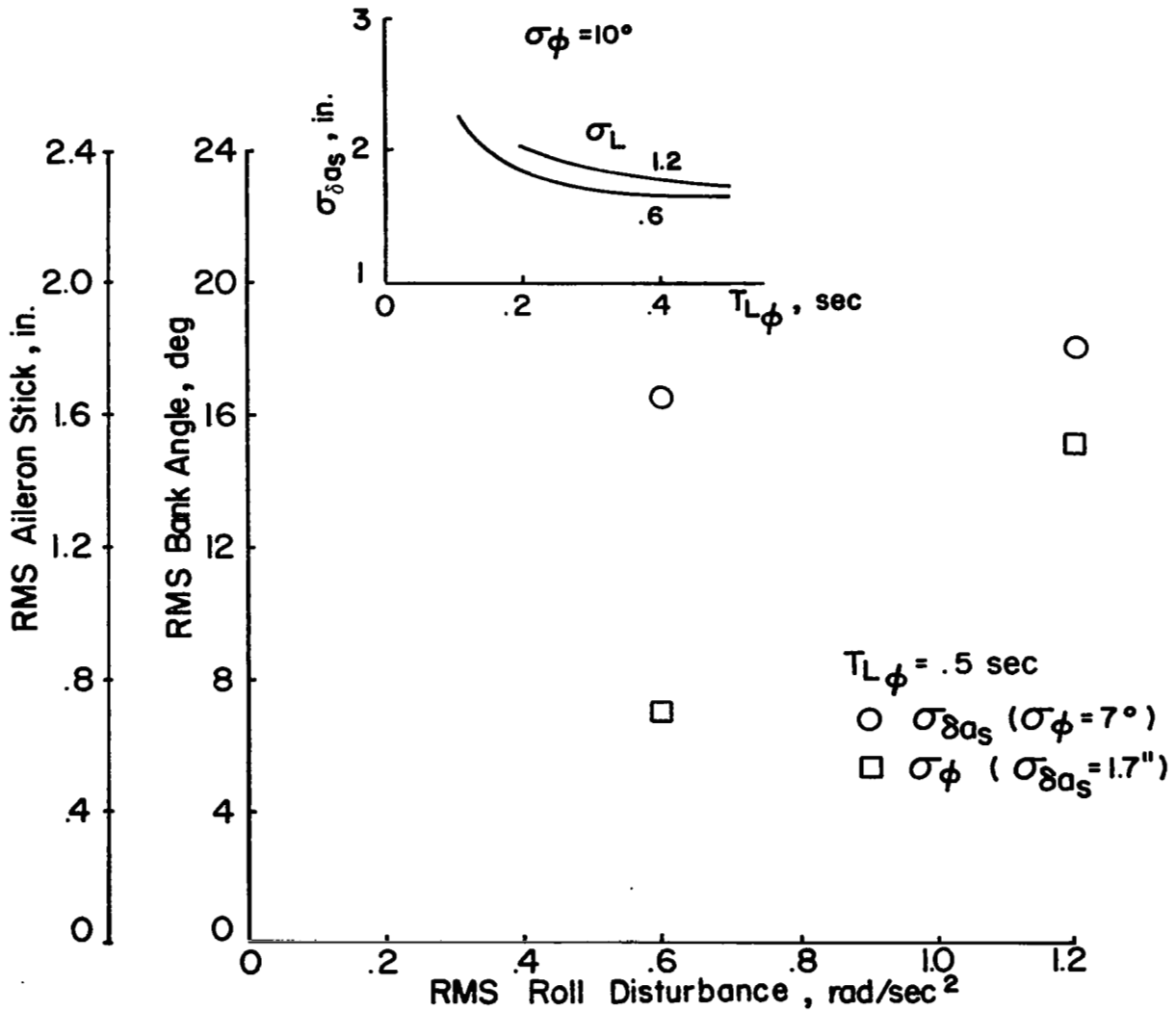
Figure 92. Effect of RMS Roll Disturbance on Roll Performance and Aileron Workload - Configuration 6

excursions and consequently reduce roll-induced excursions due to sideslip.
The increase in aileron-only workload with disturbance level for constant roll
performance is not large, whereas the increase noted in roll excursions is
substantial if a constant workload is maintained.

A variety of heading to rudder loop closures is illustrated in Figure 93.
The primary purpose is to indicate the improvement in bandwidth and stability
afforded by increasing lead time constant, T_{L_ψ}, and to show at the same time
the variation in closed loop characteristics which might be anticipated for the
uncertainty in the pilot's effective time lag ($.2 < \tau_e < .4$ seconds). If the band-
width is to be maintained near 3.0 radians/second, substantial increases in
lead are required to establish a satisfactory phase margin (φ_m = 30 degrees).
Assuming the optimistic value for pilot time lag (τ_e = .2 seconds) permits the
desired phase margin to be achieved for a lead time constant somewhat greater
than .5 seconds. However, if the more pessimistic value of pilot time lag is
used (τ_e = .4 seconds) the phase margin is reduced considerably and is barely
above the 10 degree minimum phase for a lead of T_{L_ψ} = 1.0 second. The
general conclusion to be reached from this closed loop analysis is that the
pilot is likely to be hard pressed to achieve sufficient bandwidth and phase
margin to attenuate the turbulence disturbances. He will be forced to create
some lead to maintain closed loop stability and on top of that he will have to
work hard to achieve the desired performance. The open loop pilot-airplane
transfer function based on flight test pilot describing function data is shown in
Figure 94. The crossover frequency noted is approximately 3.0 radians/
second for a slope slightly in excess of -20 db/decade. A reasonable fit of
these data, particularly in the region of crossover, is obtained using a pilot
model with the characteristics K_ψ = .05 inch/degree, T_{L_ψ} = 1.0 second.
This higher level of lead compensation, in comparison to Configuration 1,
is likely to contribute to the degradation in pilot rating observed for this
configuration for the general reasons noted previously (page 177).
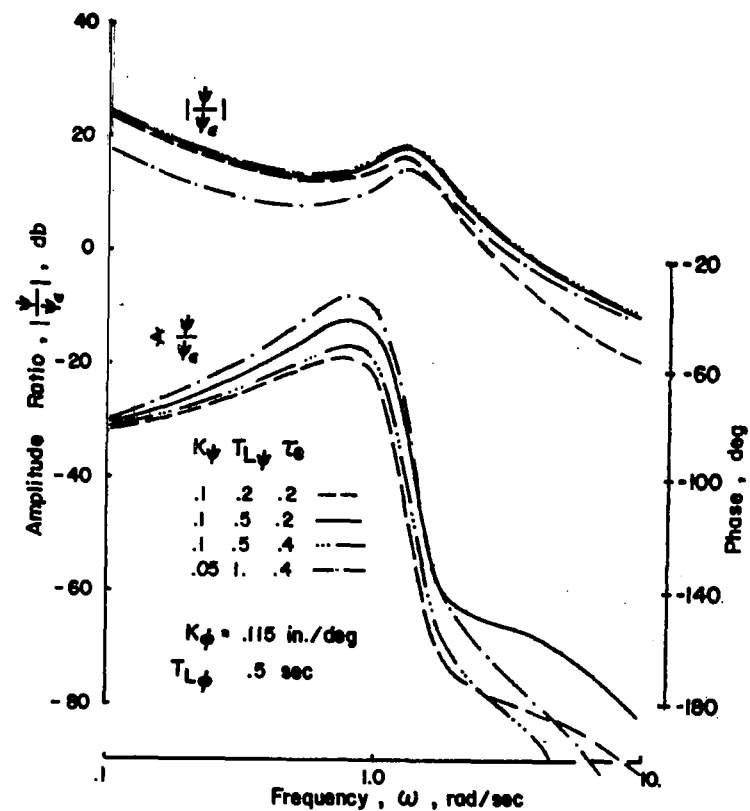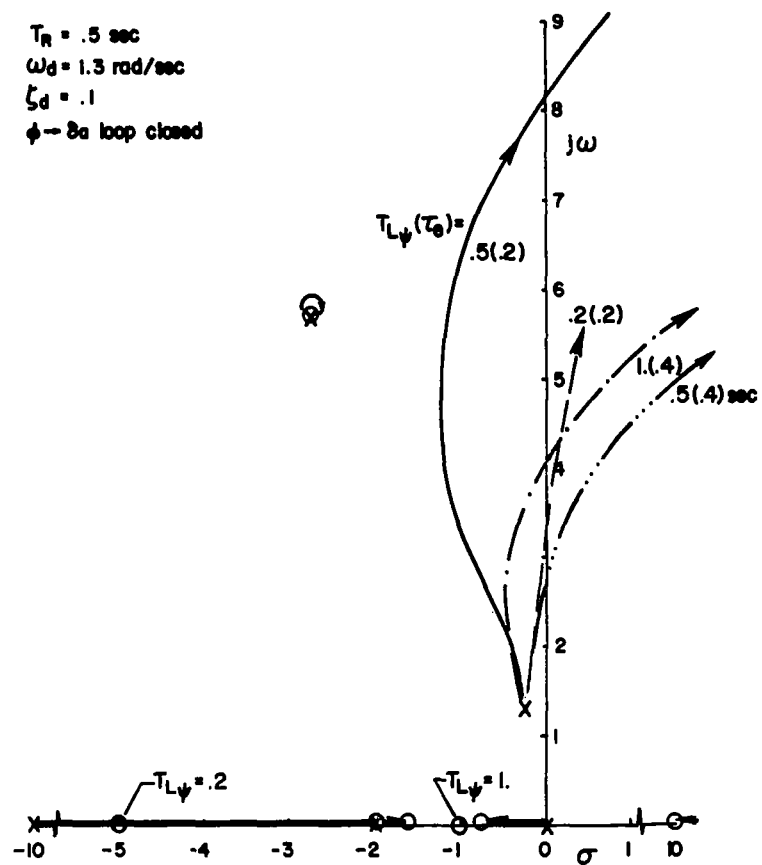
Figure 93. Heading to Rudder Closure - Configuration 6
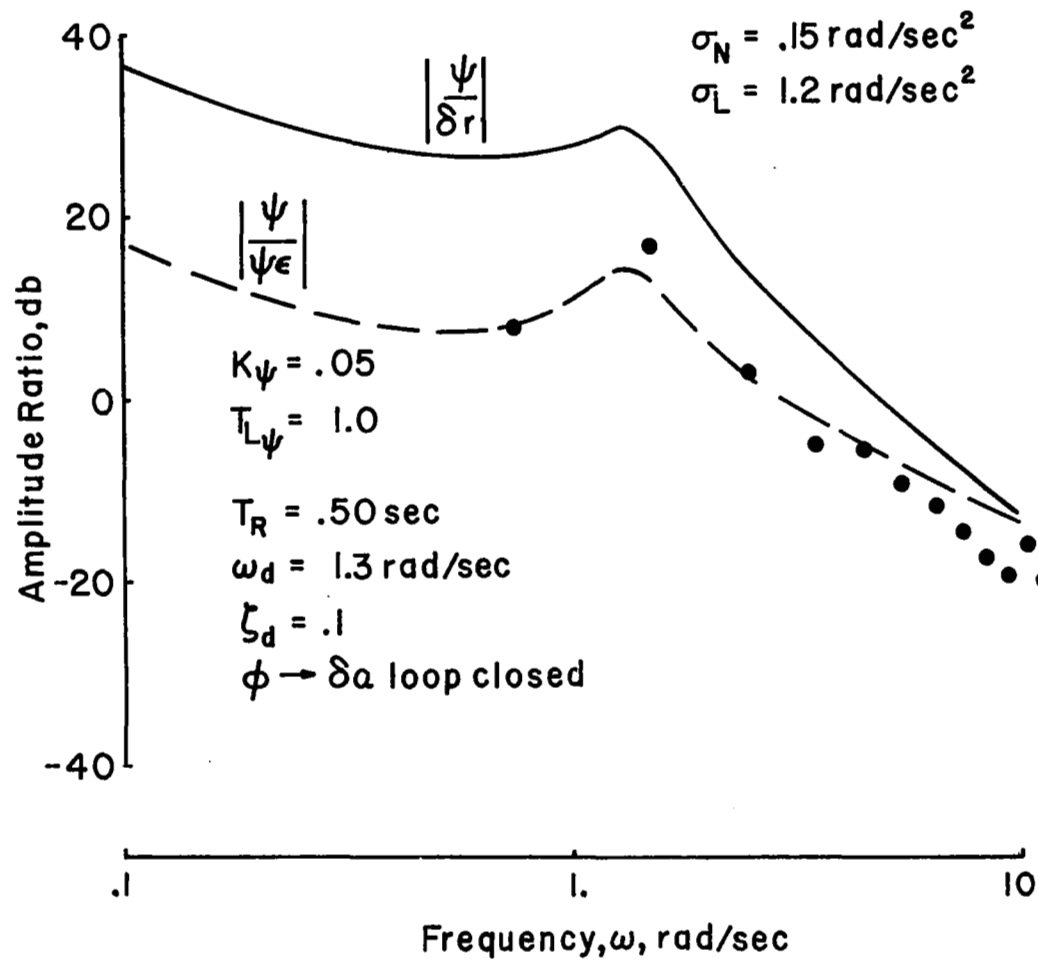
Figure 94. Flight Test Measured Pilot Compensation in Heading
Control with Rudder - Configuration 6

An indication of the effect of increasing the level of yaw turbulence on closed loop heading response to lateral gusts is given in Figure 95. A uniform increase in amplitude ratio across the frequency band is noted. The heading loop is assumed to be closed for the $T_{L_\psi} = 1.0$ radian/ second, $\tau_e = .4$ second case shown in Figure 93. The spectral distribution of energy as a function of turbulence bandwidth is shown in Figure 96. For frequencies above 1.0 radian/ second somewhat of an increase in the spectrum is apparent as $\frac{V_o}{L}$ is increased from .314 to 1.0 radian / second. No comparable change in the energy content appears as $\frac{V_o}{L}$ is further increased to 2.0 radians/ second.

Workload increase with rms yaw disturbances is substantial as shown in Figure 97. To hold yaw excursions at the 2 degree level (rms), the rudder activity shows a proportional increase greater than the increase in yaw excitation. A slight benefit in workload from increased pilot lead in the heading to rudder loop is noted. This trend in workload with increasing turbulence level corresponds to the flight test results.

In most respects, the pilot ratings and flight test performance-workload data used to evaluate the effects of turbulence magnitude and spectral bandwidth for this configuration show the same trends as noted for Configuration 1. Due to the poorer roll damping and directional stability characteristics of this configuration the absolute levels of pilot rating are worse and the magnitudes of airplane excursions and control workload are larger than for Configuration 1. The dominant influence on pilot rating is the magnitude of the turbulence, particularly yaw disturbances, because of the large attendant excursions in bank angle and heading or conversely the high control workload required to achieve acceptable task performance. The reduced roll damping and directional stability compared to Configuration 1 requires additional pilot compensation to achieve adequate closed loop bandwidths in order to suppress turbulence disturbances. The net result is either increased control workload or increased lead compensation or both.
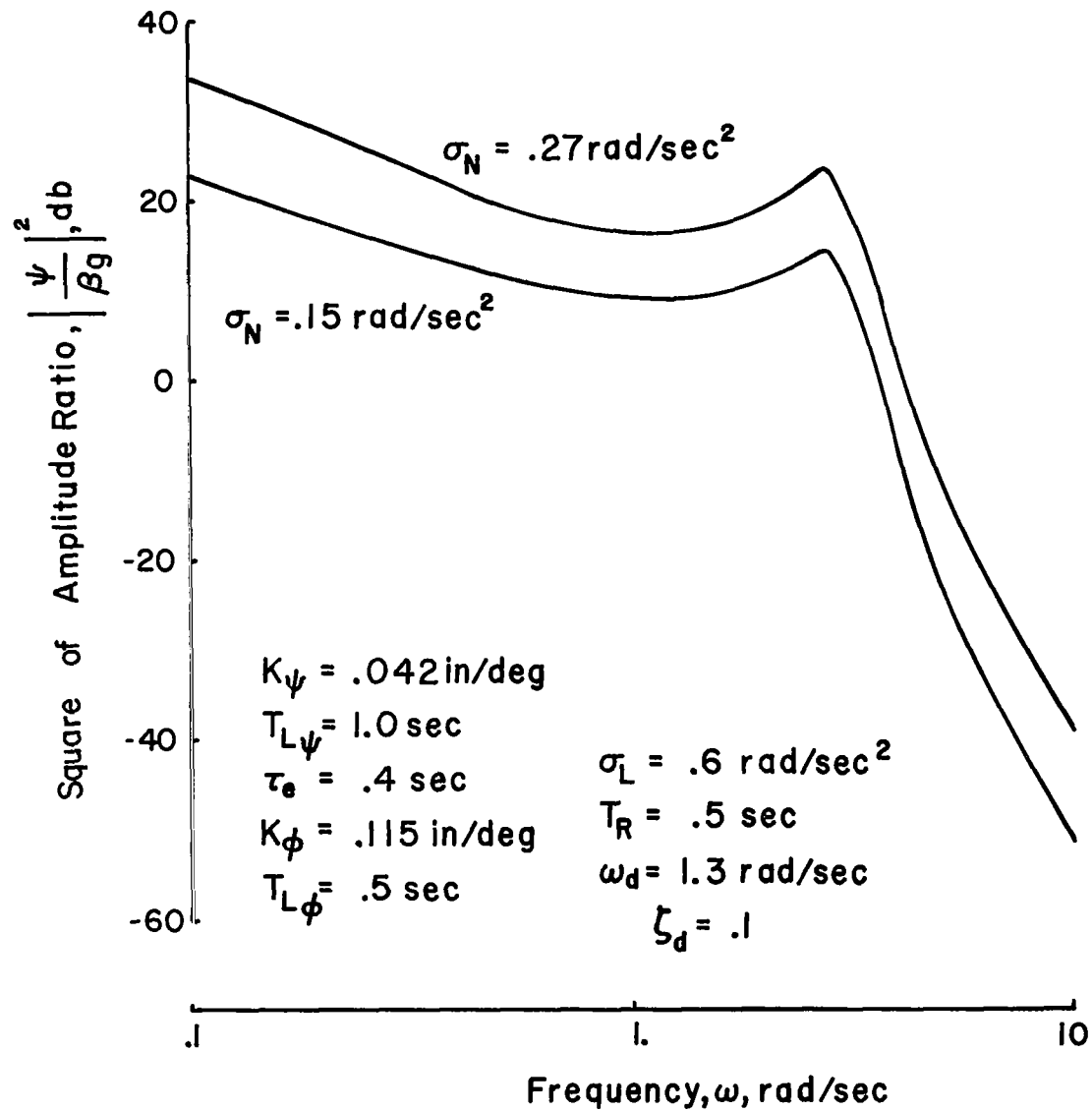
Figure 95. Closed Loop Heading Response to Lateral Gusts -
Effect of RMS Yaw Turbulence
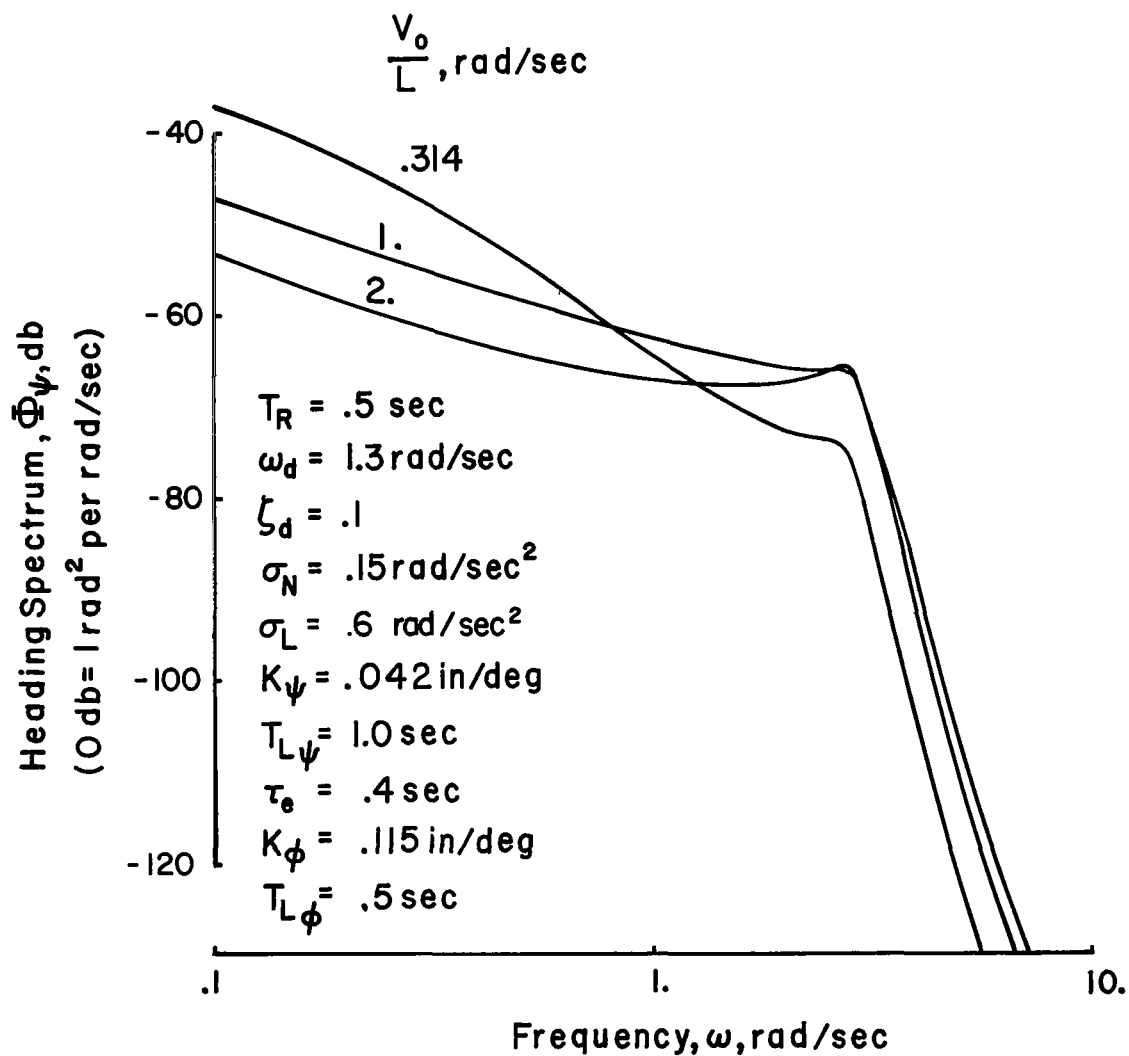
Figure 96. Effect of Turbulence Bandwidth on Heading Response - Configuration 6

The figure shows a plot of Heading Spectrum, Φ_ψ, db (0 db = 1 rad^2 per rad/sec) versus Frequency, ω, rad/sec. Curves are labeled for $\frac{V_0}{L}$, rad/sec values of .314, 1., and 2.

Parameters listed:

$T_R = .5$ sec

$\omega_d = 1.3$ rad/sec

$\zeta_d = .1$

$\sigma_N = .15$ rad/sec^2

$\sigma_L = .6$ rad/sec^2

$K_\psi = .042$ in/deg

$T_{L_\psi} = 1.0$ sec

$\tau_e = .4$ sec

$K_\phi = .115$ in/deg

$T_{L_\phi} = .5$ sec
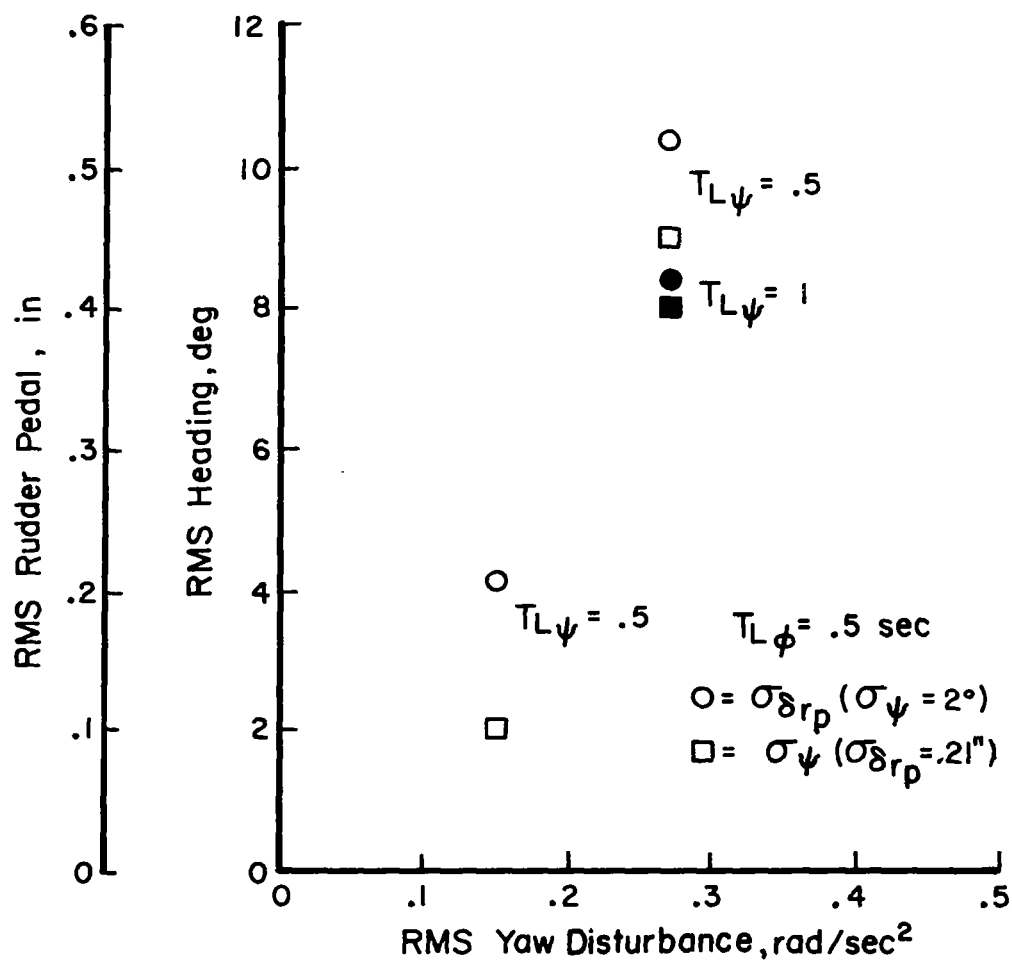
Figure 97. Effect of RMS Yaw Disturbance on Heading Performance and Rudder Workload - Configuration 6

Increasing turbulence bandwidth increases the magnitude of roll and heading excursions or conversely the aileron and rudder workloads necessary for acceptable task performance. Both flight test results and the closed loop system analyses agree in showing the dominant effect of bandwidth to correspond to the low to mid frequency range up to $\frac{V_o}{L}$ of approximately 1.0 radian/second.

Contribution of roll damping

In contrast to Configuration 1 which had a satisfactory level of roll damping (T_R = .25 seconds) and generally good closed loop characteristics, Configuration 4, with roll damping one-half that of Configuration 1, begins to make more demands on the pilot to achieve good bank angle control. Much the same as Configuration 6 which had the same low roll damping, this case requires lead compensation on the order of T_{L_φ} = .5 seconds for good closed loop characteristics. As indicated in Figure 98, at any lower levels of lead, the closed-loop roll-spiral oscillatory mode can be suppressed, but only at high gain and then at the expense of emphasizing and eventually destabilizing the Dutch roll. For the case of T_{L_φ} = .5 seconds, the pilot can increase his bandwidth substantially, while still maintaining an adequate stability margin, if this is necessary to counteract turbulence inputs. Alternatively, if the disturbances are not large, he can take advantage of the lead generated and reduce his workload (gain) and still have an adequate bandwidth for suppressing disturbances.

It is possible to compare the turbulence response characteristics of the satisfactory and unsatisfactory roll damping configurations if suitable loop closures are assumed for both cases. Using the closed loop gains, time constants and time lags considered favorable for Configurations 1 and 4, the transfer function of bank angle to lateral gusts is constructed in Figure 99. In this case, the loop was closed to give a bandwidth on the order of 4.5 radians/second. The result is a generally larger transfer of lateral gust energy into roll motions for the lower roll damping. Interestingly enough it can be shown that increasing the pilot's gain by nearly a factor of two does not appreciably alter the situation for the low roll damping. This results because the roll-spiral mode becomes poorly damped and begins to dominate roll response at the higher closed loop gain.
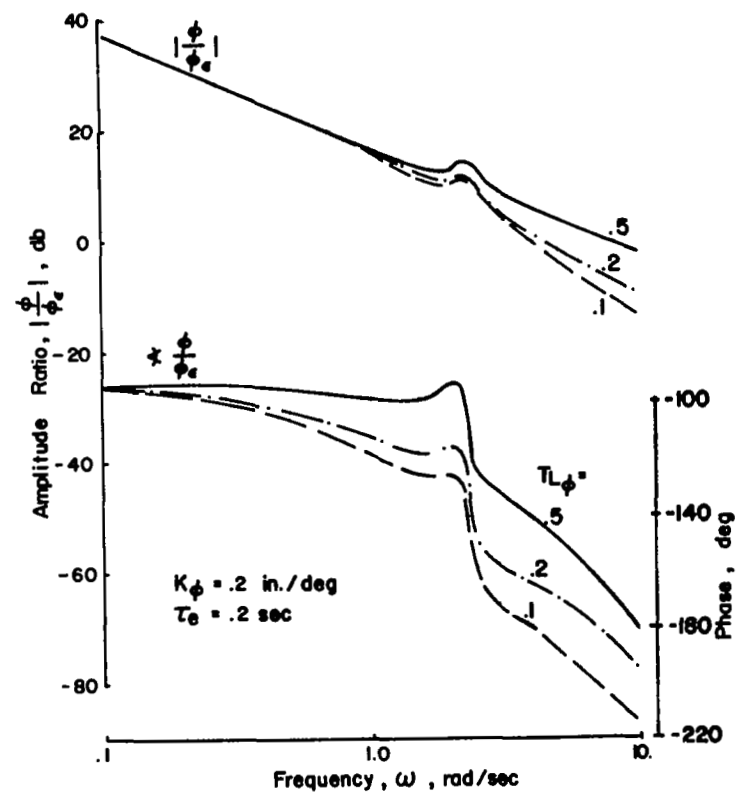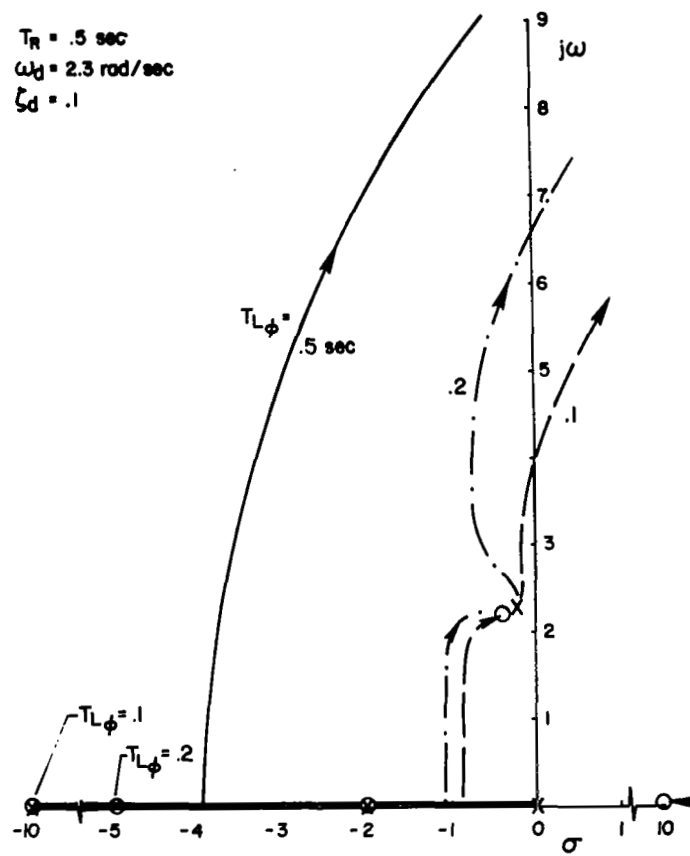
Figure 98. Bank Angle to Aileron Closure - Configuration 4
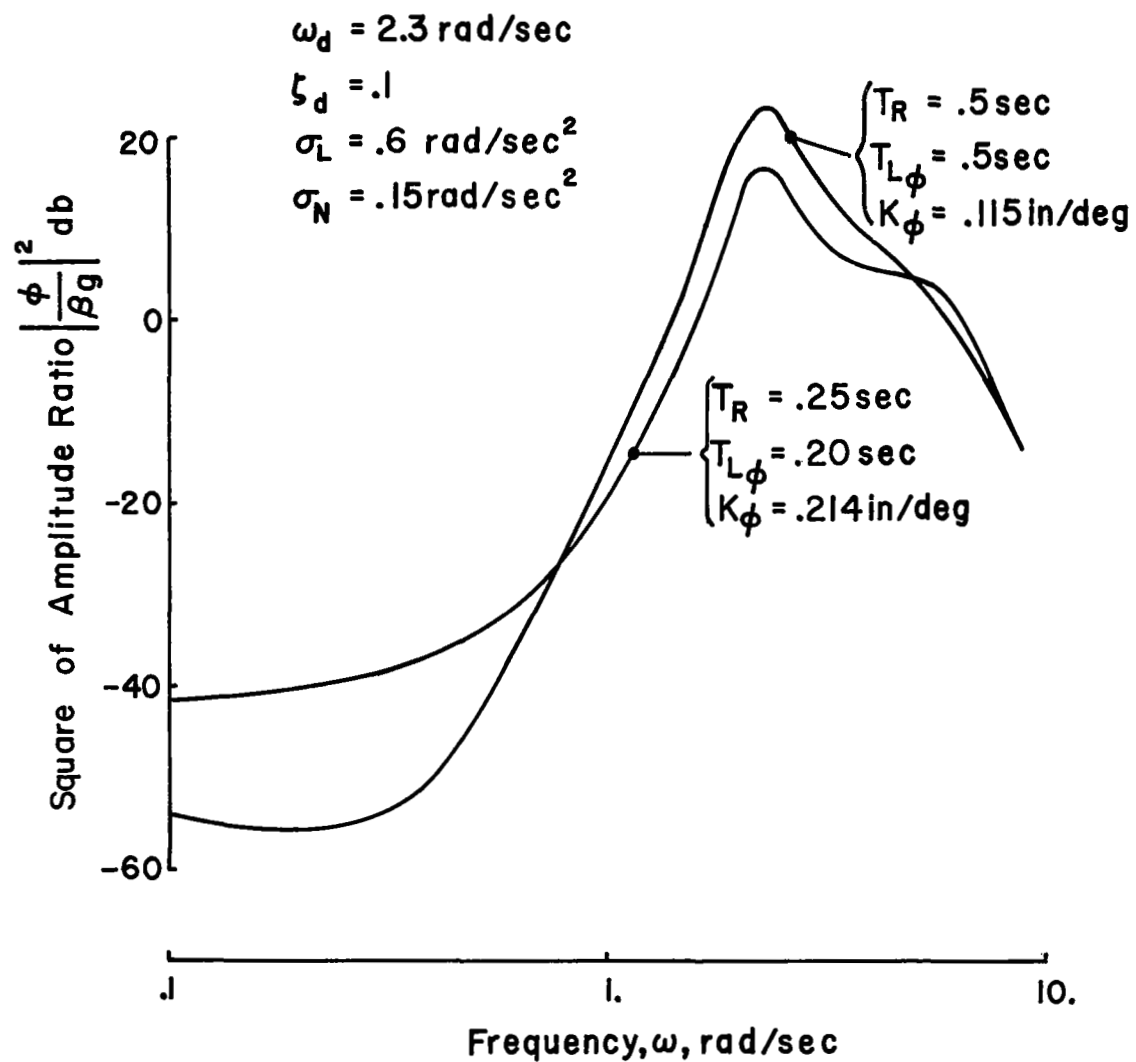
Figure 99. Effect of Roll Damping on Bank Angle Response to Lateral Gusts

Effects of turbulence bandwidth in the case of low roll damping are shown in Figure 100. The trends are similar to the higher roll damping configuration. Increasing bandwidth increases energy across the spectrum up to $\frac{V_o}{L}$ of 1.0 radian/second. Further increases in bandwidth are of little consequence.

Figure 101 illustrates the increase in aileron activity required to hold rms bank angle excursions at a constant level as roll damping is reduced. These trends are in good agreement with flight test results. An indication of the tradeoff between workload and lead compensation for the three values of roll damping is also given. The advantage of increasing lead compensation to relieve aileron workload as roll damping is reduced is apparent.

Considering the data of Figure 102, it would appear that for lower levels of roll damping a greater increase in workload is required of the pilot to maintain a desired level of performance when roll disturbances are increased. These data follow the trend suggested by pilot rating data and are consistent with the flight test variation in workload and performance. Turbulence bandwidth would appear to have the same influence on workload, regardless of roll damping. The data indicate a comparable increase in workload for increase in bandwidth to $\frac{V_o}{L} = 1.0$ radian/second.

To summarize the results of the flight test and closed loop systems analyses, roll damping seems to have two contributions, one related to the magnitude of the roll excursions and the other to the closed loop roll control characteristics. The magnitude of the open loop roll response is inversely proportional to the level of roll damping as noted on page 163, hence the closed loop bank angle excursions and aileron workload will be directly affected. Roll damping is also important to the ability to control bank angle excursions with the ailerons. Reductions in roll damping force the pilot to generate more lead compensation to maintain good closed loop characteristics. While it may be possible for the pilot to produce this lead and to achieve bandwidths and stability margins comparable to cases with better damping, too much of a demand for lead will cause the pilot to downgrade the airplane for that reason alone.
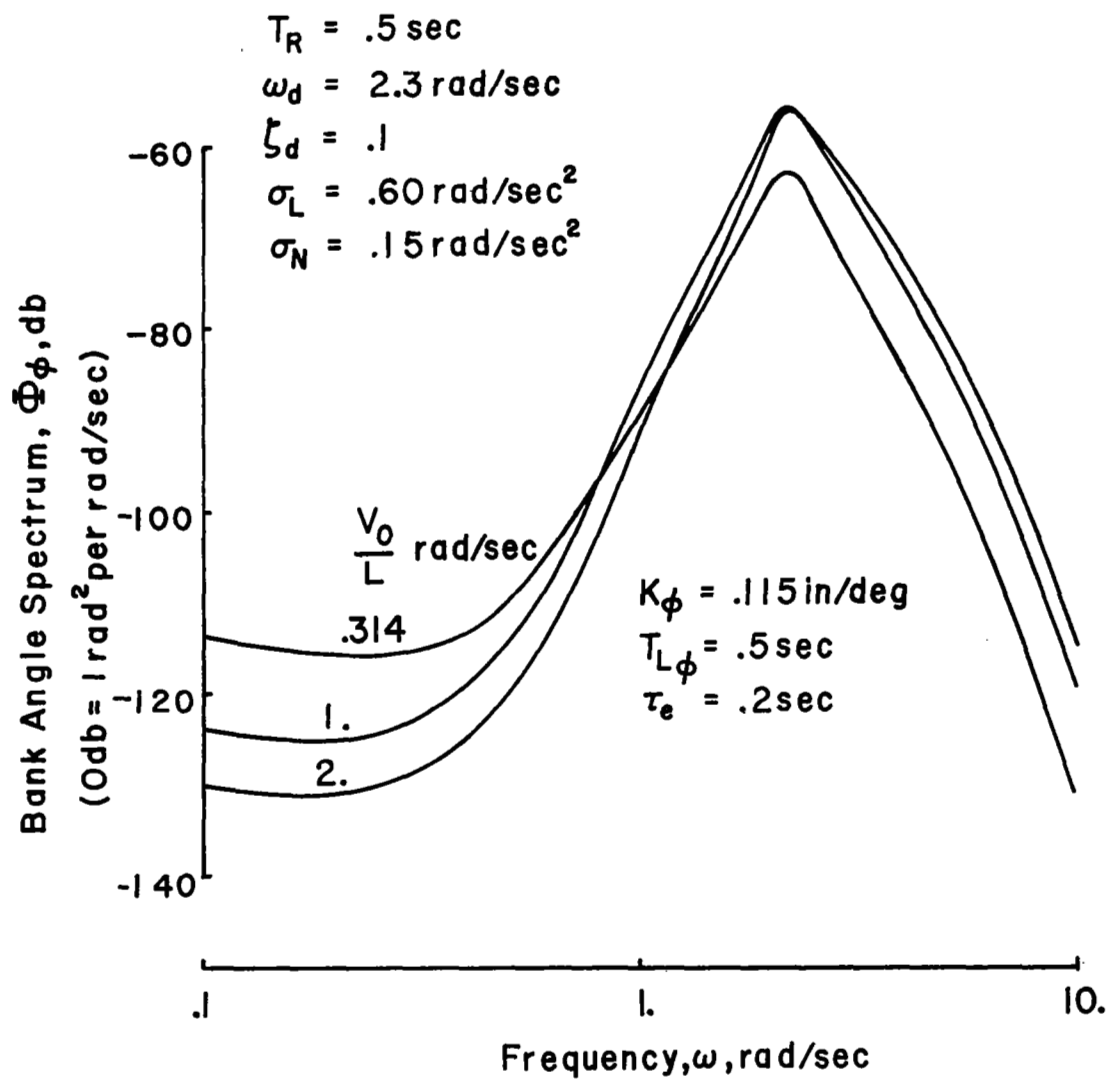
Figure 100. Effect of Turbulence Bandwidth on Bank Angle Spectra
- Configuration 4
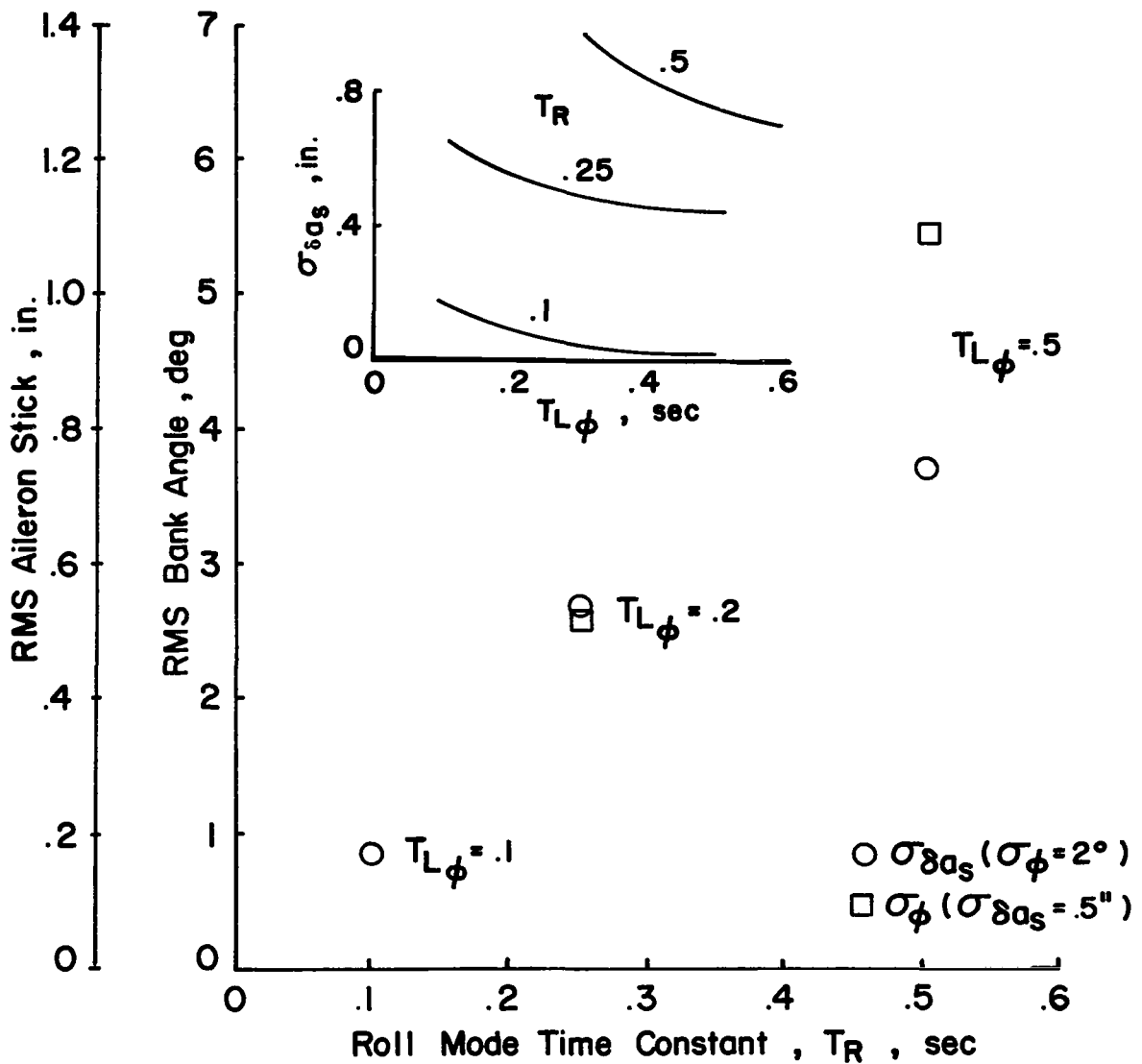
Figure 101. Effect of Roll Damping on Roll Performance and
Aileron Workload
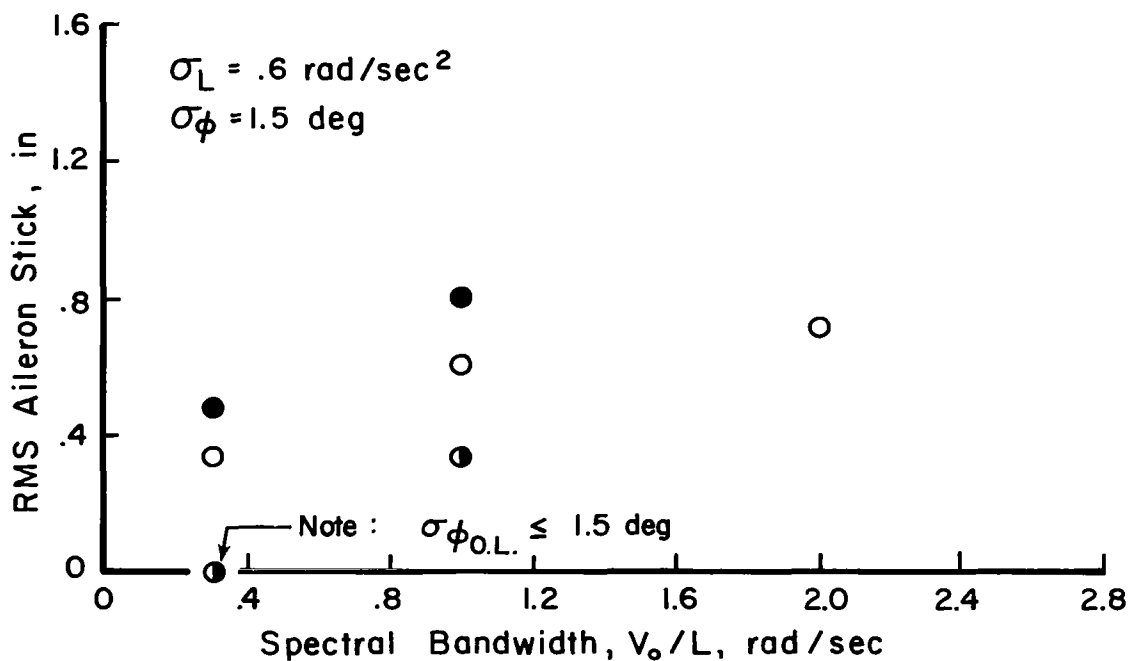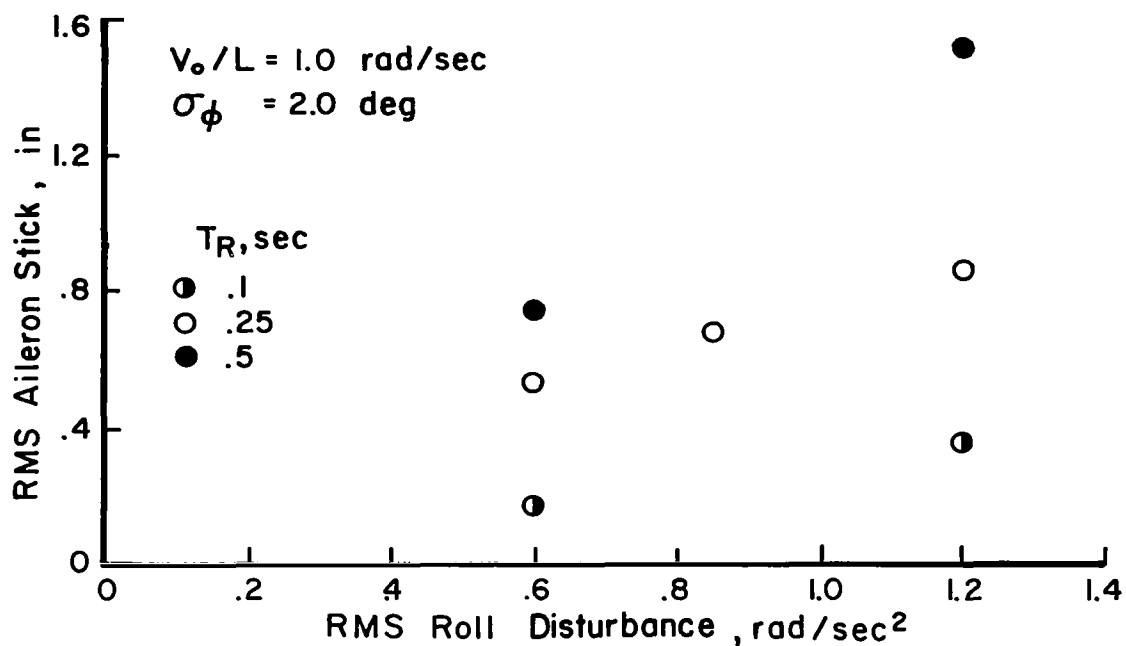
Figure 102. Effect of Roll Damping Combined with Roll Disturbance and Bandwidth on Aileron Workload

221

Increases in roll disturbances seem to lead to greater increases in roll excursions or aileron workload at the lower values of roll damping. This result is apparently due to the limitation placed on the system's closed loop bandwidth by stability requirements. In other words, the pilot can raise his gain only so far to suppress disturbances. The combined effect of low damping, which permits large roll excursions, and large disturbances, which increase the excursions even more, apparently pushes the pilot-airplane combination beyond its desired operating limits. Pilot opinion data support this result.

An increase in the derivative L_p which simultaneously increases roll damping and roll disturbance has no net effect on pilot ratings at the lower levels of L_p. Further increases in L_p above values consistent with T_R of .2 seconds begin to degrade pilot rating since increased turbulence sensitivity begins to override the additional improvement in roll axis dynamics.

Changes in turbulence bandwidth might be expected to have the same effect on bank angle excursions and aileron workload regardless of the amount of roll damping. This behavior is anticipated because it is the frequency and damping of the Dutch roll which predominantly determine the magnitude of roll excursions which will result from the turbulence energy in a given frequency band. Flight test data and the analog simulation results confirm this impression.

Contribution of directional stability

Insofar as closed loop roll control is concerned, a reduction in directional stability from the level of Configuration 1 to that of Configuration 2 causes few problems. It is apparent from the analysis of Figure 103 that the pilot, by adopting a moderate amount of lead, can achieve a suitable bandwidth and phase margin (ω_{co} = 4.75 radians/ second, ϕ_m = 41 degrees for T_{L_ϕ} = .2 seconds). The corresponding closed loop roots appear on the root locus diagram. Very
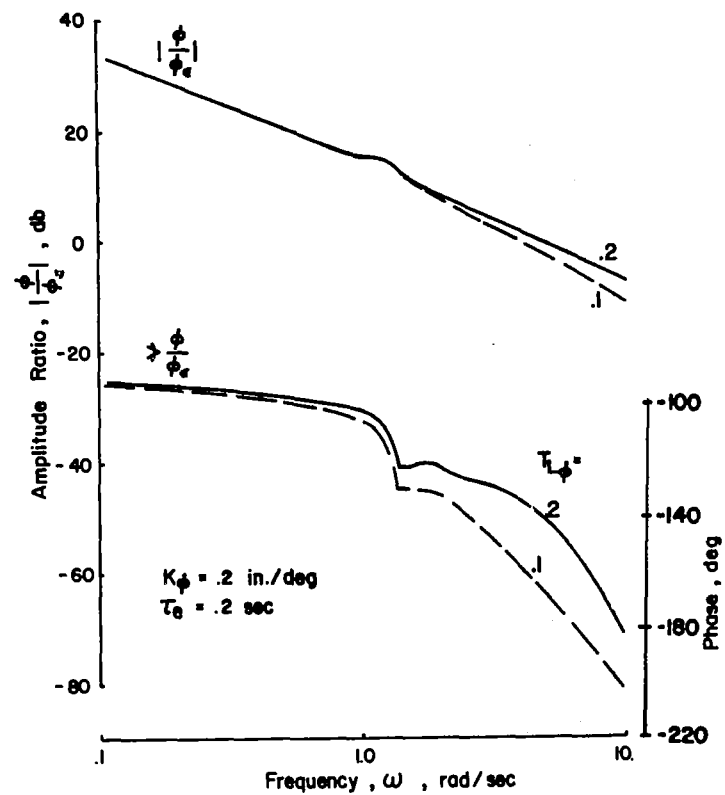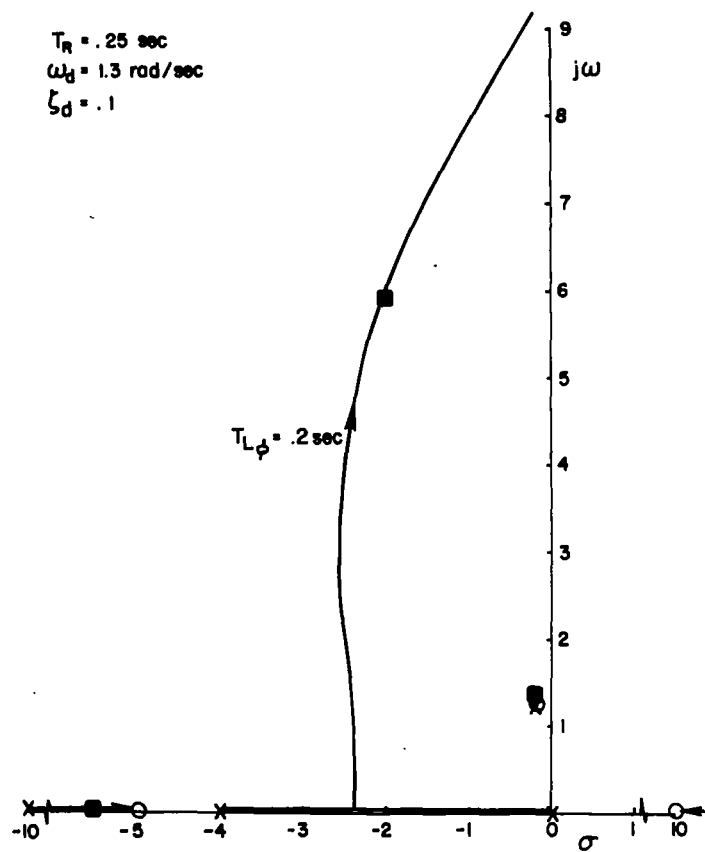
Figure 103.   Bank Angle to Aileron Closure - Configuration 2

little Dutch roll will appear due to aileron control inputs as a result of the Dutch roll pole-zero proximity. If this were not the case and the ailerons excited Dutch roll motions in the bank angle response, roll control could be difficult. The Dutch roll mode remains poorly damped after the roll loop closure. This low damping in conjunction with the low level of directional stability encourages large roll excursions if the ailerons tend to induce them.

Turbulence excitation of rolling motions is another matter, and a trouble-some one. In response to the roll disturbances induced by turbulence large roll excursions result in part due to the low Dutch roll damping and low directional stability. A comparison between closed loop roll response to turbulence for a high and low level of directional stability is shown in Figure 104 for typical bank angle to aileron closures. The dominant influence of the Dutch roll on roll response is apparent from the relative magnitude of the two peaks. Because of limitations imposed on the closed-loop bandwidth the pilot can acieve, the un-favorable influence of the Dutch roll cannot be eliminated for the single loop closure of bank angle to aileron.

An indication of the trends in aileron workload with directional stability is shown in Figure 105. Only the bank angle to aileron loop is closed in this case. A considerable increase in aileron activity to maintain a given level of roll excursions (σ_φ = 2 degrees) is indicated for ω_d less than 2 radians/second. This behavior reflects the comparison of roll spectra for ω_d = 1.3 and 2.3 radians/second of Figure 104. A similar trend is noted in roll excursions where in this case the comparison is made for constant pilot gain (K_φ). It was necessary to make the σ_φ comparison in this manner since a common value of $\sigma_{\delta a}$ did not exist for the three values of ω_d shown.

Closing the heading to rudder loop permits the pilot to achieve ac-ceptable bandwidth for yaw control, but he must introduce considerable lead in order to maintain a satisfactory stability margin. It is apparent in Figure 106 that a lead of .2 seconds is inadequate in both bandwidth and
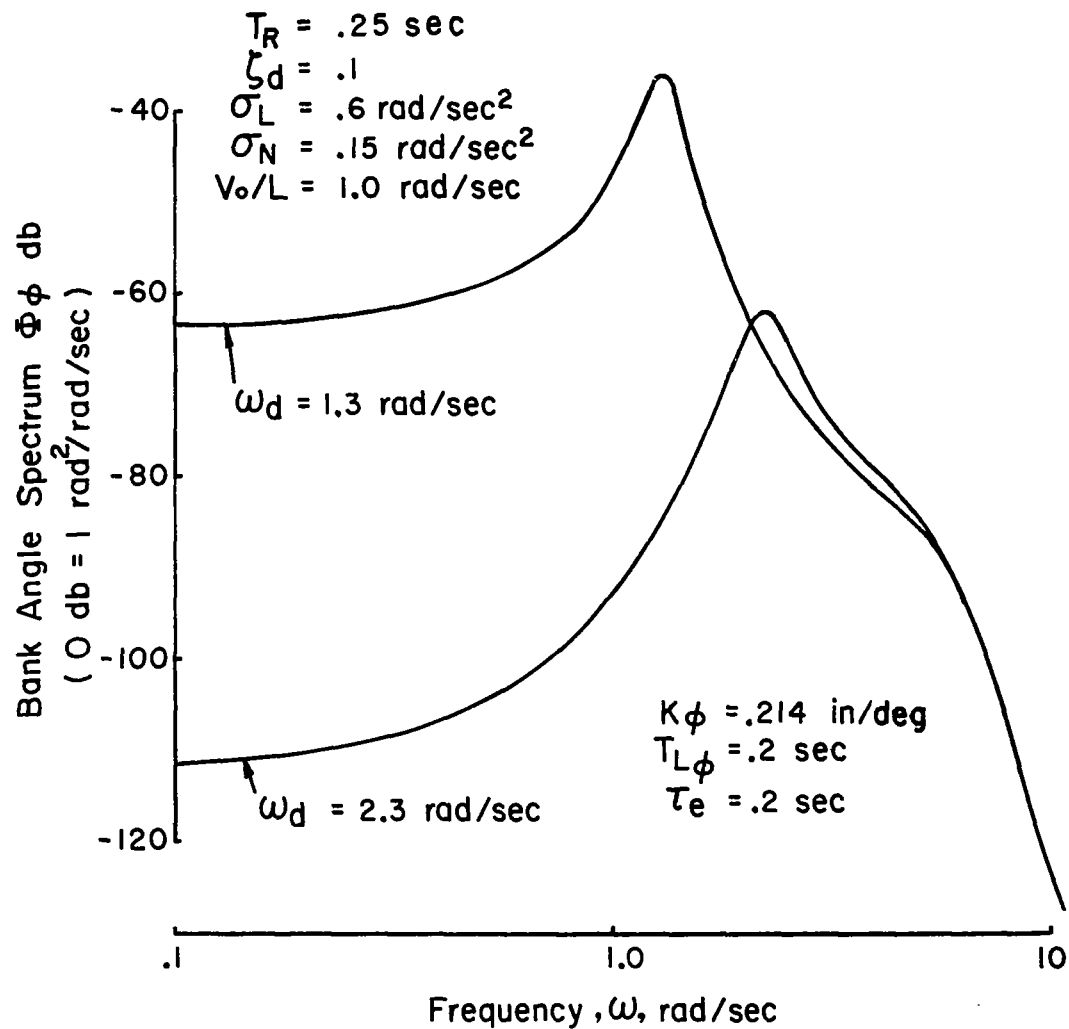
Figure 104. Effect of Directional Stability on Bank Angle Spectra
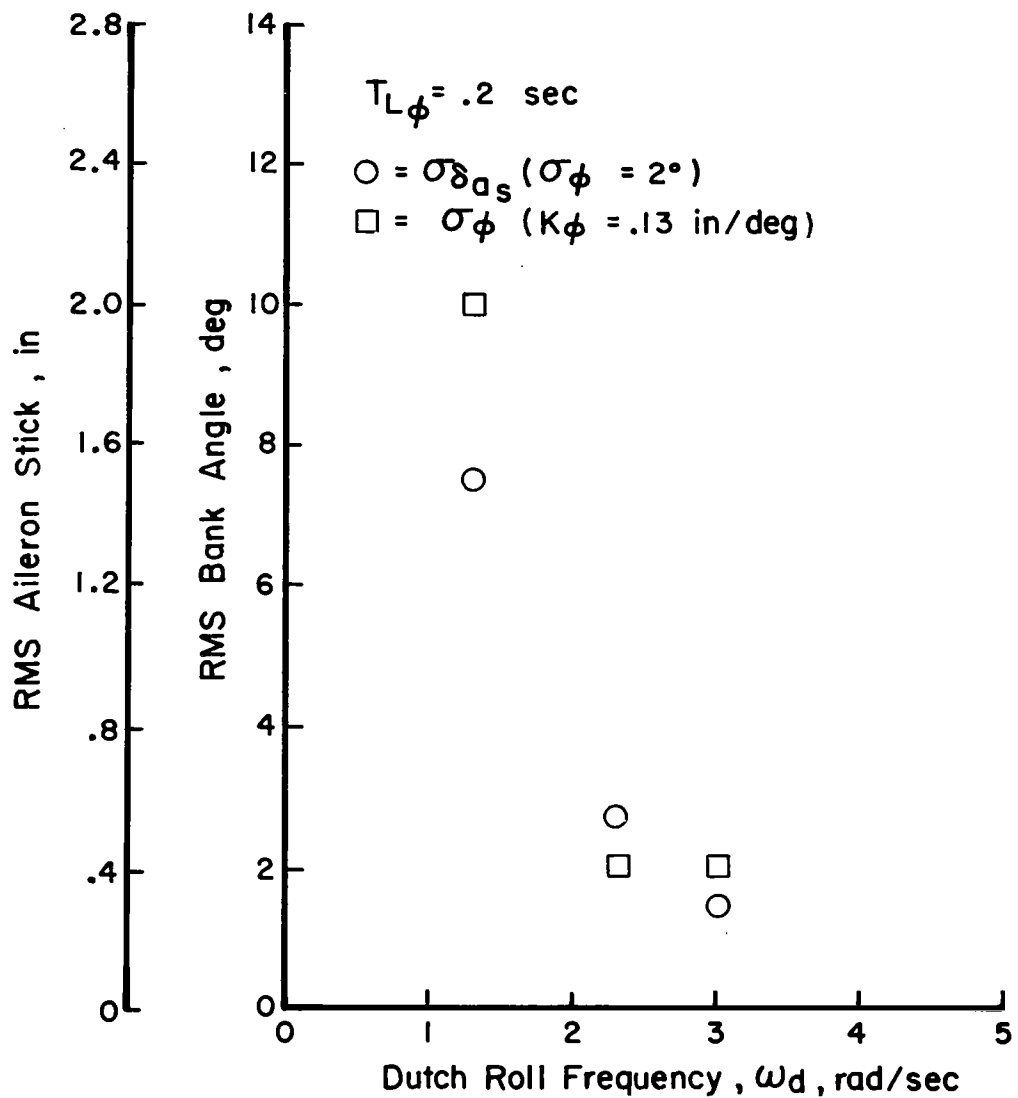
Figure 105.   Effect of Directional Stability on Roll Performance
and Aileron Workload
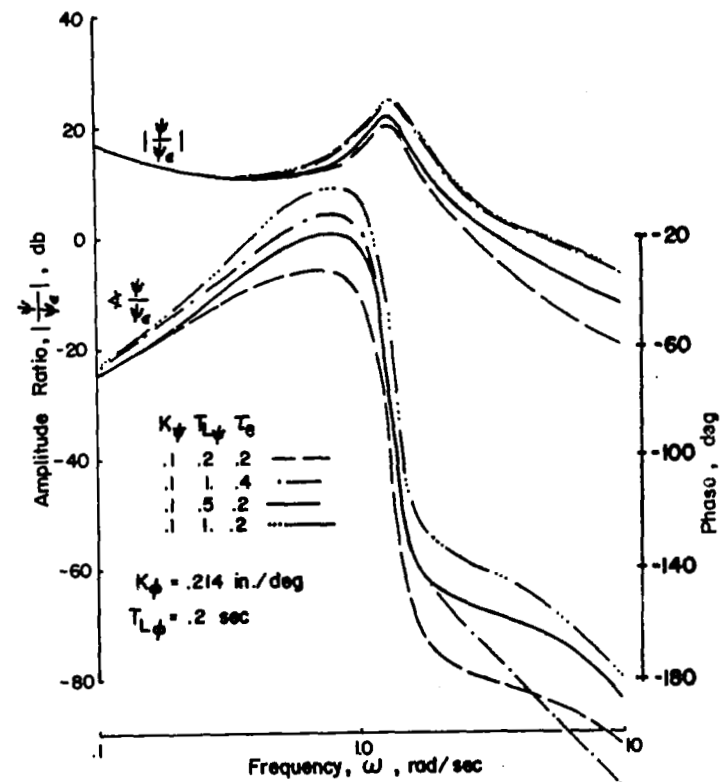
Figure 106.   Heading to Rudder Closure - Configuration 2

phase margin and that increasing the lead to .5 seconds gives a more acceptable loop closure (ω_{co} = 3.3 radians/second, φ_m = 23 degrees). If a more pessimistic pilot time lag is assumed, lead on the order of 1.0 seconds or more will be required to maintain essentially the same bandwidth and phase margin as for the T_{L_ψ} = .5 seconds, τ_e = .2 seconds case.

Pilot-airplane heading amplitude ratio data, $|\frac{\psi}{\psi_\epsilon}|$, based on flight test pilot transfer function measurements are shown in Figure 107. Data are shown for both the high and low yaw disturbance case. An excellent fit of the high σ_N results is obtained using a pilot model with the characteristics

$$K_\psi = .1 \text{ inch/degree}$$

$$T_{L_\psi} = 1.0 \text{ second}$$

In this case the crossover frequency is approximately 5.0 radians/second at a slope -20 db/decade. While the crossover frequency is considerably higher than would be anticipated considering the data of Reference 38, the presence of motion cues could aid the pilot in achieving this improvement in closed loop performance. In particular, the pilots indicated an ability to use angular acceleration cues to help them counteract both roll and yaw upsets from turbulence. Results of References 44 and 45 reveal the benefits of motion cues on closed loop control. The data of these reports indicate an increase in system bandwidth and phase margin for crossover when motion cues are present as opposed to the case when only visual cues are available to the pilot. Reference 44 suggests that the angular motion cue can for practical purposes be considered as angular rate sensing over a frequency range of approximately .3 < ω < 5.0 radians/second, due to the filtering characteristics of the semicircular canals. Thus the net effect on the pilot's describing function is to include an additional lead ($T_L s + 1$) term in a path parallel to the visual sensing and compensation path and hence to increase the pilot's overall lead time constant.

T_R = .25 sec $\qquad \zeta_d$ = .1

ω_d = 1.3 rad/sec $\qquad \phi \rightarrow \delta a$ loop closed

σ_L = .6 rad/sec^2

$\left|\dfrac{\psi}{\delta r}\right|$

$\left|\dfrac{\psi}{\psi_\epsilon}\right|$

Amplitude Ratio, db

	K_ψ	$T_{L\psi}$
— —	.1	1.0
- - -	.1	.67

σ_N

X $\quad$ .15 rad/sec^2

● $\quad$ .27 rad/sec^2

Frequency, ω, rad/sec
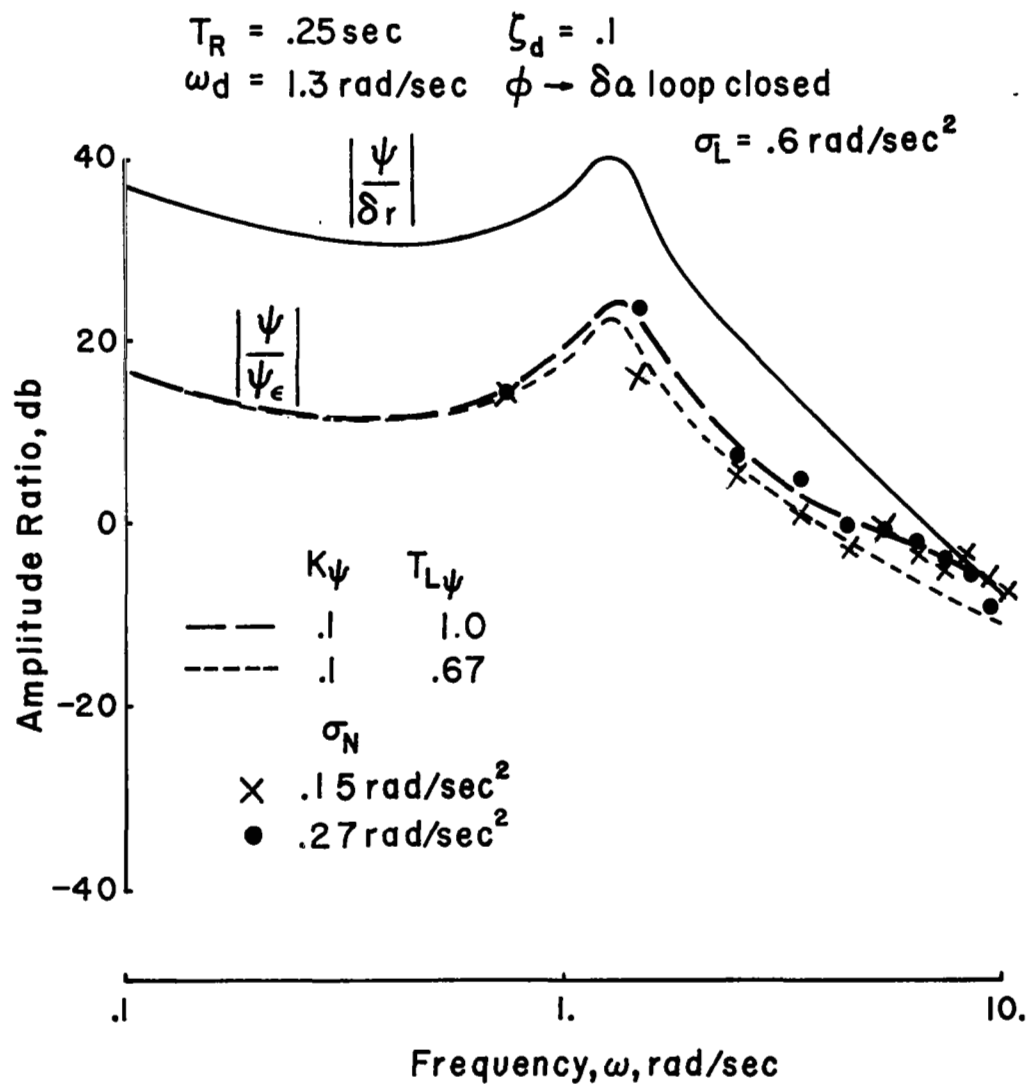
Figure 107. Flight Test Measured Compensation in Heading Control
with Rudder - Configuration 2

Data for the lower yaw disturbance level show a somewhat lower band-
width and effectively a lower magnitude of lead. For either of these cases the
compensation required exceeds that of Configuration 1 and is therefore expected
to contribute to a degradation in pilot rating.

A general increase in amplitude across the frequency spectrum occurs
for the heading to lateral gust transfer function as directional stability is re-
duced. This behavior is indicated in Figure 108. Loop closures having essen-
tially the same bandwidth and stability characteristics were adopted for the two
configurations. For the lower directional stability case, Configuration 2,
a pilot lead of 1.0 second and a conservative estimate for his effective time
lag (τ_e = .4 seconds) were used. Increasing the level of rms yaw distur-
bances increases the heading response amplitude uniformly across the spec-
trum for Configuration 2 as was noted previously in Figure 84 for Configura-
tion 1.

The effect of turbulence bandwidth on the heading response spectra is
shown in Figure 109. An increase in bandwidth from $\frac{V_o}{L}$ = .314 to 1.0 radian/
second increases the energy content of the spectra in the frequency range which
dominates the total spectral energy. This trend is comparable to the effects of
turbulence bandwidth noted in all previous examples. A further increase in
bandwidth to $\frac{V_o}{L}$ = 2.0 radians/ second does not add energy above that for the
$\frac{V_o}{L}$ = 1.0 case, and may even reduce the overall energy level because of the
deficit at lower frequencies.

Rudder workload data generally follow the trends indicated by the
frequency response data shown in Figure 108. The increase in workload as
directional stability is reduced for a constant heading performance level
(σ_ψ = 2 degrees) is indicated in Figure 110. The data shown are for head-
ing loop closures having bandwidth and stability margins on the same order
as noted in the previous root locus-Bode analysis. Rudder activity is com-
parable to flight test data in general trend although the theoretically derived
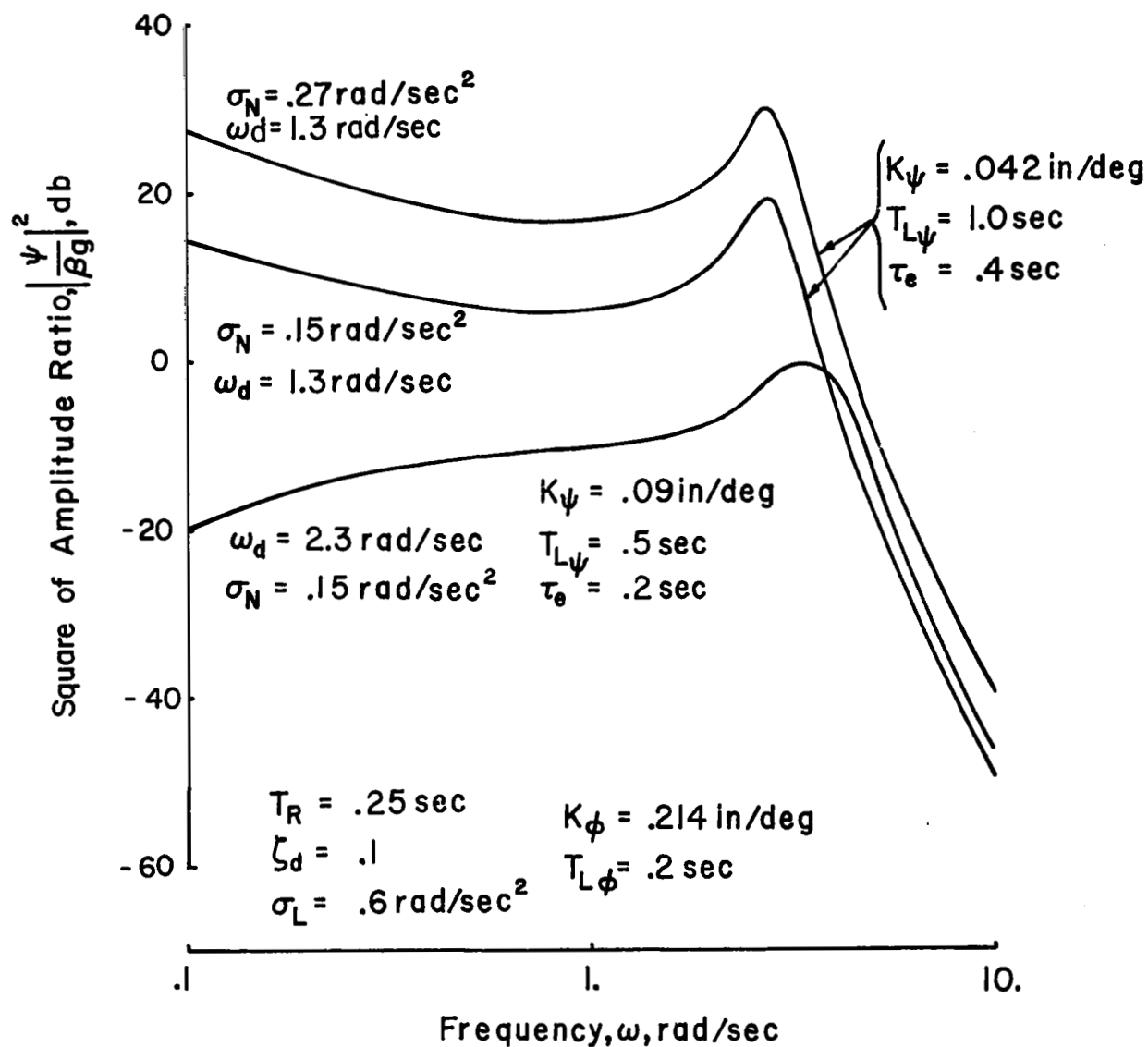
Figure 108. Closed Loop Heading Response to Lateral Gusts - Effect of Directional Stability

$T_R = .25$ sec $\quad \zeta_d = .1$

$\omega_d = 1.3$ rad/sec $\quad \sigma_L = .6$ rad/sec^2

$\dfrac{V_o}{L}$ $\quad \sigma_N = .27$ rad/sec^2

$.314$ rad/sec

1.

2.

$K_\psi = .042$ in/deg

$T_{L\psi} = 1.0$ sec

$\tau_e = .4$ sec

$K_\phi = .214$ in/deg

$T_{L\phi} = .2$ sec

Heading Spectrum, Φ_ψ, db
(0 db = 1 rad^2 per rad/sec)

Frequency, ω, rad/sec
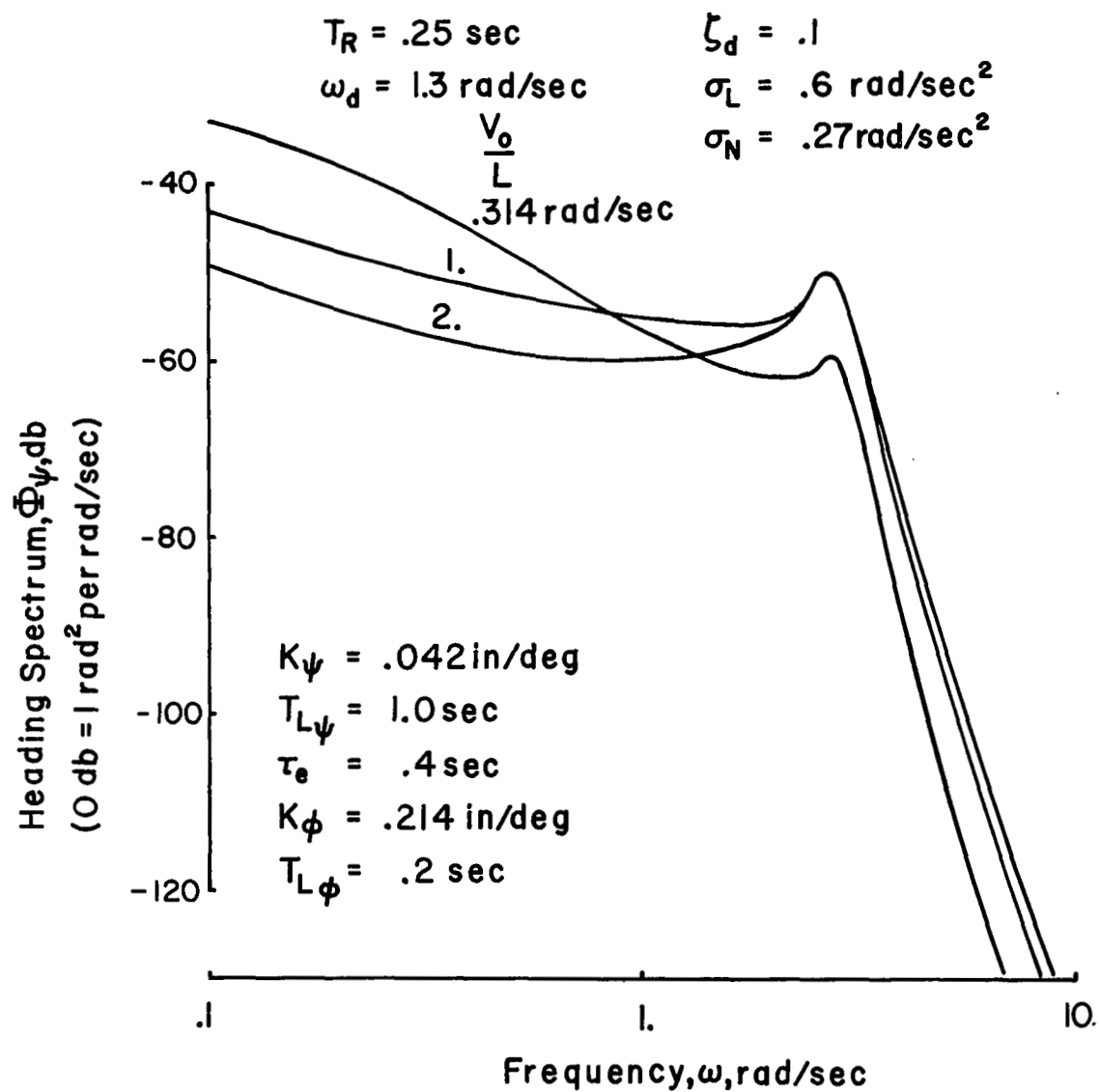
Figure 109. Effect of Turbulence Bandwidth on Heading Spectra -
Configuration 2

$T_R = .25$ sec $\qquad \sigma_N = .15$ rad/sec^2

$\zeta_d = .1$ $\qquad\qquad$ $V_o/L = 1.0$ rad/sec

$\sigma_L = .6$ rad/sec^2

$T_{L\phi} = .2$ sec

$\bigcirc$ $\sigma_{\delta r_p}$ ($\sigma_\psi = 2°$)

$\square$ σ_ψ ($\sigma_{\delta r_p} = .25"$)

$\}T_{L\psi} = .5$

$\}T_{L\psi} = .2$

$\}T_{L\psi} = .2$
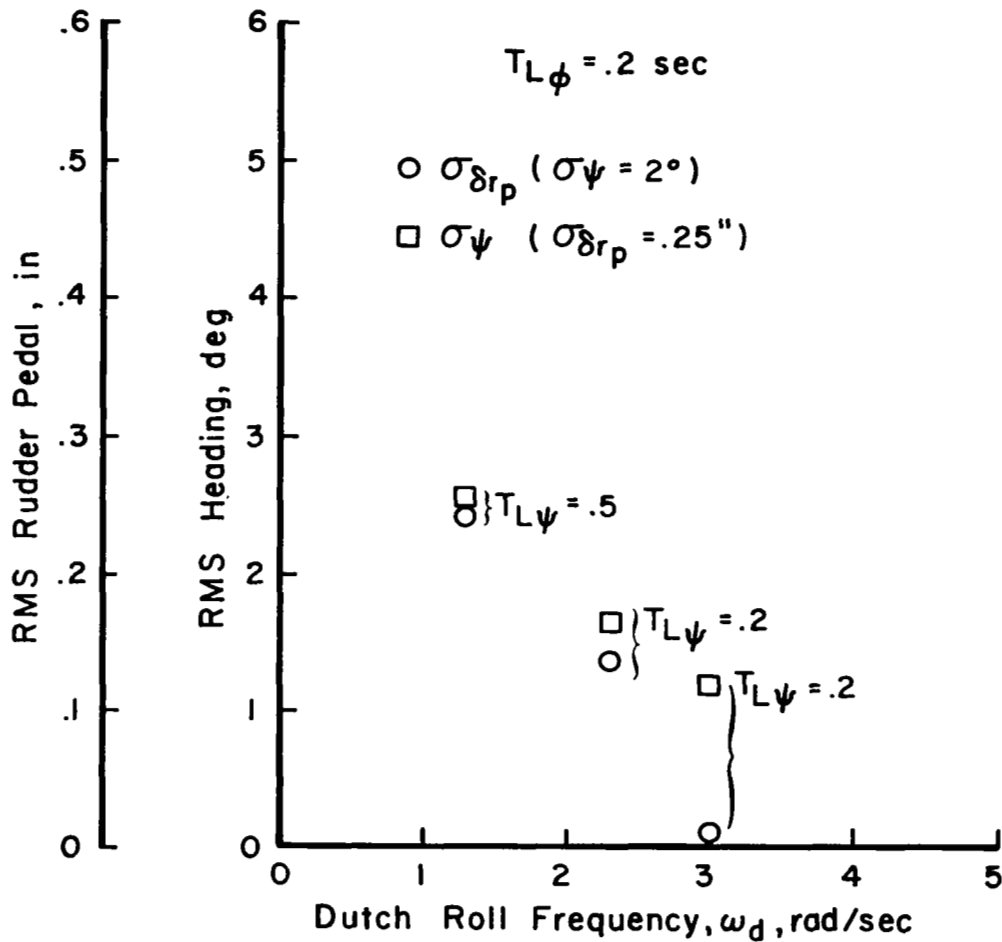
Figure 110. Effect of Directional Stability on Heading Perform-
ance and Rudder Workload

233

is somewhat lower in actual magnitude. It may be noted in Figure 111 that increasing the magnitude of yaw disturbances requires an increase of even greater proportion in workload to maintain the same level of heading excursions. The increment in workload is somewhat greater for low directional stability. Flight test data show an increase in workload with disturbance level similar to the analog simulation results.

An increase in workload with bandwidth is also apparent in Figure 111 for $\frac{V_o}{L}$ from .314 to 1.0 radian/ second for the two levels of directional stability. This result would be expected from the spectral data of Figure 109 and it also agrees with the flight test performance-workload and pilot opinion trends.

Reviewing this last subsection, it is apparent that directional stability (Dutch roll frequency) enters into the control task in a variety of ways. First of all, it is a determining factor in the open loop roll and heading response to turbulence (pages 163 and 169). Second, it has a strong bearing on the ability to control heading with the rudder. Consequently, it can be shown to influence the magnitude of bank angle and heading excursions and the aileron and rudder activity required to counteract the airplane's motions. Performance-workload studies and pilot ratings reflect the degrading effect of reducing the level of directional stability. Low directional stability forces the pilot to work hard to achieve suitable task performance and to generate substantial amounts of lead information to maintain a satisfactorily damped, wide bandwidth control loop.

The effect of increasing the level of yaw disturbances at the lowest level of directional stability is, of course, to degrade flying qualities for the heading tracking task. The extent of this degradation appears to be somewhat worse for low ω_d as compared to higher ω_d. When the dynamics of the yaw axis are poor as in the case of low directional stability, the pilot is forced to either work harder or generate more lead compensation in the rudder loop for a given level of turbulence than would be required with a good set of open loop dynamics. Pilot rating and performance-workload data and analog simulation results all seem to agree in this regard.

234
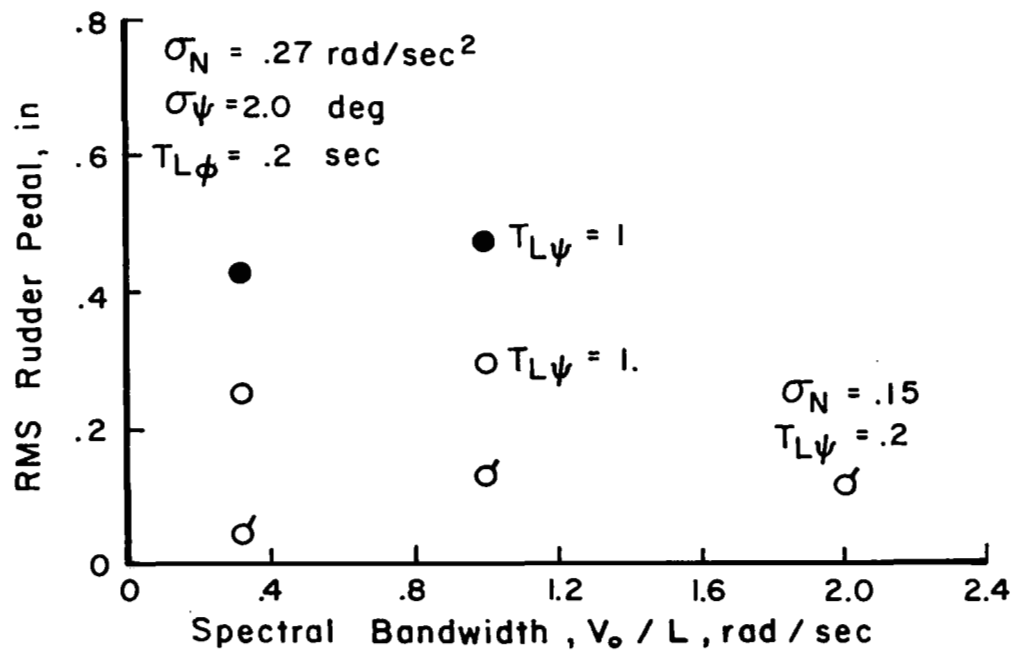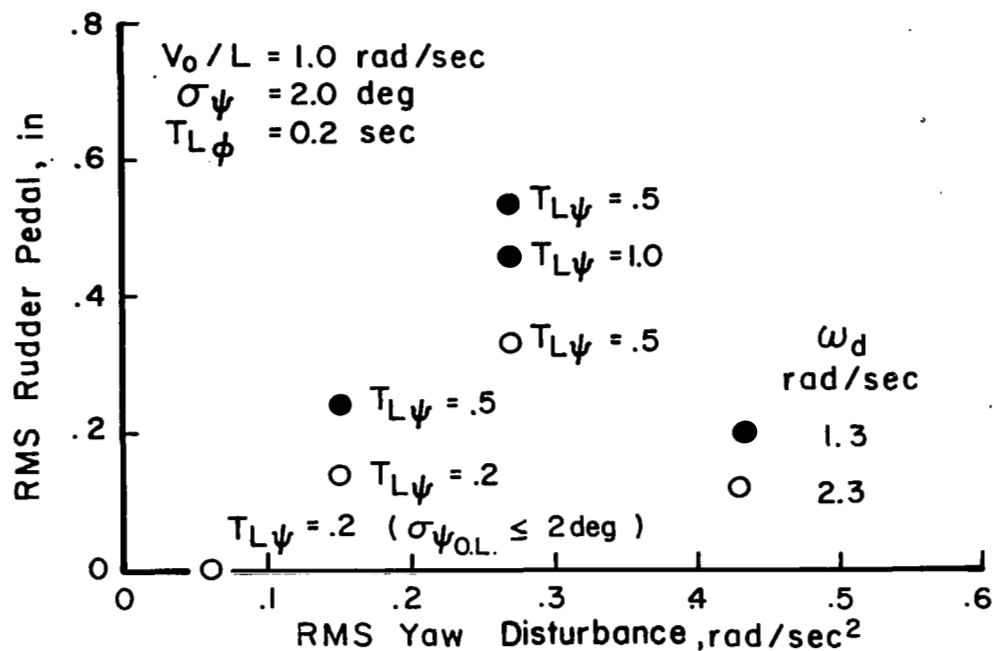
Figure 111. Effects of Directional Stability in Combination with
Yaw Disturbances and Bandwidth on Rudder Workload

235

The net influence of increasing the derivative N_β, assuming appropriate increases in directional stability and yaw turbulence disturbances, is only apparent at higher levels of the derivative. For lower values of the derivative, improvements in closed loop heading control apparently counteract the adverse influences of increased turbulence disturbances. When N_β exceeds a level appropriate to $\omega_d \cong 3.0$ radians/second, the airplane's turbulence sensitivity in yaw begins to override the favorable yaw axis dynamics and thus the overall flying qualities may be observed to deteriorate.

Turbulence bandwidth has been shown to have an influence on open loop roll and heading response because it determines in part the turbulence energy in the vicinity of the Dutch roll mode. Hence, closed loop performance and workload would be expected to depend on the turbulence bandwidth. An exception to this statement is noted for low directional stability where the lack of improvement in pilot rating with reduced bandwidth may be attributed to the pilot's objection to large, low frequency heading excursions.

Contribution   of Dutch roll damping ratio

Of all the instances where an increase in Dutch roll damping might prove beneficial, the case of low directional stability was considered the most interesting to study. Pilot ratings and commentary indicate a substantial improvement in flying qualities is possible for these configurations through an increase in damping. On the other hand, for higher levels of directional stability, little or no improvement is apparent to the pilot with increased damping.

From the indication of Figure 112, closed loop roll control is quite good with only a moderate amount of lead. The substantial difference between this case and the other low directional stability configuration is the well damped Dutch roll. As a result, roll excitation induced by control inputs or by turbulence will be of a smaller magnitude and will subside more quickly.
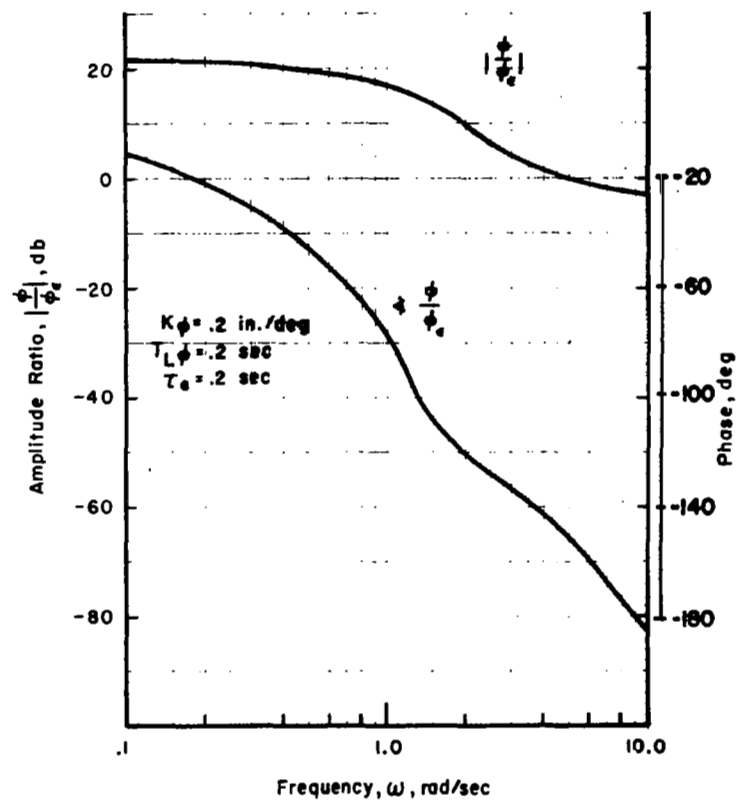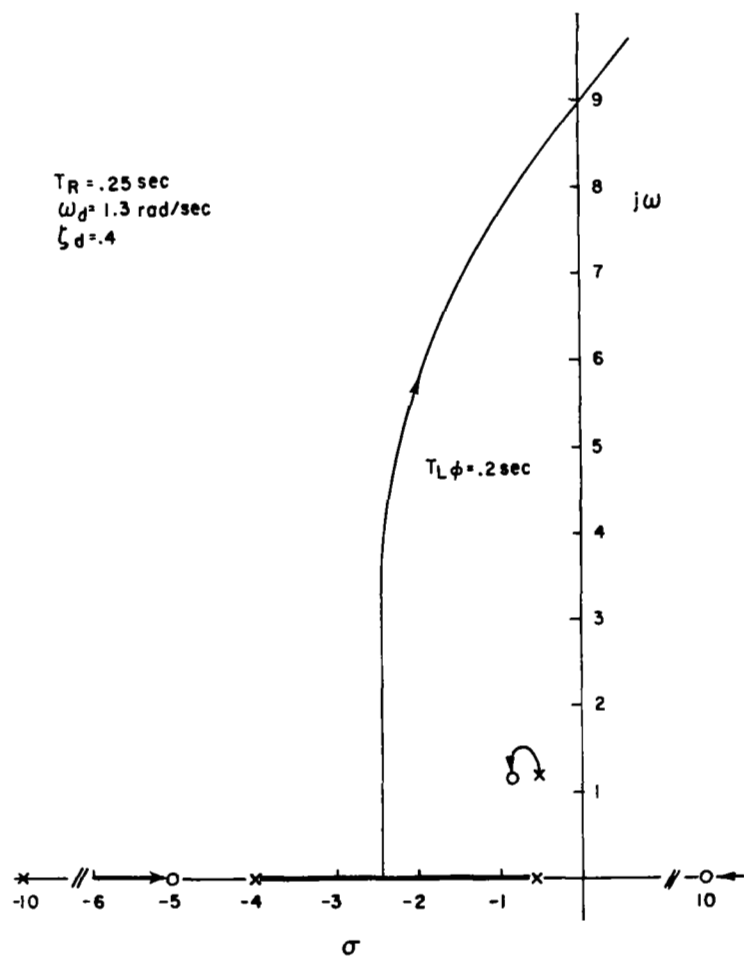
Figure 112.   Bank Angle to Aileron Closure - Configuration 7

Good heading control should be readily achieved with this configuration. Figure 113 indicates that bandwidths much in excess of the Reference 38 optimum are possible with adequate stability margins. The degree of improvement over the poorly damped configuration is apparent in Figure 114. A considerable reduction in amplitude of the heading response to lateral gust transfer function occurs in the vicinity of the Dutch roll mode with the increase in damping ratio. Finally, the improvement in workload for both bank angle and heading control, which is anticipated from the preceding analysis, is reflected in the data of Figure 115.

It is apparent from the analysis concerned with equations (88) and (89) of this subsection that Dutch roll damping is important in determining the magnitude of the airplane's open loop response, the damping of the Dutch roll in the bank angle loop closure, and the achievable bandwidth and stability of the heading loop closure. Since the pilot's greatest difficulties in the heading tracking task seemed to come from low directional stability configurations, the potential of an increase in damping ratio for improving closed loop performance was considered here. It can be demonstrated analytically that an increase in damping ratio will reduce the airplane's open loop turbulence response and will also permit the pilot to close the heading loop at higher bandwidths than is possible for a poorly damped airplane. Consequently, an improvement in task performance and workload is achieved. Flight test results, both pilot rating and performance-workload data, support this analysis.

Contribution of aileron yaw

Aileron yaw is potentially a degrading influence to both bank angle and heading control. It has previously been noted that aileron yaw can lead to objectionable Dutch roll excitation in roll, and under circumstances where the Dutch roll is poorly damped and large amounts of favorable (+) aileron yaw exist, the Dutch roll may be destabilized by closed loop roll control with ailerons only.

238
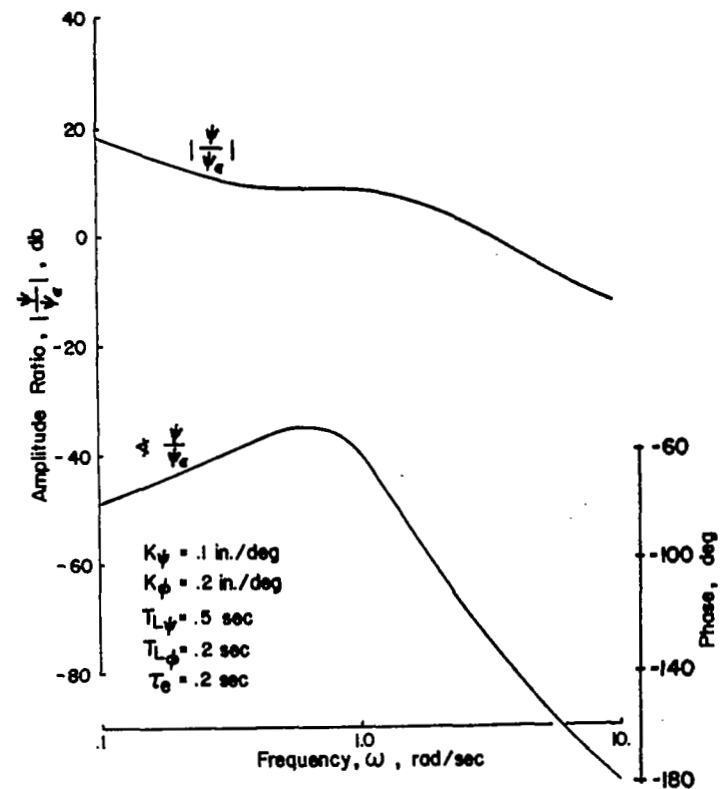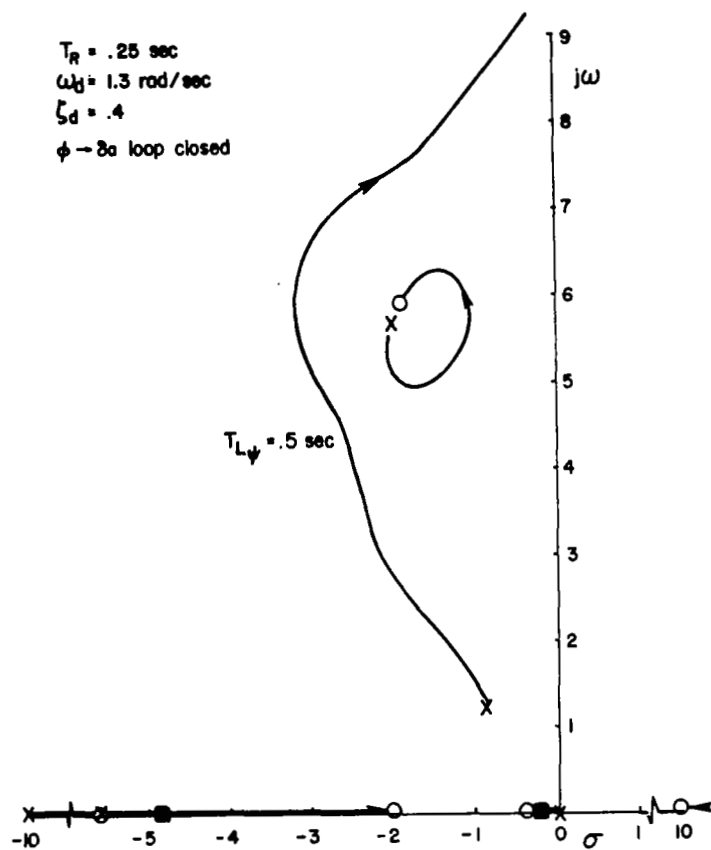
Figure 113. Heading to Rudder Closure - Configuration 7
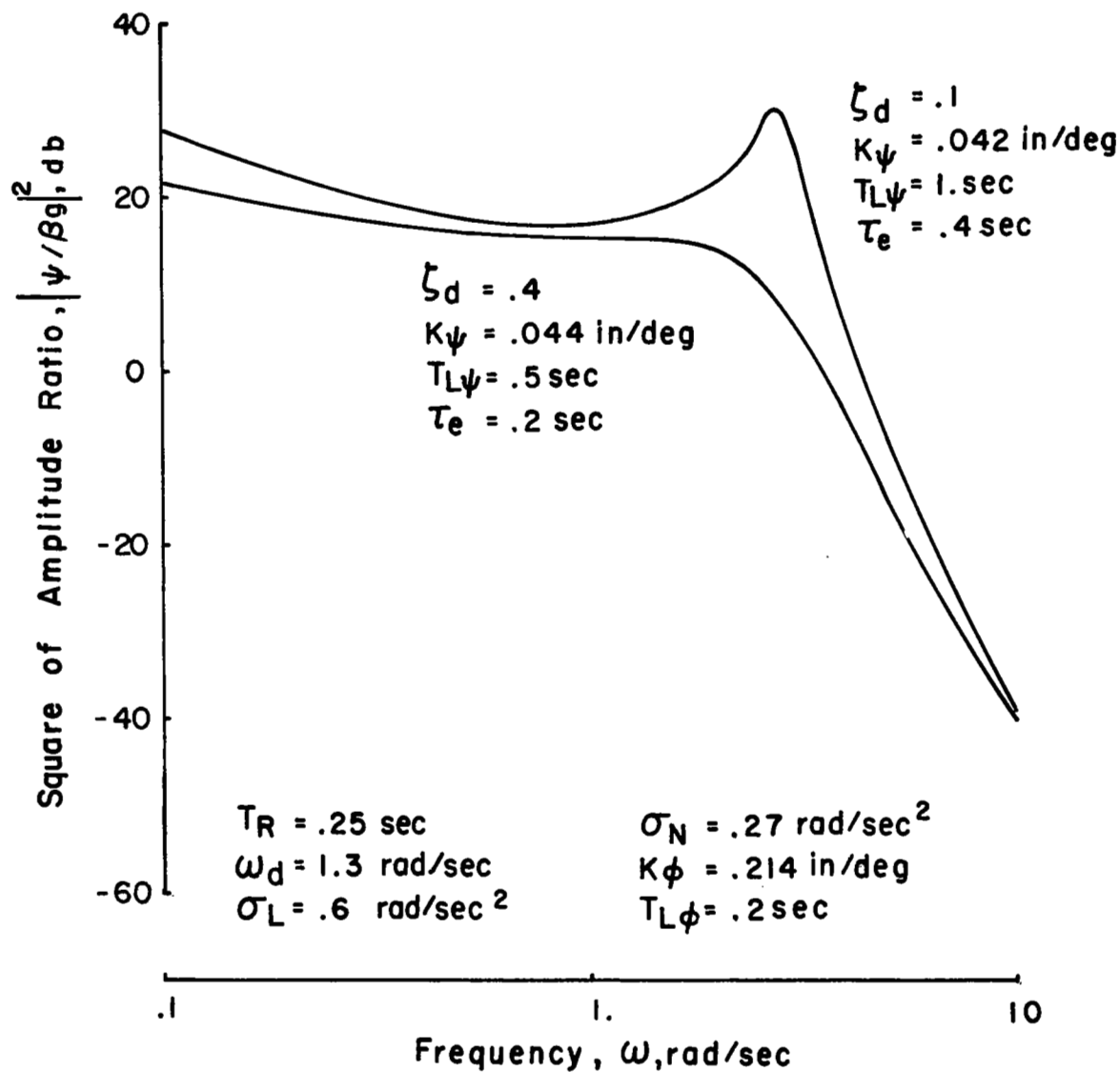
Figure 114. Closed Loop Heading Response to Lateral Gusts - Effect
of Dutch Roll Damping

$T_R = .25$ sec $\qquad \sigma_L = .6$ rad/sec^2
$\omega_d = 1.3$ rad/sec $\qquad V_o/L = 1.0$ rad/sec

$\bigcirc = \sigma_{\delta_{a_s}} (\sigma_\phi = 4^\circ)$
$\square = \sigma_\phi \ (K_\phi = .33$ in/deg$)$

$\sigma_N = .15$ rad/sec^2
$T_{L_\phi} = .2$ sec

$\bigcirc = \sigma_{\delta_{rp}} (\sigma_\psi = 2^\circ)$
$\square = \sigma_\psi \ (\sigma_{\delta_{rp}} = .34'')$

$\sigma_N = .27$ rad/sec^2
$T_{L_\phi} = .2$ sec
$T_{L_\psi} = .5$ sec
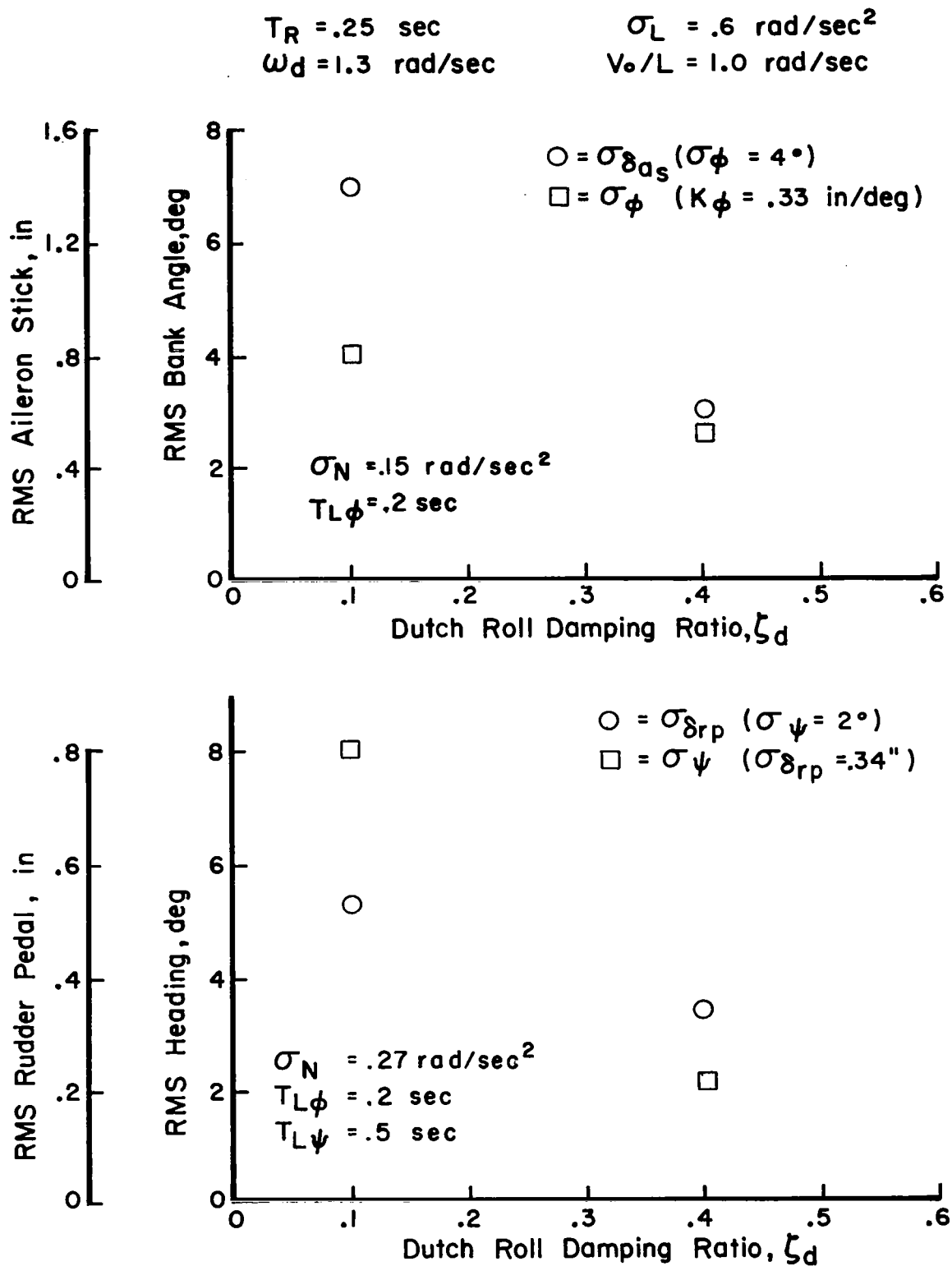
Figure 115. Effect of Dutch Roll Damping Ratio on Task Perform-
ance and Rudder Workload

241

Heading control is affected by aileron yaw due to the large yaw and sideslip excitation by aileron inputs. Under circumstances where the pilot is using ailerons vigorously to control bank angle excursions in turbulence, heading control becomes a more difficult task, or so it would seem. The lateral dynamics configuration for which aileron yaw might pose difficult problems is the low roll damping, low directional stability case. This configuration will be evaluated in the analysis to follow.

Considering the roll loop closure first, the adverse (-) aileron yaw configuration shown in Figure 116 has characteristics which are favorable and others which are undesirable. On the favorable side are the high bandwidth and good stability margins which are available. Dutch roll damping is also improved for the closed loop. An unfavorable aspect is that high gain closures will further reduce the frequency of the Dutch roll, making it more difficult to achieve satisfactory bandwidth in the subsequent heading loop closure.

Favorable (+) aileron yaw, under the circumstances shown in Figure 117, has little in its favor. Even for a substantial amount of lead, which otherwise would provide acceptable closed loop characteristics, the system is conditionally stable. The pilot is either faced with the choice of a low gain closure which would yield poor control over turbulence disturbances, or with having to work exceedingly hard in a high gain closure which at best leaves him with a very lightly damped Dutch roll and relatively large roll excitation by the ailerons. The fact that the closed loop Dutch roll has been increased in frequency over the open loop case is small consolation.

Heading loop closures for either adverse or favorable aileron yaw place considerable demands on the pilot. In the case of adverse yaw, Figure 118, the pilot is forced to generate a considerable amount of lead to reach bandwidths on the order of 3.0 radians/second. If an optimistic value of the

$T_R = .5$ sec
$\omega_d = 1.3$ rad/sec
$\zeta_d = .1$
$\dfrac{N_{\delta a}}{L_{\delta a}} = -.043$

$T_{L\phi} = .5$ sec

$j\omega$

σ

ζ

$\left| \dfrac{\phi}{\phi_q} \right|$

$\not\subset \dfrac{\phi}{\phi_q}$

Amplitude Ratio, $\left| \dfrac{\phi}{\phi_q} \right|$, db

Phase, deg

$K_\phi = .12$ in./deg
$T_{L\phi} = .5$ sec
$\tau_\theta = .2$ sec

Frequency, ω, rad/sec
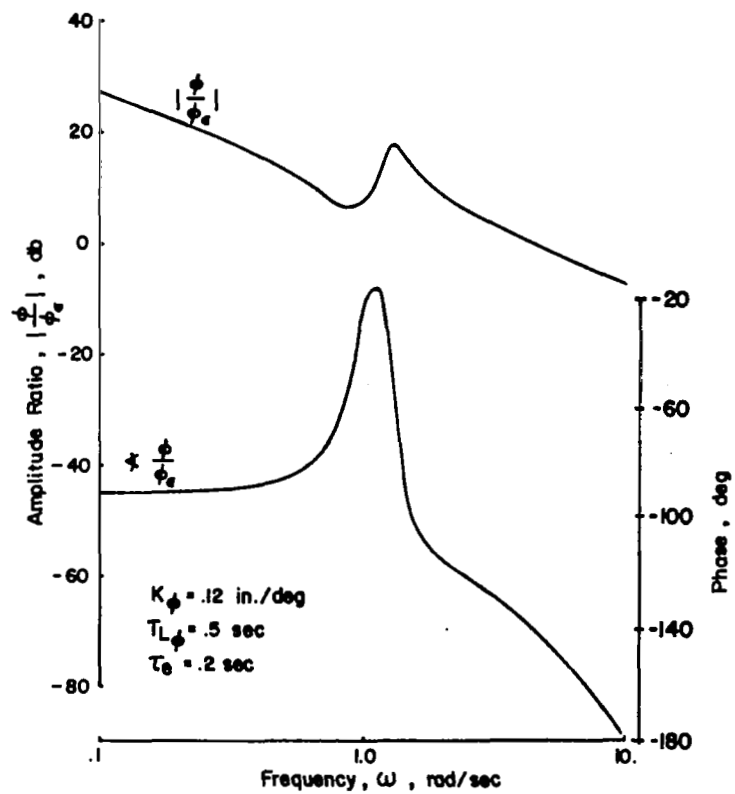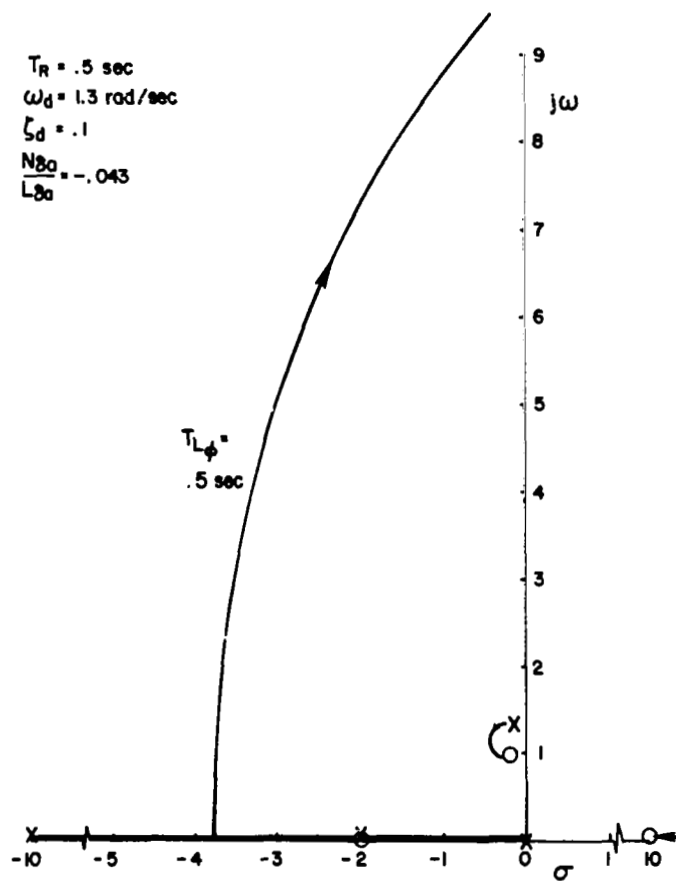
Figure 116. Bank Angle to Aileron Closure - Configuration 13
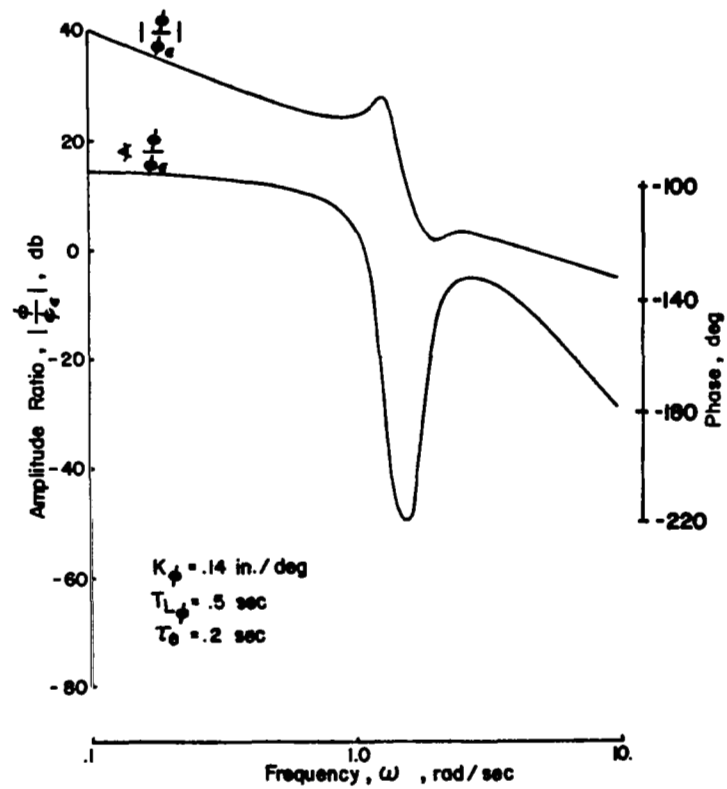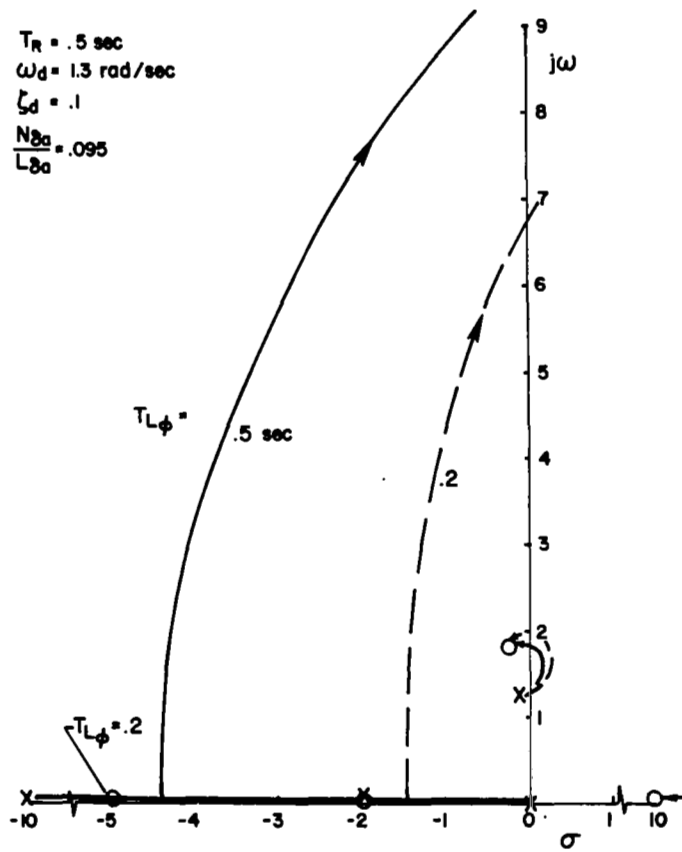
Figure 117.   Bank Angle to Aileron Closure - Configuration 14
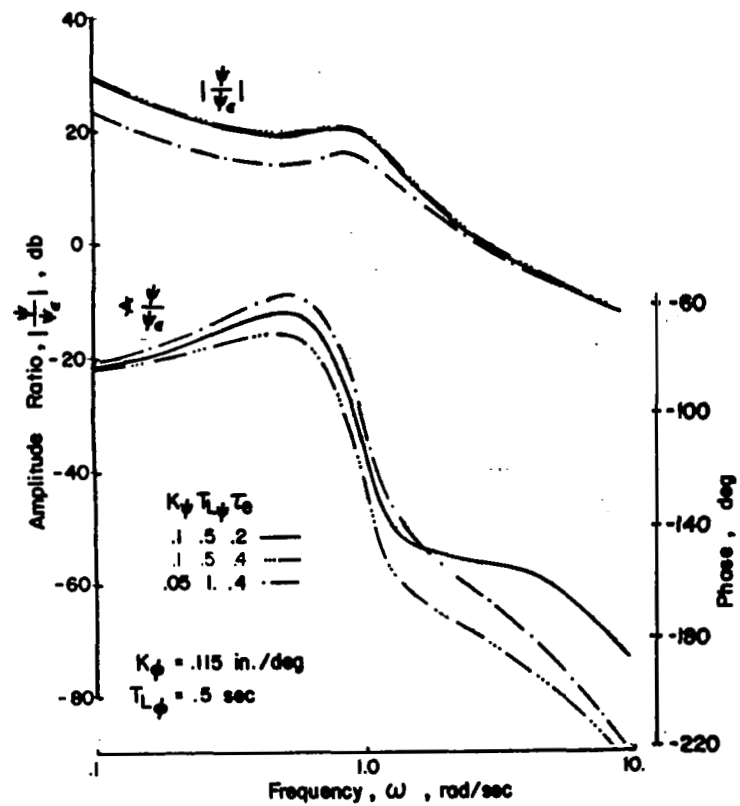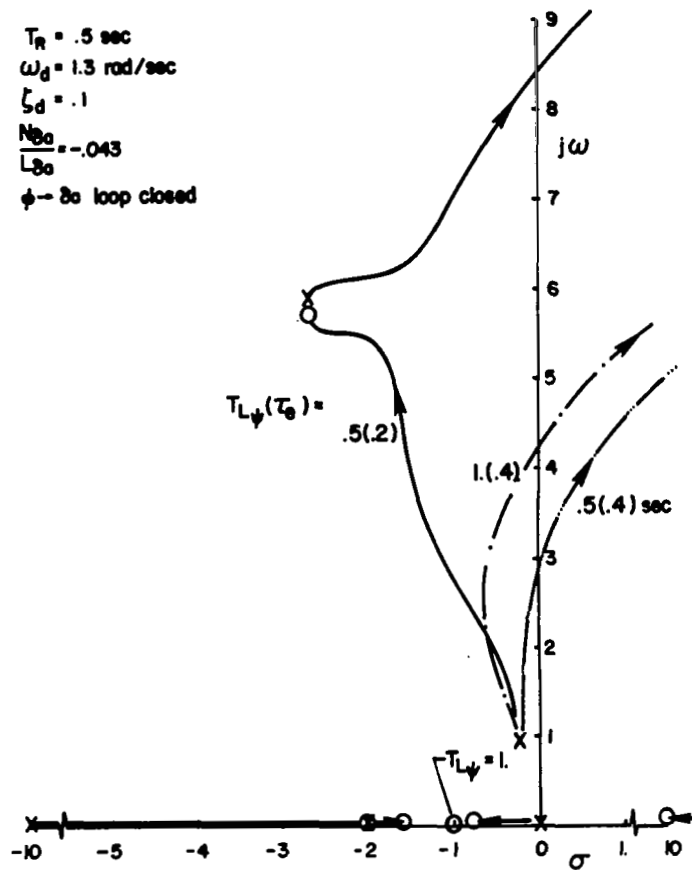
Figure 118. Heading to Rudder Closure - Configuration 13

pilot's time lag is assumed (τ_e = .2 seconds), a lead on the order of .5 seconds is sufficient to achieve the desired bandwidth with a phase margin of about 25 degrees. However, if a more conservative time lag is used (τ_e = .4 seconds), the lead time constant must be increased to at least 1.0 second to maintain the same closed loop characteristics.

For the favorable yaw configuration, Figure 119, large amounts of lead are required to provide satisfactory stability margins for bandwidths on the order of 3.0 radians/second. The obvious problem is the poorly damped Dutch roll resulting from the roll loop closure. The alternative of choosing a low gain roll loop closure would still be unsatisfactory, and an equally poorly damped Dutch roll at an even lower frequency would result from the roll loop closure and would likely produce lower bandwidths in the heading loop. It is obvious that, unless the pilot can generate a substantial amount of lead, this configuration will be difficult to control in both bank angle and heading. Pilot-airplane amplitude ratio data, based on pilot transfer function data obtained in flight, are shown in Figure 120 and indicate a crossover frequency of 3.5 radians/second. The data are well fitted with a pilot model corresponding to

$$K_\psi = .05 \text{ inches/degree}$$

$$T_{L\psi} = 1.0 \text{ second}$$

A comparison of the transfer function for heading to lateral gusts for three configurations having adverse, favorable, and neutral aileron yaw provides an indication of the effect aileron yaw has on heading control in turbulence. The state of turbulence most interesting in this particular analysis is the large roll disturbance case which would be expected to induce a high degree of aileron activity to control bank angle excursions. The three configurations are shown in Figure 121 for similar heading loop closures in order to make a comparative evaluation possible. The closed loop gain and lead compensation give the following bandwidths and phase margins for the three cases
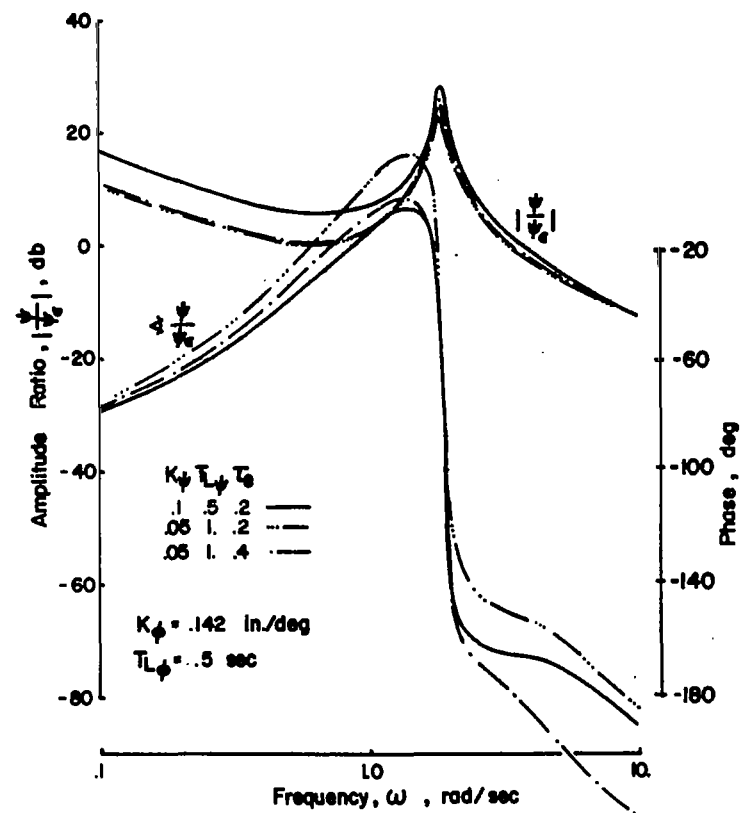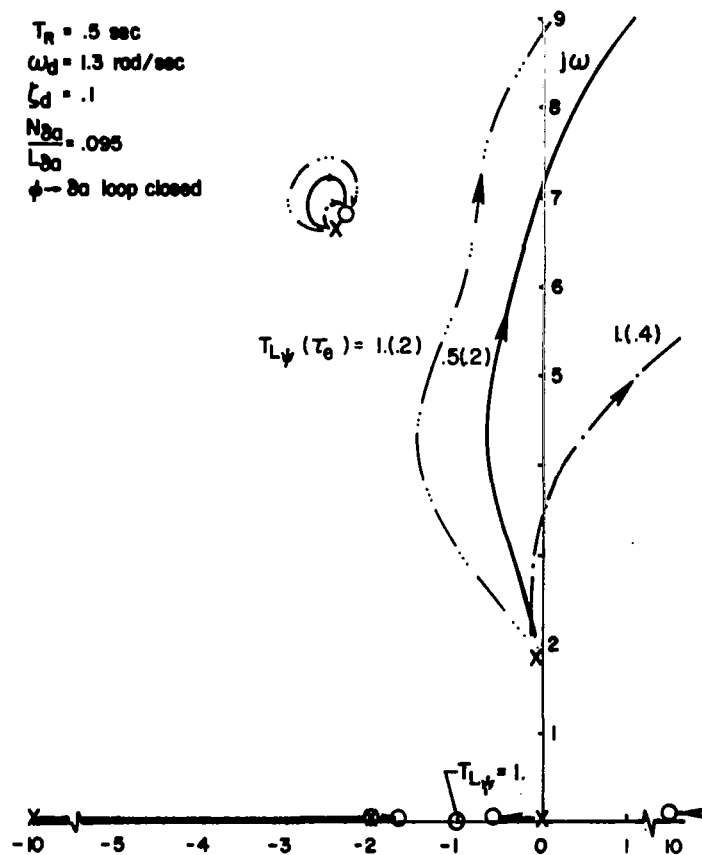
Figure 119. Heading to Rudder Closure - Configuration 14
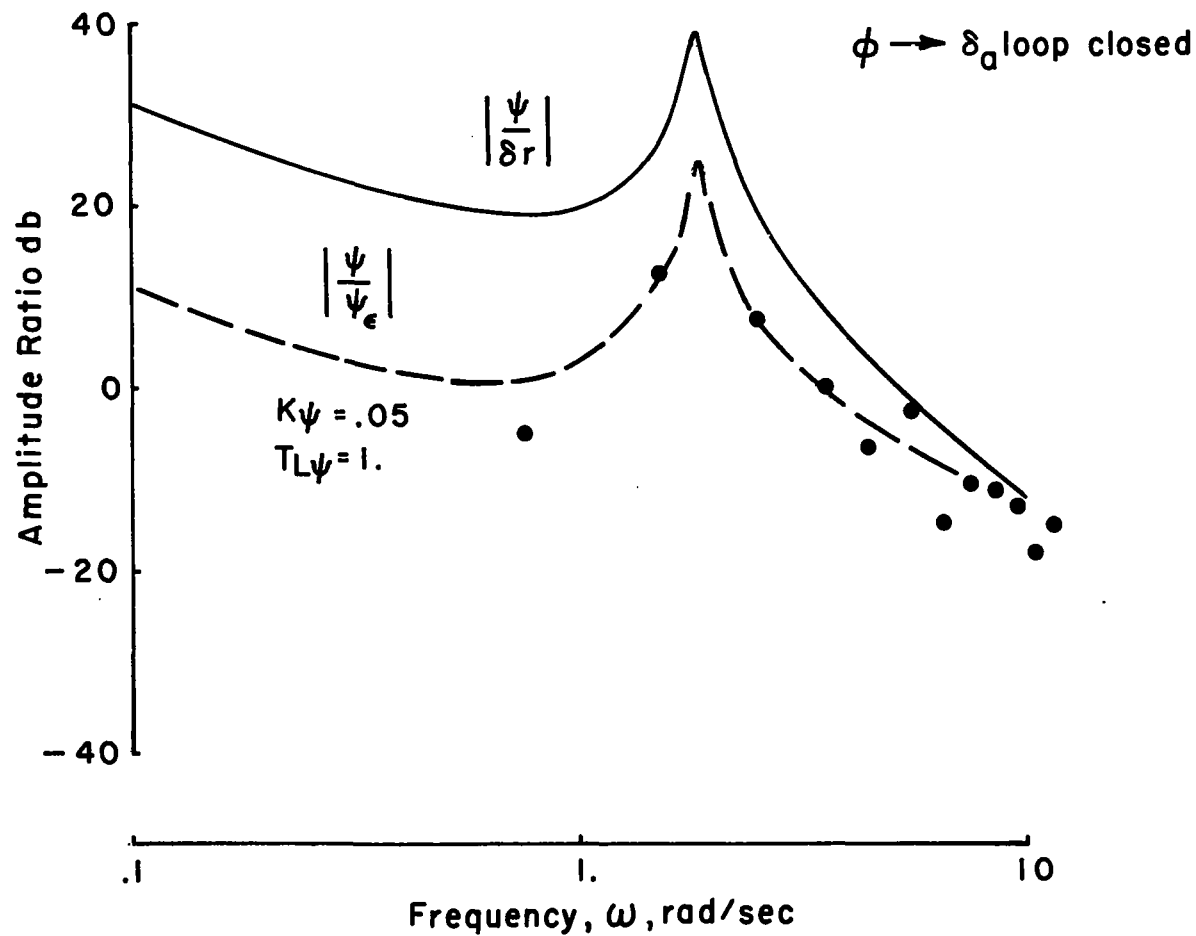
Figure 120. Flight Test Measured Pilot Compensation in Heading
Control with Rudder - Configuration 14

The figure shows a plot with the following labels and values:

Y-axis: Square of Amplitude Ratio, $|\psi/\beta_g|^2$, db, ranging from -60 to 40

X-axis: Frequency, ω, rad/sec, ranging from .1 to 10

Curve annotations:

$\begin{cases} N_{\delta_a}/L_{\delta_a} = .095 \\ \omega_\phi/\omega_d = 1.4 \\ \qquad K_\psi = .033 \text{ in/deg} \\ \qquad K_\phi = .142 \text{ in/deg} \end{cases}$

$\begin{cases} N_{\delta_a}/L_{\delta_a} = 0 \\ \omega_\phi/\omega_d = 1.0 \\ \qquad K_\psi = .042 \text{ in/deg} \\ \qquad K_\phi = .115 \text{ in/deg} \end{cases}$

$\begin{cases} N_{\delta_a}/L_{\delta_a} = -.043 \\ \omega_\phi/\omega_d = .76 \\ \qquad K_\psi = .042 \text{ in/deg} \\ \qquad K_\phi = .115 \text{ in/deg} \end{cases}$

$T_{L_\psi} = 1. \text{ sec}$
$\tau_e = .4 \text{ sec}$
$T_{L_\phi} = .5 \text{ sec}$

$T_R = .5 \text{ sec}$
$\omega_d = 1.3 \text{ rad/sec}$
$\zeta_d = .1$

$\sigma_L = 1.2 \text{ rad/sec}^2$
$\sigma_N = .15 \text{ rad/sec}^2$
$V_o/L = 1.0 \text{ rad/sec}$

Figure 121.   Closed Loop Heading Response to Lateral Gusts - Effect
of Aileron Yaw

$N_{\delta a}/L_{\delta a}$	ω_{co} radians/second	φ_m degrees
0	2.4	20
-.043	2.4	20
+.095	2.77	10

Increasing aileron yaw from neutral to adverse (-) has a fairly small effect on the energy over the frequency spectrum, at least for the increase in $N_{\delta a}/L_{\delta a}$ shown. The result is to reduce energy somewhat in the lower frequency region. Thus the net effect is likely to be a slight reduction in the level of heading excursions for the increase in adverse yaw. The underlying reason for this trend becomes apparent through a comparison of the Bode diagrams of the heading to rudder loop closure of Configurations 6 and 13 ($N_{\delta a}/L_{\delta a}$ = 0 and -.043 respectively) shown in Figures 93 and 118. Configuration 13 has a higher gain at low frequency than Configuration 6 when the two configurations have the same bandwidth. This increment in gain is sufficient to account for the reduction in heading response to lateral gusts.

Favorable yaw has an extremely degrading effect on heading response to lateral gusts. The poorly damped Dutch roll accounts for a significant part of the increase in heading excursions. An increase in gust energy transmission at lower frequencies is attributable to a reduction in low frequency gain, the converse of the situation described for adverse aileron yaw.

A trend study of aileron and rudder workload required for constant bank angle and heading performance is shown in Figure 122. The results are as anticipated from the previous closed loop analysis. Aileron activity (for only the roll loop closed) increased with aileron yaw in either the positive or
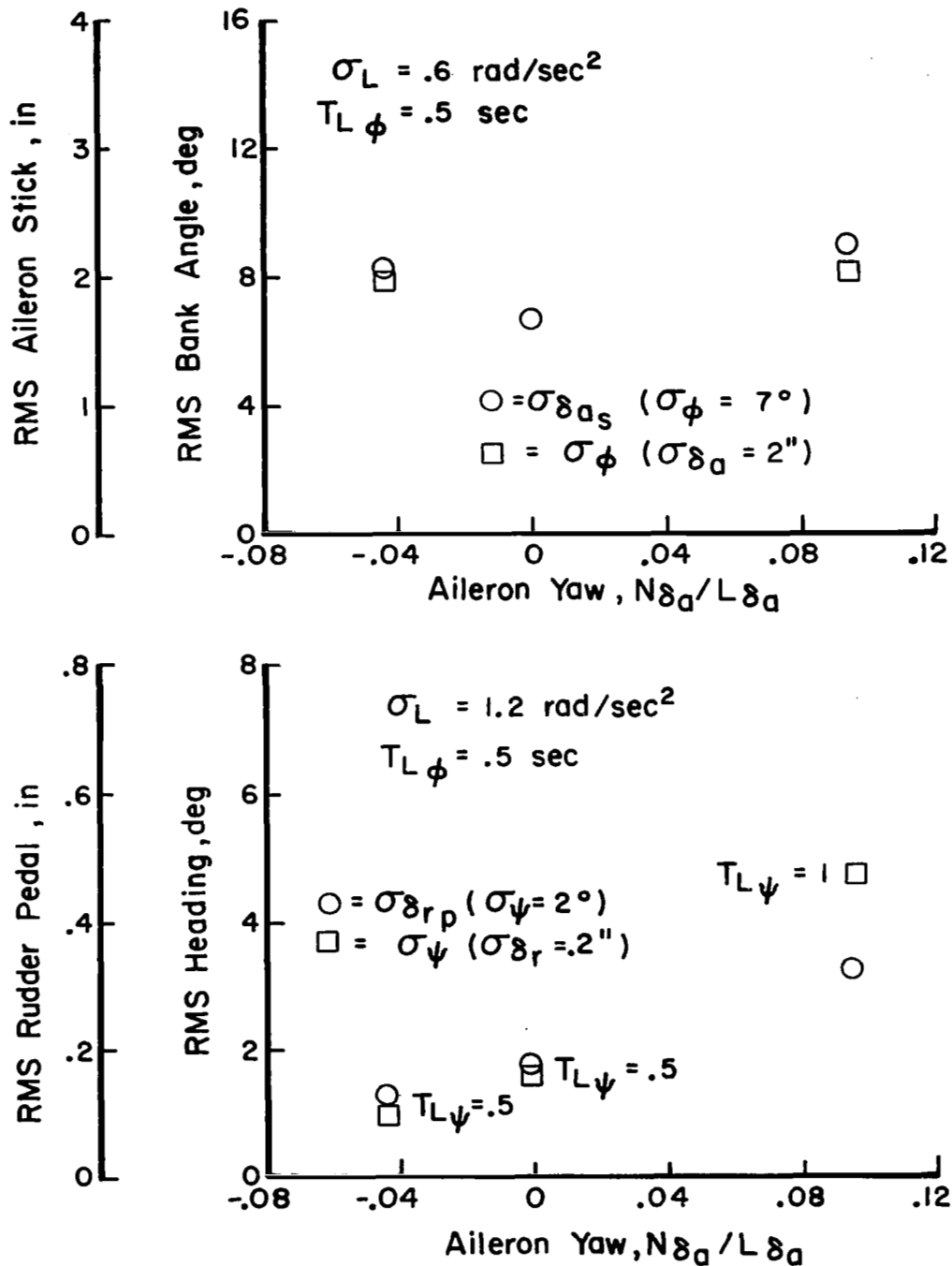
Figure 122. Effect of Aileron Yaw on Task Performance and Control Workload

negative sense. Rudder workload decreases slightly for adverse yaw and increases to a much greater extent for favorable yaw. The loop closures were made for the lead compensation noted and for an effective time lag of .2 seconds. The trends in rudder workload agree with the flight test data shown in Figure 65.

The effect of a crossfeed between the aileron and rudder may be considered to a first order approximation to be represented by a rudder-aileron interconnect. As such rudder deflection will tend to augment or attenuate aileron yaw characteristics. Therefore, the effects of a crossfeed may be evaluated in terms of the aileron yaw data previously presented.

In summary, the analytical study of aileron yaw conducted in this program indicates the most serious influence of aileron yaw to be the degraded closed loop bank angle and heading workload or performance for the case of favorable (+) aileron yaw. Low bandwidths and low stability margins are characteristic of this configuration. In contrast, large amounts of adverse (-) yaw could be tolerated and could even produce a slight improvement in closed loop heading performance. Analytical studies and flight test performance-workload data are in agreement in this matter. While the pilot rating data for this program do not unanimously confirm the undesirable influence of favorable yaw, taken as a whole the data seem to warrant the conclusion that favorable yaw does indeed degrade flying qualities for the heading control task. Results of another flight program conducted at Princeton to evaluate lateral-directional flying qualities for the ILS task serve to reinforce this conclusion. The spread in pilot rating data for large favorable yaw noted in both programs is attributed to the willingness and skill of the pilot in using rudder to control heading excursions due to lateral control activity. As indicated in the closed loop analysis it is absolutely necessary for the pilot to use rudder to achieve even remotely acceptable heading control for these configurations. It was also interesting to observe that when the pilots chose to use the rudder they did so independently of the ailerons rather than attempting to coordinate rudder with aileron inputs. Although the pilot might be

expected to coordinate rudder with ailerons in an instinctive manner to counteract aileron yaw, the best technique for control in turbulence appears to be the one used in this program. When the airplane is upset by a lateral gust, adverse aileron yaw resulting from aileron deflection to counteract the disturbance in roll actually helps to correct for the disturbance in the airplane's yaw attitude. Conventional coordination of the rudder with ailerons would counteract the beneficial effect of adverse yaw in this instance. For the case of favorable aileron yaw, coordination of rudder and aileron would indeed help to reduce yaw due to ailerons, which happen to be in a sense to increase the magnitude of yaw excursions as lateral control is used to counteract roll disturbances. However, coordination in this case demands a cross-control application of the rudder and ailerons which is unnatural for the pilot and which has received unfavorable commentary in a number of flight test programs as noted in Reference 32. The alternative technique is for the pilot to use the ailerons and rudder as separate controls as he perceives roll and yaw disturbances, and to avoid any use of the rudder in a coordinating sense.

SECTION 6

CONCLUSIONS

It is apparent from the results of this flight test program that the dominant influences on flying qualities associated with the heading control task are

- the precision of task performance, specifically rms heading excursions and to a lesser extent rms bank angle excursions,

- the control workload required of the pilot to achieve the desired task performance,

- the extent of compensation required of the pilot to overcome deficiences in the airplane's dynamics and to reduce his control workload.

The effects of turbulence disturbances and airplane dynamics on flying qualities may be explained in terms of these three factors.

The influences of turbulence and dynamics on the heading tracking task which have been identified in this program may be itemized as follows.

- The dominant influence of turbulence is the rms magnitude of aerodynamic disturbances. Yaw disturbances degrade the heading tracking task more than roll disturbances.

- Increasing turbulence bandwidth over the low to mid frequency range tested ($\frac{V_o}{L}$ = .314 to 1.0 radian/second) degrades flying qualities. This effect is of secondary importance compared to the influence of disturbance magnitude. Higher order attenuation of the disturbance spectra has no influence on flying qualities.

- Correlation between the roll and yaw disturbance components has no significant influence on the heading tracking task.

254

- Reducing roll damping adversely affects flying qualities in roll, to a greater extent when roll disturbances are large compared to the case when these disturbances are small.

- Changes in aerodynamic roll damping ($L_p = L_{p_g}$) have little influence for roll time constants between .2 and .5 seconds. Increases in aerodynamic roll damping corresponding to T_R less than .2 seconds degrades flying qualities in roll due to the increase in roll disturbance magnitude which accompanies the increase in L_p.

- Increased roll damping provided by a stability augmentation system using inertial sensing of roll rate improves flying qualities by effectively increasing roll damping without correspondingly increasing roll disturbances due to turbulence.

- Reducing directional stability degrades the heading tracking task to a more significant degree when yaw disturbances are large as compared to when these disturbances are small.

- Changes in aerodynamic directional stability ($N_\beta = N_{\beta_g}$) have little effect on the heading tracking task for Dutch roll frequencies between 1.3 and 3.0 radians/ second. Increases in aerodynamic directional stability corresponding to ω_d greater than 3.0 radians/ second degrades flying qualities in yaw due to the increase in yaw disturbance magnitude which accompany the increase in N_β.

- Increasing the Dutch roll damping ratio improves flying qualities for the lowest level of directional stability tested ($\omega_d = 1.3$ rad/ sec). No improvement with increased ζ_d occurs for the configuration having the highest directional stability tested ($\omega_d = 3.0$ rad/ sec).

- Favorable aileron yaw is detrimental to the heading tracking task, particularly for low directional stability and when roll disturbances due to turbulence are large.

• Control of heading excursions with the rudder is necessary if it is to be even possible to achieve acceptable precision in the heading control task. For this reason scatter in the pilot rating data for variations in aileron yaw is most likely due to the willingness and skill of the pilots in using the rudder. A larger sample of pilots is necessary to more conclusively define the influence of aileron yaw on flying qualities.

Analytical interrelationships between open loop turbulence response, closed loop control characteristics, and closed loop turbulence response have been defined which permit a tradeoff to be made between closed loop task performance and closed loop control workload. This tradeoff is influenced by

• the amplitude and frequency distribution of the open loop (uncontrolled) turbulence response

• the characteristics of the control loop closure(s) of interest, particularly as concerns bandwidth and stability margin at crossover, low frequency gain, and gain and compensation required of the pilot to achieve good closed loop characteristics.

Specific parameters can be identified which influence this tradeoff. Several of these parameters are noted on pages 155 through 175. Flight test measurements of the pilot's describing function indicate that

• the pilot performs in the heading-rudder loop in accordance with crossover model theory of Reference 38,

• crossover frequencies for $Y_A Y_p$ exceed the fixed base simulator data of Reference 38, apparently due to angular motion cues which permit the pilot to increase his lead compensation.

REFERENCES

1. Wilson, E. B., Report on Behavior of Aeroplanes in Gusts, NACA Report 1 Part II, 1915.

2. Seckel, E., Miller, G. E., and Nixon, W. B., Lateral Directional Flying Qualities for Power Approach, Princeton University Report No. 727, September 1966.

3. Seckel, E., Franklin, J. A., and Miller, G. E., Lateral Directional Flying Qualities for Power Approach: Influence of Dutch Roll Frequency, Princeton University Report No. 797, September 1967.

4. Mooij, H. A., Flight Evaluation of Direct Lift Control and Its Effects on Handling Qualities in Carrier Approach, Princeton University Report No. 811, December 1967.

5. Ellis, D. R. and Seckel, E., Flying Qualities of Small General Aviation Airplanes, Part 1. The Influence of Dutch-roll Frequency, Dutch-roll Damping, and Dihedral Effect, Princeton University Report No. 870, June 1969.

6. Hall, G. W. and Meeker, J. I., In Flight Evaluation of Lateral-Directional Handling Qualities for the Fighter Mission, AFFDL-TR-67-98, October 1967.

7. Harper, Robert P., Jr., In-Flight Simulation of the Lateral-Directional Handling Qualities of Entry Vehicles, WADD TR 61-147, November 1961.

8. McNeill, W. E. and Vomaske, R. F., A Flight Investigation to Determine the Lateral Oscillatory Damping Acceptable for an Airplane in the Landing Approach, NASA Memo 12-10-58A, February 1959.

9. McNeill, W. E. and Creer, B. Y., A Summary of Results Obtained During Flight Simulation of Several Aircraft Prototypes with Variable Stability Airplanes, NACA RM A56C08, May 1956.

10. Durand, T. S. and Jex, H. R., Handling Qualities in Single-Loop Roll Tracking Tasks: Theory and Simulator Experiments, ASD TDR 62-507, November 1962.

11. Graham, D. and McRuer, D., Analysis of Nonlinear Control Systems, Wiley, New York, 1961.

12. Hinze, J. O., Turbulence, McGraw-Hill, New York, 1959.

13 Karman, Th. von, "Progress in the Statistical Theory of Turbulence" Proceedings of the National Academy of Science, Vol. 34, No. 530, 1948.

14. Gault, J. D., Summary of Results from Phases I and II of LO-LOCAT, NASA Langley Research Center Meeting on Aircraft Response to Turbulence, September 24-25, 1968.

15. Press, H., Atmospheric Turbulence Environment with Special Reference to Continuous Turbulence, AGARD Report 115, April-May 1957.

16. Pritchard, F. E., A Statistical Model of Atmospheric Turbulence and a Review of the Assumptions Necessary for Its Use, AGARD Specialists' Meeting on Stability and Control, September 1966.

17. Crane, H. L. and Chilton, R. G., Measurements of Atmospheric Turbulence Over a Wide Range of Wavelength for One Meteorological Condition, NACA TN 3702, June 1956.

18. Lappe, W. O., Davidson, B., and Notess, C. B., Analysis of Atmospheric Turbulence Spectra Obtained from Concurrent Airplane and Tower Measurements, IAS Report No. 59-44, January 1959.

19. Henry, R. M., A Study of the Effects of Wind Speed, Lapse Rate, and Altitude on the Spectrum of Atmospheric Turbulence at Low Altitude, IAS Report No. 59-44, January 1959.

20. Crooks, W., High Altitude Clear Air Turbulence, AFFDL-TR-65-144, September 1965.

21. Burns, A. and Rider, C. K., Power Spectral Measurements of Clear Air Turbulence Associated with Jet Streams, ARC CP No. 940, September 1965.

22. Lumley, J. L. and Panofsky, H. A., The Structure of Atmospheric Turbulence, Wiley, New York, 1964.

23. Eggleston, J. M. and Phillips, W. H., The Lateral-Directional Response of Airplanes to Random Atmospheric Turbulence, NASA TR R-74, 1960.

24. Houbolt, J. C., Steiner, R., and Pratt, K. G., Dynamic Response of Airplanes to Atmospheric Turbulence Including Flight Data on Input and Response, NASA TR R-199, June 1964.

25. Diederich, F. W., The Response of an Airplane to Random Atmospheric Disturbances, NACA TN 3910, April 1957.

26. Diederich, F. W. and Drischler, J. A., Effect of Spanwise Variations in Gust Intensity on the Lift Due to Atmospheric Turbulence, NACA TN 3920, April 1957.

27. Eggleston, J. M. and Diederich, F. W., Theoretical Calculation of the Power Spectra of the Rolling and Yawing Moments on a Wing in Random Turbulence, NACA Report 1321, 1957.

28. Etkin, B., Theory of the Flight of Airplanes in Isotropic Turbulence - Review and Extension, AGARD Report 372, April 1961.

29. Heaslet, M. A. and Spreiter, J. R., Reciprocity Relations in Aerodynamics, NACA Report 1119, 1953.

30. Drischler, J. A., Calculation and Compilation of the Unsteady-Lift Functions for a Rigid Wing Subjected to Sinusoidal Gusts and to Sinusoidal Sinking Oscillations, NACA TN-3748, October 1956.

31. Burnham, J. and Lee, J. T., "Thunderstorm Turbulence and Its Relationship to Weather Radar Echoes," Journal of Aircraft, September-October 1969.

32. Ashkenas, I. L., A Study of Conventional Airplane Handling Qualities Requirements, Part II. Lateral-Directional Oscillatory Handling Qualities, AFFDL-TR-65-138, November 1965.

33. Hill, R. L., The Effect of the Spiral Mode on the Lateral-Directional Airplane in the Landing Approach, Senior Independent Project, Princeton University, May 1969.

34. Hall, G. W., An In-Flight Investigation of Lateral-Directional Dynamics for Cruising Flight, FAA ADS 69-13, December 1969.

35. Ellis, D. R., Flying Qualities of Small General Aviation Airplanes, Part 2. The Influence of Roll Damping, Roll Control Sensitivity, Dutch-roll Excitation, and Spiral Stability, Princeton University Report No. 896, 1970.

36. Cooper, G. E. and Harper, R. P., Jr., The Use of Pilot Rating in the Evaluation of Aircraft Handling Qualities, NASA TN D-5153, April 1969.

37. Shirley, R. S., Application of a Modified Fast Fourier Transform to Calculate Human Operator Describing Functions, NASA TM X-1762, March 1969.

38. McRuer, D. T., Graham, D., and Krendel, E. S., "Manual Control of Single-Loop Systems, Parts I and II," Journal of the Franklin Institute, Vol. 283, Nos. 1 and 2, January and February 1967.

39. Ashkenas, I. L., A Study of Conventional Airplane Handling Qualities Requirements, Part I. Roll Handling Qualities, AFFDL-TR-65-138, November 1965.

40. Chalk, C. R., et al, Background Information and User Guide for MIL-F-8785 B (ASG), "Military Specification - Flying Qualities of Piloted Airplanes," AFFDL-TR-69-72, August 1969.

41. Ashkenas, I. L. and McRuer, D. T., The Determination of Lateral Handling Quality Requirements from Airframe-Human Pilot System Studies, WADC TR 59-135, June 1959.

42. Craig, S. J., Campbell, A., Klein, R. H., and Walton, R., Analysis of VTOL Handling Quality Requirements, Part II. Lateral Hover and Lateral-Directional Control in Low Speed Flight, Systems Technology, Inc., TR-181-1, June 1969.

43. Anderson, R. A., A New Approach to the Specification and Evaluation of Flying Qualities, AFFDL-TR-69-120, November 1969.

44. Stapleford, R. L. and Peters, R. A., Experiments and a Model for Pilot Dynamics with Visual and Motion Inputs, NASA CR-1325, May 1969.

45. Shirley, R. S. and Young, L. R., "Motion Cues in Man-Vehicle Control," IEEE Transactions on Man-Machine Systems, Vol. MMS-9, No. 4, December 1968.

46. Etkin, B., "A Simple Method for the Analog Computation of the Mean-Square Response of Airplanes to Atmospheric Turbulence," Journal of the Aerospace Sciences, October 1961.

47. McRuer, D., Ashkenas, I., and Graham, D., Aircraft Dynamics and Automatic Control, Systems Technology, Inc., August 1968.

48. Anonymous, EAI TR-48 Analog Computer Reference Handbook, Electronics Associates, Inc., September 1967.

APPENDIX A

SPECTRAL COMPONENT REPRESENTATION OF GUST FIELD

It was noted in Section 3 that a shortcoming of the spectral component representation technique for predicting turbulence disturbances was its tendency toward error in the high frequency region of the spectrum. For the lateral-directional problem some disparities occur between the predictions of rolling moments due to vertical gusts and yawing moments due to lateral gusts as obtained from the modified strip theory technique and from the spectral component representation method. Predictions for L_{v_g} using the two methods are essentially identical. The following discussion identifies the differences between the L_{w_g} and N_{v_g} predictions.

Rolling Moment due to Vertical Gusts

The expression for $\Phi_{L_{w_g}}$ according to Equation 35 is

$$\Phi_{L_{w_g}}(\omega) = (\frac{\sigma_w}{V_o} L_p)^2 \frac{V_o}{\pi L} \Phi_{w_e}(\omega, \frac{V_o}{b}) \qquad (A1)$$

From Reference 28 the prediction of $\Phi_{L_{w_g}}$ by the spectral component representation is

$$\Phi_{L_{w_g}}(\omega) = (\frac{\sigma_w}{V_o} L_p)^2 \frac{V_o}{\pi L} \Phi_{ww}(\omega, \frac{V_o}{b}) \qquad (A2)$$

It is apparent that these two expressions are identical except for the spectral terms Φ_{w_e} and Φ_{ww}. The magnitude of the rolling moment is scaled proportional to the level of the roll damping derivative and the rms gust intensity in both expressions. A comparison of the two spectral terms is shown in Figure A1.
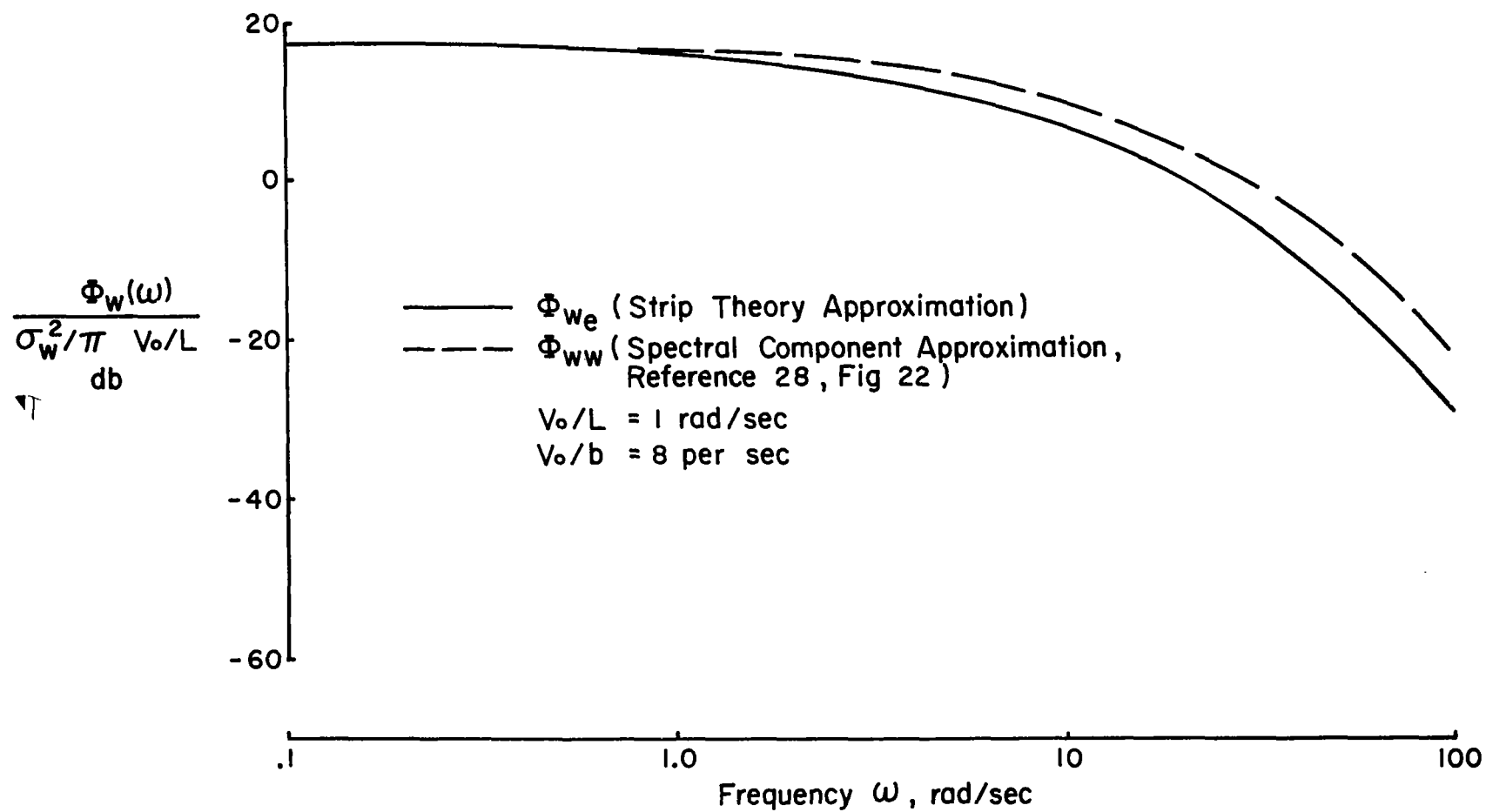
Figure A1.   Comparison of Strip Theory and Spectral Component
Prediction of the $\bar{\Phi}_w$ Spectrum

The spectrum Φ_{ww} shows higher energy levels in comparison to the strip theory prediction Φ_{w_e} with increasing frequency. As is evident from the results of this program the higher frequency components of the spectrum, particularly at lower energy levels, have little influence on flying qualities associated with the evaluation task. Consequently this difference between the two rolling moment spectra would be expected to have little significance to the evaluation of the flying qualities problem considered in this research.

Yawing Moment due to Lateral Gusts

It was noted in Section 3 that the yawing moment due to lateral gusts predicted by the spectral component technique is given by

$$N_{v_g} = N_\beta \frac{v_{g_{cg}}}{V_o} + N_r \left(\frac{\partial v_g}{\partial x}\right)_{cg} \tag{A3}$$

where the spatial gradient $\dfrac{\partial v_g}{\partial x}$ may be related to the time derivative $\dot{v}_g$ for a frozen gust field by

$$\frac{\partial v_g}{\partial x} = \frac{\partial v_g}{\partial t}\frac{\partial t}{\partial x} = \frac{\dot{v}_g}{V_o} \tag{A4}$$

The strip theory prediction of Section 3 which assumes the yawing moment disturbances to be contributed by the vertical tail may be written

$$N_{v_g} = N_{\beta_{VT}} \frac{v_g}{V_o}\left(t - \frac{\ell_v}{V_o}\right) \tag{A5}$$

Comparing the two expressions and assuming that the N_β and N_r terms of the spectral component representation also are contributed by the vertical tail,

$$N_{\beta_{VT}} \doteq -\ell_v\, Y_{\beta_{VT}} \tag{A6}$$

$$N_{r_{VT}} \doteq \frac{\ell_v^2}{V_o}\, Y_{\beta_{VT}} \tag{A7}$$

A3

gives the following result

$$N_{v_g} \doteq -\ell_v Y_{\beta_{VT}} \frac{v_{g_{cg}}}{V_o} + \frac{\ell_v^2}{V_o} Y_{\beta_{VT}} \frac{\dot{v}_{g_{cg}}}{V_o} \qquad \text{Spectral Component} \qquad (A8)$$

$$N_{v_g} \doteq -\ell_v Y_{\beta_{VT}} \frac{v_g}{V_o}(t - \frac{\ell_v}{V_o}) \qquad \text{Strip Theory} \qquad (A9)$$

Transforming into the frequency domain

$$N_{v_g} \doteq -\ell_v Y_{\beta_{VT}} \frac{v_g}{V_o}(s) + \frac{\ell_v^2}{V_o} Y_{\beta_{VT}} s \frac{v_g}{V_o}(s)$$

$$\doteq -\ell_v Y_{\beta_{VT}} \frac{v_g}{V_o}(s) \lceil 1 - \frac{\ell_v}{V_o} s \rceil \qquad (A10)$$

for the spectral representation, and

$$N_{v_g} \doteq -\ell_v Y_{\beta_{VT}} \frac{v_g}{V_o}(s) \, e^{-\frac{\ell_v}{V_o} s}$$

$$\doteq -\ell_v Y_{\beta_{VT}} \frac{v_g}{V_o}(s) \left(\frac{1 - \frac{\ell_v}{2V_o} s}{1 + \frac{\ell_v}{2V_o} s} \right) \qquad (A11)$$

for the strip theory approximation, using a first order Padé representation

for the transport lag $e^{-\frac{\ell_v}{V_o} s}$.

A comparative plot of the transfer function $(\frac{N_{v_g}}{\beta_g})$ for the two approximations is shown in Figure A2. A divergence between the two cases appears at high frequency. The spectral component representation shows a
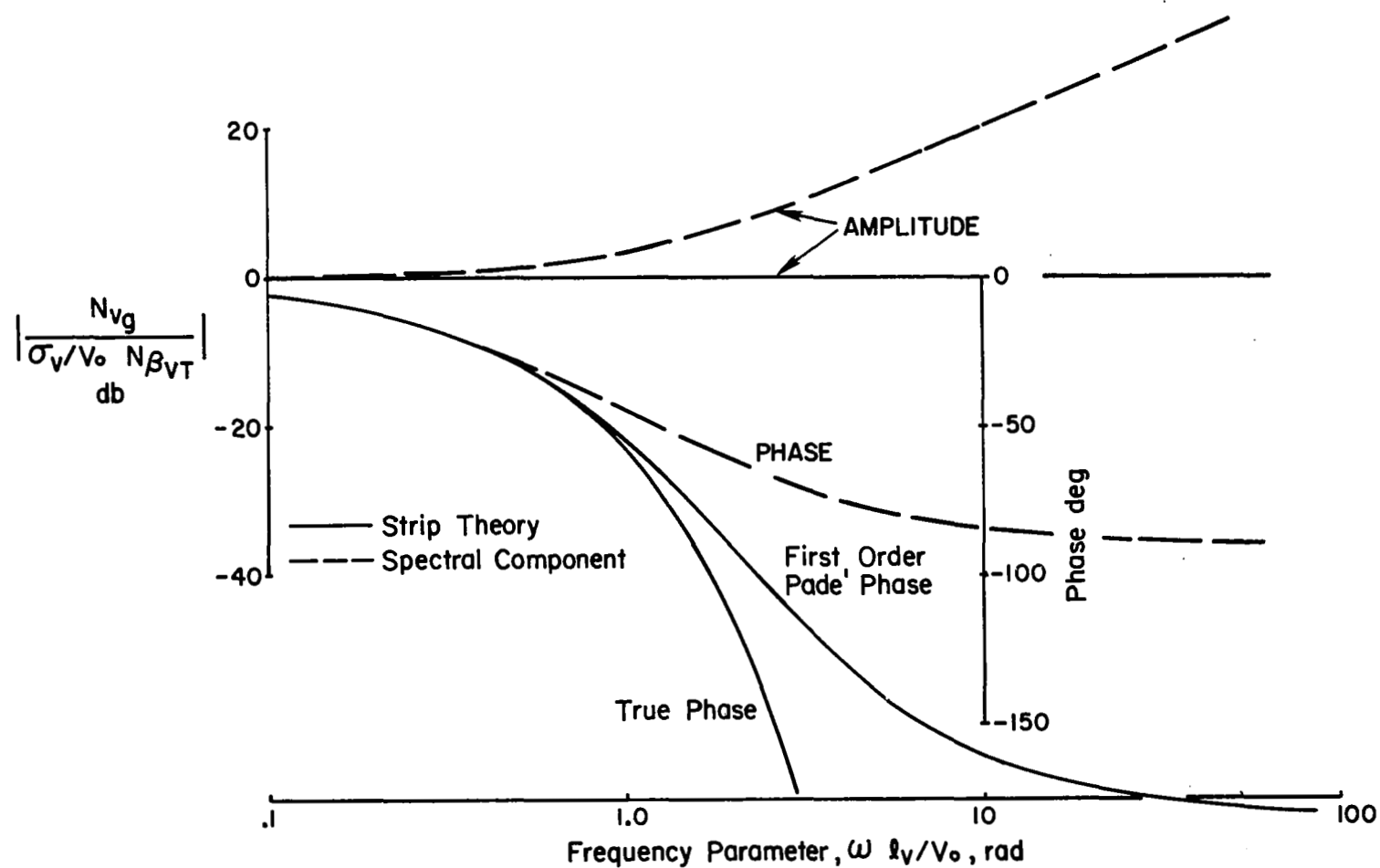
Figure A2. Comparison of Strip Theory and Spectral Component
Approximation of Yawing Moment Due to Lateral Gusts

higher energy level and smaller phase lag at high frequency than for the strip theory case. The difference between the two techniques is due to the overestimation of the gust intensity at the vertical tail by the spectral technique based on the linear gradient of the gust field at the airplane's c.g. The strip theory approximation uses the exact gust velocity combined with a transport lag to account for the time required for the gust to traverse from the wing to the tail. While no error is noted in the amplitude representation for this case, the Padé approximation of the time lag does cause a discrepancy in phase at high frequency.

The assumption that the entire yawing moment contribution comes from the tail should be the source of no appreciable error. The amplitude error which results from disregarding contributions of the fuselage and wing can be expected to be of such a low level to be inconsequential to the piloting problem. The phase error introduced by this approximation appears to be unimportant to the pilot. The yawing disturbances are observed by the pilot as a random process and the phase characteristics which arise because the airplane encounters a particular gust progressively rather than instantaneously are lost to the pilot who sees only a continuous random disturbance.

Differences which exist at higher frequencies between the strip theory and spectral component representations of the yawing moment disturbances are not likely to be important to the simulation for flying qualities evaluations. Neither the phase or amplitude error should be particularly apparent to the pilot at these higher frequencies. However, if it is desired to correct the amplitude and phase of the spectral component representation, the yaw disturbance simulation of this method may be attenuated at high frequency by a low pass filter

$$\left(\frac{1}{Ts + 1}\right)$$

where the filter time constant as suggested by equation (A11) is

$$T = \frac{\ell_v}{V_o}.$$

A6

APPENDIX B

DEFINITION OF TURBULENCE PARAMETERS

Based on equations 77 and 78 of Section 4 which define the power spectral densities of the airplane's bank angle and heading response to turbulence, the various contributions of turbulence may be identified. The individual spectral terms associated with turbulence which may be singled out are

- the rolling moment spectra due to vertical and lateral gusts,

$\Phi_{L_{w_g}}$ and $\Phi_{L_{v_g}}$

- the yawing moment spectra due to lateral gusts, $\Phi_{N_{v_g}}$

- the cross spectral density of rolling and yawing moments,

$\Phi_{L_{v_g} N_{v_g}}$.

These spectral densities may be characterized by their rms energy content and the distribution of this energy as a function of frequency. From this point of view, the turbulence contributions may be characterized by

- rolling moment due to vertical gusts - $\sigma_{L_{w_g}}$, ω_{w_1}, ω_{w_2}

- rolling moment due to lateral gusts - $\sigma_{L_{v_g}}$, ω_{v_1}

- yawing moment due to lateral gusts - $\sigma_{N_{v_g}}$, ω_{v_1}

- cross correlation of rolling and yawing moments - ρ_{LN}.

The derivation of the rms rolling and yawing moments is based on the integral over all positive frequencies of the power spectral density

$$\sigma^2 = \int_0^\infty \Phi(\omega)\, d\omega \qquad (B1)$$

The expressions for the various rms rolling and yawing moment disturbances are

● rolling moment due to vertical gusts

$$\sigma^2_{L_{w_g}} = \int_o^\infty \Phi_{L_{w_g}}(\omega)\,d\omega \tag{B2}$$

or, based on equation (54)

$$\sigma^2_{L_{w_g}} = \int_o^\infty \frac{\Phi_{L_{w_g}}(0)}{(T_{w_1}^2\omega^2 + 1)(T_{w_2}^2\omega^2 + 1)}\,d\omega$$

$$= \frac{\frac{\pi}{2}\Phi_{L_{w_g}}(0)}{(T_{w_1} + T_{w_2})} \tag{B3}$$

where

$$\Phi_{L_{w_g}}(0) \doteq 9\left(\frac{\sigma_w}{V_o}L_p\right)^2\frac{V_o}{\pi L}$$

$$\frac{1}{T_{w_1}} = \omega_{w_1} = .35\left(\frac{V_o}{b}\right)^{3/4}\left(\frac{V_o}{c}\right)^{1/4}$$

$$\frac{1}{T_{w_2}} = \omega_{w_2} = 5.7\left(\frac{V_o}{b}\right)^{3/4}\left(\frac{V_o}{c}\right)^{1/4}$$

Since $T_{w_1} \gg T_{w_2}$, $\sigma^2_{L_{w_g}}$ may be approximated by

$$\sigma^2_{L_{w_g}} \doteq \frac{\frac{\pi}{2}\Phi_{L_{w_g}}(0)}{T_{w_1}}$$

$$\doteq 1.57\left(\frac{\sigma_w}{V_o}L_p\right)^2\frac{V_o}{L}\left(\frac{V_o}{b}\right)^{3/4}\left(\frac{V_o}{c}\right)^{1/4} \tag{B4}$$

- rolling moment due to lateral gusts

$$\sigma^2_{L_{v_g}} = \int_o^\infty \frac{\Phi_{L_{v_g}}(0)}{(T_{v_1}^2 \omega^2 + 1)} \, d\omega \qquad \text{(B5)}$$

where

$$\Phi_{L_{v_g}}(0) = (\frac{\sigma_v}{V_o} L_\beta)^2 \frac{L}{\pi V_o}$$

$$T_{v_1} = \frac{L}{\sqrt{3} \, V_o}$$

Thus $\sigma^2_{L_{v_g}}$ becomes

$$\sigma^2_{L_{v_g}} = \frac{\pi}{2} \frac{\Phi_{L_{v_g}}(0)}{T_{v_1}}$$

$$= \frac{\sqrt{3}}{2} (\frac{\sigma_v}{V_o} L_\beta)^2 \qquad \text{(B6)}$$

- yawing moment due to lateral gusts

$$\sigma^2_{N_{v_g}} = \int_o^\infty \frac{\Phi_{N_{v_g}}(0)}{(T_{v_1}^2 \omega^2 + 1)} \, d\omega \qquad \text{(B7)}$$

where

$$\Phi_{N_{v_g}}(0) = (\frac{\sigma_v}{V_o} N_{\beta_{VT}})^2 \frac{L}{\pi V_o}$$

$$T_{v_1} = \frac{L}{\sqrt{3} \, V_o}$$

B3

which gives a result for yawing moment similar to the rolling moment for lateral gusts

$$\sigma^2_{N_{v_g}} = \frac{\pi}{2} \frac{\Phi_{N_{v_g}}(0)}{T_{v_1}}$$

$$= \frac{\sqrt{3}}{2} \left(\frac{\sigma_v}{V_o} N_{\beta_{VT}}\right)^2 \tag{B8}$$

The normalized cross correlation function ρ_{LN} may be defined by

$$\rho_{LN} = \frac{R_{LN}(0)}{\sigma_L \sigma_N} \tag{B9}$$

where $R_{LN}(0)$ is the cross correlation between rolling and yawing moments for zero time lag.

Since there is no correlation between lateral and vertical turbulence components, the only contribution to the cross correlation comes from rolling and yawing moments due to vertical gusts. Recalling that these rolling and yawing moments may be expressed

$$L_{v_g}(t) = L_\beta \frac{v_g(t)}{V_o} \tag{B10}$$

$$N_{v_g}(t) = N_{\beta_{VT}} \frac{v_g}{V_o}\left(t - \frac{\ell_v}{V_o}\right) \tag{B11}$$

the cross correlation between them becomes

$$R_{LN}(\tau) = \frac{L_\beta N_{\beta_{VT}}}{V_o{}^2} R_{vv}\left(\tau - \frac{\ell_v}{V_o}\right) \tag{B12}$$

The turbulence correlation function R_{vv} is normally expressed in terms of a spatial rather than a time variable. Thus for the time-spatial equivalence $(x-x_o) = V_o (t-t_o)$

$$R_{vv} (r) = R_{vv} [V_o (\tau - \frac{\ell_v}{V_o})]$$ (B13)

For $\tau = 0$

$$R_{vv} (r_o) = R_{vv} (-\ell_v)$$

The correlation function corresponding to the spectral function for lateral gusts

$$\Phi_{vv} (\omega) = \frac{\sigma^2_v \frac{L}{\pi V_o}}{(\frac{\omega L}{3V_o})^2 + 1}$$ (B14)

is

$$R_{vv} (r) = \frac{\sqrt{3}}{2} \sigma^2_v e^{-\sqrt{3} \frac{r}{L}}$$ (B15)

and for the case at hand

$$R_{vv} (\ell_v) = \frac{\sqrt{3}}{2} \sigma^2_v e^{-\sqrt{3} \frac{\ell_v}{L}}$$ (B16)

Collecting the results of (B4), (B6), (B8), (B12), and (B16), for the normalized cross correlation function gives

B5

$$\rho_{LN} = \frac{\frac{\sqrt{3}}{2} (\frac{\sigma_v}{V_o})^2 \; L_\beta \; N_{\beta_{VT}} \; e^{-\sqrt{3}\frac{\ell_v}{L}}}{\sigma_{N_{v_g}} \sqrt{\sigma_{L_{w_g}}^2 + \sigma_{L_{v_g}}^2}}$$

$$= \frac{e^{-\sqrt{3}\frac{\ell_v}{L}}}{\sqrt{(\frac{\sigma_{L_w}}{\sigma_{L_v}})^2 + 1}} \qquad\qquad (B17)$$

APPENDIX C

ANALOG COMPUTER SIMULATION

An analog computer simulation of the closed loop pilot-airplane system was performed to study the trends of rms task performance and control workload as a function of turbulence parameters and airplane dynamics. Use was made of a transient analog representation of the turbulence disturbances in order to substantially reduce the time involved in obtaining the rms measurement of turbulence response.

References 46 and 47 point out that the mean square response of a system excited by a random input is equivalent to the integral of the square of the transient response of the system to a properly scaled and filtered impulse function. This equivalence holds if the energy spectral density of the transient response is identical to one-half the power spectral density of the response to the random input. For the turbulence response problem described by equation (4) of Section 1, the power spectral density of the tracking error is

$$\Phi_{\epsilon\epsilon}(\omega) = \left| \frac{Y_G}{1 + Y_A Y_p} \right|^2 \Phi_{ff}(\omega) \tag{C1}$$

while the energy spectral density of the error to some transient input f_t is

$$\epsilon_t(j\omega)\,\epsilon_t(-j\omega) = \left| \frac{Y_G}{1 + Y_A Y_p} \right|^2 f_t(j\omega)\,f_t(-j\omega) \tag{C2}$$

For the equivalent relationship between the integral square of the transient response and the mean square of the random input response to hold

$$\epsilon_t(j\omega)\,\epsilon_t(-j\omega) = \frac{1}{2}\,\Phi_{\epsilon\epsilon}(\omega) \tag{C3}$$

Since the tracking error in control theory terms represents the response of a linear filter (the closed loop pilot-airplane system) to an input $f(t)$, the random input f (the turbulence disturbances) and its transient analog f_t must be related by

$$f_t(j\omega) \, f_t(-j\omega) = \frac{1}{2} \, \Phi_{ff}(\omega) \tag{C4}$$

Reference 46 discusses the representation of the turbulence disturbance input by an equivalent transient input. It is noted that a decaying exponential function of the form

$$f_t = a_t \, e^{-\lambda t} \tag{C5}$$

will satisfy the requirements of equation (C4). Since

$$f_t(j\omega) \, f_t(-j\omega) = \frac{a_t^2}{\omega^2 + \lambda^2} \tag{C6}$$

and for a turbulence spectrum of the form

$$\Phi_{ff}(\omega) = \frac{\Phi_{ff}(0)}{(\frac{L}{\sqrt{3} \, V_o})^2 \, \omega^2 + 1} \tag{C7}$$

the terms a_t^2 and λ of the transient analog are defined as follows to satisfy equation (C4)

$$\lambda = \sqrt{3} \, \frac{V_o}{L} \tag{C8}$$

$$a_t^2 = \frac{1}{2} \, \lambda^2 \Phi_{ff}(0)$$

$$= \frac{3}{2} \, (\frac{V_o}{L})^2 \, \Phi_{ff}(0) \tag{C9}$$

C2

The actual pilot-airplane system to be simulated was shown in Figure 25. The so-called linear filter of the preceding equations, denoted by $\dfrac{Y_G}{1 + Y_A Y_p}$, corresponds to the pilot-airplane combination with rudder and aileron loops closed and with a particular turbulence transfer function. Both rolling and yawing moment disturbances are provided in the simulation. For the approximations to the roll and yaw disturbances noted in equations (68), (73), and (75) the following definitions of a_t and λ are made.

$\dfrac{L_{w_g}}{}$

$$\Phi_{L_{w_g}}(\omega) = \frac{\Phi_{L_{w_g}}(0)}{(T_{w_1}^2 \omega^2 + 1)(T_{w_2}^2 \omega^2 + 1)}$$

$$\lambda = \frac{1}{T_{w_1}} \qquad \text{(the higher frequency attenuation associated with } T_{w_2} \text{ is disregarded)} \qquad \text{(C9)}$$

$$a_{L_w} = \frac{3}{T_{w_1}} \frac{\sigma_w}{V_o} L_p \sqrt{\frac{V_o}{L}} \qquad \text{(C10)}$$

$\dfrac{L_{v_g}}{}$

$$\Phi_{L_{v_g}}(\omega) = \frac{\Phi_{L_{v_g}}(0)}{T_{v_1}^2 \omega^2 + 1}$$

$$\lambda = \frac{1}{T_{v_1}} = \sqrt{3} \frac{V_o}{L} \qquad \text{(C11)}$$

$$a_{L_v} = \frac{\sigma_v}{V_o} L_\beta \sqrt{3 \frac{V_o}{L}} \qquad \text{(C12)}$$

$$\frac{N_{v_g}}{}$$

$$\Phi_{N_{v_g}}(\omega) = \frac{\Phi_{N_{v_g}}(0)}{T_{v_1}^2 \omega^2 + 1}$$

$$\lambda = \sqrt{3} \; \frac{V_o}{L} \tag{C13}$$

$$a_{N_v} = \frac{\sigma_v}{V_o} N_\beta \sqrt{3 \frac{V_o}{L}} \tag{C14}$$

To account for the cross-spectral relationship between the roll and yaw disturbances, Φ_{LN}, the transient input corresponding to the yaw disturbance is made to lag the roll disturbance input by a time increment equal to $\frac{\ell_v}{V_o}$ seconds. The validity of this technique may be demonstrated by defining the power spectral density and energy spectral density of the tracking error ϵ. The power spectral density $\Phi_{\epsilon\epsilon}$ has been presented previously in equation (85), Section 3 as

$$\Phi_{\epsilon\epsilon}(\omega) = \left|\frac{N_L^\epsilon}{\Delta'}\right|^2 \Phi_L(\omega) + \left|\frac{N_N^\epsilon}{\Delta'}\right|^2 \Phi_N(\omega)$$

$$+ 2 R_e \left[\frac{N_L^\epsilon}{\Delta'}\right] \left[\frac{N_N^\epsilon}{\Delta'}\right]^* \Phi_{LN}(j\omega) \tag{C15}$$

Following the procedure of Reference 47, pp 10-57 to 10-59 which utilizes the Laplace transform of the system's transient response and the final value theorem to define the energy spectral density, produces the result

$$\epsilon(j\omega)\,\epsilon(-j\omega) = \left|\frac{N_L^\epsilon}{\Delta'}\right|^2 L(j\omega)\,L(-j\omega) + \left|\frac{N_N^\epsilon}{\Delta'}\right|^2 N(j\omega)\,N(-j\omega)$$

$$+ 2R_e \left[\frac{N_L^\epsilon}{\Delta'}\right] \left[\frac{N_N^\epsilon}{\Delta'}\right] * L(j\omega)\,N(-j\omega) \tag{C16}$$

Hence, to satisfy the requirement that

$$\epsilon(j\omega)\,\epsilon(-j\omega) = \frac{1}{2}\,\Phi_{\epsilon\epsilon}(\omega)$$

it is necessary that

$$L(j\omega)\,L(-j\omega) = \frac{1}{2}\,\Phi_L(\omega) \tag{C17}$$

$$N(j\omega)\,N(-j\omega) = \frac{1}{2}\,\Phi_N(\omega) \tag{C18}$$

$$L(j\omega)\,N(-j\omega) = \frac{1}{2}\,\Phi_{LN}(\omega) \tag{C19}$$

The transient analogs for pure rolling and yawing disturbances have already been treated. The cross-spectral density of roll and yaw disturbances is

$$\Phi_{LN}(\omega) = 2\left(\frac{\sigma_v}{V_o}\right)^2 L_\beta N_\beta \frac{L}{V_o}\left(\frac{1}{T_{v_1}^2\omega^2+1}\right)e^{-j\omega\frac{\ell_v}{V_o}} \tag{C20}$$

If the transient analogs for roll and yaw are

$$L_{v_t}(t) = a_{L_v}\,e^{-\lambda t} \tag{C21}$$

$$N_{v_t}(t) = a_{N_v}\,e^{-\lambda\left(t-\frac{\ell_v}{V_o}\right)} \tag{C22}$$

C5

then the energy cross-spectral density for L and N is

$$L_v(j\omega) N_v(-j\omega) = (\frac{\sigma_v}{V_o})^2 L_\beta N_\beta \frac{L}{V_o} (\frac{1}{T_{v_1}^2 \omega^2 + 1}) e^{-j\omega \frac{\ell_v}{V_o}} \tag{C23}$$

and the relationship between Φ_{LN} and $L(j\omega) N(-j\omega)$ is satisfied.

A diagram of the analog computer program is shown in Figure C1. The computer used was an Electronics Associates, Inc. model TR-48 shown in Figure 34 of Section 4. Wiring diagrams for the open loop airplane, pilot model and the turbulence transient analog are presented. The pilot model utilizes a time delay represented by a first order Padé approximation. The time delay of the yaw disturbance transient analog is provided by an electronic comparator whose function is described in Reference 48. Integral square readouts of any response variable of interest are provided. Potentiometer settings are listed in Table C1.

Lateral - Directional Airplane

Figure C1.   Analog Computer Diagram

Figure C1. Continued

TABLE C1

ANALOG COMPUTER POTENTIOMETER SETTINGS

Pot	Parameter	Scaling	Pot	Parameter	Scaling
1	Y_{v_g}	Y_{v_g}	17	K_φ	K_φ
2	$Y^*_{\delta r}$	$Y^*_{\delta r}$	18	$K_{\dot\varphi}$	$10\,K_{\dot\varphi}$
3	Y_v	Y_v	19	K_{ψ_a}	K_{ψ_a}
4	g/V_o	g/V_o	20	$K_{\dot\psi_a}$	$10\,K_{\dot\psi_a}$
5	L_{β_g}, L_{P_g}	$.01\,L_{\beta_g}$ $.01\,L_{P_g}$	21	K_{ψ_r}	K_{ψ_r}
6	L_{δ_a}	$.01\,L_{\delta_a}$	22	$K_{\dot\psi_r}$	$10\,K_{\dot\psi_r}$
7	L_{δ_r}	$.1\,L_{\delta_r}$	23	$\Big\}\ 2/\tau_{e_a}$	$.2/\tau_{e_a}$
8	L_β	$.01\,L_\beta$	24		
9	L_r	$.1\,L_r$	25	$\Big\}\ 2/\tau_{e_r}$	$.2/\tau_{e_r}$
10	L_p	$.1\,L_p$	26		
11	N_{β_g}	$.1\,N_{\beta_g}$	27	$\Big\{\ \sigma_{\beta_g}\sqrt{3.46\dfrac{V_o}{L}}$ $\ \sigma_{P_g}\sqrt{1.43\dfrac{V_o}{L}}\Big/T_1$	
12	N_{δ_a}	N_{δ_a}	28	$\sigma_{\beta_g}\sqrt{3.46\dfrac{V_o}{L}}$	
13	N_{δ_r}	$.1\,N_{\delta_r}$	29	$(\sigma_{\beta_g}\sqrt{\ \ })e^{-\frac{\ell_v}{L}}$	
14	N_β	$.1\,N_\beta$	30	$\sqrt{3}\,\dfrac{V_o}{L}\,,\ \omega_{w_1}$	
15	N_r	N_r	31	$\sqrt{3}\,\dfrac{V_o}{L}$	
16	N_p	N_p	32	$\Big\}\ \omega_{w_2}$	
			33		

APPENDIX D

SOME IMPLICATIONS OF THE TURBULENCE SIMULATION

The equations of motion describing the airplane's response to control inputs and turbulence may be written in matrix form using prime (') notation of Reference 47 to eliminate cross product of inertia terms.

$$
\begin{bmatrix}
s - Y_v & s & -g/V_o \\
-L'_\beta & -L'_r s & s(s - L'_p) \\
-N'_\beta & s(s - N'_r) & -N'_p s
\end{bmatrix}
\begin{Bmatrix} \beta \\ \psi \\ \varphi \end{Bmatrix}
=
\begin{Bmatrix} Y^*_{\delta a} \\ L'_{\delta a} \\ N'_{\delta a} \end{Bmatrix} \delta a
+
\begin{Bmatrix} Y^*_{\delta r} \\ L'_{\delta r} \\ N'_{\delta r} \end{Bmatrix} \delta r
$$

$$
+
\begin{Bmatrix} Y_{v_g} \\ L'_{\beta_g} \\ N'_{\beta_g} \end{Bmatrix} \frac{v_g}{V_o}
+
\begin{Bmatrix} Y_{w_g} \\ L'_{w_g} \\ N'_{w_g} \end{Bmatrix} \frac{w_g}{V_o}
\tag{D1}
$$

Note from Table 5 that $I_{xz} = 0$, hence primed and unprimed derivatives are equivalent. The terms on the right hand side of the equation provide for aileron and rudder control inputs and for turbulence disturbances due to lateral and vertical gusts. For the simulation conducted in this program the derivative $L'_{\delta r}$ and the turbulence contributions from Y_{w_g} and N'_{w_g} were eliminated. The contribution to Y_{v_g} was produced by the rudder as a byproduct of the N'_{v_g} simulation, hence $Y_{v_g} = Y^*_{\delta r} \dfrac{N'_{\beta_g}}{N'_{\delta r}}$.

As was noted in Section 4, the general approach to the test program provided for separate variations in the turbulence disturbances and the airplane's lateral-directional dynamics. The purpose of this approach was to permit the separate and distinct influences of turbulence and airplane dynamics to be distinguished in the results. An obvious example is the separation of the effects of yaw disturbance magnitude which are proportional to the level of N'_{β_g} and the effects of directional stability (Dutch roll frequency) which are related to

N'_β . A noteworthy implication of this approach is that the aerodynamic deriva-
tives appearing in the turbulence disturbance matrices are not, in general,
equivalent to their counterparts appearing in the characteristic matrix, i. e.,

$$L'_{\beta_g} \neq L'_\beta$$

$$N'_{\beta_g} \neq N'_\beta \qquad (D2)$$

$$L'_{P_g} \neq L'_P$$

L'_{β_g}, N'_{β_g}, and L'_{P_g} are the aerodynamic derivatives which scale the magni-
tudes of the L_{v_g}, N_{v_g}, and L_{w_g} turbulence disturbances (see Section 3). The
consequence of these circumstances is that the transfer functions relating to
the airplane's response and the turbulence disturbances will be of a somewhat
different form than for the more typical case where the derivatives of equa-
tion (D2) are equivalent. It is worthwhile discussing these differences since
frequently in turbulence response studies the turbulence and dynamics deriva-
tives are assumed to be equivalent. An exception to this case would arise if
some form of stability augmentation were provided which altered the dynamics
derivatives while remaining insensitive to atmospheric disturbances and hence
not affecting the turbulence derivatives. The following discussion considers
the effect of these inequalities on the airplane's heading and bank angle response
to turbulence.

Heading Response

In matrix form, the airplane's heading response to turbulence may be
written

$$\psi = \left(\frac{N^\psi_{v_g}}{\Delta}\right)\frac{v_g}{V_o} + \left(\frac{N^\psi_{w_g}}{\Delta}\right)\frac{w_g}{V_o} \qquad (D3)$$

where Δ is the characteristic matrix. The numerators of the transfer func-
tions may be expanded to indicate the general form and to contrast that form with

the case where the derivatives of equation (D2) are equivalent. First consider-
ing the lateral gust transfer function numerator

$$
N^{\psi}_{v_g} = \begin{vmatrix} s-Y_v & Y_{v_g} & -g/V_o \\ -L'_{\beta} & L'_{\beta_g} & s(s - L'_p) \\ -N'_{\beta} & N'_{\beta_g} & -N'_p s \end{vmatrix}
$$

$$
= -N'_{\beta_g} (s^3 + a_2 s^2 + a_1 s + a_o) \tag{D4}
$$

where

$$
a_2 = Y_{v_g} \frac{N'_{\beta}}{N'_{\beta_g}} + L'_{\beta_g} \frac{N'_p}{N'_{\beta_g}} - Y_v - L'_p
$$

$$
a_1 = (Y_{v_g} L'_{\beta} - Y_v L'_{\beta_g}) \frac{N'_p}{N'_{\beta_g}} + (Y_v - Y_{v_g} \frac{N'_{\beta}}{N'_{\beta_g}}) L'_p
$$

$$
a_o = \frac{g}{V_o} (L'_{\beta_g} \frac{N'_{\beta}}{N'_{\beta_g}} - L'_{\beta}) \tag{D5}
$$

However, when

$$
L'_{\beta} = L'_{\beta_g}, \quad N'_{\beta} = N'_{\beta_g}, \quad \text{and} \quad Y_v = Y_{v_g}
$$

then

$$
a_2 = L'_{\beta} \frac{N'_p}{N'_{\beta}} - L'_p
$$

$$
a_1 = a_o = 0.
$$

For the case where $L'_\beta \dfrac{N'_p}{N'_\beta} \ll L'_p$ the numerator reduces to

$$N^\psi_{v_g} = -N'_\beta \; s^2 (s - L'_p) \tag{D6}$$

and the transfer function becomes

$$\left[\frac{\psi}{\beta_g}\right] = \left[\frac{N'_\beta \; s^2 (s - L'_p)}{s(s + 1/T_S)(s + 1/T_R)(s^2 + 2\zeta_d \omega_d s + \omega_d^2)}\right] \tag{D7}$$

A reasonable approximation to this transfer function when $L'_p \doteq -1/T_R$ and $1/T_S \doteq 0$ is

$$\left[\frac{\psi}{\beta_g}\right] = \left[\frac{N'_\beta}{(s^2 + 2\zeta_d \omega_d s + \omega_d^2)}\right] \tag{D8}$$

Considering the vertical gust case, the numerator may be expanded

$$N^\psi_{w_g} = \begin{vmatrix} s - Y_v & 0 & -g/V_o \\ -L'_\beta & L'_{w_g} & s(s - L'_p) \\ -N'_\beta & 0 & -N'_p s \end{vmatrix}$$

$$= -L'_{w_g} N'_p \; (s^2 + b_1 s + b_0) \tag{D9}$$

where

$$b_1 = -Y_v$$

$$b_0 = \frac{g}{V_o} \frac{N'_\beta}{N'_p} \tag{D10}$$

Whether $L'_{p_g} = L'_p$ or not is of no consequence to the character of the transfer function since L'_{p_g} acts only to scale the magnitude of the response and does not affect the factors of the numerator polynomial.

It is interesting to consider the effect of the L'_{β_g} and N'_{β_g} inequalities on the airplane's closed loop heading response to lateral gusts. A comparison of the closed loop transfer function $|\frac{\psi}{\beta_g}|$ for the cases where $L'_{\beta_g} = L'_\beta$, $N'_{\beta_g} = N'_\beta$ and $L'_{\beta_g} \neq L'_\beta$, $N'_{\beta_g} \neq N'_\beta$ is shown in Figure D1 for Configuration 1. Examples for two yaw disturbance levels are presented. In Figure D2 the same comparison is made for a low level of directional stability, Configuration 2, and a high level of yaw disturbance. No significant effects due to the inequality of the turbulence and dynamics derivatives are noted in either of these figures. The differences between the transfer functions at low frequency should be of little consequence since the turbulence inputs are attenuated in this frequency region. Hence, whether the equality between turbulence and dynamics derivatives is maintained or not should have no effect on the results of the simulation, at least for the conditions shown. Further assessment of these effects should be made if it is desired to interpret the results of the simulation for configurations other than those discussed here.

Bank Angle Response

The airplane's bank angle response to turbulence may be written

$$\varphi = [\frac{N^\varphi_{v_g}}{\Delta}] \frac{v_g}{V_o} + [\frac{N^\varphi_{w_g}}{\Delta}] \frac{w_g}{V_o} \tag{D11}$$

Considering the roll response to lateral gusts, the numerator may be expanded

$$N^\varphi_{v_g} = \begin{vmatrix} s - Y_v & 1 & Y_{v_g} \\ -L'_\beta & -L'_r & L'_{\beta_g} \\ -N'_\beta & (s - N'_r) & N'_{\beta_g} \end{vmatrix}$$

$$= -L'_{\beta_g} (s^2 + c_1 s + c_o) \tag{D12}$$

D5
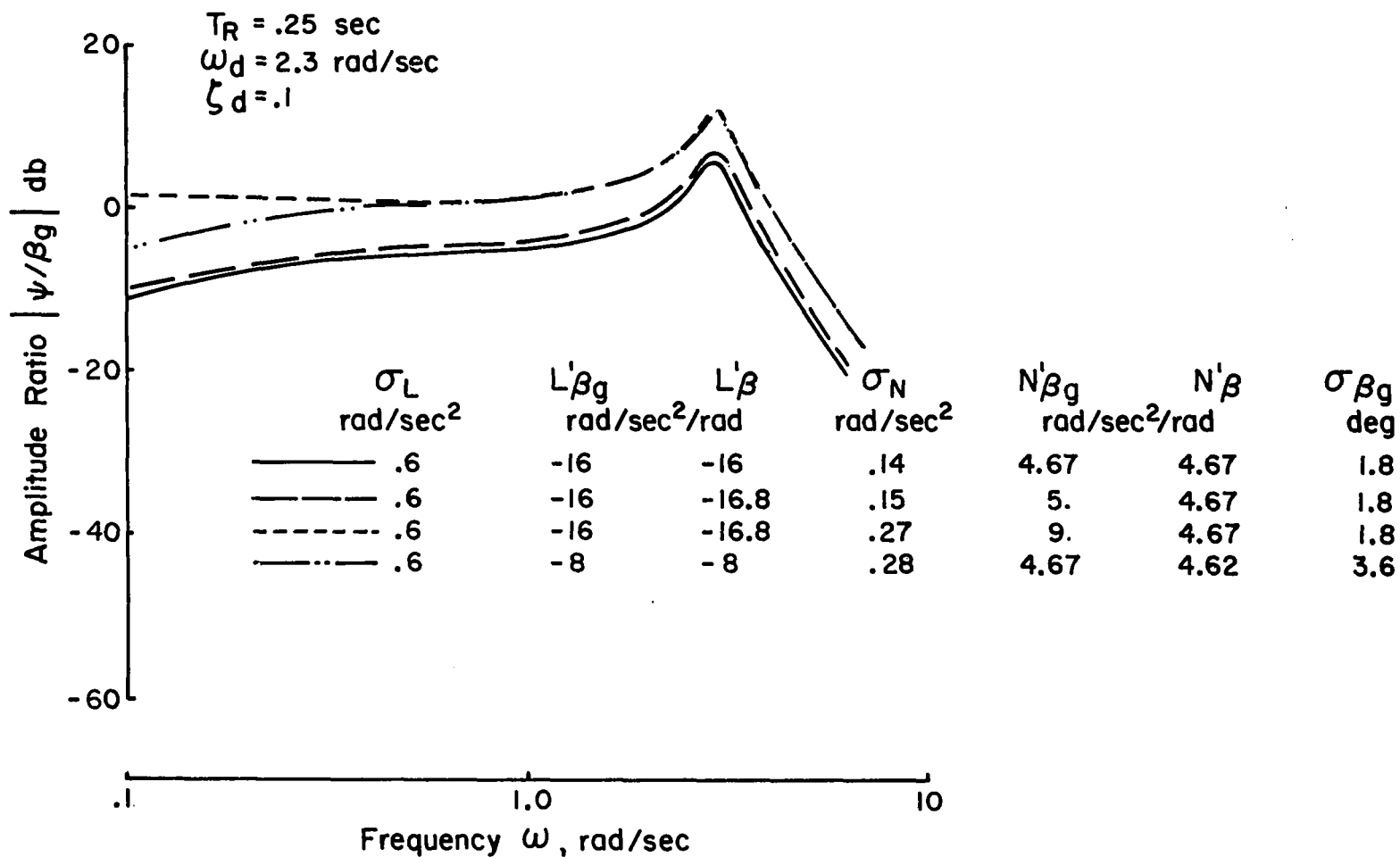
Figure D1. Effect of $L\beta'_g \neq L'\beta$, $N'\beta_g \neq N'\beta$ on Closed Loop Heading Response to Lateral Gusts

Plot showing:
$T_R = .25$ sec
$\omega_d = 1.3$ rad/sec
$\zeta_d = .1$

y-axis: Amplitude Ratio $|\psi/\beta_g|$ db, from -60 to 20
x-axis: Frequency ω, rad/sec, from $.1$ to 10

σ_L rad/sec^2	L'_{β_g} rad/sec^2/rad	L'_β	σ_N rad/sec^2	N'_{β_g} rad/sec^2/rad	N'_β	σ_{β_g} deg
.6	-2.7	-2.7	.27	1.5	1.5	10.8
.6	-16	-16	.27	9	1.5	1.8
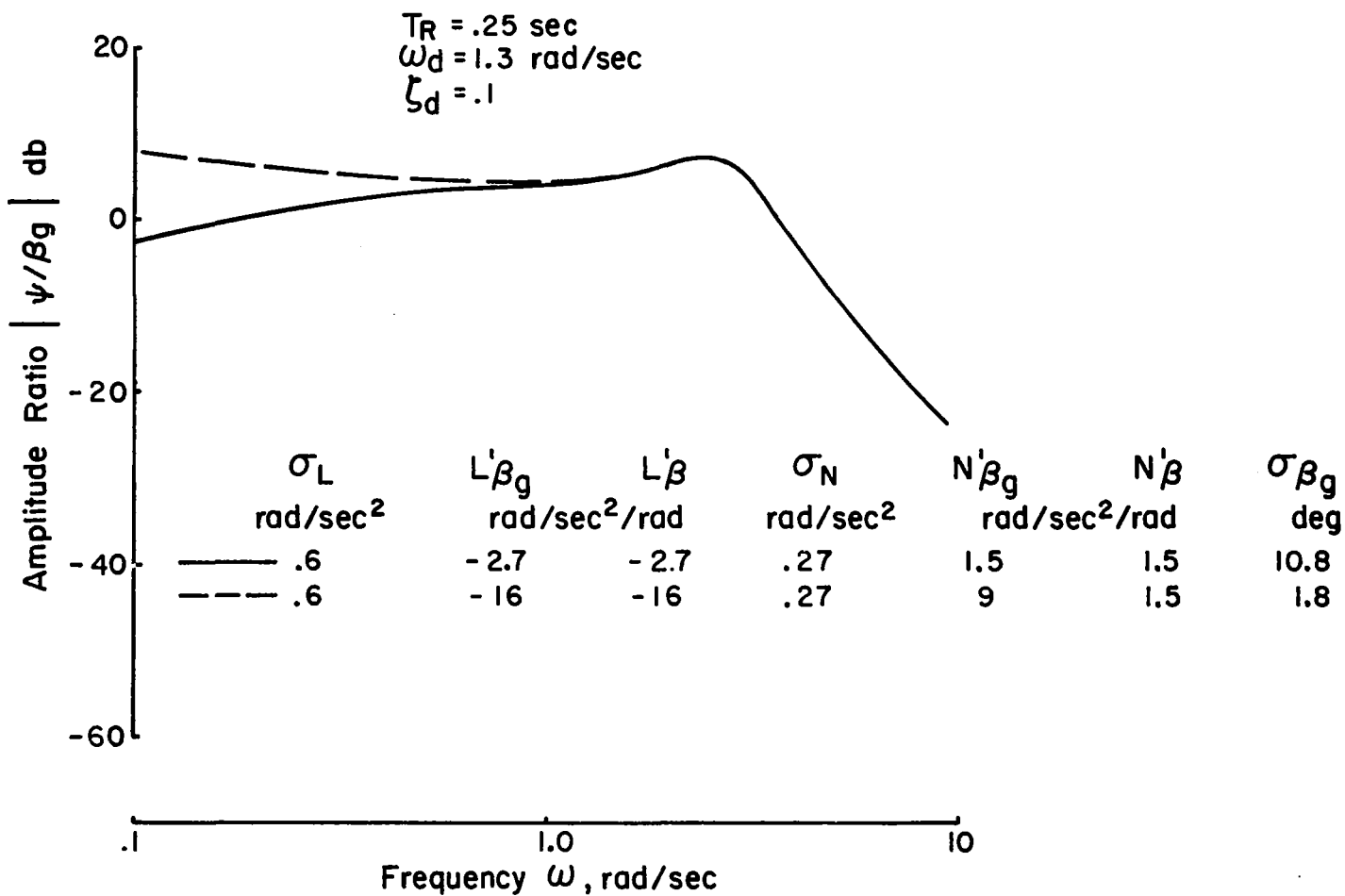
Figure D2.   Effect of $L'_{\beta_g} \neq L'_\beta$, $N'_{\beta_g} \neq N'_\beta$ on Closed Loop Heading Response to Lateral Gusts

where

$$c_1 = -\frac{1}{L'_{\beta_g}}[L'_{\beta_g} Y_v - L'_\beta Y_{v_g} + L'_{\beta_g} N'_r - L'_r N'_{\beta_g}]$$

$$c_0 = -\frac{1}{L'_{\beta_g}}[Y_{v_g}(L'_\beta N'_r - L'_r N'_\beta) - Y_v(L'_{\beta_g} N'_r - L'_r N'_{\beta_g})$$

$$+ L'_\beta N'_{\beta_g} - L'_{\beta_g} N'_\beta] \tag{D13}$$

When $L'_{\beta_g} = L'_\beta$, $N'_{\beta_g} = N'_\beta$, $Y_{v_g} = Y_v$, and for a neutral spiral mode,
$1/T_S = 0$ (which implies $L'_\beta N'_r = N'_\beta L'_r$) this numerator reduces to

$$N^\varphi_{v_g} = -L'_{\beta_g} s^2 \tag{D14}$$

and the transfer function of bank angle to lateral gusts is

$$[\frac{\varphi}{\beta_g}] = \frac{L'_\beta s}{(s + 1/T_R)(s^2 + 2\zeta_d \omega_d s + \omega_d^2)} \tag{D15}$$

For the vertical gust case

$$N^\varphi_{w_g} = \begin{vmatrix} s - Y_v & 1 & 0 \\ -L'_\beta & -L'_r & L'_{w_g} \\ -N'_\beta & s - N'_r & 0 \end{vmatrix}$$

$$= -L'_{w_g}(s^2 + d_1 s + d_0) \tag{D16}$$

where

$$d_1 = -Y_v - N'_r$$

$$d_0 = N'_\beta + Y_v N'_r \tag{D17}$$

Again the equivalence of L'_{p_g} and L'_p is of no consequence to the factorization of the numerator. The derivative L'_{p_g} merely serves to scale the magnitude of the transfer function.

The effects of the L'_{β_g} and N'_{β_g} inequalities on the airplane's closed loop roll response are indicated in Figures D3, D4, and D5. The closed loop transfer function $|\frac{\varphi}{\beta_g}|$ is shown for Configuration 1 and for a high and low level of roll disturbance in Figure D3. For the low level of roll disturbance ($\sigma_L = .6$ rad/sec^2) the two cases ($L'_{\beta_g} = L'_\beta$, $N'_{\beta_g} = N'_\beta$ and $L'_{\beta_g} \neq L'_\beta$, $N'_{\beta_g} \neq N'_\beta$) are in reasonably good agreement. It should be noted however that both the L'_β and N'_β turbulence and dynamic derivatives are nearly equivalent in this instance. However, for the higher roll disturbance ($\sigma_L = 1.2$ rad/sec^2) the two cases are substantially different. A considerable disparity exists at low frequency where the transfer function for which $L'_{\beta_g} = -32.$, $L'_\beta = -16.8$ substantially exceeds that where $L'_{\beta_g} = -32.$, $L'_\beta = -32.$ Over a mid-frequency range, the relationship of the two transfer functions is reversed. Good agreement between the two cases only exists at higher frequencies. The factors of the transfer functions are given below and illustrate the basis of the discrepancy.

$\sigma_L = 1.2$ rad/sec^2, $\sigma_N = .15$ rad/sec^2	
$L'_{\beta_g} = -32.$, $L'_\beta = -16.8$	$L'_{\beta_g} = -32$, $L'_\beta = -32$
$N'_{\beta_g} = 5$, $N'_\beta = 4.67$	$N'_{\beta_g} = 4.67$, $N'_\beta = 4.67$
$N^\varphi_{v_g} = L'_{\beta_g}(s^2 + .47s + 2.08)$	$N^\varphi_{v_g} = L'_{\beta_g} s^2$

σ_L	L'_{β_g}	L'_β	σ_N	N'_{β_g}	N'_β	σ_{β_g}
rad/sec^2	rad/sec^2/rad	rad/sec^2/rad	rad/sec^2	rad/sec^2/rad	rad/sec^2/rad	deg
.6	-16	-16	.14	4.67	4.67	1.8
.6	-16	-16.8	.15	5.	4.67	1.8
1.2	-32	-16.8	.15	5.	4.67	1.8
1.2	-32	-32	.14	4.67	4.67	1.8

T_R = .25 sec
ω_d = 2.3 rad/sec
ζ_d = .1

Amplitude Ratio $\left|\phi/\beta_g\right|$, db

Frequency ω, rad/sec
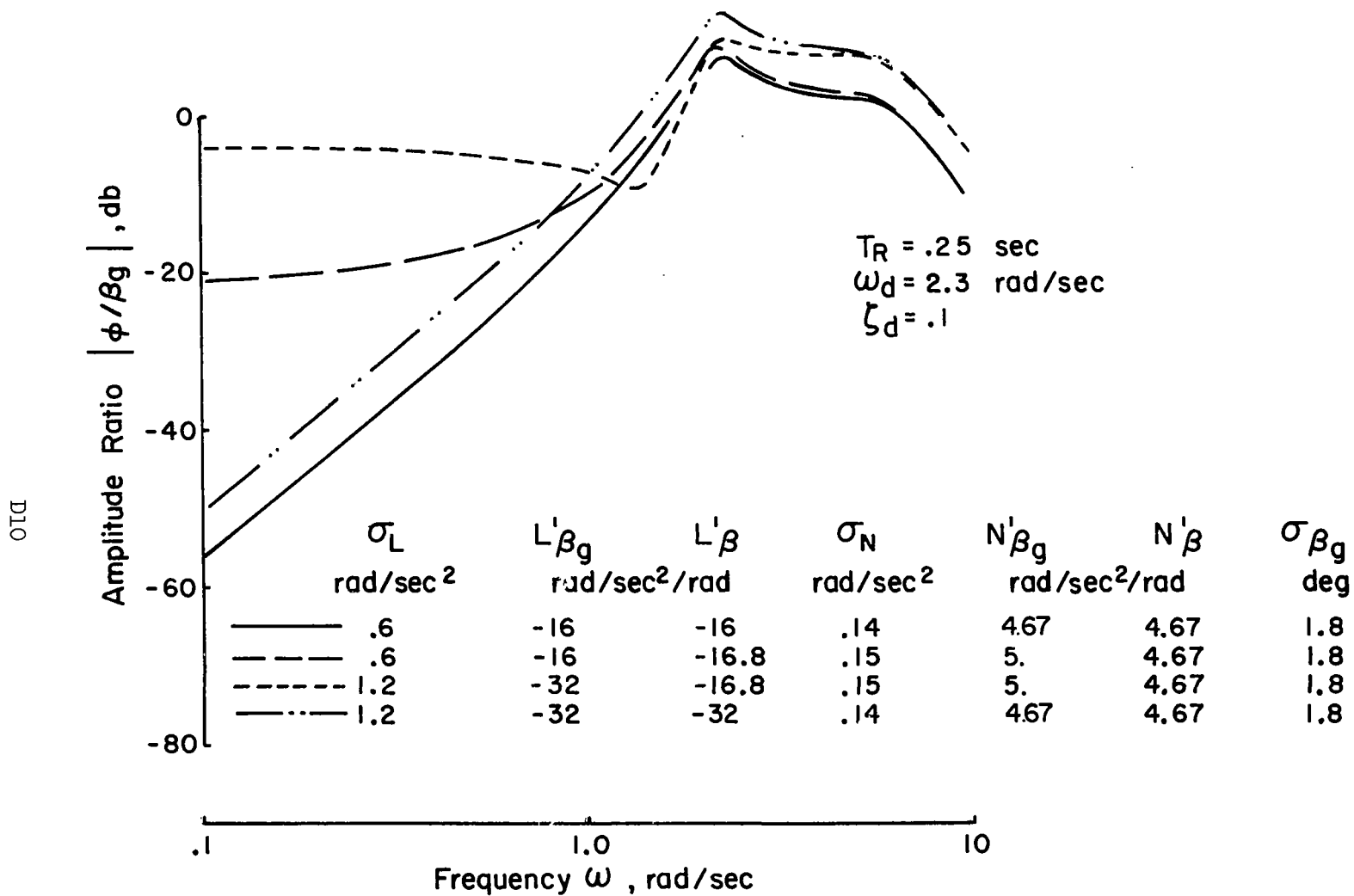
Figure D3.   Effect of $L'_{\beta_g} \neq L'_\beta$, $N'_{\beta_g} \neq N'_\beta$ on Closed Loop
Roll Response to Lateral Gusts

Amplitude Ratio $|\phi/\beta_g|$, db

$T_R = .5$ sec
$\omega_d = 2.3$ rad/sec
$\zeta_d = .1$

20

0

-20

-40

-60

σ_L rad/sec^2	L'_{β_g} rad/sec^2/rad	L'_β	σ_N rad/sec^2	N'_{β_g} rad/sec^2/rad	N'_β	σ_{β_g} deg
——— 1.2	-32	-32	.15	4.87	4.87	1.8
–– –– 1.2	-32	-16	.15	5.	4.87	1.8

.1   1.0   10

Frequency ω, rad/sec
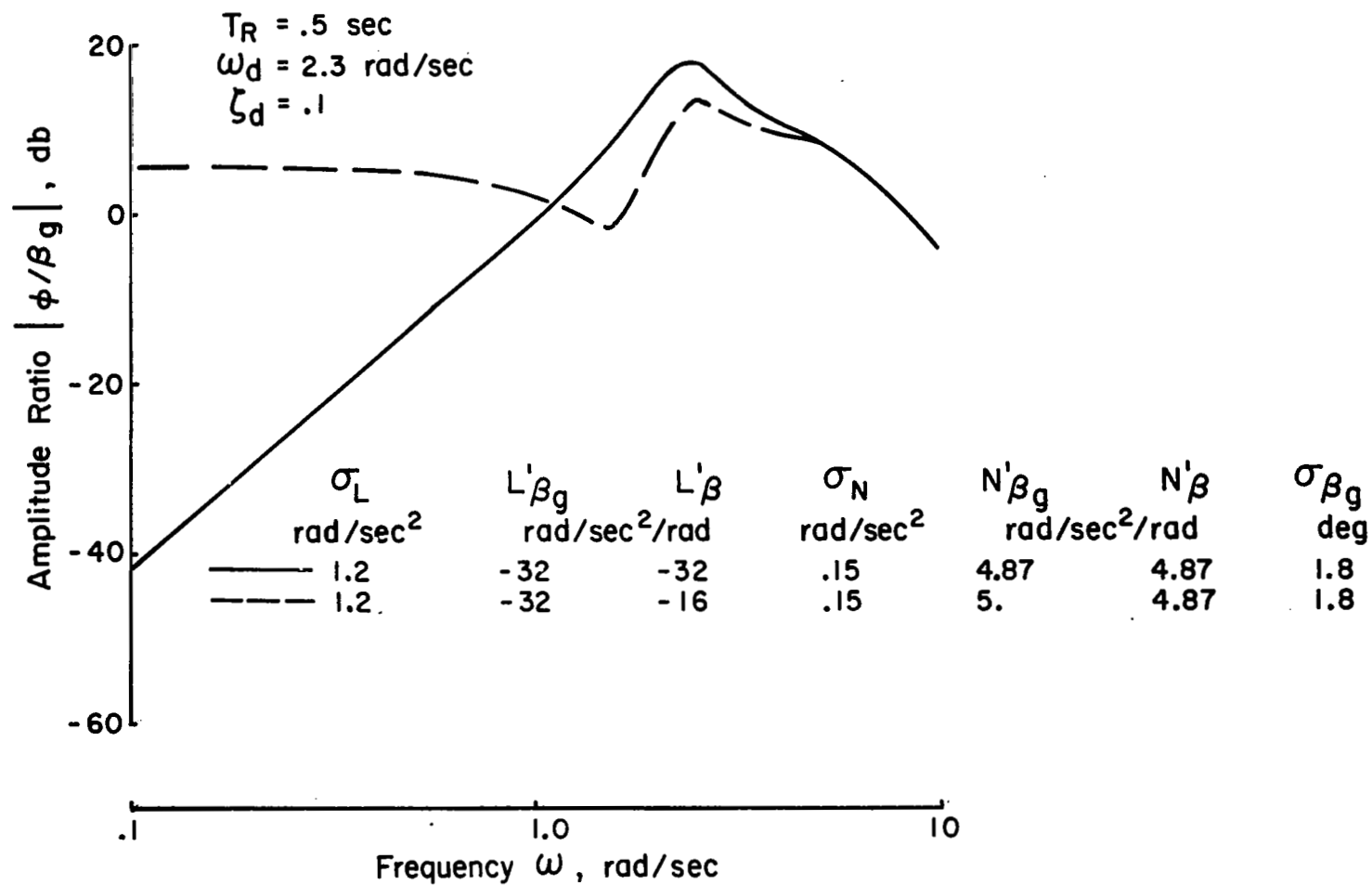
Figure D4.   Effect of $L'_{\beta_g} \neq L'_\beta$, $N'_{\beta_g} \neq N'_\beta$ on Closed Loop
Roll Response to Lateral Gusts

σ_L	L'_{β_g}	L'_β	σ_N	N'_{β_g}	N'_β	σ_{β_g}
rad/sec^2	rad/sec^2/rad		rad/sec^2	rad/sec^2/rad		deg
.6	2.67	2.67	.27	1.5	1.5	10.8
.6	-16.00	-16.00	.27	9.0	1.5	1.8

$T_R = .25$ sec
$\omega_d = 1.3$ rad/sec
$\zeta_d = .1$
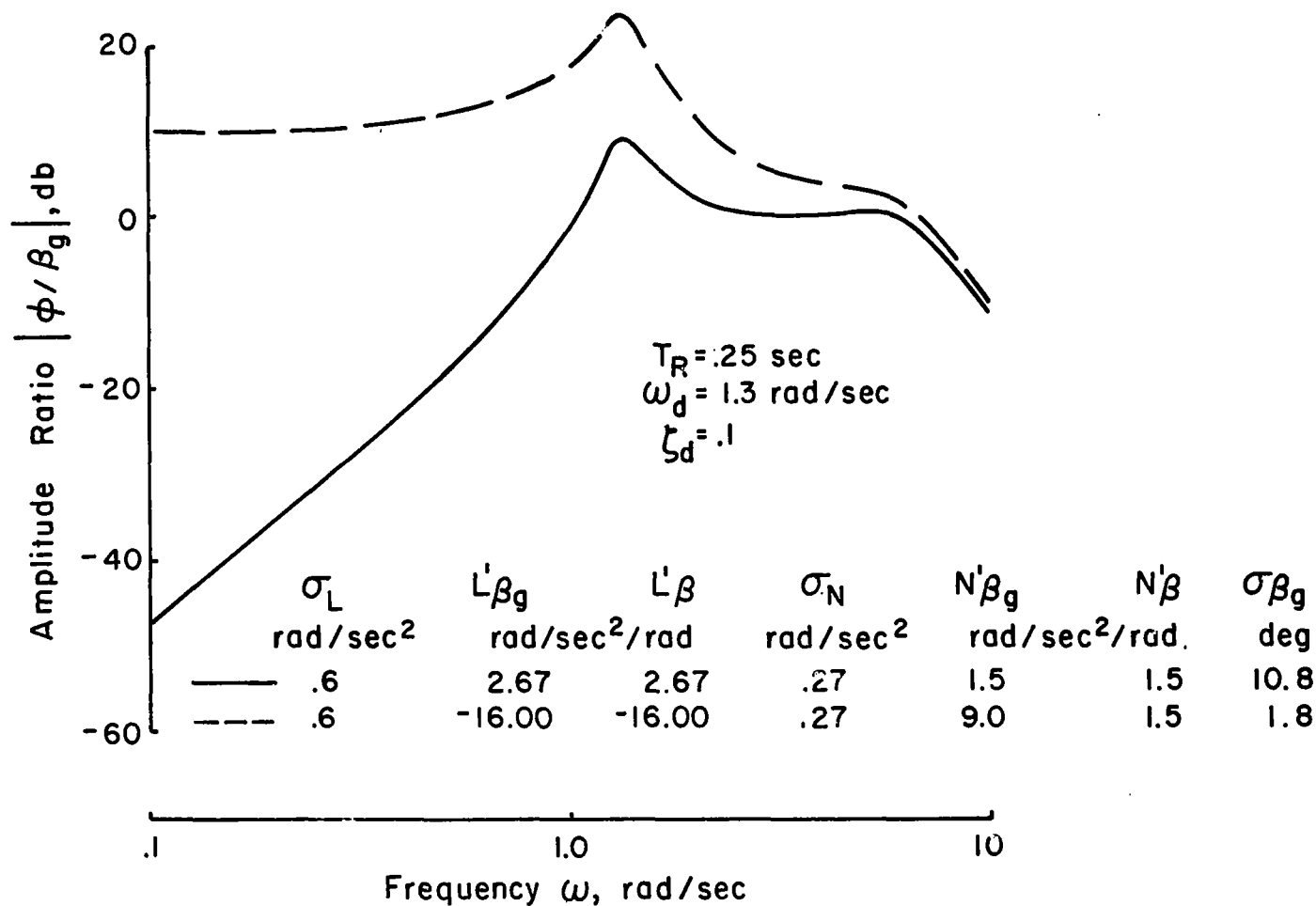
Figure D5.   Effect of $L'_{\beta_g} \neq L'_\beta$, $N'_{\beta_g} \neq N'_\beta$ on Closed Loop
Roll Response to Lateral Gusts

In Figure D4, the $\left|\dfrac{\varphi}{\beta_g}\right|$ transfer function is shown for Configuration 4 and a high roll disturbance level to indicate what effect, if any, a reduction in roll damping has on the problem. The same sort of discrepancies appear between the two cases of interest as were noted for the high roll disturbance level for Configuration 1. Furthermore, the magnitude of the difference between the two transfer functions is essentially the same.

Figure D5 presents another comparison of the roll response characteristics, but in this case for low directional stability, Configuration 2, and a high yaw disturbance. The purpose here was to consider a situation having a large mismatch between N'_{β_g} and N'_β as opposed to the previous instances having large differences between L'_{β_g} and L'_β. Again considerable differences exist between the cases of equal and unequal turbulence and dynamics derivatives, particularly in the low to mid-frequency regions. The numerator factors for this case are

$\sigma_L = .6$ rad/sec^2, $\sigma_N = .27$ rad/sec^2	
$N'_{\beta_g} = 9.$, $N'_\beta = 1.5$	$N'_{\beta_g} = 1.5$, $N'_\beta = 1.5$
$(\sigma_{\beta_g} = 1.8$ deg$)$	$(\sigma_{\beta_g} = 10.8$ deg$)$
$N^{\varphi}_{v_g} = L'_{\beta_g}(s - 2.64)(s + 2.82)$	$N^{\varphi}_{v_g} = L'_{\beta_g} s^2$

It is apparent that substantial differences may exist between the closed loop roll response characteristics of cases where the airplane's turbulence and dynamics derivatives are either equal or unequal. When roll turbulence response is a dominant influence on the flying qualities of the evaluation task it is possible that the character of the roll response discussed herein would be significant to the pilot. If roll turbulence is of secondary interest to the pilot, then the precise character of the roll response to turbulence should be of less concern. In

any event, some discretion should be exercised in the application of the results of this program in cases where roll turbulence response appears as the chief contributor to degraded flying qualities.

APPENDIX E

SUMMARY OF PILOT OPINION RATINGS AND COMMENTARY

Config. Dynamics / Turb.	Pilot	Mean Rating	No. of Ratings	Max. Deviation	Comments
1/1	A (primary)	2.7	2	±.2	No difficulty. Very little turbulence.
	B	-	-	-	
	C (secondary)	-	-	-	
	D	-	-	-	
1/2	A	3.	3	0.	No difficulty. Low turbulence level.
	B	3.1	3	+.4	
	C	3.5	2	±.5	
1/3	A	4.	4	0.	ψ problems. Moderate δ_r compensation. Acceptable performance. Large β. No φ difficulty when using δ_a and δ_r. δ_a alone unacceptable due to roll-yaw coupling.
	B	3.8	1	0.	
1/4	A	3.3	2	±.2	No ψ problem. φ excursions a little more than desired.
1/5	A	4.3	3	-.3	ψ control difficult. Considerable δ_r compensation. φ no problem.
1/6	A	3.4	2	±.4	ψ OK. φ annoying. Moderate δ_a compensation.
1/7	A	4.	4	-.5	ψ less of a problem than φ. Large φ excursions. Moderate δ_a and δ_r compensation.
	B	4.	1	0.	

Config. Dynamics / Turb.	Pilot	Mean Rating	No. of Ratings	Max. Deviation	Comments
1/8	A	4.6	4	+.4	ψ difficulties dominant. Large excursions in ψ and β. Considerable δr compensation. φ no problem.
	B	4.2	2	±.4	
	C	6.	1	0.	
1/9	A	3.3	2	±.3	φ difficult. Nothing in ψ.
1/10	A	3.8	3	-.3	Large φ and ψ excursions.
1/11	A	3.3	4	-.8	No problem in ψ or φ.
1/12	A	2.9	3	±.1	No difficulty with ψ or φ.
	B	3.	1	0.	
1/13	A	4.2	3	+.3	Some difficulty with φ and ψ. Moderate compensation with δ_a and δ_r.
	B	4.	1	0.	
1/14	A	4.4	3	+.6	Large excursions in ψ, β, φ. Considerable δ_r compensation.
	B	3.3	1	0.	
1/15	A	3.5	2	0.	Some unpleasant ψ excursions. δ_r required to compensate.
1/16	A	3.8	3	-.3	No serious problems in φ or ψ. Noted higher frequency roll upsets.
	B	3.5	1	0.	
1/17	A	3.8	4	-.3	φ and ψ about the same difficulty. Moderate δa compensation. High frequency upsets in roll, low frequency in yaw.
	B	3.	1	0	
1/19	A	3.3	3	-.3	Mildly unpleasant in φ and ψ. Minimum δa and δr.
	B	2.5	1	0	
1/20	A	2.8	2	±.3	Minimum δa and δr compensation.
	B	2.5	1	0	

Config. Dynamics Turb.	Pilot	Mean Rating	No. of Ratings	Max. Deviation	Comments
1/21	A	3.2	5	+.3	Minimum δa and δr compensation.
	B	3.	3	±.5	No problem with ψ
	C	3.5	3	±.5	
	D	3.	1	0	
1/22	A	4.5	6	±.5	ψ problems dominate. Extensive
	B	3.8	1	0	δr compensation. φ not difficult.
	C	6.	1	0	
1/23	A	3.8	2	±.3	Some φ excursions require δa com-
	B	3.	1	0	pensation. No ψ activity.
1/24	A	4.3	2	±.3	Moderate δr required for desired
	B	4.5	1	0	ψ performance. No φ difficulties.
1/25	A	4.3	2	±.3	No ψ problem. Quite a bit of δa
	B	3.5	1	0	required to keep φ excursions ac-
					ceptable.
1/26	A	4.5	4	±.5	Considerable δa required to achieve
	B	3.5	1	0	desired φ performance. ψ easier
	C	5.	1	0	to control than φ.
	D	3.8	2	±.2	
1/27	A	5.	6	±.5	Large ψ and φ excursions. Work-
	B	4.	1	0	ing hard on δa and δr. Rapid up-
	C	6.	3	0	sets. Poor ψ precision.
	D	5.	1	0	
1/28	A	3.7	3	+.3	ψ and φ comparable. No problem
	B	3.	1	0	
1/29	A	4.8	4	+.5	Primarily ψ problem, but some in
	B	4.	1	0	φ, too. Requires too much com-
					pensation with δa and δr.
1/30	A	4.	3	0	ψ OK. Large φ excursions. Mod-
	B	3.5	1	0	erate δa compensation.
	C	4.	1	0	

Config. Dynamics / Turb.	Pilot	Mean Rating	No. of Ratings	Max. Deviation	Comments
1/31	A	5.3	3	+.5	Large ψ and β excursions. Working very hard on δr to get accept-
	B	4.3	1	0	able ψ performance. Some φ prob-
	C	7.	1	0	lems. Considerable compensation.
1/32	A	3.2	2	±.2	Small excursions. Minimal com-
	B	3.5	1	0	pensation.
1/33	A	4.3	4	+.7	Moderately difficult in yaw . Mod- erate δr compensation.
1/34	A	4.	3	0	Annoying φ performance. Small
	B	3.8	1	0	ψ excursions.
	C	3.5	.1	0	
1/35	A	4.5	5	±.5	Both φ and ψ are problems. Mod-
	B	3.8	1	0	erate δr compensation.
	C	5.	1	0	
1/36	A	7.	1	0	Task performance inadequate.
	C	9.	1	0	Best workload not sufficient.
1/37	A	7.5	1	0	Excursions so large that perfor- mance is inadequate. Required workload too high.
1/39	A	3.3	2	±.1	Mildly unpleasant. Minimal com- pensation.
1/40	A	3.5	1	0	Just a little upset in roll and yaw.
1/41	A	3.3	2	±.2	A little unpleasant.
1/42	A	3.8	2	±.3	A little annoying in roll. Minor δa compensation.
1/43	A	4.4	2	±.4	Large roll upsets. Moderate δa compensation.

Config. Dynamics / Turb.	Pilot	Mean Rating	No. of Ratings	Max. Deviation	Comments
1/44	A	4.3	2	±.3	ψ problem. A lot of high frequency energy. Moderate δa compensation.
1/45	A	4.1	2	±.8	Large, abrupt roll upsets. Considerable δa required. Roll affects heading.
1/46	A	4.3	1	0	Lot of φ activity. Moderate δa compensation.
1/47	A	4.2	2	±.7	Large φ upsets. Considerable δa required.
1/48	A	4.	1	0	Abrupt roll upsets. Moderate compensation.
1/49	A	3.6	3	+.4	Minor difficulty with ψ and φ. A little too busy with δa and δr. High frequency upsets.
	B	3.	1	0	
1/50	A	4.3	3	+.7	ψ problems dominate. Continuous δr required to achieve performance. High frequency upsets.
	B	3.3	1	0	
1/51	A	4.5	4	±.5	No ψ problems. Objectionable φ excursions. Considerable δa compensation. Ignored high frequency.
	B	3.	1	0	
1/52	A	5.1	5	+.4	φ more of a problem than ψ. Considerable δa, moderate δr required. High frequency upsets. Must be very active to keep up with disturbances.
	B	3.8	1	0	
	C	4.5	1	0	

Config. Dynamics/Turb.	Pilot	Mean Rating	No. of Ratings	Max. Deviation	Comments
1/53	A	4.3	2	±.3	Annoying φ problems. ψ less difficult to control.
1/54	A	5.7	3	-.4	Very objectionable φ and ψ excursions. Best compensation barely adequate. Abrupt upsets.
	B	4.	1	0	
1/55	A	4.6	3	-.6	ψ control difficult. Considerable δr compensation. High frequency upsets.
	B	3.8	1	0	
2/2	A	4.6	4	±.4	Large ψ and β excursions. Difficult to control ψ. Considerable δr required.
2/3	A	6.	2	0	Very objectionable. Large ψ and β. Using nearly all available δr. φ somewhat of a problem.
	B	5.	1	0	
2/7	A	4.8	2	± 3	Both φ and ψ difficult. δa compensation fairly easy. Considerable δr compensation.
2/8	A	5.6	4	-.6	ψ and β excursions entirely too large. Best δr compensation required. φ is a problem, especially when β is large.
	B	4.8	1	0	
2/21	A	4.4	2	±.4	φ and ψ not too difficult. Easily compensated.
	B	3.5	1	0	
2/22	A	5.2	3	-.2	Considerable ψ problems. Nearly best δr compensation. φ not difficult.
	B	4.	2	0	

Config. Dynamics Turb.	Pilot	Mean Rating	No. of Ratings	Max. Deviation	Comments
2/25	A	4.3	2	±.8	Not much ψ excursion, but still difficult to control. φ objectionable. Moderate δa.
2/26	A	4.7	3	+.3	ψ not much of a problem. φ diffi-
	B	3.5	1	0	cult. Considerable δa.
2/27	A	5.6	4	-.6	ψ and φ very difficult. Large β.
	B	4.2	2	±.4	Working hard on δr and δa.
2/29	A	5.4	2	±.4	Difficult ψ problem. Nearly best δr compensation.
2/30	A	5.3	2	±.3	Problems in φ and ψ. Considerable compensation. Sloppy in ψ.
2/31	A	5.8	5	-.3	Large ψ and β. φ control difficult. Best δa and δr compensation required.
2/34	A	4.6	3	-.6	φ somewhat worse than ψ. Easily compensated.
2/35	A	4.9	3	±.1	ψ excursions large. Considerable δr compensation. Performance barely adequate.
2/49	A	3.9	3	±.4	Large ψ and β excursions. Low $N\beta$. More than minimum compensation.
2/50	A	4.8	2	±.3	Most of the problem in ψ. Con-
	B	4.5	1	0	siderable δr compensation.
2/51	A	4.3	2	0	Annoying φ problems. Not too easily compensated. ψ not difficult.

Config. Dynamics/Turb.	Pilot	Mean Rating	No. of Ratings	Max. Deviation	Comments
2/52	A	5.	2	0	Moderately objectionable in φ.
	B	4.3	1	0	Large ψ excursions. Considerable δr compensation.
3/2	A	2.8	3	-.3	No ψ or φ problems.
3/3	A	3.9	2	±.1	Some ψ problems. Easily compensated. Some large, low frequency ψ excursions.
3/7	A	3.8	1	0	φ excursions easily compensated. No ψ problem.
3/8	A	4.1	2	±.1	Both φ and ψ excursions easily compensated.
3/21	A	3.5	1	0	No problem.
3/22	A	3.5	3	±.5	Some ψ excursions. Easily compensated.
3/26	A	4.	1	0	φ annoying.
3/27	A	4.4	5	+.6	Not too difficult in ψ or φ. Moderate compensation.
3/29	A	4.3	1	0	Large ψ excursions. Not easily compensated with δr.
3/30	A	5.	1	0	φ moderately objectionable. Considerable δa compensation.
3/31	A	4.8	3	-.3	ψ moderately objectionable. Considerable δr compensation. φ fairly easily compensated.
3/34	A	4.	1	0	φ annoying.
3/35	A	3.8	3	-.3	Small φ excursions. ψ excursions only occasionally large.

Config. Dynamics/Turb.	Pilot	Mean Rating	No. of Ratings	Max. Deviation	Comments
3/49	A	3.	1	0	No φ or ψ problems.
3/50	A	3.8	1	0	Annoying ψ excursions. Requires some compensation. High frequency upsets.
3/51	A	3.5	1	0	A little problem with φ.
3/52	A	4.	1	0	Abrupt φ and ψ upsets. Fairly easily handled.
4/2	A	3.4	3	±.1	Roll damping less than desired.
	B	3.	1	0	Fairly large φ excursions. Not hard to control.
4/3	A	4.	2	0	Some difficulty with ψ. δr control
	B	4.	1	0	good. Very little φ response except when ψ is large.
4/7	A	4.5	3	+.3	φ control problems. Considerable
	B	4.	1	0	δa compensation.
4/8	A	4.8	4	-.3	Large φ and ψ excursions. Con-
	B	4.5	1	0	siderable δa compensation. Had
	C	8.	1	0	to work on ψ with δr.
4/21	A	3.8	3	-.8	φ a bit of a problem. Moderate
	B	3.2	1	0	δa compensation.
	C	4.3	2	±.8	
4/22	A	4.3	2	±.3	φ and ψ troublesome φ problem
	B	4.	1	0	worse. Moderate δa.
4/23	A	5.	1	0	φ objectionable. Working hard for
	B	3.5	1	0	adequate performance.

Config. Dynamics/Turb.	Pilot	Mean Rating	No. of Ratings	Max. Deviation	Comments
4/24	A	5.	1	0	Large φ and ψ excursions. Con-
	B	4.3	1	0	siderable compensation.
4/26	A	5.8	2	0	φ is the entire problem. Large
	B	4.	1	0	excursions. Best δa compensa-
	C	5.	2	±1.	tion.
4/27	A	5.4	3	+.6	φ very difficult. Working hard on
	B	4.5	1	0	δa. Some ψ activity. Using δr on
	C	7.3	3	-.3	ψ helped φ.
4/30	A	5.4	2	±.4	φ a constant problem. Working
					hard with δa. Some ψ problems.
4/31	A	6.4	2	±.4	φ very objectionable. Nearly best
	B	4.5	1	0	δa compensation. Can't keep φ
					under control. ψ not bad.
4/16	A	3.7	3	+.3	Very little φ activity. Had to work
	B	3.5	1	0	some with δa to keep wings level.
4/17	A	4.	3	0	Some difficulty with φ and ψ.
	B	3.5	1	0	
4/51	A	5.5	2	±.5	φ excursions so large had to work
	B				hard to hold $\varphi \pm 10^{\circ}$. ψ no problem.
4/52	A	5.9	2	±.1	φ difficult. Excessive δa to main-
	C	6.	1	0	tain control. Some ψ problems but
					easily compensated.
5/2	A	2.9	2	±.1	No problems with φ or ψ.
5/3	A	4.1	2	±.3	Had to work on φ and ψ. Not bad.
5/7	A	3.1	3	+.2	High roll damping helps. Not
					much of a problem.

Config. Dynamics/Turb.	Pilot	Mean Rating	No. of Ratings	Max. Deviation	Comments
5/8	A	4.1	3	+.4	ψ a little annoying. Some δr compensation required.
5/21	A	3.3	3	+.5	No particular problem. Occasional
	C	3.	1	0	ψ excursions easily compensated.
5/26	A	3.8	3	+.7	φ a little annoying. Not quite easily
	C	4.	1	0	handled.
5/27	A	4.3	3	+.7	Moderate φ excursions. ψ getting to be objectionable. Moderate δa and δr compensation.
5/30	A	4.	1	0	More of a φ problem. Easily handled.
5/31	A	4.	1	0	Not much of a problem.
5/51	A	3.9	3	+.9	Entirely a φ problem. Difficult to stop abrupt φ excursions.
5/52	A	4.1	3	+.7	Both φ and ψ difficult. Working hard with δa. Had to use δr, but not much.
6/2	A	3.9	3	±.1	Low roll damping and directional stability. Some large φ and ψ excursions. Moderate compensation.
6/3	A	4.9	3	±.1	Large ψ excursions. Have to work constantly to get desired performance. φ no problem.
6/7	A	4.8	3	-.3	Large φ. Considerable δa compensation. Low N_β makes ψ difficult.

Config. Dynamics Turb.	Pilot	Mean Rating	No. of Ratings	Max. Deviation	Comments
6/8	A	5.6	3	-.6	Large ψ excursions. Considerable δr compensation. Low L_p and N_β make a difficult task.
6/21	A D	3.8 4.	1 2	0 0	Easily controlled in φ and ψ.
6/22	A	4.8	3	-.3	ψ not easily compensated. φ no problem.
6/26	A D	5.3 5.8	3 2	-.3 ±.2	φ objectionable. Requires a lot of δa. ψ no problem.
⁻/27	A	5.8	3	-.3	Low N_β, low L_p. High roll to yaw. Working hard with δa and δr.
6/29	A	5.2	2	±.2	ψ difficult. Large β. Requires nearly best δr compensation.
6/30	A	6.3	3	-.8	Very large φ excursions. Couldn't get adequate φ performance. φ dominates so much, ψ problems not apparent.
6/31	A	6.5	3	±.5	Very large φ and ψ excursions. Couldn't get adequate φ performance. Uncomfortable ride.
6/16	A	4.8	3	-.3	Large φ. Working hard on δa. ψ not as bad as φ.
6/17	A	4.9	2	±.1	Both φ and ψ problems. Moderate to considerable δa and δr.
6/50	A	4.5	3	±.5	ψ difficult. Considerable compensation. High frequency upsets.
6/51	A	6.	2	0	Large φ. Working very hard on δa. ψ not as difficult but had to work on it.

Config. Dynamics / Turb.	Pilot	Mean Rating	No. of Ratings	Max. Deviation	Comments
6/52	A	6.2	2	±.4	φ and ψ difficult. Nearly best δa compensation. Working on δr, too.
7/2	A	3.4	2	±.4	Sloppy in ψ. Had to use δr somewhat.
7/3	A	4.3	2	±.7	Moderate ψ excursions. Required some δr.
	B	5.	1	0	
7/7	A	4.	2	±.5	A little unpleasant in roll. Relaxing on δr.
7/8	A	4.5	2	±.5	Some ψ activity. Moderate workload.
	B	3.5	1	0	
7/21	A	3.3	3	+.7	Had to use δr occasionally. Very little φ.
	B	3.3	2	0	
7/22	A	3.8	2	0	ψ annoying. Had to use δr. Not much φ.
	B	4.	2	0	
7/26	A	4.1	2	±.2	Moderate δa workload.
	B	3.3	1	0	
7/27	A	4.8	4	-.3	ψ more of a problem than φ. Considerable compensation.
	B	3.8	2	±.3	
7/30	A	4.4	3	±.4	Large φ excursions. Quite a bit of δa required.
7/31	A	5.3	3	+.5	Large ψ excursions. Considerable compensation.
7/50	A	4.	1	0	Some ψ difficulty. Used δr a little.
	B	3.3	1	0	
7/51	A	4.5	1	0	Large φ excursions. Considerable δa compensation.

Config. Dynamics/Turb.	Pilot	Mean Rating	No. of Ratings	Max. Deviation	Comments
7/52	A	5.	1	0	Both φ and ψ objectionable. Considerable δr and δa compensation.
	B	4.	1	0	
8/2	A	2.9	2	±.1	No problem.
8/3	A	3.8	1	0	Some annoying ψ activity.
8/7	A	3.5	1	0	A little φ problem.
8/8	A	3.8	1	0	Some difficulty with ψ and φ.
8/21	A	3.	1	0	No problem.
8/26	A	4.	1	0	Annoying φ excursions.
8/27	A	4.8	1	0	Most of the problem with φ. Busy with δa. No ψ difficulty.
8/31	A	5.	1	0	φ problems. Moderate δa compensation. No ψ problem.
9/8	A	4.8	2	0	Objectionable ψ. Proverse yaw apparent. φ control excites yaw.
9/21	A	3.3	2	±.3	
9/26	A	4.3	1	0	φ upsets annoying. Not much going on with ψ.
9/27	A	5.3	2	±.3	Quite a lot of φ activity. ψ objectionable. Some ψ due to δa.
9/31	A	5.1	2	±.4	φ not bad. ψ difficult. Large, low frequency excursions. Considerable δr compensation.
9/52	A	5.3	1	0	φ and ψ active. Considerable δr compensation.
10/8	A	3.9	3	±.1	Moderate φ and ψ excursions. Busy with δa and δr. Using δa and δr separately.

Config. Dynamics / Turb.	Pilot	Mean Rating	No. of Ratings	Max. Deviation	Comments
10/21	A	3.	2	0	No difficulty with $\dot{\psi}$.
	B	3.	1	0	
	C	3.	1	0	
10/26	A	4.2	2	±.2	φ annoying. Moderate δa work-
	B	4.	1	0	load. Adverse yaw tends to cor-
	D	3.	1	0	rect β. No ψ difficulty. Little δr
					effort.
10/27	A	4.3	3	-.8	Moderate φ and ψ excursions. φ
	B				control not difficult. ψ control a
					problem. β seems to be corrected
					by adverse yaw.
10/31	A	4.9	3	±.1	Large φ and ψ. Considerable δa
					and δr workload. Large excur-
					sions due to turbulence level.
10/52	A	4.5	1	0	Moderate φ and ψ. Didn't work too
					hard.
11/8	A	4.4	3	±.1	φ and ψ coupled. Rapid φ response.
					Low damping for ψ. Had to work
					at φ and ψ.
11/21	A	3.4	2	±.1	
	B	3.	1	0	
	D	3.	1	0	
11/26	A	4.	1	0	Moderate φ excursions. Proverse
	B	4.3	1	0	yaw feeds ψ. No problem with ψ
	D	4.4	2	±.1	control. Use δr as yaw damper.
11/27	A	5.	3	0	A lot of φ and ψ activity, some due
	B	4.8	1	0	to turbulence, some due to control
	D	7.	1	0	excitation. Requires a lot of work
					to compensate.

Config. Dynamics / Turb.	Pilot	Mean Rating	No. of Ratings	Max. Deviation	Comments
11/31	A	5.4	2	±.4	Had to work hard on δr. Active use of δa to control φ causes a lot of ψ activity.
11/52	A	4.	1	0	ψ excitation not too bad. High frequency turbulence annoying, but amplitude seems lower.
12/8	A	5.2	2	±.2	Considerable ψ problem. φ not as bad. Considerable δr required.
12/21	A	4.	1	0	φ excursions larger than desired. Moderate compensation.
12/26	A	5.5	2	0	Large φ excursions. Considerable δa required. ψ not difficult.
12/27	A	5.4	2	±.4	Large φ and ψ excursions. Considerable δa and δr compensation.
12/31	A	6.	2	0	Very large φ and ψ. Required nearly best δa and δr capability. Used δa and δr independently. Couldn't perform as well when co-ordinating δa and δr.
12/52	A	6.	1	0	Large φ and ψ excursions. A lot of compensation required.
13/8	A	5.3	2	0	Large φ and ψ excursions. Considerable compensation. Moderate turbulence disturbing a bad airplane.
13/21	A	4.4	2	±.1	Difficult to maintain performance.
	B	3.	1	0	Large β. Sloppy airplane. Working
	C	4.5	2	±.5	fairly hard with δ_a and δ_r.

Config. Dynamics/Turb.	Pilot	Mean Rating	No. of Ratings	Max. Deviation	Comments
13/26	A	5.7	3	-.4	Large φ excursions. Requires
	B	4.	1	0	nearly best δa compensation. Close
	D	6.	1	0	to δa stops. ψ not good. Large β. Neither as bad as roll.
13/27	A	6.1	4	+.2	Large φ and ψ. Nearly best com-
	B	5.	1	0	pensation with δa and δr. Sloppy airplane.
13/31	A	6.9	2	±.1	Very large φ and ψ excursions. Could keep airplane under control, but performance not acceptable.
13/52	A	7.	1	0	Very large φ and ψ. Performance not acceptable with best effort.
14/8	A	5.2	2	±.2	ψ objectionable. Considerable δr required to correct large, low fre- quency excursions. φ not as bad as ψ.
14/21	A	4.	3	+.3	Sloppy airplane. Favorable $N_{\delta a}$
	D	5.5	2	±.5	feeds into roll. Used δr to stop Dutch roll.
14/26	A	5.4	3	±.1	Large φ. Considerable δa required.
	D	7.	1	0	Working hard on δr to damp Dutch roll. Large ψ. δa and δr inde- pendent.
14/27	A	6.	3	+.3	φ objectionable. Extensive com- pensation. Large ψ. Working hard on δr. Objectionable ride.

Config. Dynamics/Turb.	Pilot	Mean Rating	No. of Ratings	Max. Deviation	Comments
14/31	A	6.9	2	±.4	Large φ, ψ, and β. Working hard on δa and δr. Used controls independently. Not getting adequate performance.

APPENDIX F

AIRPLANE TRANSFER FUNCTIONS TO CONTROL INPUTS

Lateral Control Transfer Functions

Transfer functions of bank angle and sideslip to aileron control inputs are developed in this section. Only the transfer function numerators are considered since the characteristic roots have been previously specified in Section 3.

According to Reference 47, the airplane's bank angle response to aileron deflection is defined for small disturbances from straight and level flight by

$$\frac{\varphi}{\delta a} = \frac{N^{\varphi}_{\delta a}}{\Delta}$$

where $N^{\varphi}_{\delta a} = A_{\varphi \delta a} (s^2 + 2\zeta_{\varphi} \omega_{\varphi} s + \omega_{\varphi}^2)$

and $A_{\varphi} = L'_{\delta a}$

$$2\zeta_{\varphi} \omega_{\varphi} \doteq -(Y_v + N'_r) + \frac{N'_{\delta a}}{L'_{\delta a}} L'_r$$

$$\omega_{\varphi}^2 \doteq N'_{\beta} \left(1 - \frac{N'_{\delta a} L'_{\beta}}{L'_{\delta a} N'_{\beta}}\right)$$

for the conditions specified in Table 6-4 of Reference 47.

Sideslip response to ailerons is specified by a transfer function whose numerator normally factors in the form

$$N^{\beta}_{\delta a} = A_{\beta} \left(s + \frac{1}{T_{\beta_1}}\right)\left(s + \frac{1}{T_{\beta_2}}\right)$$

where for the case when $N'_{\delta a} \neq 0$

$$A_\beta \doteq N'_{\delta a}$$

$$\frac{1}{T_{\beta_1}} \doteq \left(\frac{g}{V_o}\right) \frac{L'_r - \dfrac{L'_{\delta a}}{N'_{\delta a}} N'_r}{L'_p - \dfrac{L'_{\delta a}}{N'_{\delta a}} \left(N'_p - \dfrac{g}{V_o}\right)}$$

$$\frac{1}{T_{\beta_2}} \doteq - L'_p + \frac{L'_{\delta a}}{N'_{\delta a}} \left(N'_p - \frac{g}{V_o}\right)$$

When $N'_{\delta a} = 0$ the numerator factors into the form

$$N^\beta_{\delta a} = A_\beta \left(s + \frac{1}{T_{\beta_2}}\right)$$

where

$$A_\beta = L'_{\delta a} \left(N'_p - \frac{g}{V_o}\right)$$

$$\frac{1}{T_{\beta_2}} = \frac{g}{V_o} \frac{N'_r}{\left(N'_p - \dfrac{g}{V_o}\right)}$$

Values of the $N^\varphi_{\delta a}$ and $N^\beta_{\delta a}$ numerators for the test configurations of this program are given in Table F1. These factors are exact calculations rather than approximate values determined from the previous equations.

TABLE F1

LATERAL TRANSFER FUNCTION NUMERATORS

Config.	Transfer Function (Aileron)						
	$N_{\delta a}^{\varphi}$				$N_{\delta a}^{\beta}$		
	A_{φ}	$\zeta_{\varphi}\omega_{\varphi} \pm j\omega_{\varphi}\sqrt{1-\zeta_{\varphi}^2}$	$\omega_{\varphi}/\omega_d$	K_d/K_{ss}	A_{β}	$-1/T_{\beta_1}$	$-1/T_{\beta_2}$
1	103.14	$-.31 \pm j\,2.16$	.950	.130	-17.64	-	- .391
2	103.14	$-.17 \pm j\,1.22$	.948	.137	- 5.26	-	- .305
3	103.14	$-.35 \pm j\,2.94$	.983	.046	-11.45	-	- .734
4	74.49	$-.382 \pm j\,5.0$	.972	.108	- 9.76	-	- .705
5	131.79	$-.242 \pm j\,5.03$	.975	.054	-22.54	-	- .243
6	74.49	$-.25 \pm j\,1.275$	1.000	.168	- 2.31	-	- 1.46
7	103.14	$-.852 \pm j\,2.1$	1.000	.168	-11.45	-	- 2.36
8	103.14	$-1.302 \pm j\,8.77$	.985	.103	-17.64	-	- 2.49
9	103.14	$-.532 \pm j\,2.56$	1.000	.103	7.95	-.324	6.98
10	103.14	$-.327 \pm j\,4.58$	.792	.549	- 8.04	-.101	- 6.67
11	103.14	$-.186 \pm j\,2.747$	1.197	.279	11.55	.034	- 5.66
12	74.49	$-.498 \pm j\,1.2$	1.000	.279	- .15	-.143	-45.50
13	74.49	$-.198 \pm j\,.968$	.760	.680	- 3.20	-.280	- 2.20
14	74.49	$-.23 \pm j\,1.808$	1.402	.433	7.10	.202	- 1.99

F3

Directional Control Transfer Functions

Roll response to rudder inputs is defined by the open loop transfer function

$$\frac{\varphi}{\delta r} = \frac{N_{\delta r}^{\varphi}}{\Delta}$$

The numerator typically factors in the following fashion

$$N_{\delta r}^{\varphi} = A_{\varphi_{\delta r}} (s^2 + 2\zeta_{\varphi_r} \omega_{\varphi_r} s + \omega_{\varphi_r}^2)$$

or

$$= A_{\varphi_{\delta r}} (s + \frac{1}{T_{\varphi_1}})(s + \frac{1}{T_{\varphi_2}})$$

For the configurations of this program where $L'_{\delta r} = 0$, the rudder roll numerator may be redefined

$$N_{\delta r}^{\varphi} = A_{\varphi_{\delta r}} (s + \frac{1}{T_{\varphi_1}})$$

where

$$A_{\varphi_{\delta r}} = L'_{\beta} Y^*_{\delta r} + N'_{\delta r} L'_r$$

$$\frac{1}{T_{\varphi_1}} = \frac{Y^*_{\delta r} (L'_r N'_{\beta} - N'_r L'_{\beta}) - N'_{\delta r} (L'_{\beta} - Y_v L'_r)}{L'_{\beta} Y^*_{\delta r} + N'_{\delta r} L'_r}$$

The rudder will command yaw rate as determined in part by the numerator

$$N_{\delta r}^{r} = A_r (s + \frac{1}{T_{r_1}})(s^2 + 2\zeta_r \omega_r s + \omega_r^2)$$

where $\qquad A_r = N'_{\delta r}$

$$\frac{1}{T_{r_1}} \doteq - L'_p$$

$$2\zeta_r \omega_r \doteq - (Y_v - \frac{Y^*_{\delta r} N'_\beta}{N'_{\delta r}} - \frac{g}{V_o} \frac{L'_\beta}{L'^2_p})$$

$$\omega_r^2 \doteq \frac{g}{V_o} \frac{L'_\beta}{L'_p}$$

under the circumstances where

$$\left| \frac{(Y_v - \frac{Y^*_{\delta r} N'_\beta}{N'_{\delta r}})^2}{4} \right| < \left| \frac{g}{V_o} \frac{L'_\beta}{L_p} \right| < \left| \frac{L_p^2}{10} \right|$$

Another possible factorization of the yaw rate to rudder numerator is

$$N^r_{\delta r} = A_r (s + \frac{1}{T_{r_1}})(s + \frac{1}{T_{r_2}})(s + \frac{1}{T_{r_3}})$$

where $\qquad A_r = N'_{\delta r}$

$$\frac{1}{T_{r_1}} \doteq - L'_p$$

$$\frac{1}{T_{r_2}} \doteq - (Y_v - \frac{Y^*_{\delta r}}{N'_{\delta r}} N'_\beta)$$

$$\frac{1}{T_{r_3}} \doteq \frac{g/V_o L'_\beta}{L'_p (Y_v - \frac{Y^*_{\delta r}}{N'_{\delta r}} N'_\beta)}$$

when the following condition holds

$$\left| \frac{g}{V_o} \frac{L'_\beta}{L'_p} \right| < \left| \frac{(Y_v - \frac{Y^*_{\delta r}}{N'_{\delta r}} N'_\beta)^2}{4} \right|$$

Exact values of the $N^\varphi_{\delta r}$ and $N^r_{\delta r}$ numerator factors are listed in Table F2 for the various test configurations.

TABLE F2

DIRECTIONAL TRANSFER FUNCTION NUMERATORS

Conf.	Transfer Function (Rudder)				
	$N_{\delta r}^{\varphi}$		$N_{\delta r}^{r}$		
	A_{φ}	$-1/T_{\varphi_1}$	A_r	$-1/T_{r_1}$	$-\zeta_r \omega_r \pm j \omega_r \sqrt{1 - \zeta_r^2}$
1	-70.15	-11.21	-45.84	-4.04	.00002 ± .868
2	-52.92	-14.39	-45.84	-4.1	-.028 ± j .85
3	-51.79	-14.69	-45.84	-4.09	-.024 ± j .881
4	-85.27	- 8.84	-45.84	-2.30	.201 ± j1.11
5	-43.53	-16.62	-45.84	-10.0	-.081 ± j .531
6	-119.62	- 6.35	-45.84	-2.33	.171 ± j1.099
7	-101.02	- 7.74	-45.84	-4.06	-.023 ± j .852
8	-217.16	- 3.58	-45.84	-3.99	.017 ± j .847
9	-100.84	- 7.55	-45.84	-3.73	.016 ± j .881
10	-73.76	-10.12	-45.84	-4.00	-.003 ± j .849
11	-20.53	-35.48	-45.84	-4.27	-.017 ± j .819
12	-100.85	- 7.55	-45.84	-2.33	.176 ± j1.102
13	-119.62	- 6.35	-45.84	-2.33	.171 ± j1.099
14	-58.20	-13.42	-45.84	-2.45	.156 ± j1.103